Department of Mechanical Engineering

Modelling of Large Diesel Intake and Exhaust System Acoustics Using One Dimensional (1D) Simulation and Experimental Verification

David Robert Bowden

This thesis is presented for the Degree of
Master of Philosophy (Mechanical Engineering)
of
Curtin University

July 2017

Author’s Declaration

To the best of my knowledge and belief this thesis contains no material previously published by any other person except where due acknowledgement has been made.

This thesis contains no material which has been accepted for the award of any other degree or diploma in any University.

David Robert Bowden

Date

Abstract

The noise levels for large capacity marine diesel engines must meet legislative requirements as a minimum and may have additional constraints on level and spectral content such as in the case of a conventionally powered (diesel / electric) submarine. Exhaust and intake system testing and development for this class of engine is generally limited to confirmation testing due to limited availability of test facilities, high cost of test hardware and testing, limited physical access, and low production volumes. These large diesel engines differ significantly from those used for automotive applications in regard to gas flow characteristics, exhaust system design, and operational modes.

To address this development constraint, the Defence Science and Technology Group (DST) has evaluated the applicability of an automotive industry one dimensional (1D) simulation software suite (Ricardo WAVE) and developed a capability to model / simulate the acoustic and gas flow performance of intake exhaust system components representative of large marine diesel engines. This capability can be used for exhaust and intake system components, complete systems, and full engine installations with savings achieved through a reduction in test samples and physical testing.

A virtual test bench approach was employed to reduce simulation run times compared to that of complete engine installations. The modelling was conducted in order of increasing complexity where simple models were validated before progressing to more complex models. Published research, theory, and experimental acoustic transmission loss test bench data were used for validation. The acoustic cavity mode resonant frequencies were experimentally measured using air jet excitation to assess the complexity of the acoustic behaviour of the large marine muffler.

An experimental acoustic transmission loss test bench was designed, constructed and developed to provide validation of the modelling / simulation process. This capability operates at room temperature and zero flow independently of the engine and engine installation and with excitation provided by a low frequency loudspeaker. The acoustic transmission loss was calculated using the four microphone and three microphone methods. The performance of the facility was validated using a plain duct, simple contraction / expansion chambers and was compared with computer simulation results.

A finite element analysis using ANSYS of a large marine muffler's shell was conducted to assess the effect of shell and structural modes on the acoustic performance. This analysis was partially validated by the experimental measurement of the muffler shell resonances.

Acknowledgements

There are many people who have contributed to this thesis and associated work and I apologize in advance to those who I have not listed. Firstly there are my Curtin University supervisors Ian Howard and Rodney Entwistle who have always encouraged me and have taught me how to do a research degree. Secondly there is my employer the Defence Science and Technology Group (DST) who enabled this work by providing support, time, the simulation software, and the experimental facilities. My retired DST colleague Ross Juniper and I conducted many on-engine large marine exhaust noise reduction trials which while productive and enjoyable prompted me to explore the simulation process as a complementary approach. Yan Tso, James Forrest, Alex Skvortsov and Chris Norwood supported the DST work program of which this thesis is a part. In addition James has been my DST supervisor for this thesis. Finally I would like to especially thank my group leader Michael Newman for his encouragement, coaching, and help with my technical and report writing.

Dedication

This thesis is dedicated to the special people in my life who have helped with my education and this thesis. Firstly there are my father David and my mother Hazel who always encouraged me to learn, to strive to achieve and to seize the educational and vocational opportunities that were not available to them when they were growing up in the 1930's and 1940's. Secondly I would like to thank my wife Tracy who always quietly encourages me to be who I am, to do what I want to do and to achieve my goals.

Table of Contents

List of Figures

List of Figures in Appendices

List of Tables

List of Abbreviations

Abbreviation / Acronym	Description
Δp	Amplitude of pressure wave (Pa)
µPa	Micro Pascals
1D	One Dimension / Dimensional
3D	Three Dimensions / Dimensional
A	Area (m^2)
a	Radius of pipe (m)
$\alpha_0(f)$	Power reflection coefficient
ANSYS	ANSYS Inc.'s finite analysis software
BEM	Boundary Element Method
BIGWAVE	Version of WAVE with more elements
c	Speed of sound (m/s)
CAD	Computer Aided Design
CCSM	(Australian) Collins Class Submarines
C_d	Coefficient of discharge
C_f	Coefficient of flow
CFD	Computational Fluid Dynamics
CFR	Cylinder Firing Rate
C_{xy}	Real component of cross (power) spectrum between points x and y
D	Orifice diameter (m)
D	Pipe internal diameter (m)
D_1	Upstream diameter (m)
D_2	Downstream diameter (m)
dB	decibel
DG	Diesel Generator
d_p	Pipe hydraulic diameter (m)
DST	(Australian) Defence Science and Technology Group
DSTO	(Australian) Defence Science and Technology Organisation
dtube	Discretization length of tube
dx	Discretization length in X direction
dy	Discretization length in Y direction
dz	Discretization length in Z direction

Abbreviation / Acronym	Description
EU	Engineering Units (HP analyser)
E_w	Noise generation efficiency (dB)
f	Frequency (Hz)
F	Froude's friction factor
FEM	Finite Element Method
FRF	Frequency Response Function
HP	Hewlett Packard
Hz	Unit of frequency, Hertz
ICP	Denotes sensor with inbuilt signal conditioning electronics
JMAX	Total number of y-junctions and ducts in WAVE model
K	Unit of temperature, Kelvin
K	Loss Coefficient
k	Wave number (m^{-1}), $k = 2\pi f/c$ or $k = 2\pi/\lambda$
k_0	Stationary wave number (m^{-1})
k_c	Convective wave number (m^{-1})
kg	Kilogram
kg/m^3	Kilograms per cubic metre
kg/s	Kilograms per second
KMAX	Number of y-junctions in WAVE model
kPa	Unit of pressure, 1000 Pascals
kW	Unit of power, 1000 Watts
l	Length (m)
l_0	End correction (m)
l_e	Effective / corrected length (m)
LM	Large Muffler
LMAX	Number of ducts in WAVE model
LMM	Large Marine Muffler
l_p	Pipe length (m)
L_v	Length of Helmholtz resonator cavity / volume (m)
Lw	Emitted sound power (dB)
m	Area ratio
m	Metre
M	Speed (Mach)
m/s	Metres per second

Abbreviation / Acronym	Description
MATLAB	MathWorks' computational mathematics software
mm	millimetre
MTU	An engine manufacturer
n	Area ratio
NACA	(US) National Advisory Council on Aeronautics
ø	diameter
ºC	Unit of temperature, degrees Centigrade
p	Sound pressure (Pa)
Pa	Unit of pressure, Pascal
P_{at}	Atmospheric pressure (mm Mercury)
PCB	Instrumentation manufacturer
p_i	Incident sound pressure (Pa)
p_r	Reflected sound pressure (Pa)
p_t	Transmitted sound pressure (Pa)
QWT	Quarter Wave Tube
Q_{xy}	Imaginary component of cross (power) spectrum between points x and y
r	Duct radius (m)
r_d	Downstream pipe radius (m)
rms	Root mean squared
rpm	Revolutions per minute
r_u	Upstream pipe radius (m)
S	Cross-sectional area of Helmholtz resonator neck (m^2)
S_{AA}	Incident auto (power) spectrum
S_{BB}	Reflected auto (power) spectrum
SDF	HP Standard Data File format
SESAM	Silencer & Exhaust Systems Acoustic Measurement
S_i	Cross-sectional area of inlet tube (m^2)
S_o	Cross-sectional area of outlet tube (m^2)
SPL	Sound Pressure Level
S_v	Cross-sectional area of Helmholtz resonator cavity / volume (m^2)
S_v	Cross-sectional area of Helmholtz resonator duct (m^2)
S_{xx}	Auto (power) spectrum at point x
t	Time (seconds)
T	Gas temperature (°C)

Abbreviation / Acronym	Description
TL	Transmission Loss
TMM	Transmission Matrix Method
U	Gas velocity (m/s)
u	Particle velocity (m/s)
v	Gas flow velocity (m/s)
V	Volts
W	Unit of power, Watts
ω	Frequency (radians)
WAVE	Ricardo's 1D computational fluid dynamics software
WaveBuild	Ricardo's 1D model creation software
WaveBuild3D	Ricardo's 3D model creation software
WavePost	Ricardo's post processing software
x_i	Distance to point i from reference position
Z	Impedance (kg/m^2)
λ	Wavelength (m)
ξ	ratio of contraction pipe diameter to expansion pipe diameter
ρ	Density (kg/m^3)

Chapter 1 Introduction

This chapter explains the background, identifies the target of this study, introduces the approaches used, and lists the thesis aims and research methods.

1.1 Background

Large capacity diesel engines are used in marine, rail, and off-highway applications as propulsion engines, in diesel electric propulsion and with generators for electrical power generation. The noise levels must meet legislative requirements as a minimum and must in some applications meet additional constraints on level or spectral content. In addition to acoustic performance, flow restriction or exhaust back pressure is important as it adversely affects the thermodynamic performance of the engine by increasing pumping work [1] and accordingly must be minimised. This criterion must be balanced against acoustic performance as acoustic performance generally improves with increasing flow restriction.

The impetus for the work in this study arose from developmental work on the Collins Class (CCSM) submarines conducted by Australia's Defence Science and Technology Organisation (DSTO) / Defence Science and Technology Group (DST) starting in the mid-1990's [2]. Accordingly, this thesis considers the particular case of a conventionally powered submarine. These are battery electric powered at depth and typically use two or three diesel generators (DG) of 1.5 MW capacity each to recharge their batteries either at periscope depth or on the surface. While all submarines rely on their stealth to evade detection, the covert operation of a conventional submarine is compromised by the need to periodically run the diesel generators to recharge the batteries. During the recharging process, the submarine is more vulnerable to detection due to the emission of a higher level of distinctive acoustic 'signatures'. This acoustic signature may enable the submarine to be detected and identified.

The submarine's far field radiated noise is a combination of hull flow noise and all on-board equipment with a significant contributor being the diesel generators. The DG's contribution is a combination shown in Figure 1.1 of intake noise, noise directly radiated from the DG structure, structure borne noise through the DG's isolators, and underwater exhaust / tailpipe noise. Due to the DG's high power output, the exhaust system's tailpipe noise is the most significant noise element radiated as far field noise.

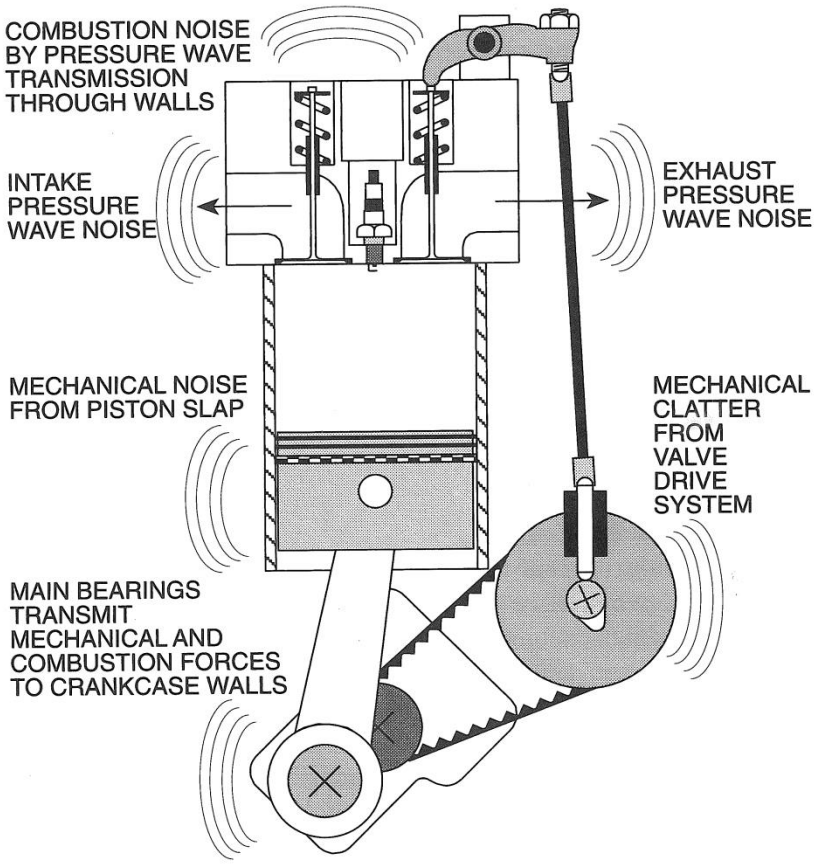

Figure 1.1 Sources of Base Engine Noise [3]

The tools and techniques explored in this thesis are equally relevant to intake systems and exhaust systems with the prime differences being the mean gas temperatures, gas temperature variation across operating range, gas flow volumes, and pressure fluctuation amplitudes. Traditionally, the acoustical properties of an intake or exhaust system have been determined by analytical means and supplemented by experimental validation. Unlike automotive applications, noise tests on large marine diesel engine installations are rare except for confirmation testing due to the limited physical access when installed, limited availability of acoustic quality engine test facilities, low production volumes, high costs of operation and limited availability of the vessel. Additionally mufflers for large marine diesel engines are large, heavy, expensive to manufacture, difficult to modify and cumbersome to manoeuvre.

Experimental verification and development of system performance is accordingly time consuming, expensive and requires dedicated test facilities [3, 4]. This has driven the emergence of analytical modelling, including software simulation, which is quicker, cheaper, and more flexible with respect to test parameters and test configurations. In the automotive industry exhaust and intake system simulation and optimization are important and well-researched areas [5-14]. However, large marine diesel engines differ significantly from those used for automotive applications in the following areas:

1. higher gas flow volumes
2. larger amplitude exhaust / cylinder blow down pulses
3. lower engine speeds
4. constant speed operation for diesel generators
5. exhausting under water in some applications.

Computer based modelling provides the capability to design and optimise the acoustical properties of the exhaust system without the necessity of manufacturing hardware. The software package used in this study can model and optimise the acoustic and flow performance of intake and exhaust systems applicable to diesel generators in a conventional submarine.

1.2 Large Marine Muffler

The focus of this study is a large two chamber marine diesel muffler as shown in Figure 1.2 and which in this study is designated Large Marine Muffler (LMM). This is purely a test muffler and is not used in any application but is similar in concept and size to that fitted to the CCSM's. To illustrate the difference to automotive components, this exhaust muffler is two metres in length and weighs 450 kilograms. It is a twin expansion chamber muffler with an interconnecting tube and has better acoustic performance than two similar expansion chambers in series. Despite its apparent simplicity, it consists of two expansion chambers, two coupled Helmholtz resonators and four quarter wave tubes. It is sometimes referred to as Helmholtz filter or a low pass filter.

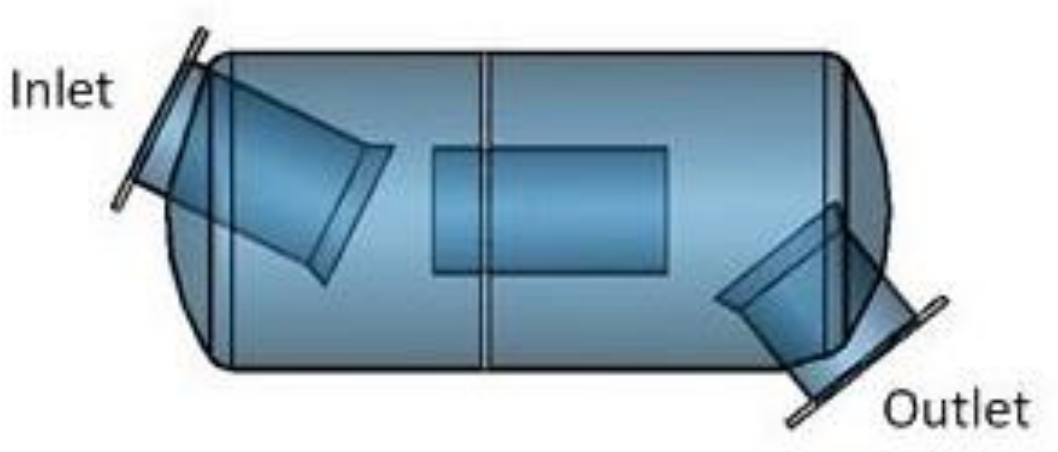

Figure 1.2 Large Marine Muffler (LMM)

1.3 Exhaust Noise Overview

1.3.1 Spectra of Exhaust Systems

The far field radiated noise due to an engine's exhaust is a function of the source level, transmission/attenuation paths, and radiation characteristics. The engine source level and spectra are dependent on engine configuration, number of cylinders, and running speed. As an example, a four stroke V16 configuration engine running at 2000 rpm will have an exhaust noise spectrum comprised of harmonics starting at the cylinder firing frequency of 17 Hz, or half (crankshaft) order with a peak at the engine firing frequency - 267 Hz or eighth (crankshaft) order. To illustrate the tonal nature of the exhaust noise, Figure 1.3 shows a repetitive tonal time signal and the resultant tonal frequency spectrum. As an example of an un-muffled exhaust noise source, Figure 1.4 shows the tailpipe third octave spectrum for a V16 marine diesel engine at 2000rpm and 2320 kW.

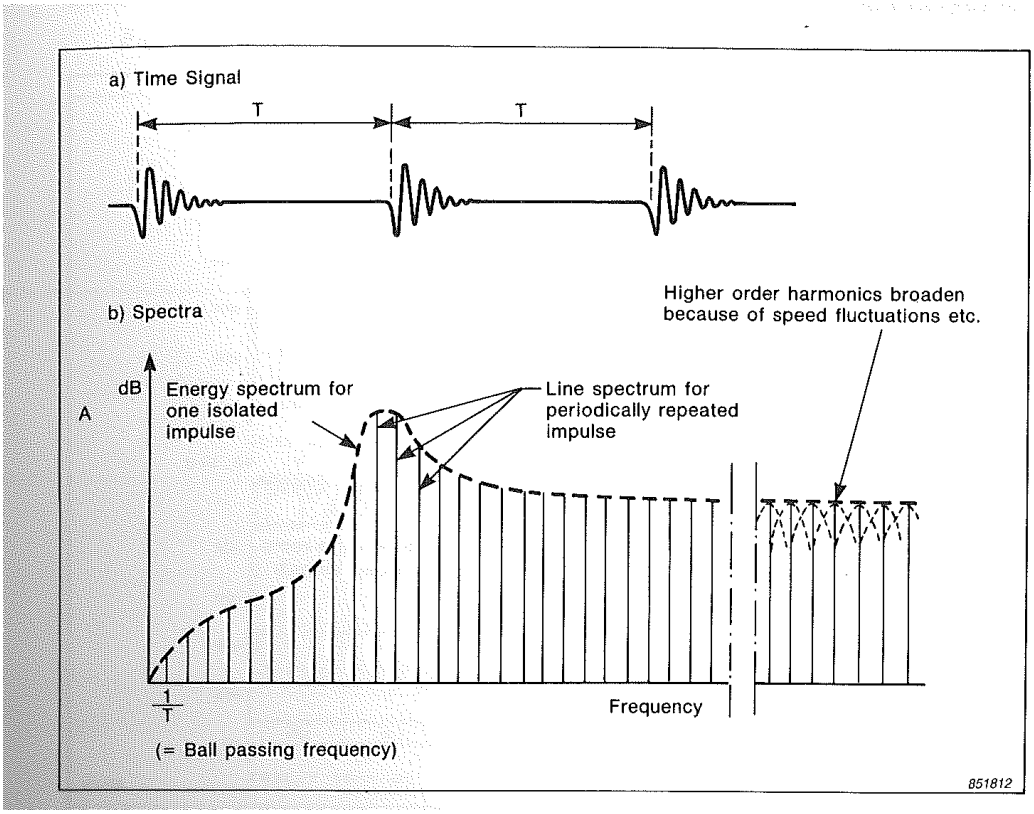

Figure 1.3 Tonal Spectrum For Repeated Pulse Time Signal [15]

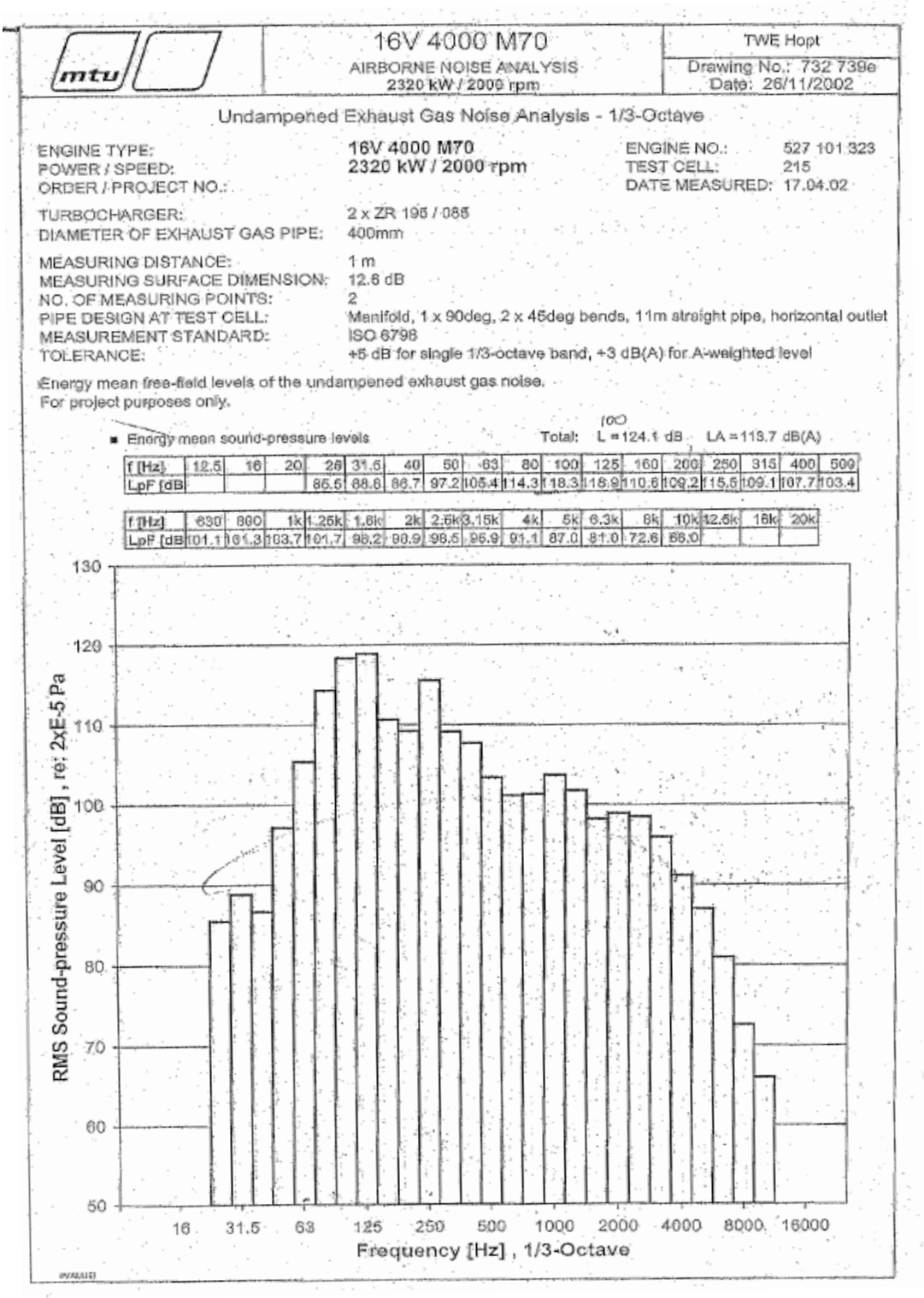

Figure 1.4 Undamped Exhaust Third Octave Spectrum, MTU 16V M70 Diesel Engine [16]

1.3.2 Exhaust Noise Reduction Strategies

Exhaust noise from internal combustion engines comprises tonal components, as mentioned in the previous section, and broadband noise generated by the high velocity exhaust gas flow through the exhaust system. The exhaust noise propagates from the source towards the outlet with partial reflections from each acoustic discontinuity / impedance change e.g. area change. Accordingly, the sound pressure level at any point is an instantaneous combination of forward travelling and backward travelling waves. As more pressure waves are reflected back towards the source and dissipated as heat, less sound energy is radiated from the outlet.

The primary basis of reducing broadband noise transmission is by increasing reflections, promoting destructive interference, and dissipating sound energy as heat by using perforations and absorptive packing. For specific tones, noise cancellation can be achieved by passively generating out-of-phase resonances with quarter wave tubes and Helmholtz resonators, or by active noise cancellation using speakers to generate out-of-phase tones to cancel the targeted tones.

1.4 Simulation

Many methods of gas flow and acoustic analysis and simulation have been devised including empirically based formula, analytical models, method of characteristics, transmission matrix method (TMM), Finite Element Method (FEM), Boundary Element Method (BEM) and computational fluid dynamics (CFD) in one-dimensional (1D) and three-dimensional (3D) forms. The gas flow and acoustic behaviour can be linear or non-linear depending upon the flow regime and the amplitude of the pressure fluctuations. Linear behaviour occurs when the fluctuations are small in comparison with the mean pressure and this allows the wave equation to be linearized and solved more easily and generally. When pressure fluctuations are high relative to the mean pressure and there is substantial mean flow, the linear assumption breaks down. Fortunately there is CFD software that can model both linear and non-linear behaviour including with gas flow.

CFD software developers in this area include Gamma Technologies, Lotus Engineering, AVL Powertrain Engineering, Optimum Power, and Ricardo. The software used in this research program is an automotive one-dimensional (1D) engine and gas dynamics simulation software package called Ricardo WAVE. This software can model general and complex compressible flow fluid networks in terms of finite volume elements. The flow of gas within pipe elements is assumed to be non-linear, one-dimensional, inviscid, compressible, and unsteady and the governing equations are conservation of mass, momentum, and energy. As reported previously [17] DST has developed a computer modelling and simulation capability based on Ricardo WAVE software capable of predicting the acoustic response and flow performance of exhaust systems representative of a large marine diesels. This computer model was validated with published test data and on-engine test data.

1.5 Transmission Loss Test Bench

To provide further validation, increase confidence in the modelling capability and overcome many of the above development constraints, DST has developed an experimental laboratory test bench [18] to measure the acoustic transmission loss performance of exhaust system components representative of large marine diesel engines. Transmission loss was selected as the preferred parameter to characterise acoustic performance as it is independent of the upstream and downstream systems which vary depending upon the installation. This test bench operates independently of the engine and engine installation with excitation provided by a low frequency loudspeaker and at room temperature and with zero flow. The advantages and disadvantages of testing at room temperature with zero flow are discussed in detail later in this thesis. Four microphones were used to measure sound pressure levels before and after the muffler with data acquisition and signal processing by a Hewlett Packard (HP) Spectrum Analyser with post processing in MATLAB software to calculate the acoustic transmission loss. This thesis describes the test bench design, instrumentation, data acquisition, development, data processing techniques and validation process.

1.6 Thesis Overview

1.6.1 Overall Aims

This study aims to investigate the ability of one-dimensional (1D) computational fluid dynamics (CFD) software modelling and simulation to predict the acoustic performance and flow restriction of intake and exhaust system components applicable to large diesel engines. An additional aim includes an examination of the methods of experimentally quantifying component acoustic performance in a laboratory environment. The aims can be summarised in the following questions:

1. Can a commercial one-dimensional (1D) software suite targeted at automotive applications be used for modelling the acoustic performance for the intake systems and exhaust systems of medium and large diesels?
2. Can a commercial one-dimensional (1D) software suite targeted at automotive applications be used for modelling the flow restriction for the intake systems and exhaust systems of medium and large diesels?
3. What are the acoustic, gas flow, and modelling differences between automotive scale intake systems and exhaust systems and those of medium and large diesels?
4. What is the best method for accurate characterization of the acoustic performance of intake and exhaust systems and system components using practical measurements at a test facility?

1.6.2 Research Method

A detailed literature search examined the applicable modelling and experimental validation techniques paying particular regard to large scale diesel components and their differences from automotive scale components and techniques. The results of this data and information gathering were used to guide and refine the modelling / simulation and verification program. Ricardo's WAVE software suite was used to model selected systems for both acoustic performance and flow restriction. Verification used theory, published results, and experimental results as available and applicable. For both acoustic and flow modelling, the variations investigated progressed from simple to complex in both configuration complexity and modelling complexity.

Experimental acoustic transmission loss testing was conducted on an existing large two chamber muffler (muffler LMM) at DST Western Australia on the experimental laboratory test bench.

The shell of muffler LMM was modelled using finite element analysis (FEA) software (ANSYS) to predict modes of vibration so as to assess their possible influences on the experimental acoustic results.

The acoustic cavity and pipe acoustic modes of muffler LMM were experimentally determined using air-jet excitation to assess their influences on the experimental acoustic results and to explore the complexity of the muffler.

1.6.3 Structure of Thesis

This thesis is structured as follows:

1. introduction
2. literature review
3. technology overview and methodologies
4. numerical experiments for acoustics and flow
5. design, construction and validation of an experimental transmission loss test bench
6. finite element modelling of the muffler shell
7. limited experimental validation of muffler cavity modes
8. experimental transmission loss test bench measurements on a large marine muffler
9. limited experimental validation of muffler shell modes
10. discussion
11. conclusions
12. appendices with more information for:
    a. muffler shell finite element analysis
    b. experimental transmission loss test bench
    c. MATLAB code used for data processing
    d. experimental measurement of muffler shell modes

Chapter 2 Literature Review

2.1 Overview

This thesis covers a number of well researched areas and to formally review all of these areas is beyond the scope of this thesis. So this literature review will concentrate on the areas which the author considers to be of direct relevance and in sufficient depth to achieve his needs. This is intended not to diminish or lessen the contribution of others to this field of research but is a necessary practical approach given the depth and breadth of the research areas touched upon by this thesis.

Exhaust and intake system modelling, simulation and measurement has long been important areas of research with many centres of research including Southampton University's Institute of Sound & Vibration Research (ISVR) [19-24], General Motors Research Laboratories [25-27], the University of Kentucky [13, 28-31], the Indian Institute of Science (IISc) [10, 11, 32-35], the University of Manchester's Institute of Science and Technology [36, 37], Cranfield University [38, 39], Queens University Belfast [3, 40], the University Polytechnic Valencia [41] and the University Polytechnic Milan [42, 43]. The acoustic modelling and simulation has progressed in sophistication and accuracy in parallel with engine performance and gas flow modelling particularly with the advent of modern computing power facilitating more complex models and modelling techniques. The acoustic modelling techniques have progressed along from analytical / mathematical, one dimensional (1D) computational fluid dynamics (CFD), three dimensional (3D) CFD, to combined 1D/3D variants in an attempt to improve accuracy under all conditions. This thesis uses a 1D commercial software suite called Ricardo WAVE.

2.2 Automotive / Small engine Applications

Significant early work targeted at piston engine helicopters was conducted by the US National Advisory Council on Aeronautics in the 1950's [44, 45]. This work comprised extensive experimental measurements benchmarked against theoretical calculations using classical mathematical models. Increasing customer expectations, high production volumes and the large development budgets of the automotive industry has driven the development of exhaust and intake system modelling and optimization techniques. Commercially available engine acoustic software is available from a number of vendors [5-8, 12] and is targeted primarily at the automotive industry.

2.3 Acoustic Measurement Techniques

While the overall system acoustic performance can be characterised by a single number such as tailpipe sound pressure level, it is useful for developmental purposes to be able to quantify the acoustic performance contribution of individual components. Considerable research [25-31, 46, 47] has been undertaken as how to best quantify and then to measure the component's acoustic performance in laboratory tests and in on-engine tests. Practical techniques have been proposed and developed for measuring theoretical component acoustic parameters such as insertion loss, level difference, and transmission loss. Some techniques are now mature enough in a controlled laboratory environment to become standard measurement techniques for acoustic material properties [48, 49]. However, the best method for practical on-engine measurements of engine exhaust and intake component performance is still under debate [13] and may be application specific.

Both Seybert, Ross & Soenarko [29-31] and Chung & Blaser [25-27] have developed experimental techniques which can resolve the complex acoustic fields as measured with pressure transducers / microphones at specific points into the required forward and backward travelling waves using wave decomposition. From the forward and backwards travelling waves, the incident acoustic power and transmitted acoustic power and the transmission loss can be calculated. The two techniques are essentially identical with one being able to be derived from the other [29, 34]. While the Chung-Blaser method is claimed to be less computationally intensive [34], this distinction is now less important due to the continually increasing performance of computers. However, the Chung-Blaser uses transfer functions and so facilitates corrections for phase and amplitude matching of the microphones.

Seybert and Ross at the University of Kentucky presented a seminal experimental technique with accompanying theory for the determination of acoustic properties in 1977 [30]. This used a sound source with random excitation and two microphones in a tube. This new technique addressed the limitations of the standing wave ratio (SWR) method previously used including slow measurement speed due to the SWR's discrete frequency sweep and the physical size limitation due to the need for the traversing microphone to actually fit inside the system under test. The new technique also addressed the impulse excitation method's difficulty of producing an acoustic pulse with sufficient energy across the desired frequency range. The method used two microphones and their measured auto (power) spectra and cross (power) spectra combined with wave decomposition to determine the auto (power) spectra and cross (power) spectra of the incident and reflected waves. The acoustic impedance, absorption, power reflection coefficient and transmission loss can then be calculated as appropriate to the item under test. The experimental apparatus used a tube diameter of 48 mm giving an upper frequency limit of 4.2 kHz and a microphone spacing of approximately 128 mm which gave solution indeterminacies at multiples of 1.35 kHz. This 4.2 kHz upper frequency limit was due to the onset of a duct lateral mode. Seybert and Ross emphasised the need for phase and amplitude matching of the microphones and presented an axial orientation technique for measuring the required correction factors. The physical diameters of their measurement tubes are far smaller than those used in this thesis.

Chung and Blaser at General Motors Research Laboratories presented the theory [26] and an experimental method [27] for measuring in-duct acoustic material properties at zero flow using the transfer function method in 1980. The method used two microphones and their transfer function relationship combined with wave decomposition to determine the complex reflection coefficient. From this coefficient, the acoustic impedance, transmission loss and sound absorption coefficient can be determined. The experimental apparatus used a tube diameter of 51 mm and a microphone spacing of 27 mm giving upper frequency limits of 4 kHz and 6.4 kHz respectively. These frequency limits are due to the onset of a duct lateral mode and wave decomposition indeterminacy respectively. The microphone phase and amplitude matching was accomplished by the use of a transfer function correction determined by switching the microphone positions with a constant source and averaging the transfer functions. Compared to those used in this thesis, the physical sizes of their measurement tubes were far smaller. Additionally, their upper frequency limit and associated microphone spacing are much higher and smaller respectively.

Seybert and Soenarko in 1981 [31] followed on from the earlier work of Seybert-Ross and Chung-Blaser and presented an error analysis of the spectral estimates used in these techniques described earlier. The experimental apparatus used a tube diameter of 52 mm and a microphone spacing of 50 mm giving upper frequency limits of 3.8 kHz and 3.45 kHz respectively. Again these physical dimensions are much smaller than those used in this thesis and their frequency range is much higher. They categorised the errors as bias or random errors. As described by Bendat in 1993 [50] random errors are a haphazard variation of results from one analysis to the next, whereas bias errors are systematic and repeatable in magnitude and direction from one analysis to the next. The bias errors of the pressure spectral densities were a function of the microphone positioning relative to the sample and the analysis frequency bandwidth used. These errors are minimised when the microphone is located close to the test item and when a small analysis frequency bandwidth is used. The random errors were found to be a function of the coherence between the acoustic source and the pressures in the duct. These errors can be minimised by ensuring a high coherence by minimising extraneous noise sources and using small microphone spacings. Large errors were noted when a standing wave node coincided with a microphone position and due to the microphone spacing when kL approached zero and kL approached π (where k is the wave number and L is the microphone spacing).

Boden and Abom [47] from the Swedish Royal Institute of Technology followed on from the work above and presented a more comprehensive theoretical and experimental examination of both the measurement errors and their effects on the calculated results of the two microphone method in1986. Random and bias errors were considered and the basic input parameters examined were those required to calculate the required acoustic parameter - transfer function, microphone spacing, the distance from a microphone to the acoustic sample and duct length. The results in Seybert and Soenarko above were confirmed with the following additional conclusions:

1. The bias error target or the transfer function should be less than 1% in magnitude and 0.6º in phase as this the typical Fourier analyser accuracy in the mid 1980's.
2. If the termination is not highly reflective this bias error can be easily met
3. If the termination is highly reflective a higher frequency resolution of less than one Hz is required.
4. The distance from the closest microphone to the sample should be a minimum of two to three diameters to minimise the effect of any lateral modes even below the cut-on frequency.

5. The error in the actual microphone spacing due to a microphone's 'acoustic centre' not coinciding with microphone's physical centre was found to be 0.5 mm for a pair of particular ¼ inch diameter microphones. This was for microphone spacings of 10.5 mm and 20.0 mm and a frequency range of 400 Hz to 4 kHz.
6. If the source end is reflective, the overall length of the duct should be kept small - five to ten diameters to minimize standing wave effects.
7. If the source end is non-reflective, then the overall length of the duct is arbitrary.
8. The two microphone method has the lowest sensitivity to errors when kL is equal to π.
9. The two microphone method should only be used when kL is in the range $0.1\,\pi < kL < 0.8\pi$ to avoid a high sensitivity to input data errors.

These guidelines and those from Seybert–Soenarko were considered and incorporated where possible into the acoustic transmission loss test bench designed for and used in this thesis. The implication of point 9 above is that multiple microphone spacings were needed to cover the thesis' subject frequency range.

Further work by Seybert [29] in 1988 presented a 'unified theoretical approach' to the two sensor methods presented over the previous ten years. He proposed that the duct acoustic properties can be derived from a general wave decomposition theory using the sound pressures measured at two points in the duct. The decomposition theory is presented in detail and experimentally verified. Using the decomposition theory, the auto (power) spectra and the cross (power) spectra for the incident and reflected wave are derived. From these the normalized impedance, power reflection coefficient and acoustic intensity are calculated. The Chung-Blaser transfer function approach described earlier was shown to be a special case of the decomposition theory.

In 2003 Tao and Seybert [13] presented a review of the techniques for measuring the acoustic transmission loss of a muffler. The wave decomposition method with an anechoic termination shown in Figure 2.1 was discussed first and this gives good results provided the anechoic termination is effective. The wave decomposition method will not work if there is reverberant behaviour after the muffler and this will be explained further in Section 5.7 of this thesis.

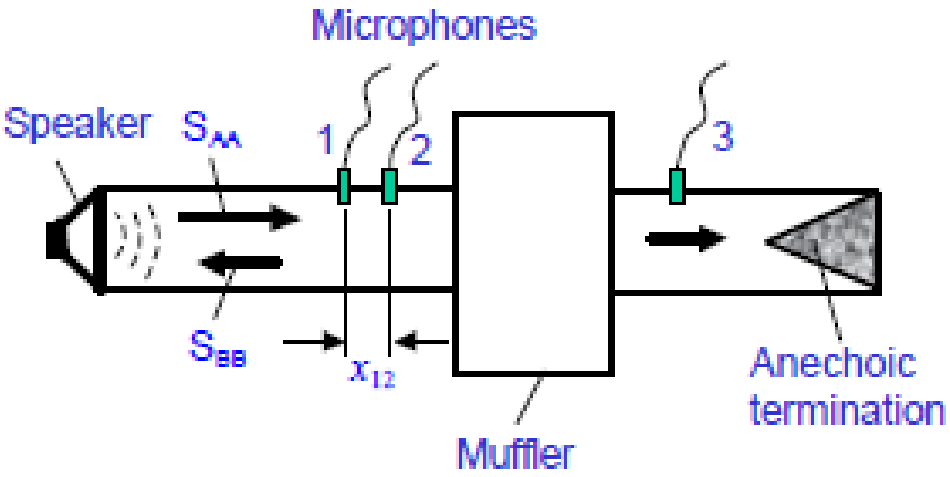

Figure 2.1 Wave Decomposition Theory Schematic [13]

Tao and Seybert recommend using the four pole / transfer matrix method shown schematically in Figure 2.2 when the termination after the muffler is reflective and consequently wave decomposition does not work. The removal of the need for an effective anechoic termination is particularly suited to applications with gas flow such as the large marine muffler in this thesis.

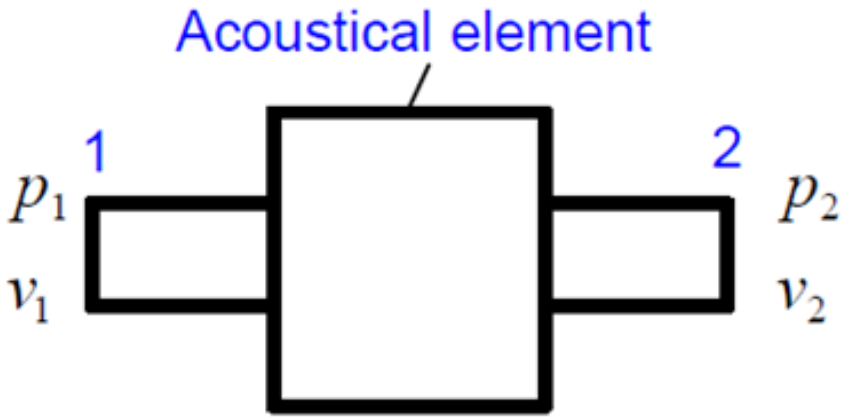

Figure 2.2 Transfer Matrix, Four Poles [13]

The transfer matrix for this is Equation (2.1):

$$\begin{bmatrix} \boldsymbol{p_1} \\ \boldsymbol{v_1} \end{bmatrix} = \begin{bmatrix} \boldsymbol{A} & \boldsymbol{B} \\ \boldsymbol{C} & \boldsymbol{D} \end{bmatrix} \begin{bmatrix} \boldsymbol{p_2} \\ \boldsymbol{v_2} \end{bmatrix} \quad (2.1)$$

Where:

p_1 and p_2 are the sound pressure amplitudes at positions 1 and 2 respectively

v_1 and v_2 are the sound particle velocity amplitudes at positions 1 and 2 respectively

A, *B*, *C* and *D* are the four parameters of the system.

Tao and Seybert presented two methods of obtaining the four pole parameters using wave decomposition and discussed their advantages and disadvantages. Validation was based on boundary element modelling (BEM) of small single and twin chamber expansion mufflers. These were 203 mm and 305 mm long respectively. The bodies were 153 mm in diameter with 35 mm diameter inlets and outlets. The first method was the two source method shown schematically in Figure 2.3. This method requires the source to be relocated or the muffler to be reversed with each configuration providing the two equations required to solve for the four unknowns.

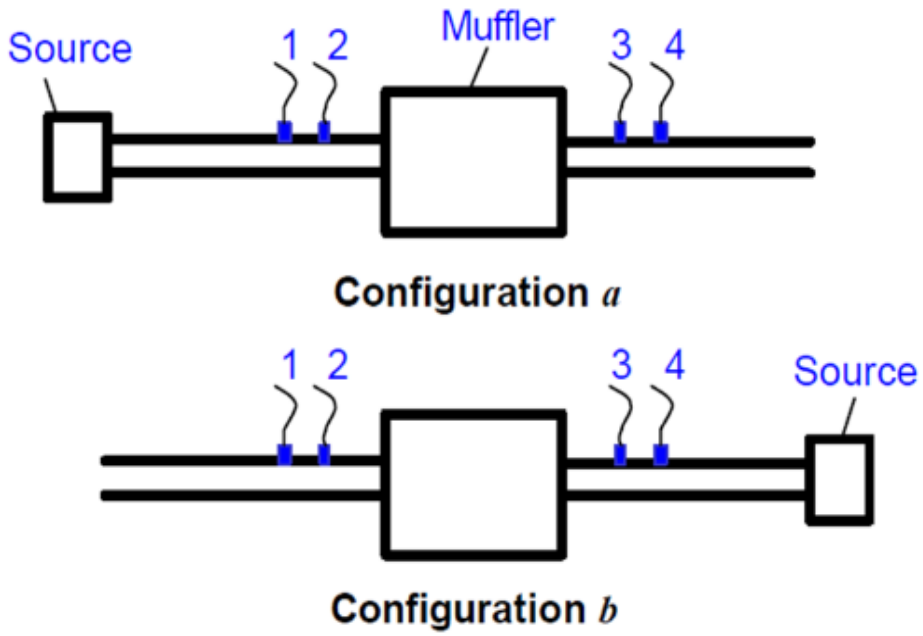

Figure 2.3 Two-Source Method, Configurations a and b [13]

While use of the two source is certainly possible for many applications it is not practical for on-engine testing or easy with the large mufflers which are the focus of this thesis.

The second method was the two load method shown schematically in Figure 2.4. This does not require the source to be changed or the muffler to be reversed. Rather it requires the test to be run with two loads / impedances Z_a and Z_b to give the required four equations. The two loads needs to be sufficiently different to ensure stability of the result.

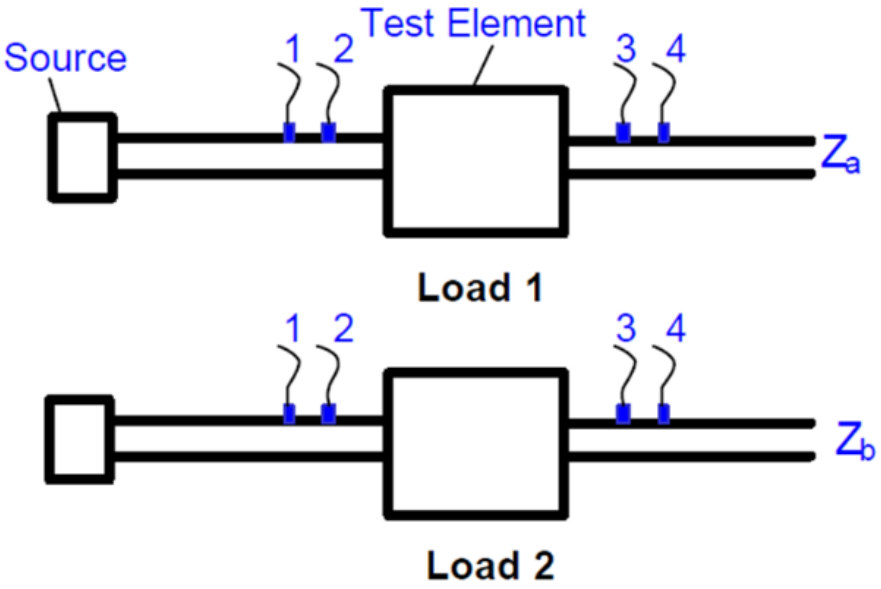

Figure 2.4 Two-Load Method, Load 1 And Load 2 Configurations [13]

This method is well suited to on-engine testing and the large marine mufflers which are the focus of this thesis. Due to the effect of changes in back pressure on the engine operation, care needs to be taken that the differences in the loads / impedances do not affect the engine combustion pressures and accompanying source levels.

As stated earlier, this work has reached a level of acceptance and maturity such that standard test methods have been published by ASTM International for measuring the sound absorption coefficients of acoustic materials using the transfer matrix two load method [48, 49]. These standard test methods typically use small diameter tubes such as the Seybert associated Spectronics Inc. apparatus [51] which has 34.8 mm diameter tubes and microphone spacings of 29.2 and 76.2 mm. For this apparatus, Spectronics Inc. quote a frequency range of 50 Hz to 5650 Hz. The first ASTM test method [49] uses two microphones with the acoustic sample against a solid backing piston. The second ASTM test method [48] uses a through approach with two microphones each side of the sample and two loads. While not aimed at muffler testing the theory and method of the transfer matrix two load method are well suited to any acoustic device [52] including those which are the focus of this thesis.

In 2013 Seybert published *A Guide to Making Effective Measurements of Sound Absorption Coefficient* [51] which detailed how to prepare acoustic material samples, use the aforementioned Spectronics Inc. apparatus, and associated measurement sources of error. In addition to the areas already covered in his earlier work he quantified the error in the actual microphone spacing due to the microphones 'acoustic centres' as 0.3 mm in a microphone spacing of 29.2 mm. While this 0.3 mm error can be significant in the small microphone spacings used for acoustic material high frequency measurements it is expected to have little effect with the 200 mm and 500 mm microphone spacings used in this thesis.

2.4 Marine / Large Diesel Applications

As opposed to the large quantity of published automotive modelling research papers, there appears to very little published research for exhaust and intake system modelling and optimization for large diesels [23, 53, 54]. In particular there is very little published work on gas flow and back pressure modelling and simulation [32, 34, 55]. This is likely to be due to lower customer requirements, a lack of a culture of publishing, and research and development work being retained as commercial property. In 2013 Ricardo [56] were unaware of anyone using their software to model large marine exhaust systems. The current commercial marine diesel approaches appear to be:

1. an engine manufacturer provides exhaust noise levels and spectra,
2. an engine manufacturer recommends and/or supplies a muffler,
3. a muffler manufacturer supplies a standard design muffler to meet a specific sound pressure level reduction, and/or
4. an acoustic consultant is engaged for a custom installation to meet special requirements.

In 2005 Johansson et al presented two papers on a proposed noise measurement technique using averaging of six microphones before and after the silencer in association with a manufacturer of large marine diesel engines - Wartsila Finland. The technique was called Silencer & Exhaust Systems Acoustic Measurement (SESAM). The first paper [57] detailed an experimental test bench (Figure 2.5) and measurement techniques. The sound levels from each set of six microphones were averaged in two ways – logarithmic average of all six and spatial averaging where the microphones were paired based on their spacing matching one quarter wavelength of the frequency of interest. This spatial averaging is claimed to compensate for standing waves in the ducts.

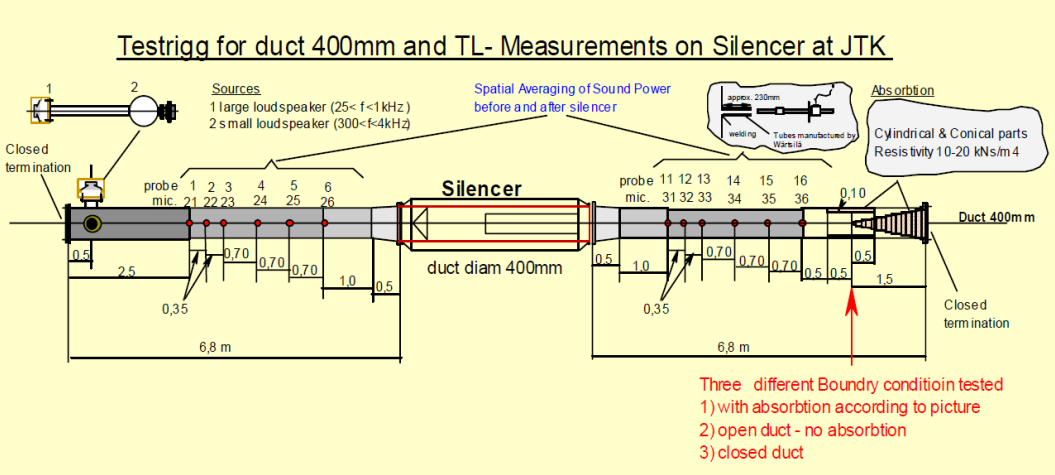

Figure 2.5 Schematic of SESAM Measurement Set-Up [57]

The second paper [58] presented the results of the above SESAM method on a running Wartsila W8L20 diesel (Figure 2.6) and with speaker excitation. The subject engine is a 70 litre capacity eight cylinder diesel rated at 1480 kW at 900 rpm. The calculated sound power in the ducts for each noise source was then compared with the radiated / tailpipe measured sound powers.

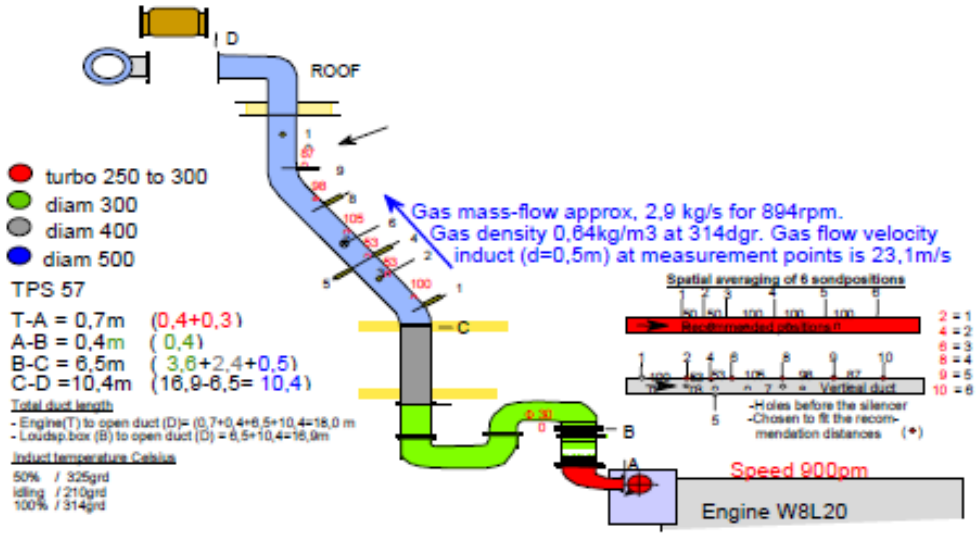

Figure 2.6 SESAM Measurement Schematic On Wartsila 8L20 Diesel [58]

In this author's opinion, the SESAM technique is promising as it does not affect engine back pressure, is simpler than the two-source and two-load methods and does not require an anechoic termination. It does not generate the four pole parameters for acoustic element but can generate the acoustic transmission loss if the sound power is calculated each side of the acoustic element.

In 2008, Ji and Wang presented a paper [59] on a variation of the boundary element method and compared the predictions with experimental test bench measurements on a large muffler – ø 550 mm and 1.5 m long. The noise source was a combustor with a centrifugal fan for flow in lieu of an engine. Their experimental technique used the four microphone transfer function two-load method with microphone error correction using the Chung-Blaser technique. Due to apparent concerns with the noise source stability 1000 averages were used. This author notes that the measurement and analysis techniques are as per the standard test methods above [48].

2.5 Effects of Gas Temperature on Acoustic Attenuation

For practical and logistical reasons associated with generating and maintaining a high gas and muffler temperature, the experimental transmission loss test bench operates at room / ambient temperature rather than at operating engine exhaust temperatures. The influence of this difference needs to be understood so that the test bench testing can be extrapolated to on-engine performance. In addition to increasing the mean gas volume flow rate, a survey of the literature showed that gas temperature affects:

1. speed of sound and resulting wavelength and wave number [60-63]
2. gas density [60, 62, 63]
3. gas viscosity [60].

To further assess the effects of temperature, it is helpful to look at the formulae for the transmission losses of reactive devices typically used in the mufflers of interest to this thesis. The transmission loss of an expansion chamber can be calculated using Equation (2.2) [34, 55].

2.5.1 Expansion Chamber

$$Transmission\ Loss\ (TL) = 10\log_{10}\left(1 + {}^{1}/_{4}\left(m + {}^{1}/_{m}\right)^{2}\sin^{2} k_0 l\right) \qquad (2.2)$$

where:

k_0 is the stationary wave number ($k = 2\pi f/c$ or $k = \omega/c$ or $k = 2\pi/\lambda$)

l is the length of the contraction / expansion (m)

m is the area ratio.

f is the frequency in Hz

ω is the frequency in radians

c is the speed of sound in m/s

λ is the wavelength in m

The wave number is the only parameter affected by temperature and results in a frequency shift with temperature as shown in Figure 2.7 for a simple large expansion chamber muffler (Muffler LM1, Figure 4.3) at gas temperatures of 25 °C and 430 °C

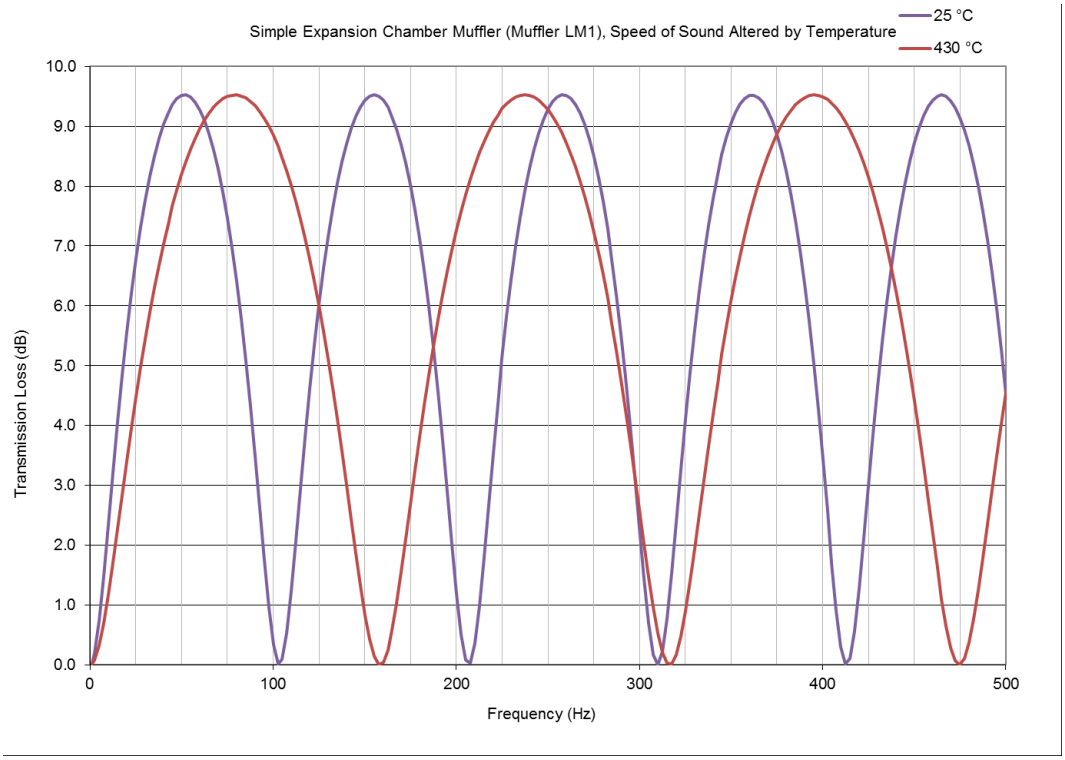

Figure 2.7 Simple Expansion Chamber, Effect of Temperature on Calculated Transmission Loss

2.5.2 Helmholtz resonator

The transmission loss of a Helmholtz resonator can be calculated using Equation (2.3) [55].

$$Transmission\ Loss\ (TL) = 10\log_{10}\left(1+\left(\frac{S}{2S_d}\frac{\left(\left({}^{S_v}/_{S}\right)\tan(kl_v)+\tan(kl_e)\right)}{\left(\left({}^{S_v}/_{S}\right)\tan(kl_e)\tan(kl_v)-1\right)}\right)^2\right) \qquad (2.3)$$

where:

S is the resonator neck cross-sectional area (m^2)

S_d is the duct cross-sectional area (m^2)

S_v is the cavity cross-sectional area (m^2)

l_v is the length of the cavity in the axial direction (m)

l_e is the effective length of the resonator neck (m)

Again the wave number is the only parameter affected by temperature and results in a frequency shift with temperature.

2.5.3 Quarter Wave Tube

The transmission loss of a quarter wave tube can be calculated using Equation (2.4) [55].

$$Transmission\ Loss\ (TL) = 10\log_{10}\left(1 + \left({}^{S}/_{2S_d}\tan(kl_e)\right)^2\right) \quad (2.4)$$

where:

S is the quarter wave tube cross-sectional area (m^2)

S_d is the duct cross-sectional area (m^2)

l_e is the effective length of the quarter wave tube (m)

Again the wave number is the only parameter affected by temperature and results in a frequency shift with temperature.

2.5.4 End Corrections

The frequencies at which reactive devices operate is driven by their effective acoustic lengths or dimensions rather than their physical lengths as explained further in Section 9.7.2. The end correction to give the effective acoustic lengths of tubes can be calculated using Equations (2.5) [55] and (2.6) [55]. In this case there is no temperature dependency for the end corrections.

$$End\ correction\ (l_0) = 0.82(1 - 1.33\xi) \quad (2.5)$$

where:

a is the radius of the contraction / pipe (m)

ξ is the ratio of contraction pipe diameter to expansion pipe diameter.

$$End\ correction\ (l_{0)} = 0.61a \tag{2.6}$$

2.5.5 Overall Effects

As shown above, the frequency based acoustic performance of the relevant acoustic devices is generally wavelength / temperature dependent. Accordingly these values can be corrected using the ratio of the speeds of sound based on a nominal exhaust temperature and the experimental test bench ambient temperature. In contrast, the transmission loss amplitudes are generally temperature independent and do not require temperature corrections.

2.6 Effects of Mean Gas Flow on Acoustic Attenuation

The experimental transmission loss test bench and the Ricardo WAVE virtual test bench both operate at zero mean flow, whereas the operating engine experiences both mean gas flow and fluctuating gas flow. The experimental transmission loss test bench operates at zero flow for practical and logistical reasons associated with the difficulty of generating approximately 3 kg/s of gas flow. For software reasons, the modelling's virtual test bench is unable to accurately maintain the pressure difference needed to generate a specific mean flow. The influence of flow differences needs to be understood so that test bench testing and WAVE modelling can be extrapolated to on-engine performance. The following are a selection of researchers who have investigated this topic.

2.6.1 Alfredson and P.O.A. L. Davies

In 1970, Alfredson and P.O.A. L Davies (ISVR) [19] noted that exhaust system mean gas flow has a significant effect on the nett energy transport within the exhaust system and that the omission of mean gas flow can lead to serious errors in predicted levels of sound radiated by the exhaust. In 1971, Alfredson and Davies [20]proposed a plus and minus mean gas flow (+M and –M, where M is the speed in Mach) term into their plane wave prediction / modelling equations. They noted that standing wave patterns can be generated by the shedding of vortices at exhaust system discontinuities. They also found that gas flow can be disruptive to acoustic performance with their linearized modelling over predicting muffler attenuation when flow was omitted. In particular, they found neglect of mean flow resulted in large scale discrepancies between theory and experiment.

2.6.2 Eriksson and Thawani

In 1985, Eriksson and Thawani [61] published a comprehensive paper on exhaust system design theory and practice. They noted that the effects of mean flow are likely to be the one of the main causes of the discrepancy between theory and measurements and defined a wave number (k) in the presence of flow called the convective wave number (k_c). This is shown in Equation (2.7) for flow in the direction of sound propagation and in the opposite direction.

$$k_c = \frac{k}{1 \pm M^2} \tag{2.7}$$

For low gas flow such as Mach 0.1, the wave number correction factor is only ± 1 % and is accordingly insignificant. At high flows such as Mach 0.4 it is significant at + 19 % and – 14%. With respect to straight through resonators with perforated pipe, they found that mean flow affects the perforate impedance term, causes dissipative losses in perforates, and changes particle velocities through the perforates. They noted that increased flow velocity through the exhaust system may actually result in an increased sound level due to aerodynamic noise generation as the high velocity flow passes various edges and perforations in the muffler. Additionally they commented that there was a possibility that the frequency of flow generated noise may coincide with internal acoustic resonances of the muffler

2.6.3 Green and Smith

In 1988, Green and Smith [62] reported on theoretical and experimental work conducted on the gas flow and the exhaust noise of heavy vehicle exhaust systems. They noted that while steady mean flow as in laboratory test facilities can cause acoustic resonances which then dominate the output spectra, on-engine the flow is not steady and these resonances are therefore not expected to develop in engine operation. In addition they proposed an empirical relationship for predicting flow generated noise as shown in Equation (2.8).

$$\boldsymbol{E_w = L_w - 10log_{10}P_{at} + 17.5log_{10}(T + 273) - 20log_{10}D - 45log_{10}U + 26.9} \tag{2.8}$$

where

E_w is noise generation efficiency (dB)

L_w is emitted sound power (dB re 10^{-12} W)

T is gas temperature (ºC)

D is internal pipe diameter (m)

U is gas flow velocity (m/s)

P_{at} is atmospheric pressure (mm Mercury)

2.6.4 Abom and Boden

In an analysis of errors in the two microphone method in ducts with flow, Abom and Boden in 1988 [46] noted the following flow related possible sources of error with respect to flow:

1. most techniques assume zero attenuation between microphones, whereas with flow the attenuation is unknown and non-zero
2. pressure fluctuations – acoustic and turbulent
3. the optimum microphone spacing range must be corrected to account for the mean flow.

2.6.5 M.E. Davies and Johnson

In 1990, M. E. Davies (Ricardo) and Johnson [64] commented on the effects of flow and advised that further flow corrections may be necessary to account for jet effects and flow / acoustic interactions within the system. One effect of the jet is to distort the directionality of the wave propagation due to the shear layer between the jet and the stationary flow. Another effect is that most energy flows straight through thus reducing the attenuation efficiency.

2.6.6 Beranek and Ver

In their 1992 book on noise and vibration [60], Beranek and Ver included a chapter on silencer / muffler acoustics. They showed that for a large dissipative muffler (1.5 metres long, 610 mm in diameter with 150 mm thick absorption material) that the attenuation varied with mean flow speed and the relative direction of the mean gas flow and the sound propagation as shown in Figure 2.8. They noted that for dissipative silencers, flow:

1. affects the effective propagation speed of sound
2. creates a velocity gradient near passage boundaries that causes refraction of sound towards (same direction) or away from the lining (opposite directions)
3. increases the effective flow resistance of baffle.

For reactive silencers, they noted that:

1. the convective wave number can be calculated using Equation (2.7) shown previously.
2. mean grazing flow has a strong effect on the impedance of the resonator throat

3. the attenuation of an expansion chamber is not significantly degraded by mean flow when the mean flow is less than 0.1 Mach.

They also advised against the use of undamped quarter wave tubes in high mean flow environments due to possible conversion of steady-flow energy into acoustical energy by aerodynamic interaction between the flow and the resonator.

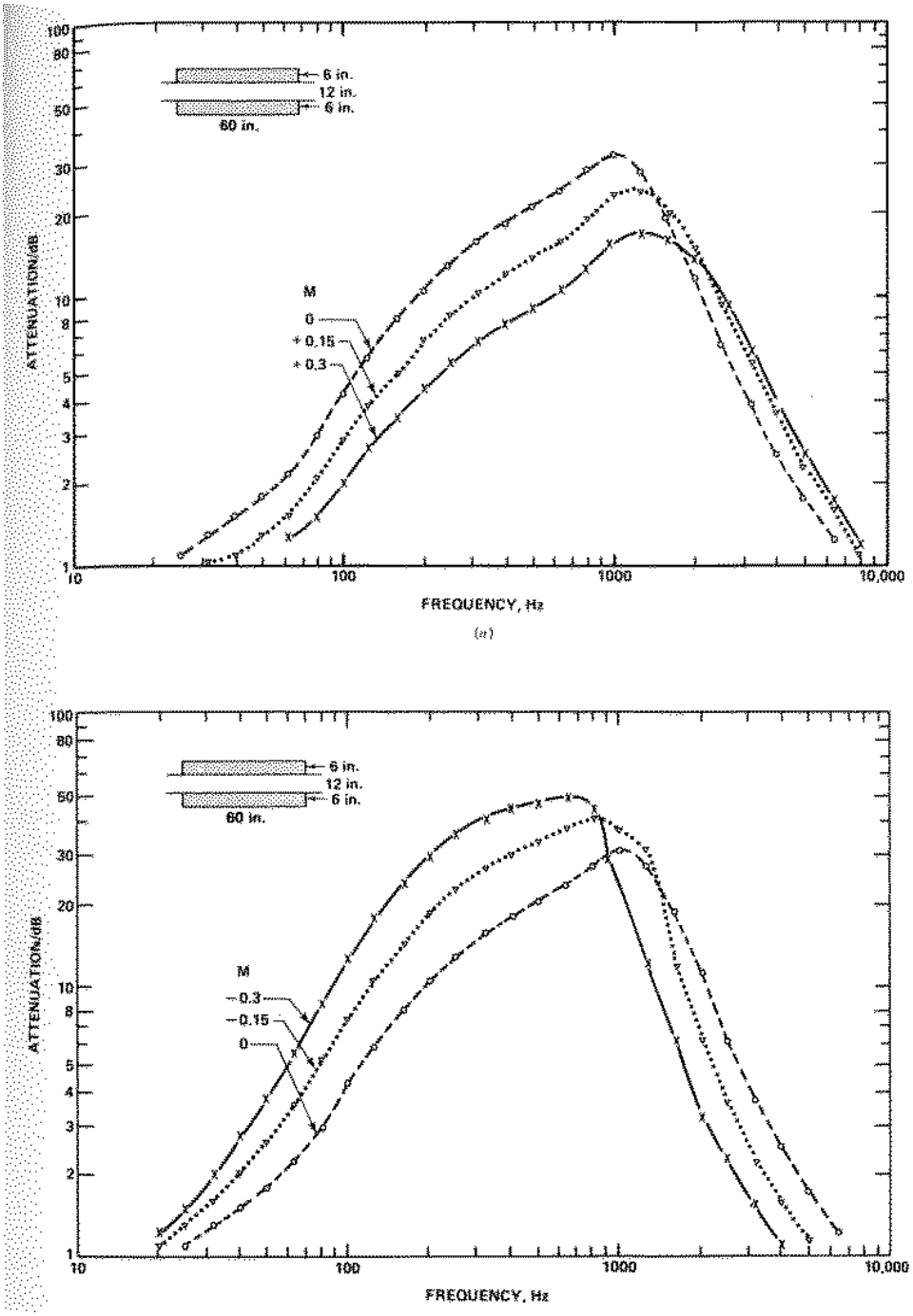

Figure 2.8 Effect of flow speed and direction on sound attenuation [60]
(a) flow and sound propagation in same direction
(b) flow and sound propagation in opposite directions

2.6.7 Crocker and P.O.A.L Davies

In 1998, Crocker [65] edited a handbook on acoustics which included a chapter on silencer / muffler acoustics by Davies (ISVR). They noted that there are significant effects arising from the presence of a mean flow including corrections to the axial wave number based on the speed of the mean flow and the relative direction of the sound propagation. In essence, the wavelength is stretched relative to that in the free field for waves travelling in the direction of flow and contracted for those travelling in the reverse direction, due to the convection by the mean flow.

2.6.8 Allam and Boden

In 2005, Allam & Boden [66] presented a paper addressing duct acoustic two-port data in the presence of flow. They noted that flow noise can cause contamination of the measured pressure signals with the flow noise masking the acoustic signals. To overcome the potentially poor signal to noise ratio and the difficulty of designing an anechoic termination that is effective at low frequencies, they proposed:

1. Using the two source method
2. locating excitation speakers on a side branch with 50% porosity perforations
3. signal processing techniques to reduce adverse effects of flow noise at microphones.

2.6.9 Bies and Hansen

Bies & Hansen noted in 2009 [55]:

1. that for a short narrow duct the effective length / end correction depends upon the mean flow and the relative direction of the mean flow and the sound propagation
2. acoustic resistance is affected by mean flow
3. for quarter wave tubes and Helmholtz resonators, the effective length / end correction factor is affected by the mean grazing flow
4. an increase in mean duct flow reduces side branch resonator acoustic performance because the resistive part of the impedance usually increases
5. mean flow can decrease the cut-on frequency for either upstream or downstream propagation
6. other researchers had reported decrease in insertion loss from 30 dB to 10 dB for flow speeds above 40m/s due to increased damping caused by the flow
7. other researchers had reported a 20% increase in resonance frequency in presence of 70 m/s flow.

2.6.10 Munjal

M. L. Munjal in 2013 [32] and 2014 [34] commented on the effects of mean flow on muffler acoustic performance. He commented that while the forward wave moves faster (c_0 + M) and the reflected wave moves slower (c_0 - M) due to convective effect of mean flow, this can be neglected in the whole of muffler analysis as a first approximation. For a more thorough analysis however the dissipative effect of the mean flow at the area discontinuities and perforates, because of the flow separation, plays a crucial role in the muffler performance and must be incorporated appropriately. The convective wave number can be calculated using Equation (2.7) shown previously. Mean flow increases attenuation at higher frequencies and decreases it at lower frequencies. Mean flow affects downstream convective, sideways diffraction, and the absorption properties of materials by scattering through vortices and other non-linear effects. The amount of flow generated noise can set an insertion loss noise floor which limits muffler acoustic performance.

2.6.11 Howard and Craig

In a study of quarter wave tube orifice geometries, Howard and Craig in 2013 [67] commented that the acoustic performance of silencing elements decreases with an increase in gas flow above a Mach 0.1 threshold. Apart from possible whistling, the effects of grazing flow are to change the reactive and resistive components of the resonator neck's impedance. These impedance changes will cause the resonant frequencies to increase or decrease depending upon the effects of the increasing flow on each impedance term.

2.6.12 Howard and Cazzolato

In 2015 Howard & Cazzolato [63] commented on the acoustic performance of quarter wave tubes in the presence of grazing flow. They strongly recommended further investigation with respect to end corrections for a variety of tube interface geometries and grazing flows. Additionally they noted that mean flow can result in aero-acoustic phenomena, vortex shedding and excitation of quarter wave tubes and Helmholtz resonators.

2.6.13 Large Marine Muffler

To put the preceding flow speed comments into context, the mean gas flow rates for a simple large twin expansion chamber muffler (Muffler LM4, Figure 4.7) were calculated for a gas temperature of 430 °C and a mass flow rate of 3.1 kg/s - Table 2-1. The mean gas flow in the muffler body is well under the Mach 0.1 threshold whereas the flow in the ducts and interconnecting tube is slightly above this threshold.

Table 2-1 Flow Rates for Simple Large Two Chamber Muffler (LM4)

Muffler LM4	Diameter (mm)	Mean Flow Rate (m/s)	Mean Flow Rate (Mach)
Inlet / Outlet Duct	340	68	0.13
Muffler Body	820	12	0.02
Interconnecting Tube	300	87	0.16

2.6.14 Overall Effects

Mean flows of less than Mach 0.1 are expected to have minimal effects on acoustic attenuation. Notwithstanding this, the presence of mean gas flow in an intake or exhaust system results in:

1. flow generated noise
2. a change to the effective speed of sound due to a Doppler effect which depends upon the direction and speed of the gas flow
3. changes to end corrections / effective acoustic lengths
4. changes to wave propagation damping
5. aero-acoustic interactions including excitation of acoustic modes
6. higher losses through perforates and absorptive material
7. an inability to design and use of an effective anechoic termination
8. flow noise masking acoustic performance / degrading signal to noise ratio.

Chapter 3 One Dimensional (1D) Modelling - Overview

This chapter gives an overview of the CFD method and software used in this study for modelling and simulating the acoustic and flow characteristics and also addresses the likely effect of finite amplitude waves.

3.1 Ricardo WAVE Software

Ricardo WAVE software can model general and complex compressible flow fluid networks in terms of finite volume elements, which include constant area or tapered pipes/ducts, junctions of multiple ducts, orifices, and termination points such as infinite plenums (ambients), anechoic boundaries and special machinery elements such as engine cylinders, piston compressors, turbochargers and supercharger (compressors and turbines), and pumps [12]. These elements can be attached to the pipe networks to serve as sources or absorbers of pulsating flows [12]. The flow of gas within elements is assumed to be non-linear, one-dimensional, inviscid, compressible, and unsteady and the governing equations are conservation of mass, momentum, and energy [68]. According to Ricardo [68], the basic methodology incorporated in WAVE has been extensively tested against a set of reference cases, including:

1. shock wave propagation in a duct
2. pressure wave reflection from closed and open ends of a duct
3. steady-state flow through a duct with an abrupt change of cross sectional area
4. flow through an orifice
5. pipe flow with friction
6. pipe flow with heat transfer
7. flow through junctions of three ducts.

DST group has a licence for the Ricardo one-dimensional (1D) engine and gas dynamics simulation software suite WAVE . This software is used by DST for the prediction and optimisation of diesel generator performance under submarine operating conditions. Figure 3.1 shows a typical WAVE model of a turbocharged six cylinder diesel engine [12]. The models consist of the individual elements that make up the engine and exhaust system. These elements are connected at nodes to represent the flow of intake and exhaust gases. Simulations are conducted by the code solver that performs all the calculations needed to simulate the engine operation.

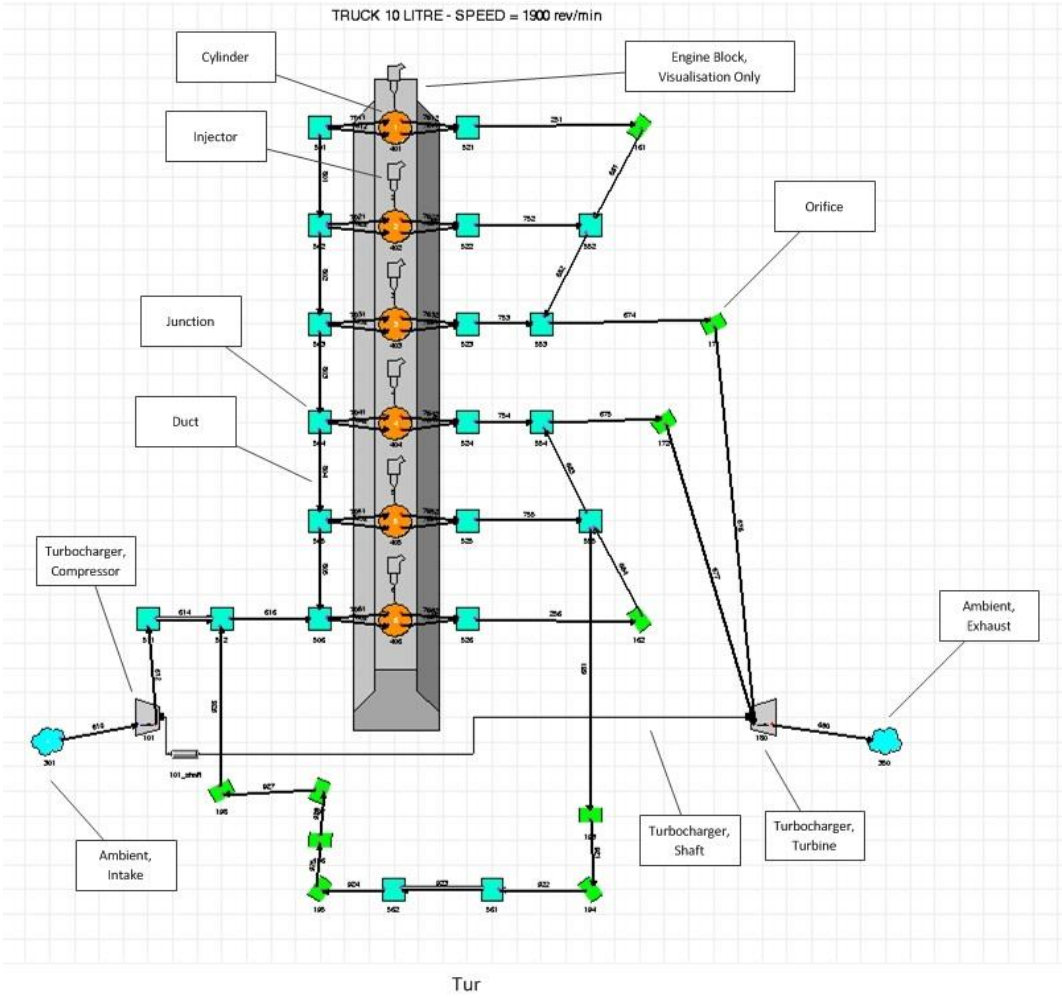

Figure 3.1 Schematic of Six Cylinder Diesel Engine WAVE Model, after [12]

3.2 Modelling Methodology

The software models gas flow systems by breaking down the physical layout into 1D elements.

Figure 3.2 shows a simple 1D model with three elements to represent an expansion chamber muffler. These elements are further subdivided by WAVE into 1D sub-volumes to give the required physical and frequency resolution as shown in

Figure 3.3 where a half wave is subdivided into seven discrete steps. In the direction of sound propagation / flow the Ricardo guidelines [68] are to divide the highest frequency wavelength of interest into six to ten sub-elements. The 1D elements have longitudinal dimensions that are at least ten times the transverse dimensions and are used with the assumption that there are no lateral modes. Using 1D elements instead of three-dimensional

(3D) elements markedly reduces the element complexity and number of elements which in turn greatly reduces solution run times. WAVE can model more complex systems by meshing with multiple 1D elements (see

Figure 3.4) to give a quasi-3D model. Note that these multiple 1D elements are only connected in the longitudinal direction and not connected in the transverse direction as 3D elements would be. Ricardo's WaveBuild3D is a model creation module designed to import geometry from CAD files and create acoustic quality meshes consisting of multiple 1D elements.

As lateral modes within a 1D duct are not considered, the effective frequency range and mesh size must take into account the duct's characteristic lateral mode frequency [27, 69]. While plane waves of any frequency can propagate relatively attenuated, the cut-on / cut-off frequency is the effective upper frequency limit for a plain duct or element due to the effects of the first lateral mode. The cut-on frequency (for the lateral mode) refers to the frequency at which the lateral mode starts propagating. The cut-off frequency (for a duct) is again the frequency at which the lateral mode starts propagating. Accordingly the terms cut-on and cut-off frequencies are effectively equivalent for the purposes of plane wave 1D propagation. For a 300 mm diameter circular duct at 430 °C, this is approximately 1 kHz and is effectively equivalent to a half wavelength across the corrected diameter [70].

Figure 3.2 Three Duct / Element Model [68]

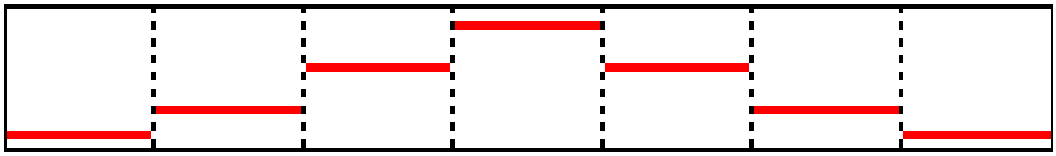

Figure 3.3 Subdivision of 1D Duct to Improve Frequency and Spatial Accuracy [68]

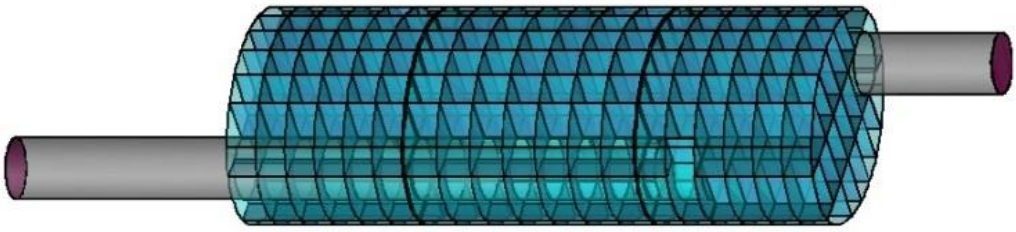

Figure 3.4 Complex Meshed (1D) Model [68]

3.3 Governing Equations

The duct is one dimensional as shown in the "Fluid Control Volume" in Figure 3.5 in that the gas flow parameters (pressure, density, particle velocity and area) vary only in the longitudinal direction and with time.

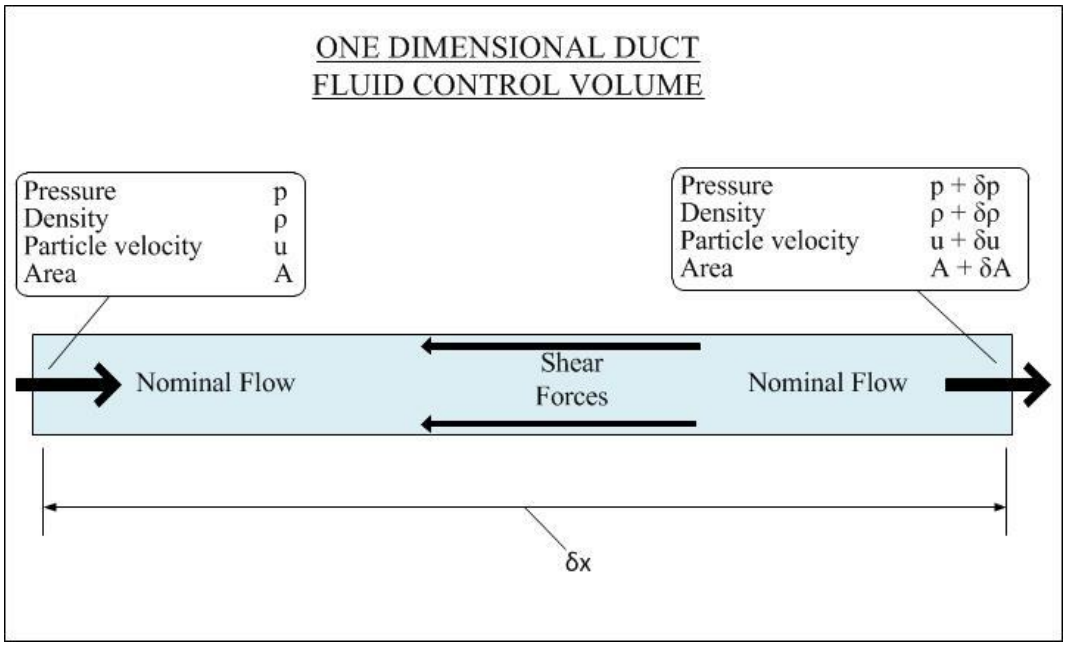

Figure 3.5 One Dimensional (1D) Duct Fluid Control Volume, after [71, 72]

The details of the flow as calculated in the flow network are obtained as a solution of quasi-one dimensional compressible flow equations and are then written in a finite difference form for each of these volumes. The governing equations are conservation of mass, momentum, and energy as defined in Figure 3.6. A staggered mesh system is used, with equations of mass and energy solved for each volume and the momentum equation solved for each boundary between volumes as shown in Figure 3.6. The solution of the governing equations is obtained by the application of a finite difference technique, utilizing the finite-volume approach, to the discretization of the partial differential equations. The time-differencing is based on the explicit technique, with the Courant condition determining the time step [12, 68].

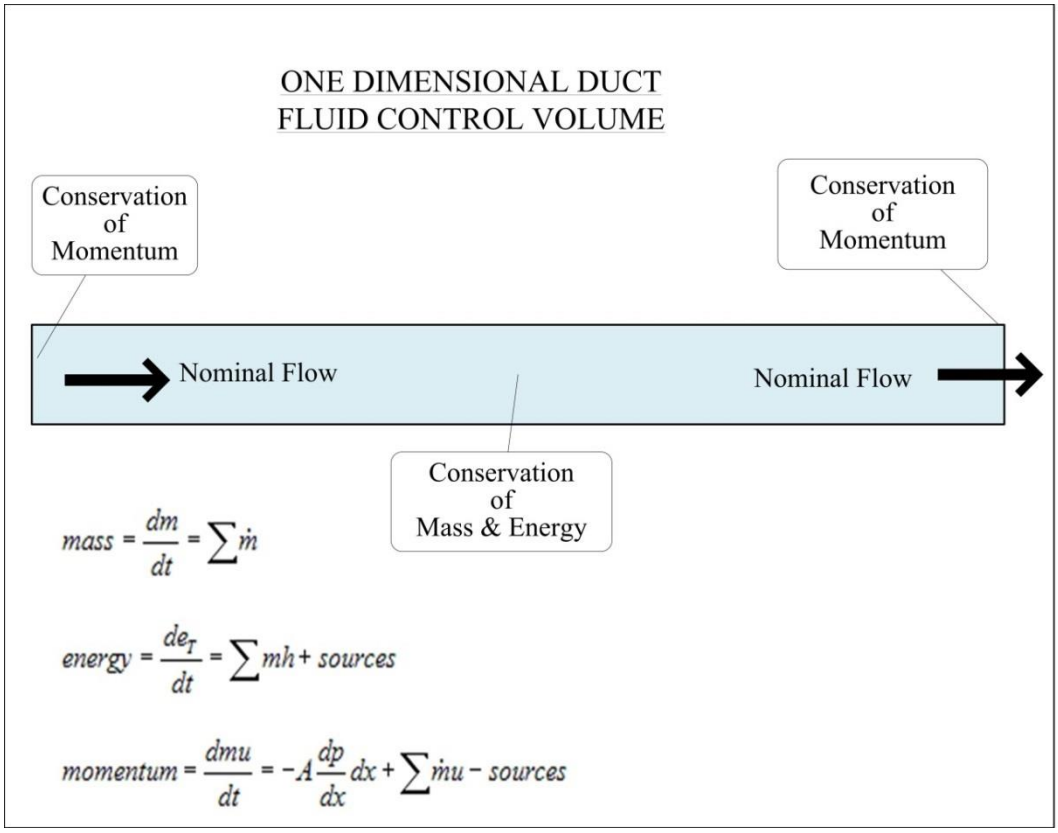

Figure 3.6 1D Duct Conservation of Mass, Energy & Momentum, after [12, 68]

3.4 Finite Amplitude Considerations

The high amplitudes of the pressure fluctuations in the exhaust system give rise to finite amplitude pressure waves in addition to linear acoustic waves. The primary difference is that the waveforms of the finite amplitude pressure waves continually change as they propagate away from the source as shown in Figure 3.7. This is because the higher pressure components of the dynamic wave affect the density of the propagation medium resulting in a change in the speed of sound. So different pressure amplitudes propagate at different speeds and this leads to a steepening of the pressure waveform and the formation of a shock wave. The shock wave formation time and distance can be derived from Equations (3.1) and (3.2) respectively [19].

$$\boldsymbol{T(seconds)} = \frac{\boldsymbol{p_0}}{(\boldsymbol{5 \times f \times \Delta p})} \tag{3.1}$$

$$\boldsymbol{Distance\ (metres)} = \boldsymbol{T\ (c \pm v_0)} \tag{3.2}$$

where:

p_0 is the ambient pressure (Pascals)

f is the wave frequency (Hz)

Δp is the amplitude of the pressure wave (Pascals)

c is the mean speed of sound (m/s)

v_0 is the mean velocity of the gas flow (m/s).

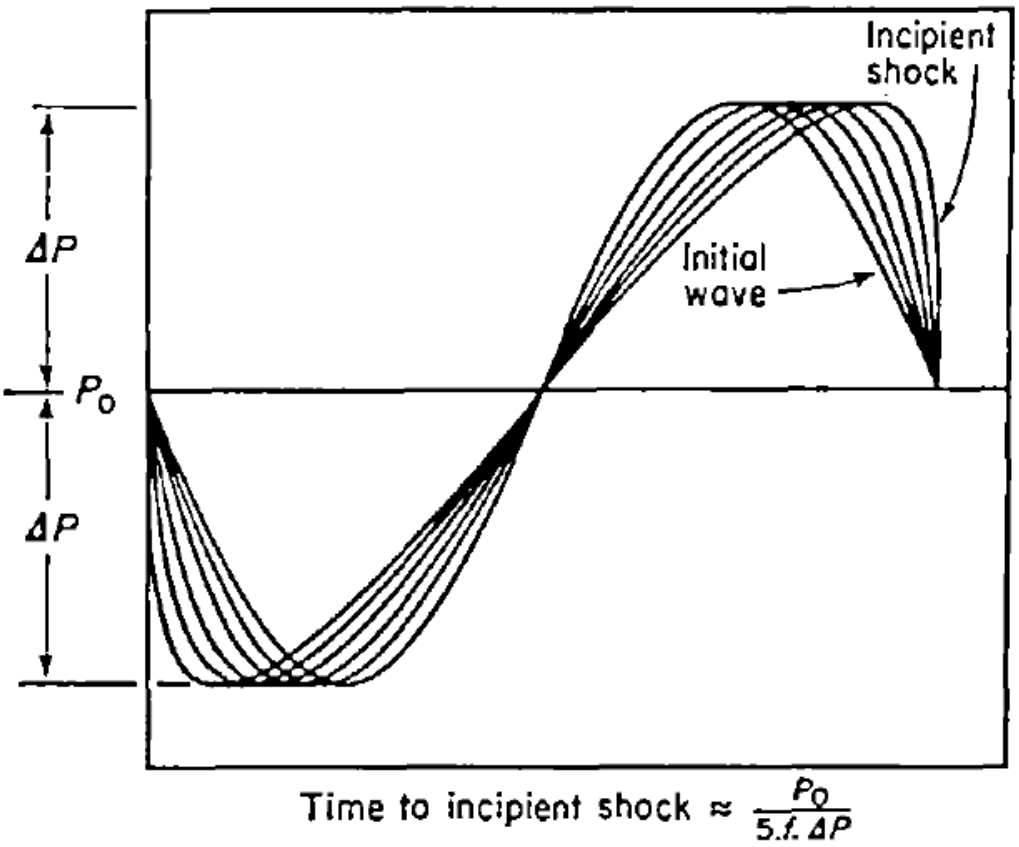

Figure 3.7 Variation of Sinusoidal Wave with Time / Propagation [19]

The importance of this is that it introduces nonlinear effects into the wave propagation and may invalidate linear theory and modelling. The actual speed of propagation is the speed of sound in the medium ± the local gas flow mean velocity. To assess the impact of this, the actual amplitudes in the exhaust systems, in the experimental test bench and in the WAVE modelling are relevant. The typical values of the maximum sound pressure levels in exhaust systems are 155 dB re 20µPa at 300 Hz and 135 dB re 20µPa at 100 Hz [34]. The input sound pressure level in the experimental test bench was set at 120 dB re 20µPa and this is accordingly used in the corresponding WAVE modelling.

Figure 3.8 and Table 3-1 show the distances to shock wave formation at a typical engine exhaust temperature (430 ºC) with a typical gas flow rate (50 m/s). Even at 155 dB re 20µPa, the distances (61 metres at 100 Hz and 6.1 metres at 1000 Hz) are generally much larger than typical exhaust systems and can be discounted even though a submarine exhaust could be 30 metres long.

Table 3-2 and Figure 3.9 show the distances to shock wave formation for the test bench at 25 ºC with zero flow. At 120 dB re 20µPa, the distances are larger than the test bench and muffler and can be discounted, namely 44 metres at 100 Hz and 4.4 metres at 1000 Hz

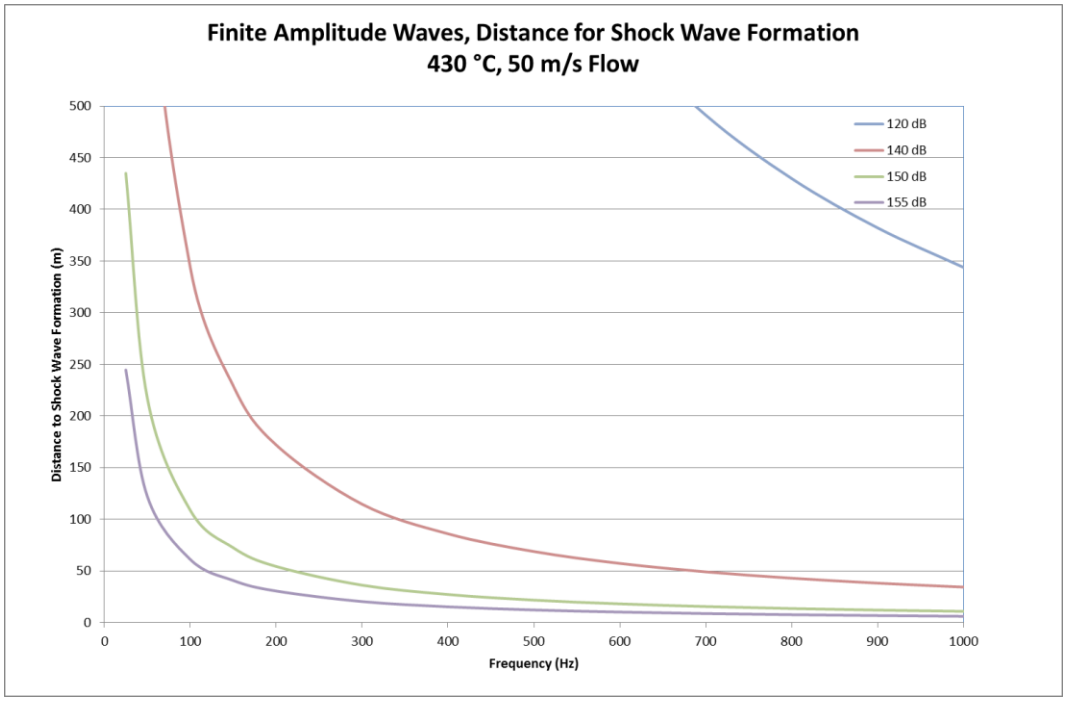

Figure 3.8 Finite Amplitude Waves, Shock Wave Formation Distance, 430 °C, 50 m/s Flow, for 120 dB, 140 dB, 150 dB and 155 dB re 20µPa

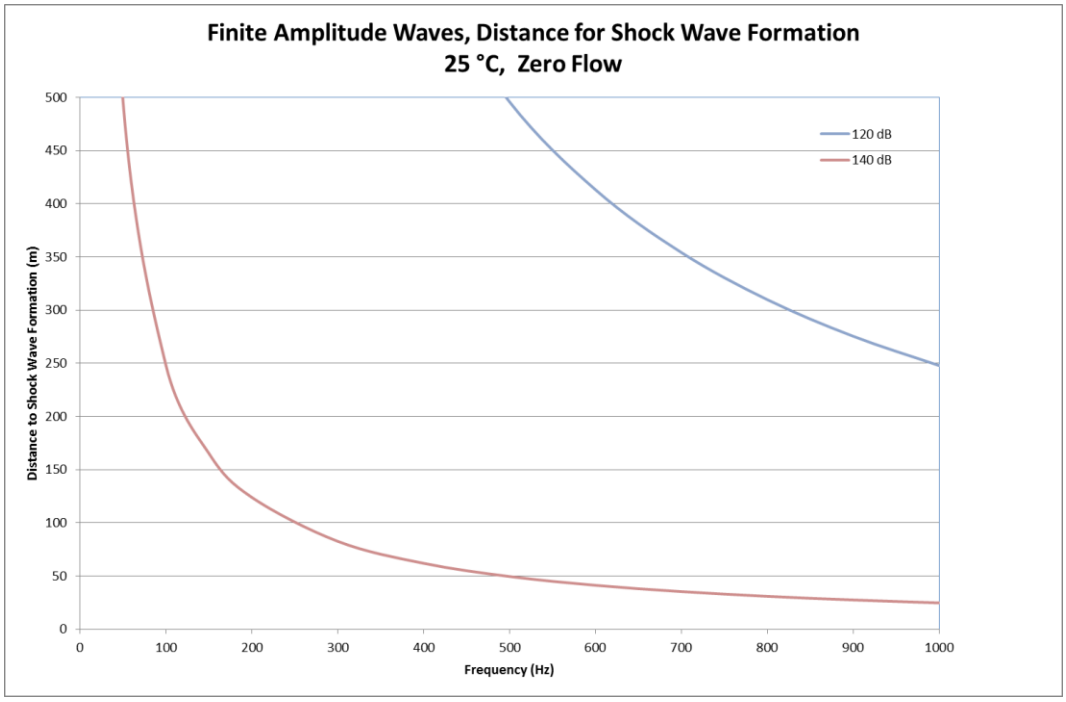

Figure 3.9 Finite Amplitude Waves, Shock Wave Formation Distance, 25 °C, Zero Flow, for 120 dB and 140 dB re 20µPa

Table 3-1 Finite amplitude shock wave, Formation distances (metres), 430 °C, 50 m/s Flow

Sound Pressure Level (dB re 20µPa)	Frequency (Hz)										
	100	150	200	300	400	500	600	700	800	900	1000
120	3439	2293	1720	1146	860	688	573	491	430	382	344
140	344	229	172	115	86	69	57	49	43	38	34
150	109	73	54	36	27	22	18	16	14	12	11
155	61	41	31	20	15	12	10	8.7	7.6	6.8	6.1

Table 3-2 Finite Amplitude Shock Wave, Formation Distances (metres), 25 °C, Zero Flow

Sound Pressure Level (dB re 20µPa)	Frequency (Hz)										
	100	150	200	300	400	500	600	700	800	900	1000
120	2479	1653	1240	826	620	496	413	354	310	275	248
140	248	165	124	83	62	50	41	35	31	28	25
150	78	52	39	26	20	16	13	11	10	9	8
155	44	29	22	15	11	8.8	7.3	6.3	5.5	4.9	4.4

3.5 Meshing

The WaveBuild3D meshing strategy for a complex shape / volume is to construct an overall volume consisting of internal volumes / cavities, planar elements and tube sections. The meshing elements consist of ducts, simple Y-junctions, complex Y-junctions, perforates, openings, ambients, external connectors, orifices and mass-less ducts. The sequence of meshing is that:

1. tubes are individually meshed,
2. cavities are individually meshed,
3. all open and internal tube ends are connected to cavities and
4. all perforates are meshed (including openings and planar items which join together adjacent cavities and tubes).

The meshing is in three dimensions dx, dy, and dz with the direction convention shown in Figure 3.10.

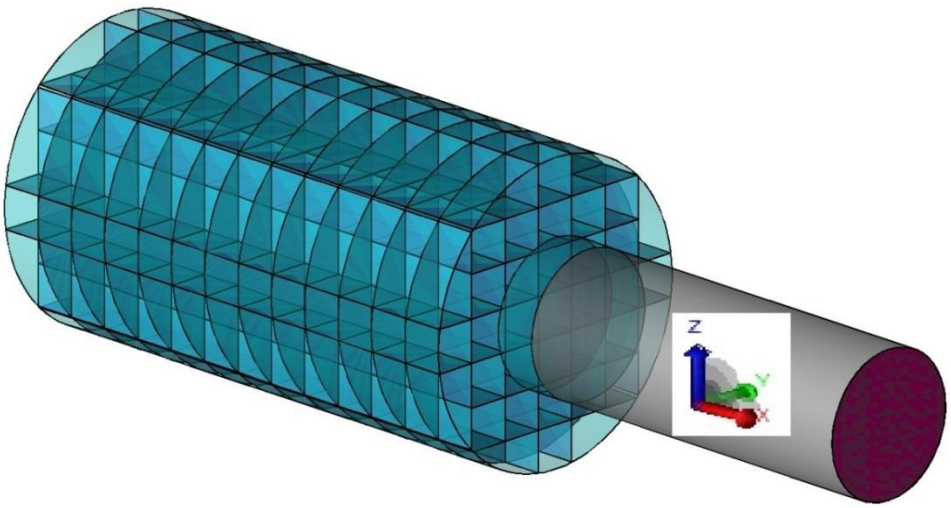

Figure 3.10 Discretisation Axes X, Y & Z

3.6 Acoustic Modelling

WAVE has numerous tools and capabilities to perform acoustic characterisation and noise simulations of full engines, partial models, and individual components such as an exhaust muffler. Ricardo claims that good correlation with experimental data is typically achieved for complex automotive exhaust systems up to 1000 Hz and for simple automotive concentric tube mufflers up to 4000 Hz [68]. Note that as WAVE is incapable of predicting flow variations due to turbulence, it cannot directly calculate flow noise. Instead WAVE optionally uses an empirical flow noise correlation [62] to add flow noise to the WAVE predictions.

For the testing and simulation of individual components and subsystems, WAVE includes an acoustic piston / speaker and an anechoic termination to construct a virtual test bench (see Figure 3.11) which is capable of determining the transmission loss and / or acoustic level difference of a component between two locations. Unfortunately WAVE's anechoic termination does not fix an ambient pressure so the acoustic virtual transmission loss test bench cannot be used in conjunction with flow. The benefit of running partial and component models is greatly reduced running times. For example, a full engine model may take four hours to run but a virtual test bench run of a meshed large muffler would take ten minutes. Engine source characteristics can be extracted from full engine models for later use in partial systems.

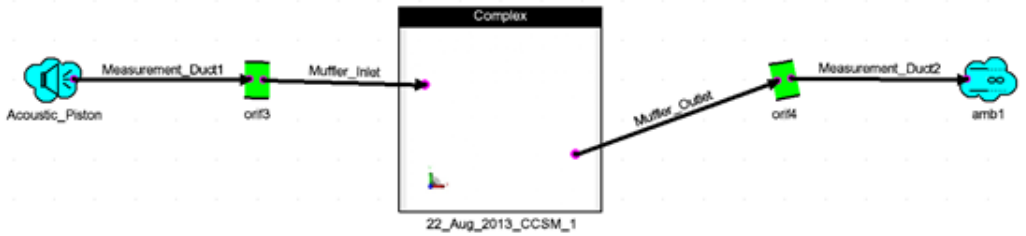

Figure 3.11 Schematic of WAVE Acoustic Virtual Test Bench

The acoustic transmission loss is calculated using a computer analogue of the Chung-Blaser [26, 27] experimental technique. Transmission loss is the difference in sound power level between the incident wave entering, and the transmitted wave exiting the component. This measurement / calculation requires two pressure transducers on either side of the silencer as shown in Figure 3.12 in order to measure the incident and transmitted acoustic power flows.

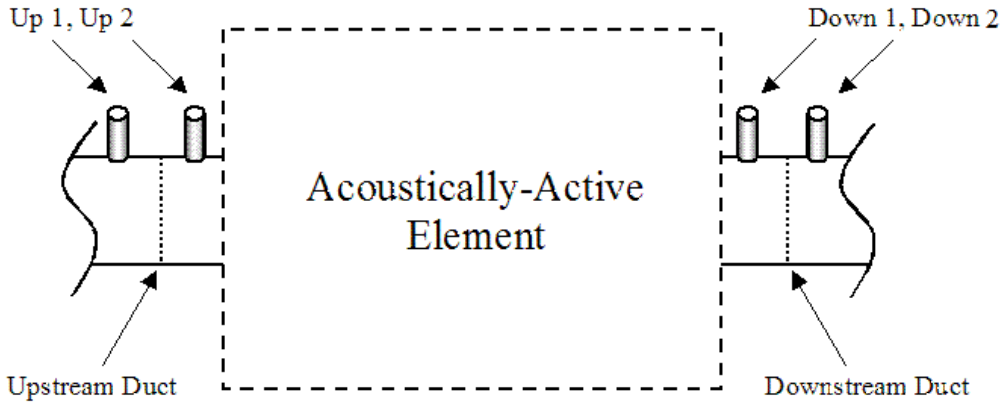

Figure 3.12 General Arrangement of Chung-Blaser Four Microphone Method [68]

A post processor Ricardo's WavePost provides acoustic-specific post-processing capabilities, including noise radiation models and acoustic processing and analysis tools. For example, resonances and standing waves can be identified using run speed sweeps and spatial animations.

3.7 Flow Modelling

WAVE also has the capability to perform gas flow analysis of full engines, partial models, and components. The flow coefficients for elements are either assigned manually or automatically generated by WAVE. Note that the gas flow performance is influenced by geometric details of the components such as the inlet and outlet edge shapes. In complex flow regimes, a more detailed solid model with a mesh finer than that used for acoustic modelling may be needed. A 1D mesh or a coupled 1D and 3D CFD approach may be needed.

For the flow testing of partial systems and components, WAVE can be used to construct a virtual test bench (see Figure 3.13) to determine the gas flow rate through the component due to a specific pressure difference.

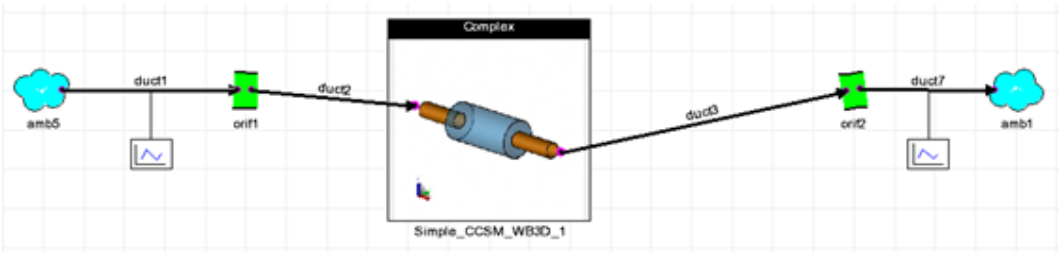

Figure 3.13 Schematic of WAVE Flow Virtual Test Bench

Chapter 4 Flow Modelling (1D) Methodology

This chapter explains the flow modelling approach, the validation data, the WAVE modelling methodology and quantifies the subject simplified large mufflers (LM) and large marine muffler (LMM).

4.1 Overview

4.1.1 Measure of Flow Performance

The normal measures of the flow performance of a component are the flow rate through and the coefficient of flow (C_f) or coefficient of discharge (C_d) for a specific pressure difference across the component. Both coefficients express the actual measured flow as a fraction of the theoretical flow and are useful measures of flow efficiency. The two coefficients are generally interchangeable and identical provided the theoretical flow areas are identical. An example of where they differ is the case of a poppet valve in a cylinder head where different flow areas are used. These measures of performance can be obtained from a WAVE flow virtual test bench or full engine model. This report will be confined to flow rates on a virtual test bench at a constant pressure difference.

Using a test bench approach allows development independent of the engine and/or complete exhaust system. Additionally the simulation run times are greatly reduced. The virtual test bench consisted of an inlet ‘ambient’ pressure, an inlet duct before the test element, the element being tested, an outlet duct after the test element, and an outlet ‘ambient’ pressure. The methodology employed was to specify a pressure difference and use the resultant gas mass flow rate as a measure of flow efficiency. The modelling / simulation provides a lot of flexibility and capability by enabling the following parameters to be specified and varied - gas temperatures, wall temperatures, heat transfer, termination type, gas type, and pressures at inlet and outlet.

4.1.2 Modelling Strategy

The modelling was conducted in order of increasing complexity in such a way that simpler models could be evaluated and validated before progressing onto more complex models as follows:

1. ten individual large mufflers with design increments from simple expansion chamber muffler to complex twin chamber muffler (Muffler LM 1 to 10) with theoretical validation, and
2. a complex large marine muffler (Muffler LMM) with limited validation from on-engine testing of similar mufflers.

4.1.3 Model Construction

The models for the test elements were constructed using a variety of approaches - Wavebuild, WaveBuild3D, and computer aided design (CAD) software depending upon the complexity of the models. The models consisted of:

1. single 1D elements
2. multiple 1D elements (meshed)
3. geometry imported from CAD files and then meshed.

The large twin expansion chamber marine muffler (Muffler LMM) shown in Figure 4.1 and Figure 4.2 was available for experimental acoustic transmission loss testing and was according selected for modelling. This muffler is two metres in length, 800 mm in diameter and weighs 450 kg. It is different dimensionally to those fitted to CCSM's but is similar enough in concept to warrant investigation.

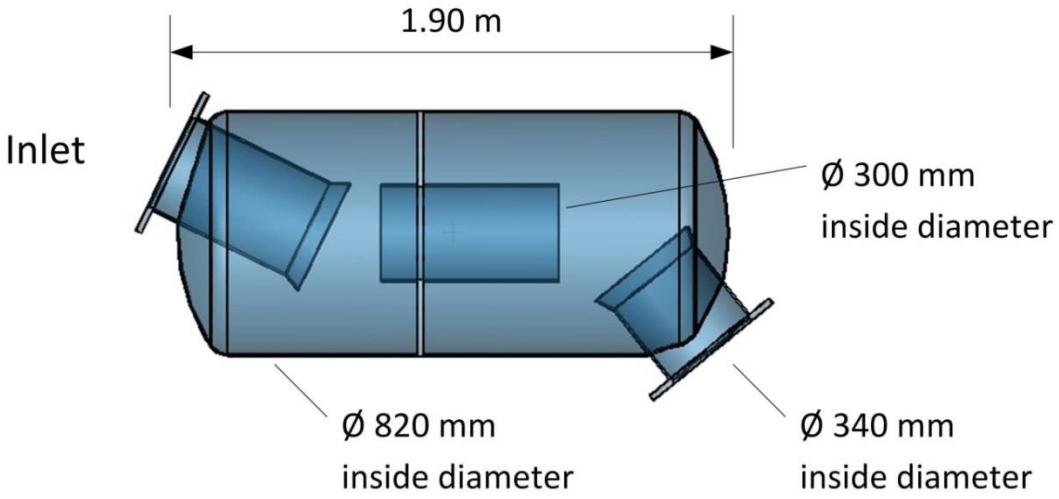

Figure 4.1 Large Marine Muffler (LMM), Cross-section

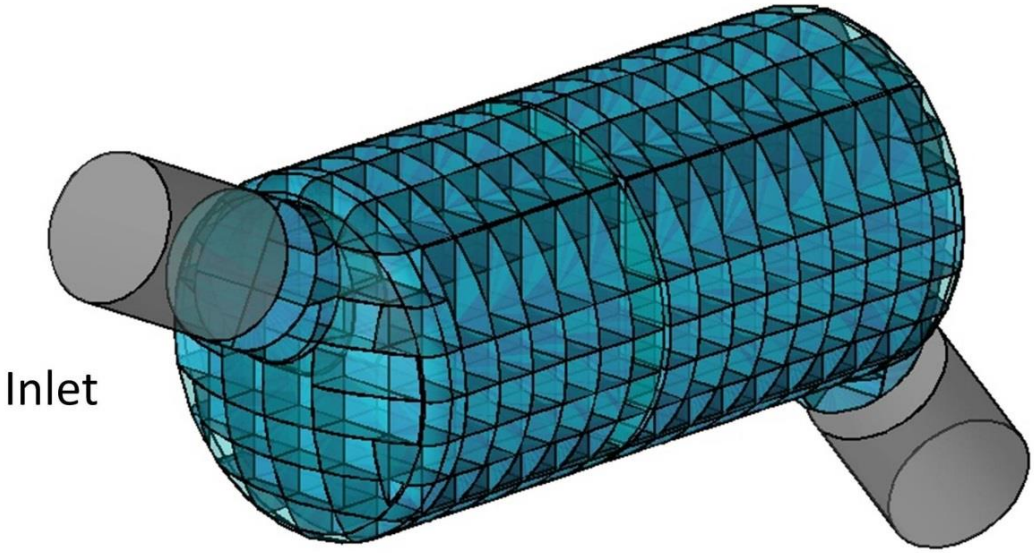

Figure 4.2 Large Marine Muffler (LMM), Meshed

Ten simplified large expansion chamber mufflers (Mufflers LM1 to LM10 inclusive) were designed to examine the effects of iterations from a large single expansion chamber (LM1) to a typical large marine muffler (LM10 and LMM). The inlet and outlet pipes are 340 mm in diameter and one metre long and with a muffler body 820 mm in diameter and 1.675 metres long. These mufflers are shown in Figure 4.3 to Figure 4.13 with the basic elements in Figure 4.3, Figure 4.5, Figure 4.6, and Figure 4.7 being repeated in Figure 4.8 to Figure 4.13 inclusive.

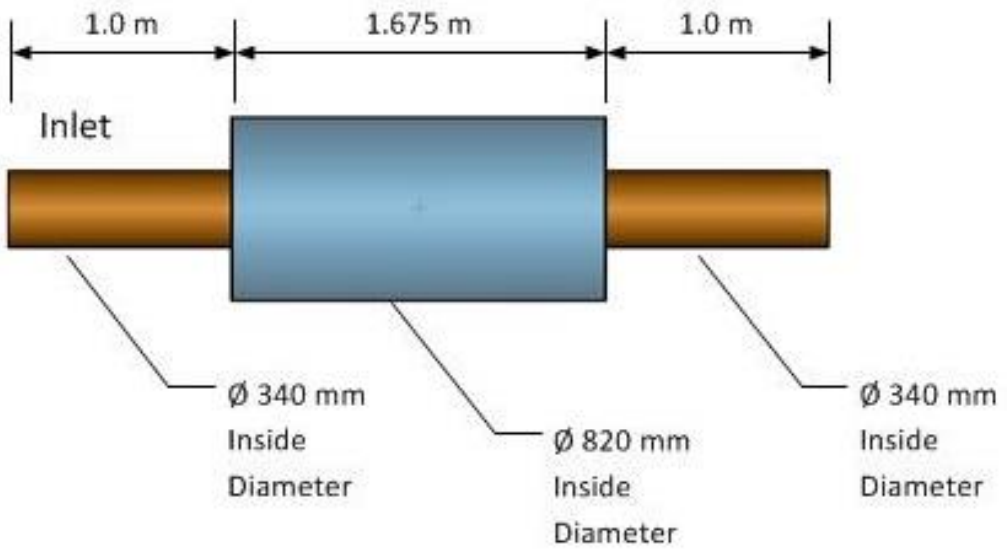

Figure 4.3 Simple Large Muffler LM1

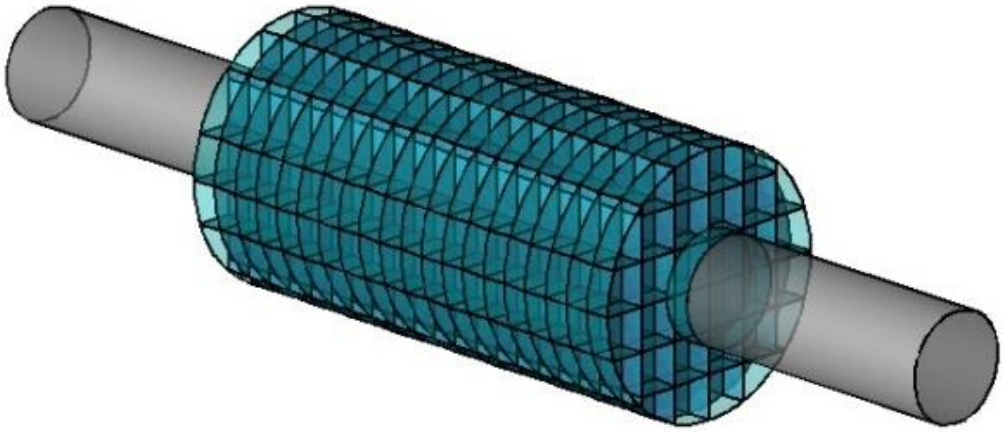

Figure 4.4 Simple Large Muffler LM1, Meshed

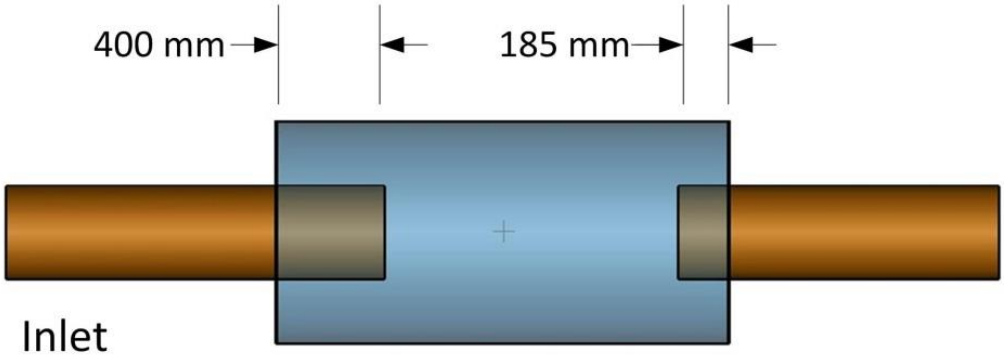

Figure 4.5 Simple Large Muffler LM2, Other Details / Dimensions as per LM1

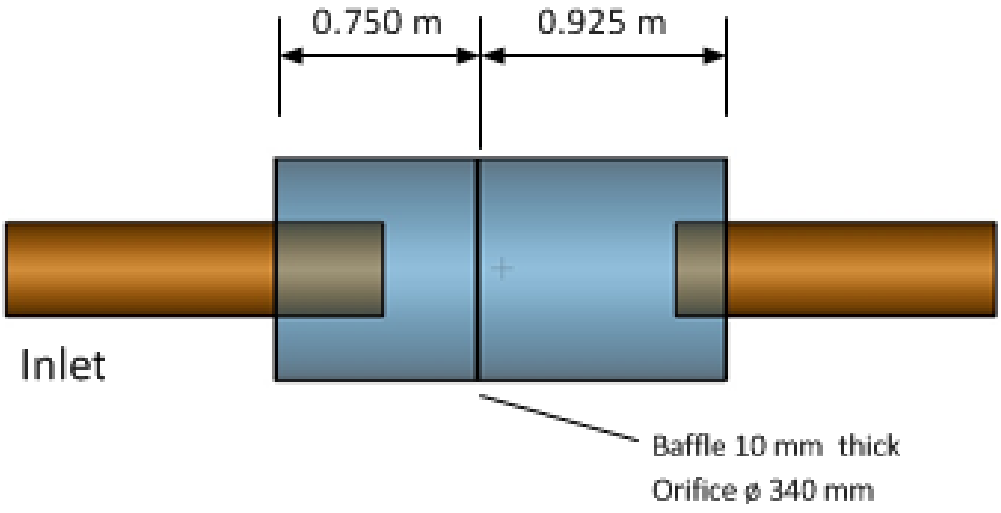

Figure 4.6 Simple Large Muffler LM3, Other Details / Dimensions as per LM2

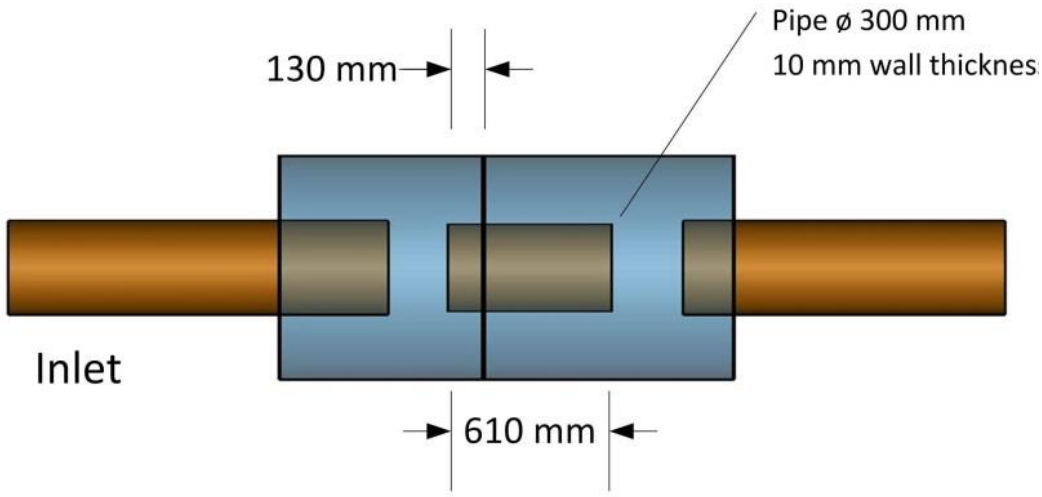

Figure 4.7 Simple Large Muffler LM4, Other Details / Dimensions as per LM3

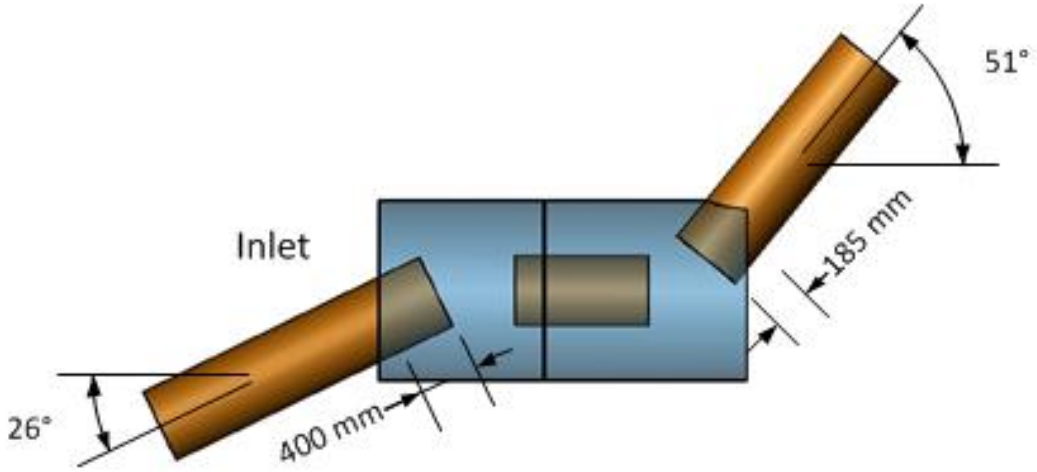

Figure 4.8 Simple Large Muffler LM5, Other Details / Dimensions as per LM4

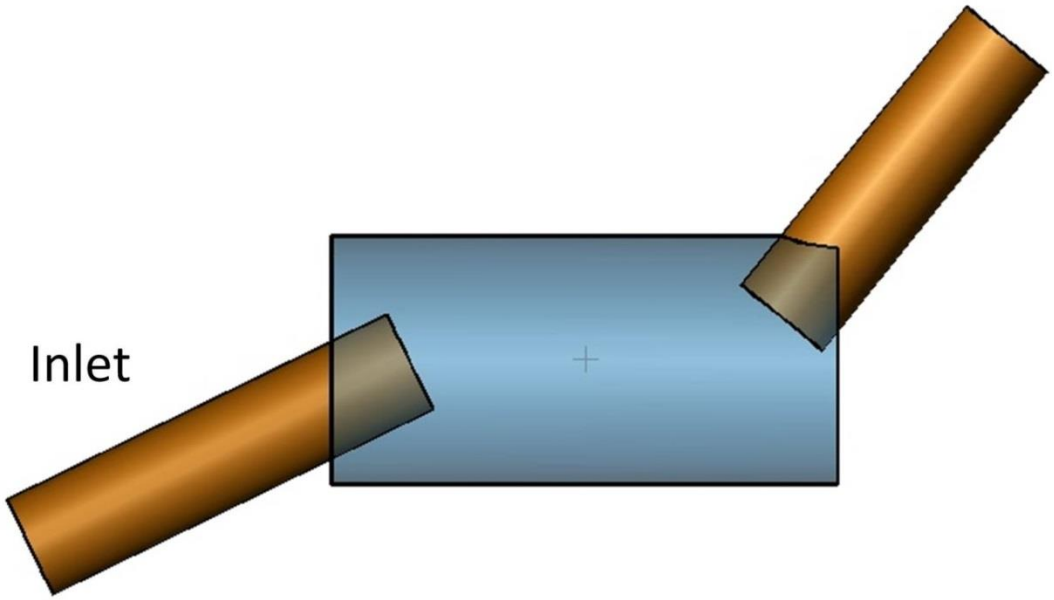

Figure 4.9 Simple Large Muffler LM6, Other Details / Dimensions as per LM5

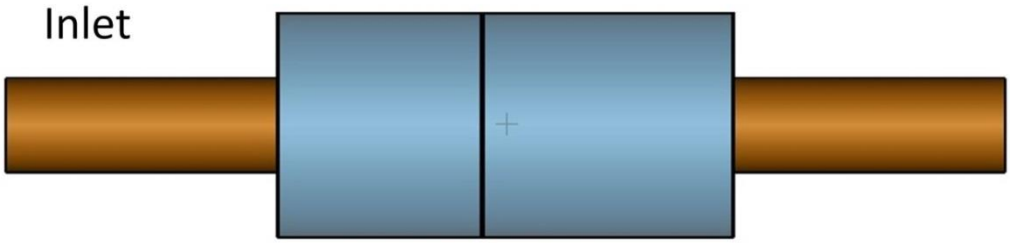

Figure 4.10 Simple Large Muffler LM7, Other Details / Dimensions as per LM3

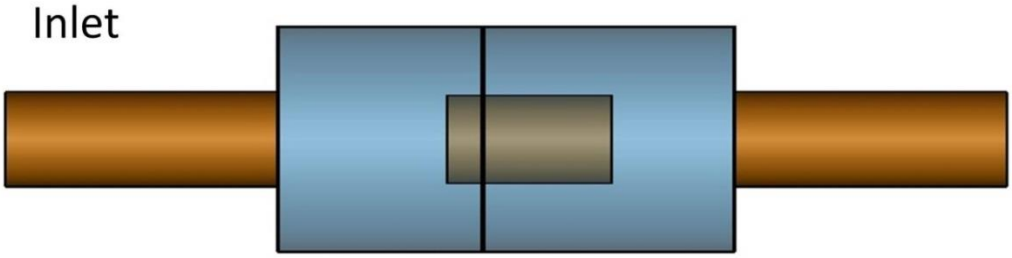

Figure 4.11 Simple Large Muffler LM8, Other Details / Dimensions as per LM4

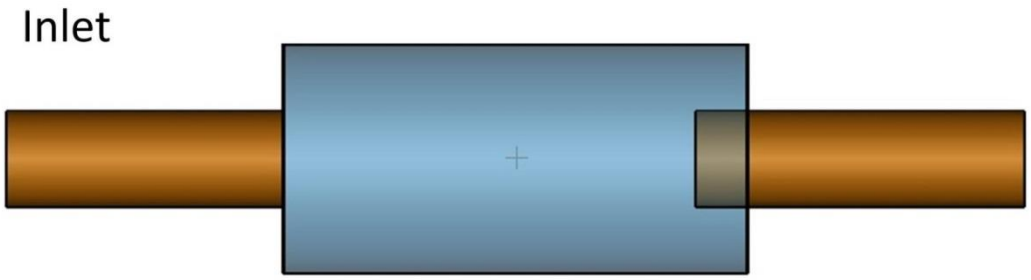

Figure 4.12 Simple Large Muffler LM9, Other Details / Dimensions as per LM2

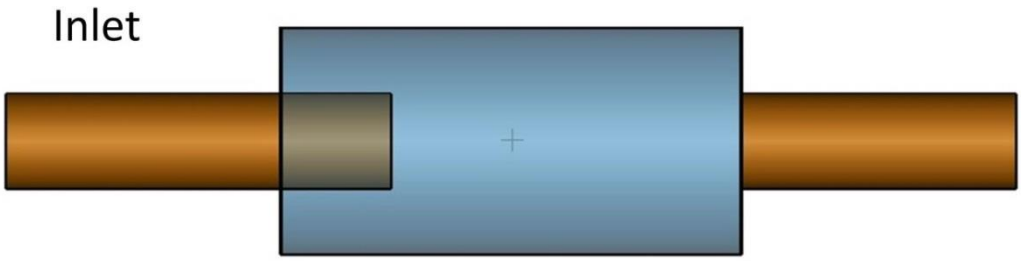

Figure 4.13 Simple Large Muffler LM10, Other Details / Dimensions as per LM2

The configuration elements of these mufflers (LM1 to LM10 and LMM) are summarised in Table 4-1.

Table 4-1 Summary of Features of Large Mufflers, LM1 to 10 and LMM

Muffler	Meshed	Extended Inlet	Centre Baffle	Interconnecting Tube	Extended Outlet	Angled inlet & Outlet
Simplified Large Expansion Chamber Mufflers (LM)						
LM1 (meshed)	Yes	No	No	No	No	No
LM1 (ducts)	No	No	No	No	No	No
LM2	Yes	Yes	No	No	Yes	No
LM3	Yes	Yes	Yes	No	Yes	No
LM4	Yes	Yes	Yes	Yes	Yes	No
LM5	Yes	Yes	Yes	Yes	Yes	Yes
LM6	Yes	Yes	No	No	Yes	Yes
LM7	Yes	No	Yes	No	No	No
LM8	Yes	No	Yes	Yes	No	No
LM9	Yes	No	No	No	Yes	No
LM10	Yes	Yes	No	No	No	No
Large Marine Muffler (LMM)						
LMM	Yes	Yes	Yes	Yes	Yes	Yes

4.2 Flow Validation data

4.2.1 Overview

There is only limited data available as the on-engine pressure drop for Muffler LMM is currently unknown. However testing with similar mufflers gives an indicative flow restriction value. The gas flow rate through the subject exhaust system was measured at various operating conditions during the New Class Submarine (Collins) project in 1990 [73]. At full load the exhaust gas mass flow rate was measured as 3.1 kg/s with an exhaust gas temperature of 430 °C.

For most of the simple construction mufflers (LM1 to LM10 inclusive) and duct systems the flow restriction can be readily calculated using the Coefficient of Discharge or the Loss Coefficient methods. Mufflers LM5 and LM6 have compound angle flows and are not readily solved using the aforementioned methods.

4.2.2 Loss Coefficient Flow Methodology

A common approach [34, 55, 74] for calculating the pressure drop due to flow in a duct or pipe system is to use the flow Loss Coefficient (*K*) for each part of the system, e.g. pipe, expansion, contraction, valve, or orifice. The coefficient is related to the dynamic head as shown in Equation (4.1) [74]. The approach is to sum the *K* values for each part of the system to give the overall pressure drop. As distinct to the discharge coefficient, a *K* of 0.0 indicates no flow restriction / zero pressure drop and the pressure drop increases as *K* increases.

$$\boldsymbol{Pressure\ drop}\ (\Delta \boldsymbol{p}) = \boldsymbol{K}\frac{\boldsymbol{1}}{\boldsymbol{2}}\boldsymbol{\rho U^2} \qquad (4.1)$$

where:

K is the Loss Coefficient

ρ is the density (kg/m^3)

U is the gas velocity (m/s).

For a pipe or duct the flow Loss Coefficient K_p is given by Equation (4.2) [32]. *K* is typically 0.05 for a mild steel circular pipe one metre long and 340 mm in diameter as typically used in the subject mufflers. *K* is 0.03 for the bodies of these mufflers - 1.675 metres long and 820 mm in diameter.

$$\boldsymbol{Loss\ Coefficient\ Pipe}\ (\boldsymbol{K_p}) = \boldsymbol{F}\frac{\boldsymbol{l_p}}{\boldsymbol{d_p}} \qquad (4.2)$$

where:

F is the Froude's friction factor (typically 0.016 for mild steel pipes)

l_p is the pipe length (m)

d_p is the pipe hydraulic diameter (m).

For a sudden expansion or extended inlet, the Loss Coefficient K_e derived by Equations (4.3) and (4.4) [32] is typically 0.69 for a sudden expansion from 340 mm to 820 mm diameter.

$$\boldsymbol{Loss\ Coefficient\ Expansion\ K_e = (1 - n)^2} \tag{4.3}$$

$$\boldsymbol{n = \left(\frac{r_u}{r_d}\right)^2} \tag{4.4}$$

where:

r_d is downstream radius (m)

r_u is the upstream radius (m).

For a sudden contraction or extended outlet, the Loss Coefficient K_e derived using Equation (4.3) is typically 0.41 for a sudden contraction from 820 mm to 340 mm diameter.

From these values for *K*, it is apparent that the majority of the pressure drop is due to geometry changes rather than pipe friction and in the majority of cases pipe friction can be ignored.

For muffler LM1 the calculated Loss Coefficients are:

Inlet pipe friction (one metre long, ϕ 340 mm)	*K*= 0.05
Sudden expansion	*K*= 0.69
Body pipe friction (1.675 metres long, ϕ 820 mm)	*K*= 0.03
Sudden contraction	*K*= 0.41
Outlet pipe friction (one metre long, ϕ 340 mm)	*K*= 0.05
Total	*K*= 1.20

The mean flow rate (*U*) in the inlet pipe is 80 m/s (from WAVE modelling) and the nominal density at 1 bar is 0.5043 kg/m^3. Note that the mean flow rate in the muffler body is reduced by the area ratio (0.415). The total Loss Coefficient is the sum of these with correction for the lower mean flow rate in the body. Using Equation (4.1) to (4.5), the total pressure drop is 2.03 kPa.

$$\textbf{\textit{Pressure drop}}\ (\Delta p) = \left(0.05 + 0.69 + 0.03 \times 0.415^2 + 0.41 + 0.05\right) \times \frac{1}{2} \times 5043 \times 80^2 \quad (4.5)$$

Similar calculations for muffler LM2 (extended inlet and outlet) give a higher pressure drop of 2.08 kPa for the same flow rate. This is due to friction in the longer inlet and outlet pipes being only partially offset by the effectively shorter body. Muffler LM8 is more complex being muffler LM1 with an internal baffle and interconnecting tube. This gave a calculated pressure drop of 3.95 kPa for the same flow rate.

The pressure drops for the same flows (80 m/s inlet velocity and 3.75 kg/s mass flow rate) using the Loss Coefficient method are summarised in Table 4-2.

Table 4-2 Summary of Calculated Flow Coefficients *K* and Pressure Drop

Muffler	Flow Coefficient *K*	Pressure Drop (kPa)	Flow % relative to LM1
LM1	1.20	2.03	100
LM2	1.23	2.08	98
LM8	2.33	3.95	52

4.3 WAVE Modelling Flow Methodology

4.3.1 Mufflers LM1 to LM10

The large expansion chamber mufflers (LM) were modelled on the virtual test bench at 700 K (≈ 430 °C) with a pressure difference (5 kPa) that was selected to give the required mass flow rate (approximately 3.1 kg/s). These models were constructed and meshed in Wavebuild3D with increasing level of complexity to examine the sensitivity of the flow performance to design changes. For comparison a simple expansion chamber (LM1) was also modelled using ducts rather than meshed.

4.3.2 Muffler LMM

The large twin chamber marine muffler LMM was correspondingly modelled on the virtual test bench at 700 K (≈ 430 °C) with a pressure difference (12.5 kPa) that gave approximately 3.1 kg/s gas flow rate. Note that muffler LMM also has flared extended inlet and outlet tubes which can be expected to reduce flow restrictions by smoothing abrupt area and directional changes.

4.3.3 Coefficient of Discharge

Where there are changes in the physical geometry of adjoining elements, the impediment to gas flow can be characterised by the flow coefficients C_f or C_d. A C_d of 1.0 has no flow restriction / zero pressure drop, whereas the pressure drop increases as the C_d decreases.

The C_d / gas flow performance is strongly influenced by the geometric details of components such as the inlet and exhaust entry shapes as shown by the six contractions in Figure 4.14 [68] and the sudden expansion in Figure 4.15 [68].

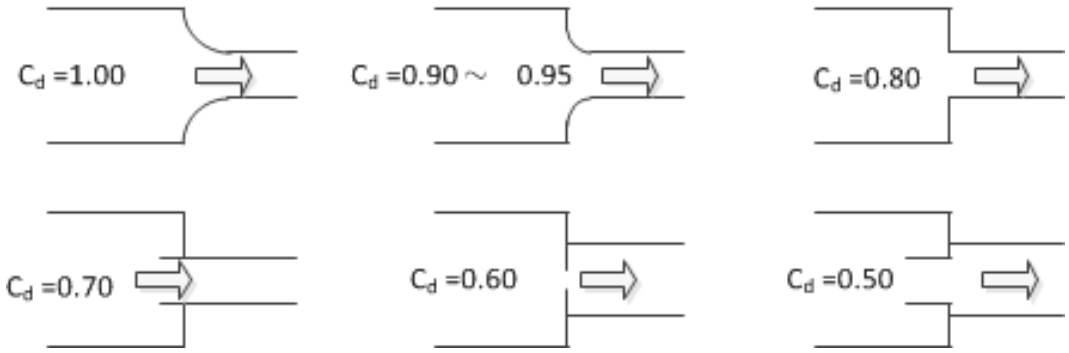

Figure 4.14 Coefficients of Flow, Various Contraction Configurations, after [68]

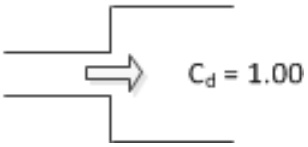

Figure 4.15 Coefficient of Flow, Sudden Expansion, after [68]

In WAVE the flow coefficients (coefficients of discharge C_d) for elements are either assigned manually if known or automatically generated based on upstream diameter, downstream diameter, and effective orifice diameter. The relationship used by WAVE [68] is shown in Equation (4.6). This gives a C_d of 0.61 for a step contraction from ø 820 mm to ø 340 and a C_d of 1.0 in the case of a sudden area increase from ø 340 mm to ø 820 mm.

$$\boldsymbol{C_d = 1 - \left[1 - \left[\frac{D}{D_1}\right]^4\right] * \left[0.2 + 0.2 * \left[1 - \left[\frac{D}{D_2}\right]^4\right]\right]} \qquad (4.6)$$

Where:

D is the orifice diameter

D_1 is the upstream diameter

D_2 is the downstream diameter.

Chapter 5 Acoustic Modelling (1D) Methodology

This chapter explains the measures of acoustic performance, the WAVE modelling methodology and parameters, the effects of lateral modes, sound pressure wave decomposition and the experimental acoustic transmission loss test bench.

5.1 Measurement of Acoustic Performance

The sound pressure level at any point in the exhaust system is the instantaneous combination of multiple forward travelling and backward travelling waves. The sound pressure level at a point as measured by a microphone or pressure transducer is accordingly dependent upon the systems both downstream and upstream of the measurement point. This has implications when measuring and characterising the acoustic performance of single elements and subsystems.

Three common ways of characterising and measuring the acoustic performance of systems or components such as a muffler are level difference (noise reduction), insertion loss (external), and transmission loss [13]. Level difference is the difference in sound pressure levels across the component of interest. Insertion loss is the sound pressure level difference at a reference point, usually outside the exhaust system, with and without the presence of the component. Both level difference and insertion loss are dependent upon the systems around the component of interest.

Transmission loss is defined as the difference in sound power level between the incident wave entering and the transmitted wave exiting the component. It is purely attributable to the component of interest and is theoretically independent of the upstream and downstream systems. For the purposes of muffler modelling and development, transmission loss is often the preferred parameter to characterise the exhaust component due to its independence from the surrounding exhaust systems and source.

Various experimental techniques can be used to evaluate the transmission loss and typically use two pressure transducers on either side of the test component to measure the upstream and downstream sound pressure levels and post processing to separate the forward and backward travelling waves – Figure 3.12. This method is based on plane wave propagation and an anechoic termination at the system exit. An effective anechoic termination is difficult to achieve in practice [13, 75, 76], though techniques have been proposed to compensate for a reflective termination [13].

5.2 Excitation / Source Characteristics

5.2.1 Input spectra

In WAVE modelling, the input "speaker" is generally used as a multi-sine or white noise source. The multi-sine source imposes a gas velocity made up of a constant term with a superimposed random-phase multi-sine term. No withstanding this, the input spectrum is flexible and can be tailored to suit the analysis with options including:

1. random noise
2. swept sine
3. white noise
4. multi-sine
5. specific engine spectra
6. targeted frequencies

5.2.2 Sound Pressure Level and Particle Velocity

As stated earlier in Section 3.4, 120 dB re 20μPa was selected as the input sound pressure level in the experimental test bench and in the corresponding WAVE modelling. The WAVE simulation uses an input particle velocity rather than a sound pressure level and this is calculated using impedance calculations for ambient air. Equation (5.1) calculates the impedance.

$$\boldsymbol{Impedance\ Z_a = {}^{p}/_{u} = \rho_0 \times c_0} \qquad (5.1)$$

Where

p is the rms sound pressure (Pa)

u is the rms particle velocity (m/s)

ρ_0 is the density of the medium (kg/m^3)

c_0 is the speed of sound (m/s).

In air at 25 °C and 1 atmosphere pressure (101.325 kPa),

ρ_0 is 1.1839 kg/m^3

Z_a is 409.4 kg/m^2.

Equation (5.2) calculates the sound pressure corresponding to the sound pressure level (p_{ref} is 20μ Pa). Note that as sound pressure level is a mean square quantity, the calculated sound pressure is correspondingly a root mean square (rms) quantity.

$$\boldsymbol{p = p_{ref} \times 10^{\frac{dB}{20}} = 2x10^{-5} \times 10^{\frac{dB}{20}}} \qquad (5.2)$$

Equation (5.3) is used to calculate the equivalent particle velocity. For 120 dB re 20μPa this is 50 mm/s and Table 5-1 summarises calculated sound pressures and particle velocities for sound pressure levels of 25 to 150 dB re 20μPa.

$$\boldsymbol{u = \frac{p}{Z_a}} \qquad (5.3)$$

Table 5-1 Calculated Sound Pressures and Particle Velocities at Standard Temperature and Pressure

Sound Pressure Level (dB re 20μPa)	**Sound Pressure (rms) *p* (Pa)**	**Particle Velocity (rms) *u* (mm/s)**
25	0.0004	0.001
50	0.006	0.015
75	0.11	0.27
90	0.63	1.53
100	2.0	4.8
110	6.3	15.3
120	20.0	48.4
120.3	20.6	50.0
125	35.6	86.1
130	63.2	153.1
150	632.5	1531.5

5.3 Frequency Range

Engine configurations ranging from 6 to 16 cylinders were analysed by the author to determine the required frequency range for the modelling and experimental test bench. Diesel generators typically run at 1500 rpm or 1800 rpm for power generation at 50 Hz or 60 Hz respectively. Using the cylinder firing rate (CFR) to give the lower limit and the fifth harmonic of the CFR to give the upper limit [68], the required frequency range was therefore 75 Hz to 1000 Hz as shown in Table 5-2 for a nominal run speed of 1500 rpm for four-stroke engines.

Table 5-2 Engine Derived Frequency Range, 1500 Rpm, Even Firing

Number of Cylinders	**6**	**8**	**12**	**16**
Cylinder Firing Crankshaft Order	3	4	6	8
Half Order (Hz) (four stroke)	12.5	12.5	12.5	12.5
Dominant Firing Frequency Hz) (Even firing engine configuration)	75	100	150	200
Fifth Harmonic Frequency (Hz)	375	500	750	1000

As the acoustic performance of devices is generally wavelength / temperature dependent, these values were then corrected using the ratio of the speeds of sound based on a nominal exhaust temperature (430 °C) to give ambient temperature (25 °C) equivalent frequencies of 50 Hz to 655 Hz. This gave a target range of 30 Hz to 700 Hz for the room temperature test facility.

5.4 Lateral Frequencies

As the two microphone method assumes plane wave propagation, the first lateral mode cut-on frequency in the measurement duct sets an upper limit for testing. The lateral cut-on frequency can be calculated using Equation (5.4) [70] and for circular cross sections is effectively equivalent to a half wavelength across the corrected diameter.

$$f_c = 1.8412 * c/(2 * \pi * r) \quad (5.4)$$

Where:

r is the duct radius

c is the speed of sound.

Using Equation (5.4), the lateral cut-on frequencies for a 330 mm diameter duct and a 820 mm diameter muffler body / duct are 614 Hz and 247 Hz respectively at 25 °C. At 430 °C, the equivalent duct and muffler body cut-on frequencies are 941 Hz and 379 Hz respectively. Note that the duct cut-on frequency at 614 Hz is inside the target frequency range at 25 °C as is the cut-on frequency of 914 Hz in the on-engine installation at 430 °C. In addition to the effect of the cut-on frequencies on the wave decomposition in the measurement ducts, they also indicate the presence of lateral modes in the exhaust system. Table 5-3 summarises the cut-on frequencies for a range of exhaust components and diameters at 25 °C and 430 °C for which the corresponding speeds of sound are 346 and 530 m/s respectively. From this analysis we can see that lateral modes are an important influence in large scale components but much less so for automotive components

Table 5-3 Lateral Mode Frequencies, Exhaust System Components

Typical device	Pipe diameter (m)	Cut–on Frequency (Hz) at 430° C and 530 m/s	Cut-on Frequency (Hz) at 25° C and 346 m/s
Automotive Exhaust Piping	0.05	6212	4056
Automotive Exhaust Piping	0.075	4142	2704
Automotive Muffler	0.1	3106	2028
Automotive Muffler	0.2	1553	1014
TL Bench Measurement Ducts	0.33	941	614
Marine Exhaust Piping	0.34	914	596
Marine Muffler Body	0.82	379	247
Marine Muffler Body	1	311	203

5.5 Discretization

The frequency and spatial resolution is determined by the selected discretization size (dx) which should be between 1/6th and 1/10th of the wavelength of the highest frequency of interest. Table 5-4 summarises the recommended dx values for the two microphone spacings and the two temperatures.

Table 5-4 Meshing Parameters – dx Discretization Size Resulting From Upper Limit Frequency Based On Microphone Spacing

Temperature (°C)	Microphone Spacing (mm)	Upper frequency (Hz)	Lambda (m)	dx (mm) for 6 elements per wavelength	dx (mm) for 10 elements per wavelength
25	500	275	1.258	210	126
25	200	690	0.501	84	50
430	500	425	1.247	208	125
430	200	1060	0.500	83	50

5.6 Microphone Spacing

The relative spacing of each microphone in the microphone pairs is critical in that it affects the effective frequency range and resultant measurement accuracy. There has been considerable work in this area and the following guidelines [47] were used to ensure accuracy. These are graphically represented in Figure 5.1 for an air temperature of 25 °C. The optimum microphone spacing is achieved when $ks = \pi/2$, and the effective range is achieved at $0.1\pi < ks < .8\pi$ where k is the wave number ($k = 2\pi f/c$ or $k = 2\pi/\lambda$), f is the frequency and s is the microphone spacing. In addition to the accuracy requirements, the wave decomposition is indeterminate when the microphone spacing is half a wavelength ($\lambda/2$).

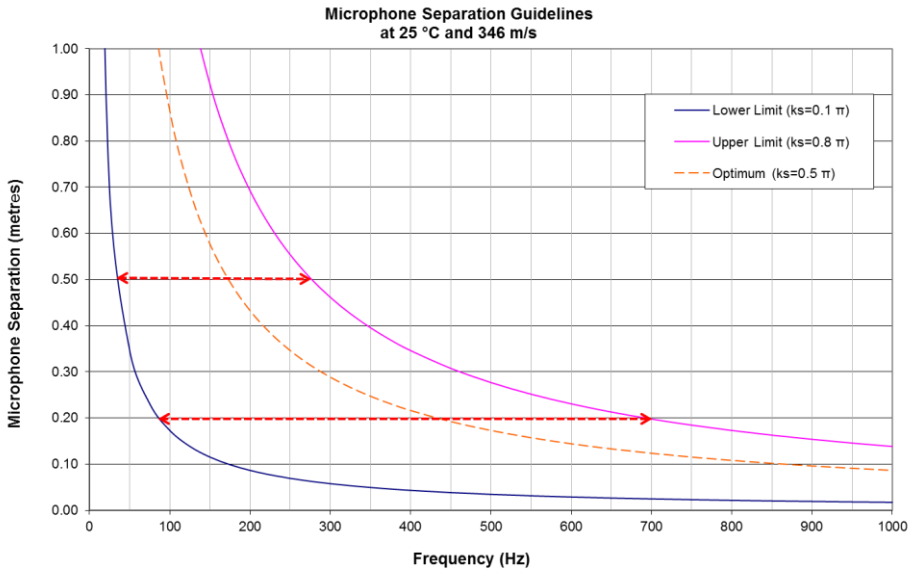

Figure 5.1 Microphone Spacing Guidelines, 25 °C, after [47]

It can be seen from Figure 5.1 that the two spacings (200 mm and 500 mm) cover the required frequency range of 35 Hz to 690 Hz at 25 °. At 430 °C, these two spacings cover the frequency range of 55 Hz to 1060 Hz. These frequency limits and the λ/2 indeterminacy frequency for both spacings and both temperatures are summarised in Table 5-5.

Table 5-5 Summary of Microphone Spacing Guidelines

Temp (°C)	Speed of Sound (m/s)	Spacing (mm)	Lower Limit (Hz)	Optimum (Hz)	Upper Limit (Hz)	Frequency (Hz) for λ/2
25	346	500	35	175	275	345
25	346	200	85	430	690	865
430	530	500	55	265	425	530
430	530	200	132	660	1060	1325

5.7 Wave Decomposition

As stated earlier, the sound pressure level at any point in the exhaust system is an instantaneous combination of multiple forward travelling and backward travelling waves. This is shown schematically in Figure 5.2 where S_{AA} and p_i and S_{BB} and p_r are the incident and reflected auto (power) spectra and sound pressures respectively.

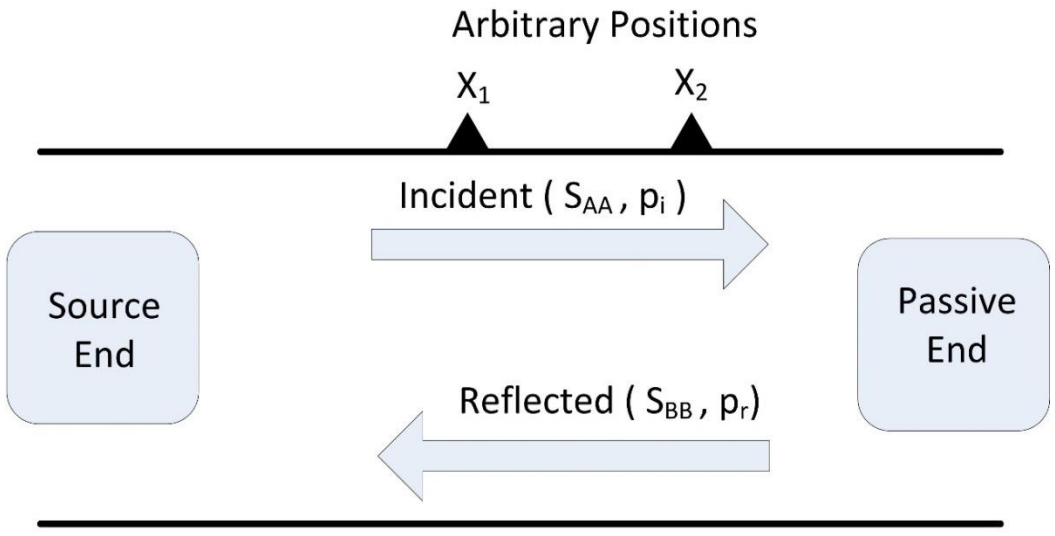

Figure 5.2 Wave Decomposition in Duct

Both Chung-Blaser [26, 27] and Seybert-Ross-Tao [13, 29, 30] have developed experimental techniques which can resolve the complex acoustic fields as measured at specific points into the required forward and backward travelling waves. From the forward and backwards travelling waves, the incident acoustic power and transmitted acoustic power and the transmission loss can be calculated. The two techniques are essentially identical with the Chung-Blaser method being able to be derived from the Seybert-Ross-Tao method [11, 29]. The wave decomposition is achieved using Equations (5.5) to (5.9) inclusive [13, 29].

Incident wave spectra (S_{AA})

$$\boldsymbol{S_{AA} = [S_{11} + S_{22} - 2C_{12}\cos\ k(x_1 - x_2) + 2Q_{12}\sin k(x_1 - x_2)]/4\sin^2 k(x_1 - x_2)} \quad (5.5)$$

Reflected wave spectra S_{BB}

$$\boldsymbol{S_{BB} = [S_{11} + S_{22} - 2C_{12}\cos k(x_1 - x_2) - 2Q_{12}\sin k(x_1 - x_2)]/4\sin^2 k(x_1 - x_2)} \quad (5.6)$$

Amplitude (rms) of the incident wave sound (p_i)

$$\boldsymbol{p_i = \sqrt{S_{AA}}} \quad (5.7)$$

Amplitude (rms) of the reflected wave sound pressure (p_r)

$$\boldsymbol{p_r = \sqrt{S_{BB}}} \quad (5.8)$$

The transmission loss calculation is calculated using Equation (5.9):

$$\boldsymbol{Transmission\ Loss\ = 20\log_{10}(p_i/p_t) + 10\log_{10}(S_i/S_0)} \quad (5.9)$$

The effectiveness of the anechoic termination (power reflection coefficient) is calculated using Equation (5.10) [29]:

$$\boldsymbol{\alpha_0(f) = S_{BB}(f)/S_{AA}(f)} \quad (5.10)$$

where:

$S_{AA}(f)$ is the incident wave auto (power) spectrum

$S_{BB}(f)$ is the reflected wave auto (power) spectrum

$S_{11}(f)$ is the pressure auto (power) spectrum at (arbitrary) point x_1

$S_{22}(f)$ is the pressure auto (power) spectrum at (arbitrary) point x_2

$C_{12}(f)$ is the real part of the pressure cross (power) spectrum between points x_1 and x_2

$Q_{12}(f)$ is the imaginary part of the pressure cross (power) spectrum between points x_1 and x_2

x_1 is the distance to an arbitrary point from a reference position (m)

x_2 is the distance to an arbitrary point from a reference position (m)

(x_1-x_2) is the microphone spacing (m)

p_i is the rms amplitude of the incident wave sound pressure (Pa)

p_r is the rms amplitude of the reflected wave sound pressure (Pa)

p_t is the rms amplitude of the transmitted wave sound pressure (incident wave sound pressure after the test item (Pa)

S_i is the area of the area of the inlet tube area (m^2)

S_o is the area of the area of the outlet tube area (m^2)

$\alpha_0(f)$ is the power reflection coefficient.

5.8 Acoustic Transmission Loss Bench

The experimental and the WAVE virtual test bench consisted of a speaker for excitation, a measurement duct with two microphones before the test element, the element being tested, a measurements duct with two microphones after the test element, and an anechoic termination. The transmission loss bench is shown schematically in Figure 5.3 and uses wave decomposition before and after the item of interest to calculate the incident (p_i) and the transmitted (p_t) sound pressures. From these pressures the incident and transmitted sound pressures and the sound transmission loss are calculated. The transmission loss was calculated by WAVE using the Chung-Blaser [26, 27] experimental technique. The experimental transmission loss bench uses the Seybert-Tao [13] techniques and data processing and is covered in more detail in Section 9.6.

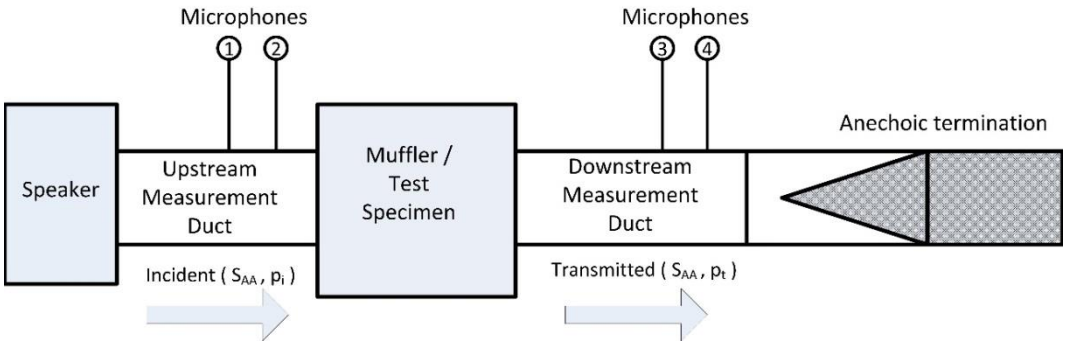

Figure 5.3 Transmission Loss Bench Schematic

Chapter 6 Numerical Experiments – Flow Modelling

This chapter covers the flow modelling of the simplified large mufflers (LM) and large marine muffler (LMM). It presents the flow results and provides comparisons by grouping into logical groups to illustrate the effects of design iterations.

6.1 Virtual Test Bench

The WAVE flow simulation software was used as a virtual test bench with nominal exhaust gas temperatures of 700 K (≈ 430 °C). The pressure difference across the test mufflers was selected to give a nominal mass flow rate of 3.1 kg/s. The discretisation sizes were chosen to give the finest mesh possible within the constraints of the software. Table 6-1 summarises the modelling parameters. Note that WAVE automatically applies a C_d of 0.80 to the upstream ambient to inlet pipe interface thus reducing the effective pressure difference across the test element.

Table 6-1 WAVE Flow Modelling Parameters

Parameters	WAVE Flow Modelling
Speed of Sound	530 m/s
Temperature	700 K (≈ 430 ºC)
Pressure Difference, LM Mufflers	5 kPa
Pressure Difference, LMM Muffler	12.5 kPa
Pressure downstream	1.0 bar
Cut-on Frequency for Ducting (ø 340 mm)	915 Hz
Cut-on Frequency for Muffler Body (ø 820 mm)	380 Hz
Measurement Type	Mass flow

6.2 Simplified Large Expansion Chamber Mufflers

The flow rate of simplified large expansion chamber mufflers (LM) were simulated in WAVE at 5 kPa overall pressure difference and the results are summarised in Table 6-2 and Figure 6.1. These large expansion chamber mufflers (Mufflers LM1 to LM10 inclusive) were designed to evaluate the effects of geometry variations.

Table 6-2 Flow Results Summary, Large Mufflers (LM1 to LM10)

Test Mufflers	Mass Flow (kg/s)	Mass Flow % relative to LM1
LM1	3.67	100
LM1 (ducts)	3.57	97
LM2	4.03	110
LM3	3.30	90
LM4	3.22	88
LM5	2.61	71
LM6	3.25	89
LM7	3.29	90
LM8	3.23	88
LM9	4.03	110
LM10	4.00	109

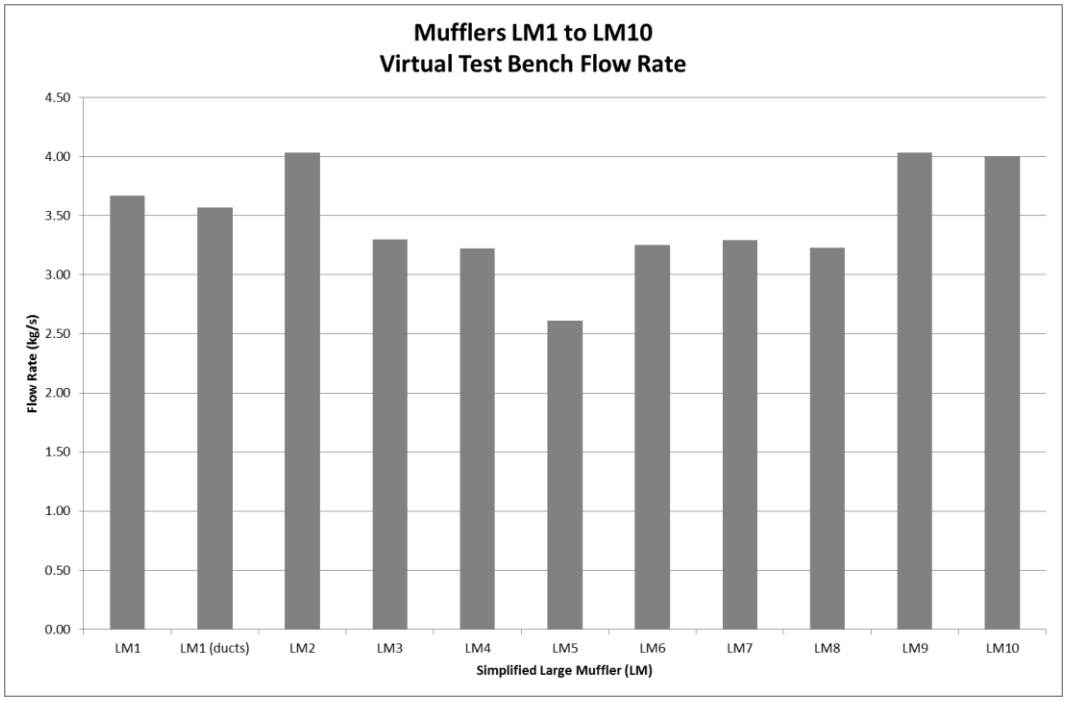

Figure 6.1 Flow Results Summary, Large Mufflers (LM1 to LM10)

These results show a high sensitivity to design variations. To simplify the results and to show the effects of successive iterations, the ten mufflers were divided into four subsets:

6.2.1 LM1 (meshed) versus LM1 (ducts)

This compares a single large expansion comprised of three cylindrical ducts (Figure 4.3) versus the same geometry meshed (Figure 4.4) into multiple 1D elements (one cavity, two tubes, 642 Y-junctions, 1754 ducts). The difference is minimal with the flow rates being 3.57 and 3.67 kg/s for the three duct muffler and the meshed muffler respectively.

6.2.2 LM1 to LM5

This progression is from a simple single expansion chamber (LM1) to a twin expansion chamber with interconnecting tube, angled extended inlet, and angled extended outlet (LM5) with the results summarised in Figure 6.2.

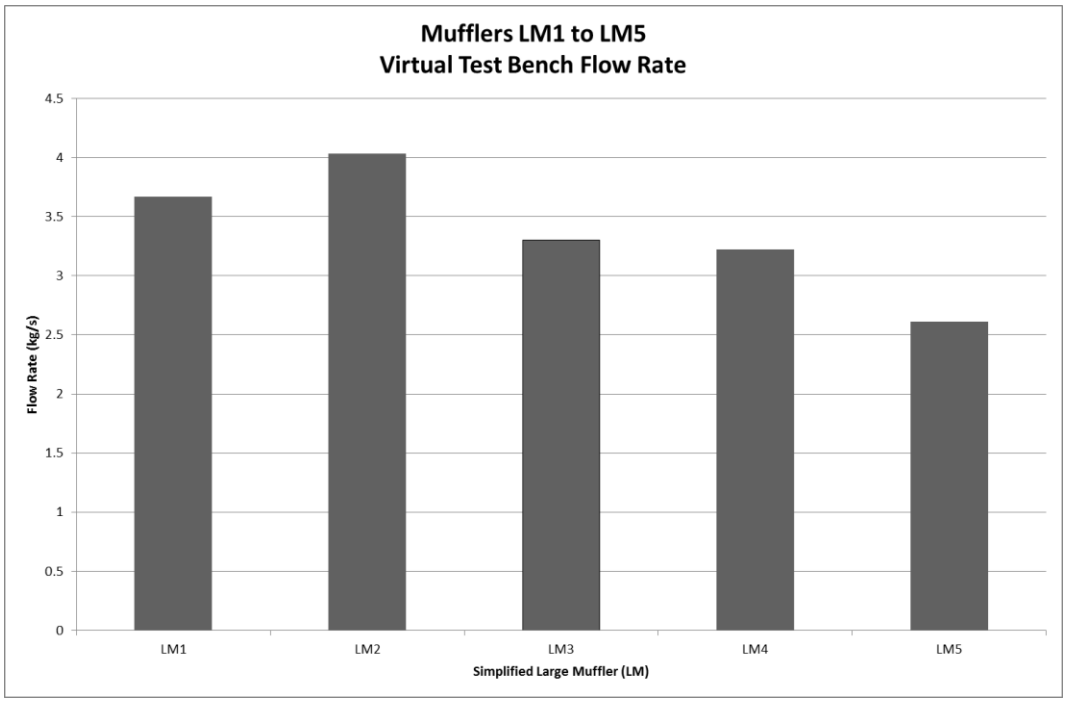

Figure 6.2 Flow Results Summary, Large Mufflers (LM1 to LM5)

The flow rate reduction with increasing complexity and flow impediments is shown by LM1, LM3, LM4 and LM5. However LM2 shows higher flow compared to LM1 when no increase was expected and this is the opposite trend to that in the flow coefficient method earlier. The extended inlet and the sudden expansion should have similar flow coefficients [34]. The sudden contraction and extended outlet should also have similar flow coefficients [34]. In muffler LM2, the longer inlet pipe / extended inlet friction and the longer outlet pipe / extended outlet friction should increase the flow restriction. This is not completely offset by the slightly reduced body pipe friction due to the shorter body. Clearly this is a topic for future investigation.

6.2.3 LM1 to LM2

This series consists of single expansion chamber mufflers (no centre baffle / interconnecting tube) with progression from a simple expansion chamber (LM1) to a simple expansion chamber with extended inlet, and extended outlet (LM2). The series splits the progression from LM1 to LM2 with LM9 which has only an extended outlet and LM10 which has only an extended inlet and the results are summarised in Figure 6.3.

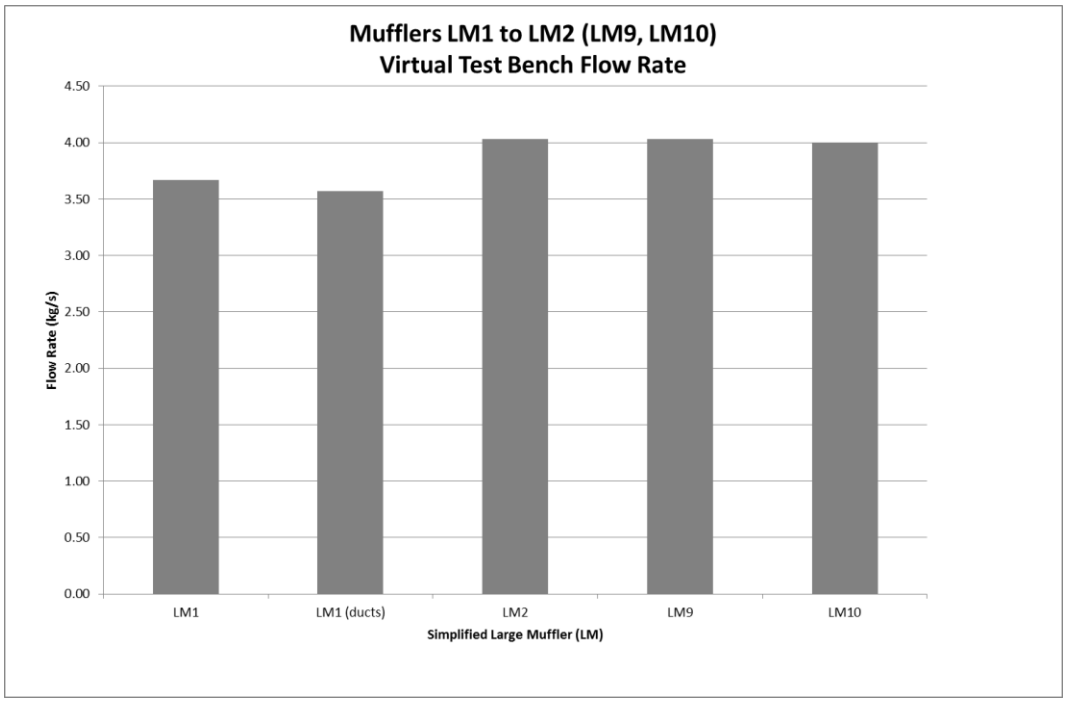

Figure 6.3 Flow Results Summary, Large Mufflers (LM1, LM2, LM9 and LM10)

Again the results for LM2, LM9 and LM10 show a 10% higher flow than LM1 which is counterintuitive for the reason stated previously and again will be the subject of future investigation.

6.2.4 LM1, LM2, LM6

This series consists of single expansion chambers with no centre baffle or interconnecting tube. The series makes the progression from LM1 to LM2 with coaxial extended elements to LM6 which has the extended inlet and extended outlet at angles to the body with the results summarised in Figure 6.4.

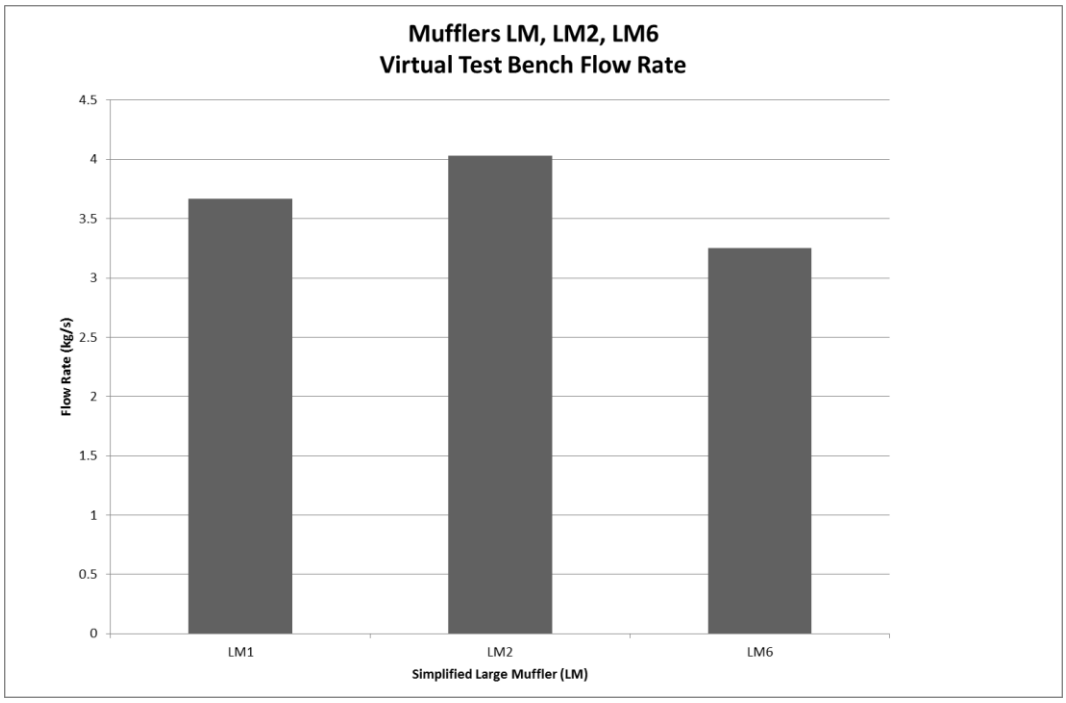

Figure 6.4 Flow Results Summary, Large Mufflers (LM1, LM2 and LM6)

The flow rate reduction with increasing complexity and flow impediments is shown as expected with LM6 having a lower flow rate compared to LM2 and LM1.

6.2.5 LM1, LM7, LM8

This series consists of single expansion chambers with no extended inlets or extended outlets. The series makes the progression from LM1 to LM7 with a centre baffle to LM8 with a centre baffle and interconnecting tube. The results are summarised in Figure 6.5.

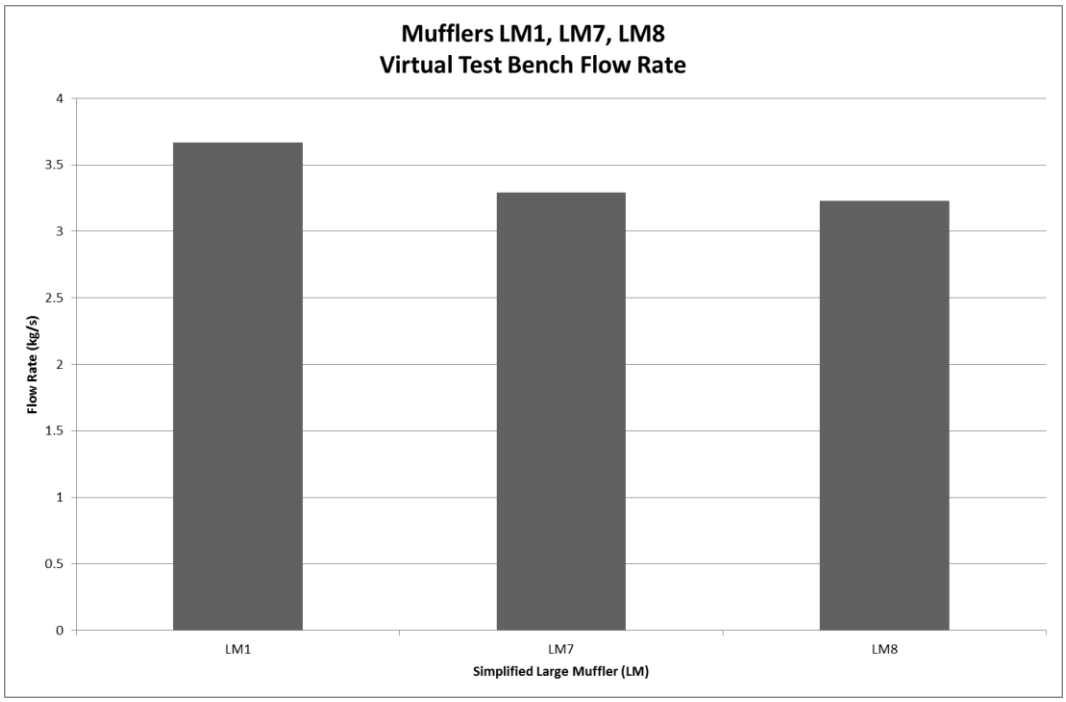

Figure 6.5 Flow Results Summary, Large Mufflers (LM1, LM7 and LM8)

The flow rate reduction with increasing complexity and flow impediments is as expected.

6.3 Large Marine Muffler

The flow rate of a large marine muffler (Muffler LMM) was simulated in WAVE at 700 K (≈ 430 °C) with a 12.5 kPa overall pressure difference. The sensitivity of the results to mesh size was investigated and the results are summarised in Table 6-3 and Figure 6.6 with an 8% (minimum to maximum) range. The on-engine pressure drop for this muffler is currently unknown however extrapolating from testing with similar mufflers suggests that the pressure drop will be in the five to ten kPa range [77]. The calculated flow rate is lower for a given pressure difference than the test data with similar mufflers suggests. This may possibly be due to the low discharge coefficients automatically selected in WAVE modelling.

Table 6-3 Flow Results Summary, Large Marine Mufflers (LMM), Discretisation Sweep

Nominal flow ≈ 3.1 kg/s, 700 K, 12.5 kPa pressure difference			
Muffler B, WB3D	**dx, dy, dz, dtube (mm)**	**Flow (kg/s)**	**Flow (%)**
B400	140, 100, 100, 100	3.07	102
BBW	80, 80, 80, 80	2.87	96
BBW1	50, 100, 100, 50	2.81	94
BBW2	100, 100, 100, 100	3.00	100

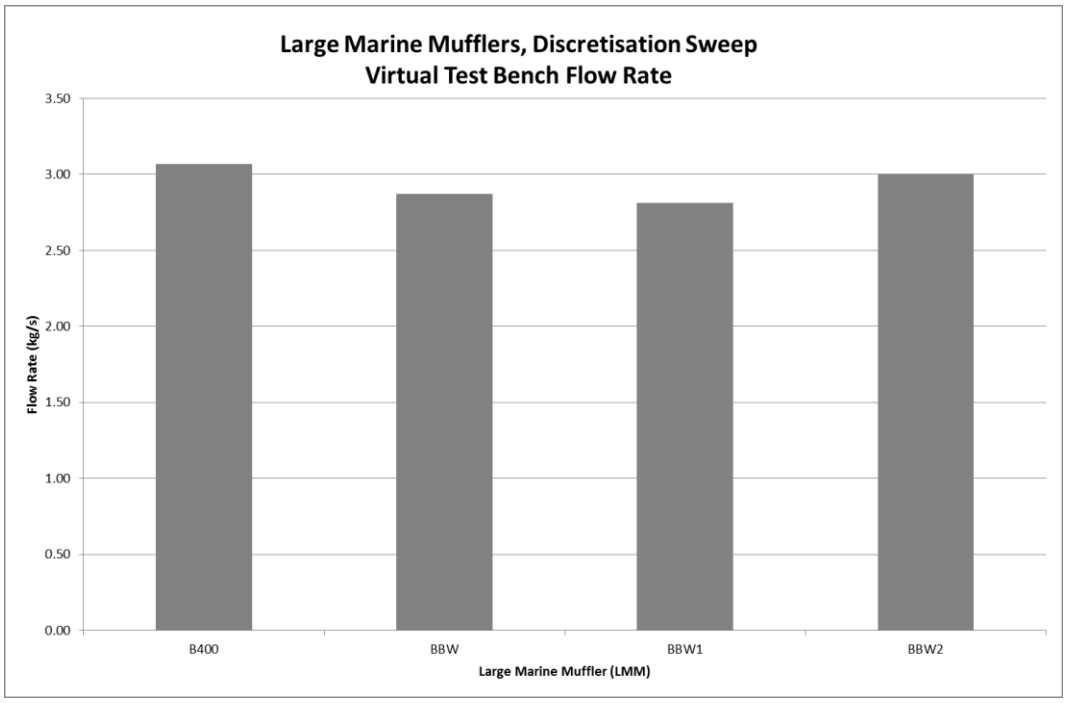

Figure 6.6 Flow Results Summary, Large Marine Mufflers (LMM)

Chapter 7 Numerical Experiments - Acoustic Modelling

This chapter covers the acoustic modelling approach and the modelling of:

1. simple and complex exhaust devices from published research
2. simple contraction / expansion chambers
3. the simplified large mufflers (LM)
4. the large marine muffler (LMM).

It presents the acoustic transmission loss results and provides comparisons by grouping into logical groups to illustrate the effects of design iterations for the LM and LMM mufflers. In addition, a discretisation size sweep was undertaken for the LMM muffler.

7.1 Modelling Overview

7.1.1 Modelling Strategy

The modelling was conducted in order of increasing complexity in such a way that simpler models could be validated and evaluated before progressing onto more complex models:

1. simple National Advisory Council on Aeronautics (NACA) mufflers with validation by theory and published results [44, 45]
2. complex NACA mufflers with validation by theory and published results [44, 45]
3. large mufflers with design increments (Muffler LM 1 to 10) with limited theoretical validation
4. a complex large marine muffler (Muffler LMM) with validation by experimental acoustic transmission loss test bench.

7.1.2 Model Construction

The models for the test elements were constructed using a variety of approaches (Wavebuild, WaveBuild3D, and CAD files) depending upon the complexity of the models. The models consisted of:

1. single 1D elements
2. multiple 1D elements (meshed)
3. geometry imported from CAD files and then meshed.

7.1.3 WAVE Modelling Parameters

Table 7-1 summarises the modelling parameters generally used with variations noted in the relevant sections.

Table 7-1 WAVE Acoustic Modelling Parameters, General

Parameters	WAVE Acoustic, 25°C	WAVE Acoustic, 700 K
Speed of Sound (m/s)	346	530
Temperature	25 °C	700 K (≈ 430 °C)
Pressure (bar)	1.01	1.0
Flow	zero	zero
Minimum Frequency (Hz)	1	1
Maximum Frequency (Hz)	400 or 700	400 or 700
Cut-on Frequency (Hz) for Ducting (ø 340 mm)	595	915
Cut-on Frequency (Hz) for Muffler Body (ø 820 mm)	245	380
Microphone Spacing (mm)	200 & 500 mm	200 & 500
Input Spectra	Multi-sine	Multi-sine
Input Amplitude (mm/s)	50	50
Discretisation Length	dx	dx

7.2 NACA Muffler Testing

Significant early work targeted at piston engine helicopters was conducted by the US National Advisory Council on Aeronautics (NACA) in the 1950's [44, 45]. This work comprised extensive experimental measurements using the standing wave ratio method benchmarked against theoretical calculations using classical analytical models. As noted in their reports, the correlation between their theoretical calculations and measured results with respect to transmission loss magnitude reduced as the complexity of the mufflers increased, e.g. multi-chamber mufflers. Approximately 80 mufflers and exhaust elements were evaluated at zero flow on an acoustic transmission loss experimental test bench at an ambient temperature of 27 °C. The schematic and the actual test bench are shown in Figure 7.1 and Figure 7.2 respectively. Selected items were then tested on a running helicopter engine as shown in Figure 7.3. These studies were very well documented and are widely used for validation of exhaust system testing and modelling [21].

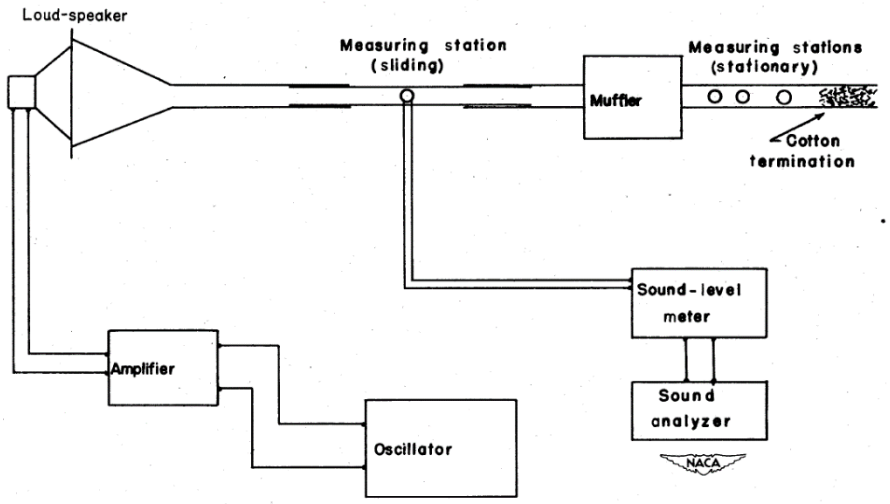

Figure 7.1 NACA Test Bench Schematic [44]

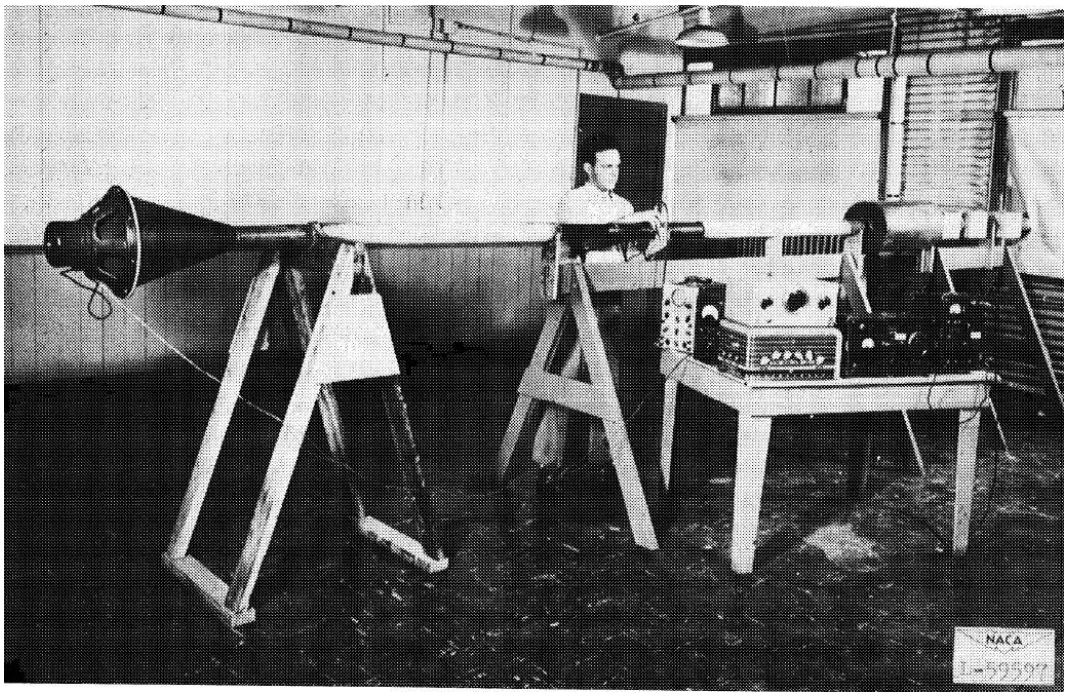

Figure 7.2 NACA Test Bench Photo [44]

Figure 7.3 NACA Helicopter Engine Noise Test Facility [45]

7.3 Simple NACA Models

The transmission loss testing of a range of simple mufflers has been reported by NACA [44, 45] under 'Test Bench' conditions with an ambient temperature of 27 °C. Table 7-2 summarises the parameters used for the corresponding WAVE modelling.

Table 7-2 WAVE Acoustic Modelling Parameters, General

Parameter	For modelling of NACA Mufflers
Speed of Sound (m/s)	347
Temperature (°C)	27
Pressure (bar)	1.01
Flow	zero
Frequency Minimum (Hz)	1
Frequency Maximum (Hz)	700 or 1000
Microphone Spacing (mm)	150
Input Spectra	Multi-sine
Input Amplitude (mm/s)	50
Discretisation Length (dx) (mm)	50

NACA experimental results and WAVE modelling results are presented in the following sections for the simple expansion chamber, quarter wave tube, and Helmholtz resonator devices listed in Table 7-3.

Table 7-3. Summary of NACA Simple Mufflers [44, 45]

Description	No of Chambers	NACA Muffler No	Variable
Expansion Chamber	Single	1,2,3,4	Expansion ratio
Expansion Chamber	Single	5,6,2,7	Length
Quarter Wave Tube	n/a	68,69,70	Length
Helmholtz Resonator	n/a	24,25,26	Volume
Helmholtz Resonator	n/a	29,25,30	Area of Tube
Helmholtz Resonator	n/a	31,25,32	Length of Tube

7.3.1 Single Expansion Chamber with variable Expansion Ratio

In expansion chamber mufflers the sudden change in cross sectional area reflects energy / waves back towards the source thus reducing sound transmission along the pipe. NACA mufflers 1, 2, 3, and 4 are single expansion chambers 610 mm long with 76 mm diameter inlet and exhaust pipes and body diameters of 152, 305, 456, and 610 mm respectively. Figure 7.4 from NACA [44] shows the dimensions, calculated transmission losses, and experimental results. Figure 7.5 shows WAVE modelling results of transmission losses using the same ambient conditions as the NACA testing.

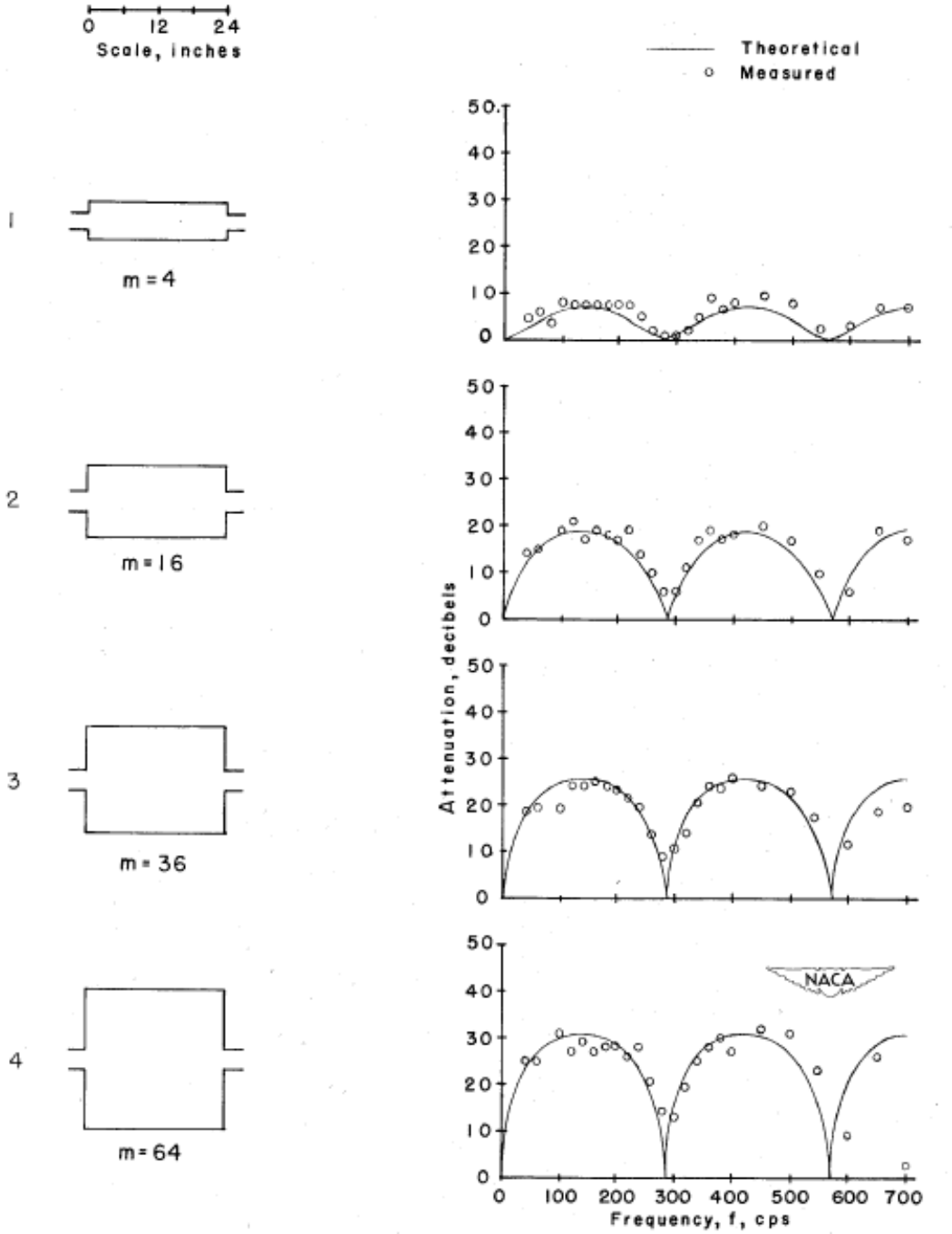

Figure 7.4 NACA Expansion Chamber Mufflers, Effect of Expansion Ratio [44]

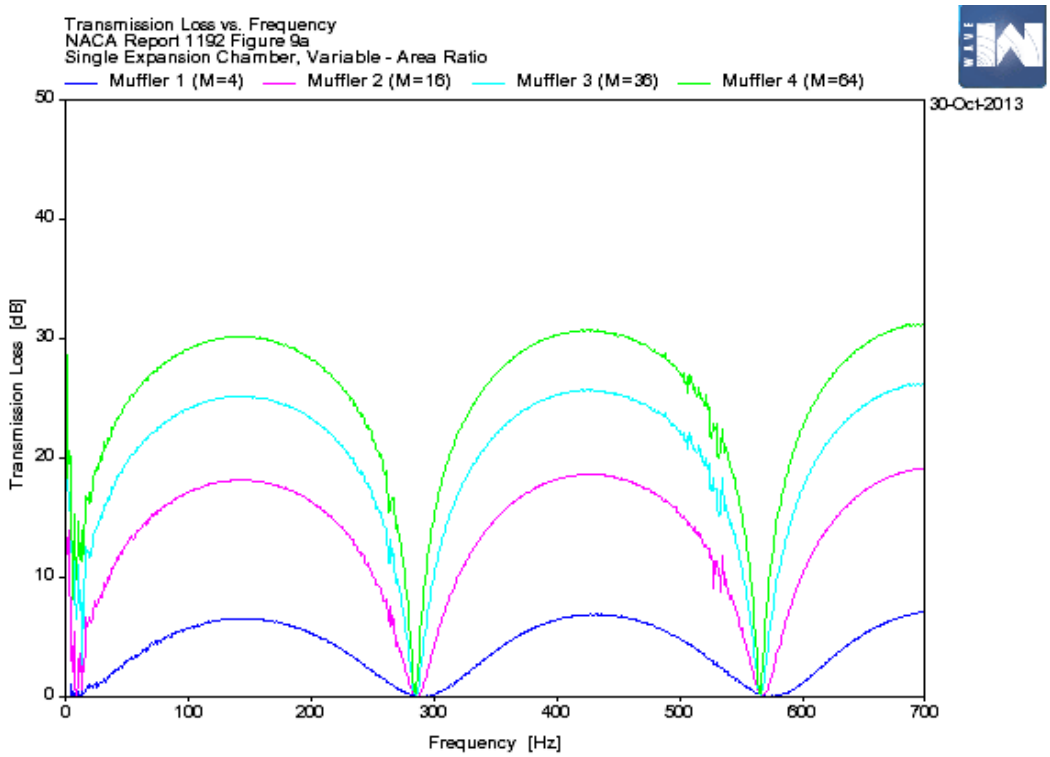

Figure 7.5 WAVE Modelling Results Equivalent to Figure 7.4

The WAVE modelling results show good agreement with NACA results with respect to frequencies and transmission loss curve shapes. The peak transmission losses show very good agreement for NACA mufflers 3 and 4 which have high area ratios (36 and 64 respectively). However the WAVE modelling predicts lower peak transmission losses compared to NACA measurements and theoretical predictions for NACA mufflers 1 and 2 which have lower area ratios (4 and 16 respectively). The reason for this is unclear and warrants further investigation. It can be seen that the peak transmission losses increase with the expansion ratio. Also, maximum transmission losses occur at frequencies when the length of the expansion chamber corresponds to one quarter of the acoustic wavelength and its odd multiples, as predicted by classical theory. Similarly the minimum transmission losses occur at one half of the acoustic wavelength and its odd multiples.

7.3.2 Single Expansion Chamber with Variable Length

NACA mufflers [44] 5, 6, 2, and 7 are single expansion chambers 305 mm in diameter with 76 mm diameter inlet and exhaust pipes and body lengths of 76, 305, 610, and 1220 mm respectively. Figure 7.6 and Figure 7.7 show NACA and WAVE results respectively.

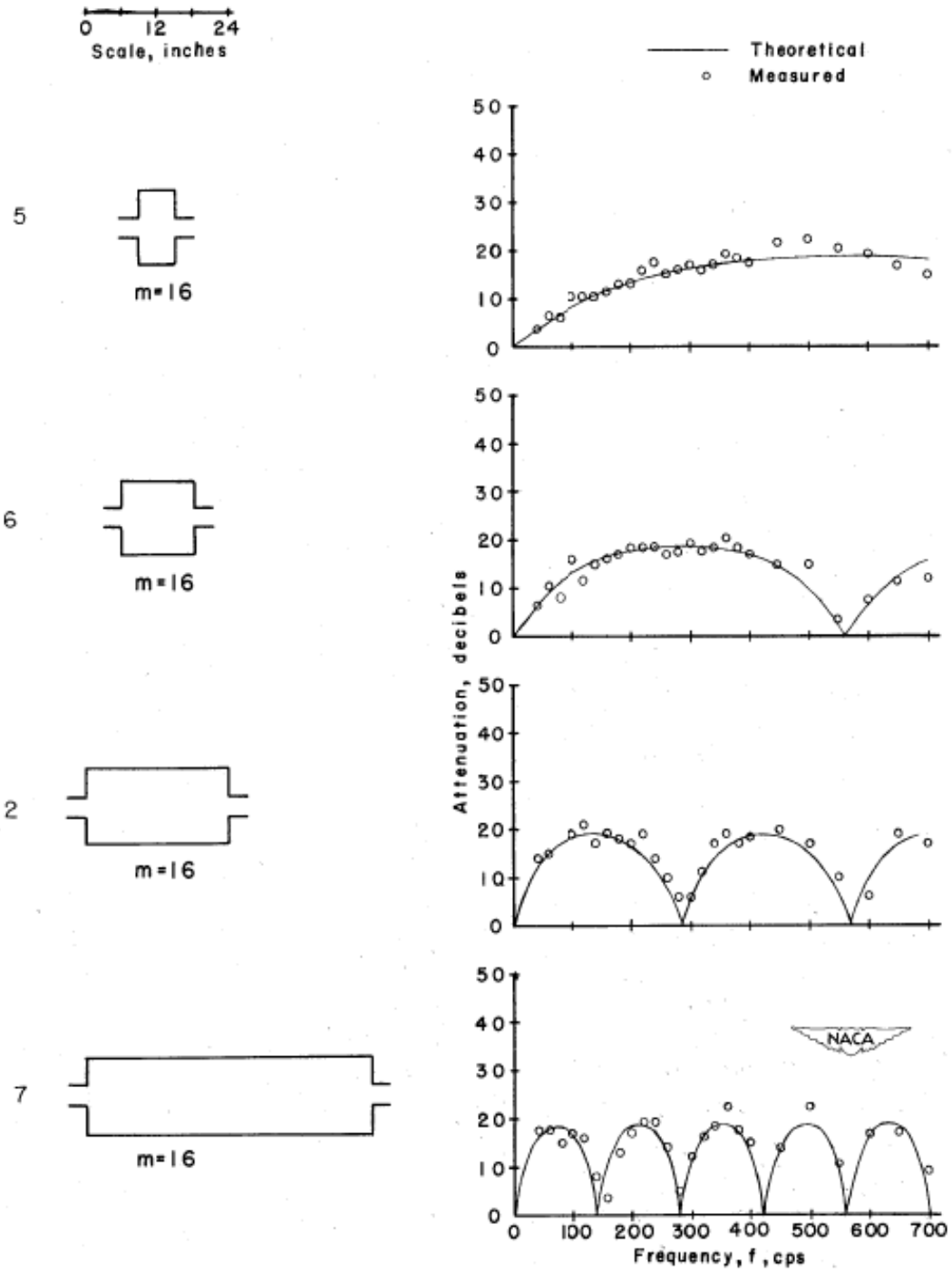

Figure 7.6 NACA Expansion Chamber Mufflers, Effect of Length [44]

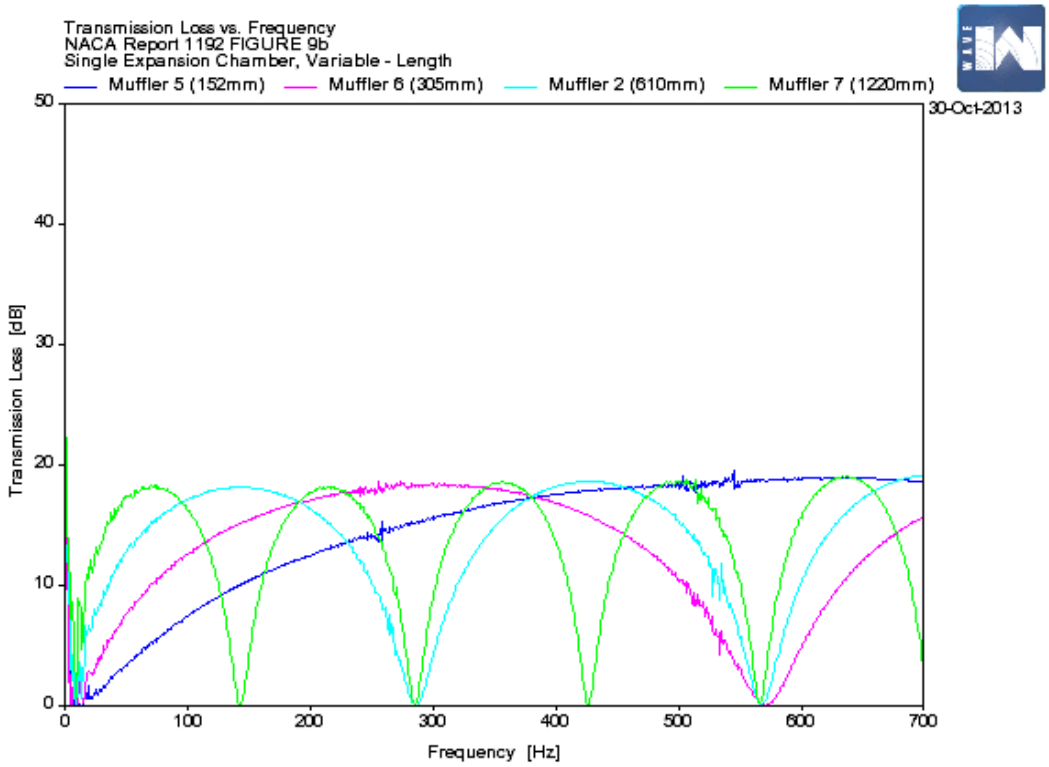

Figure 7.7 WAVE Modelling Results Equivalent to Figure 7.6

The WAVE modelling results show good agreement with NACA results. It can be seen that for an expansion ratio of 16, the maximum transmission losses are approximately 20 dB. The low frequency noise is believed to be an aberration of the modelling software and not real. As in the previous section, maximum transmission losses occur at frequencies when the length of the expansion chamber corresponds to one quarter of the acoustic wavelength and its odd multiples, as predicted by classical theory. For single expansion chambers the expansion ratio governs the maximum transmission loss that can be achieved by the muffler while the chamber length controls the frequency at which maximum attenuation takes place.

7.3.3 Quarter Wave Tubes with Variable Length

A quarter wave tube (QWT) works over a narrow frequency range to attenuate a specific tuned frequency. The device works by generating a sound pressure that is 180 º out of phase to the incident sound pressure at the mouth of the QWT. This is achieved by the sound pressure at the mouth travelling down the QWT and being reflected at the closed end. The 180 º phase change occurs when the total distance is equivalent to one half wavelength (the length of tube is a quarter of the acoustic wavelength) and its odd multiples. Quarter wave tubes of 76 mm diameter with lengths of 1065, 710, and 560 mm connected to a 76 mm diameter pipe are shown in Figure 7.8 [44] as NACA mufflers 68, 69 and 70 respectively. Also shown in the figure are the calculated transmission losses and experimental results. Figure 7.9 shows WAVE modelling results of the predicted transmission losses.

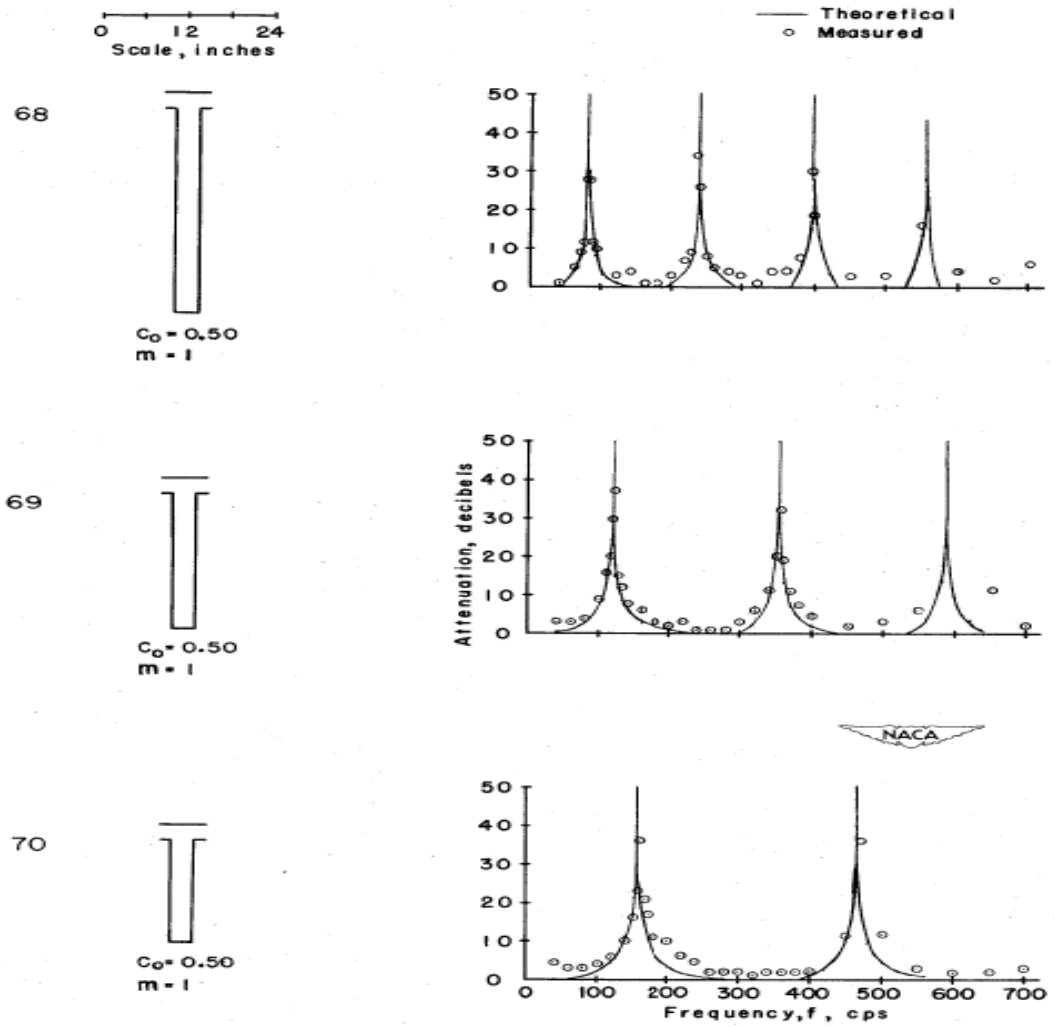

Figure 7.8 NACA Quarter Wave Tube, Effect of Length [44]

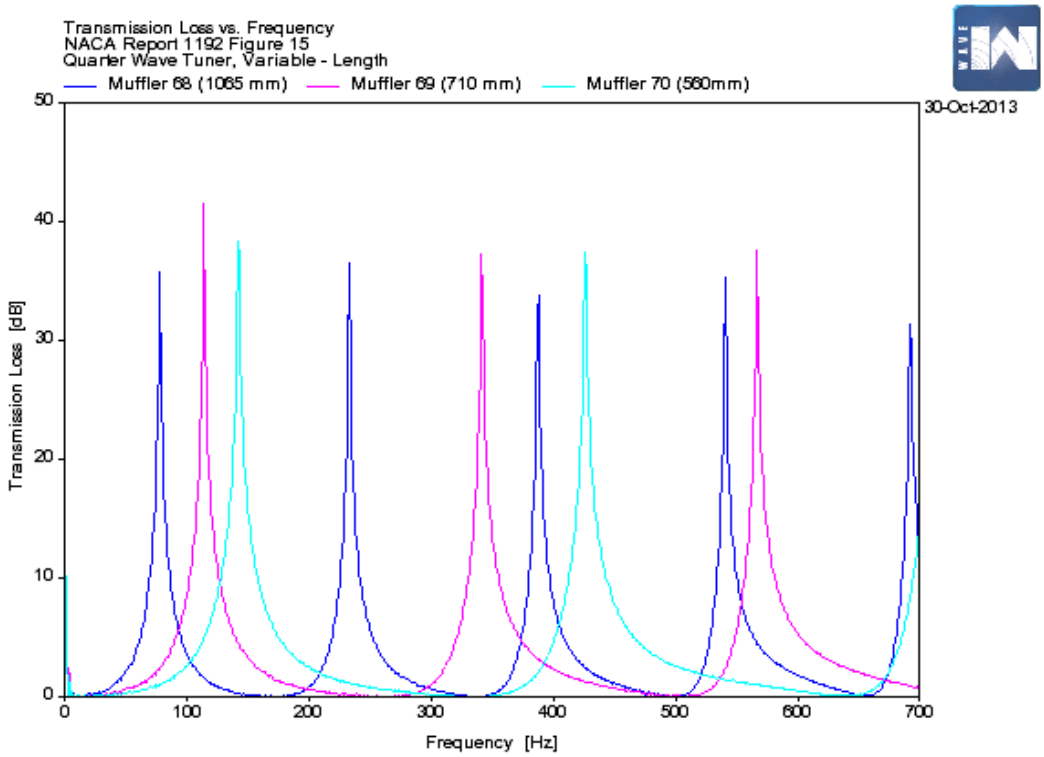

Figure 7.9 WAVE Modelling Results Equivalent to Figure 7.8

The WAVE modelling results show good agreement with NACA results. The tuned, narrow band nature of noise attenuation can be observed from both NACA and WAVE modelling results. As expected, the tuned frequencies occur when the tube length corresponds to a quarter of the acoustic wavelength and its odd multiples.

7.3.4 Helmholtz Resonators with Variable Volume

A Helmholtz resonator consists of a cavity of air coupled to the main pipe through a narrow tube. In simple physical terms, a Helmholtz resonator operates as a spring-mass vibration system with the volume of gas in the narrow tube acts as a mass element, while the volume of gas in the cavity acting as a spring element. At a specific frequency depending on the geometry, the tube / cavity resonates and generates a sound pressure 180 º out of phase resulting in sound cancellation. NACA mufflers 24, 25, and 26 are Helmholtz resonators with fixed tube dimensions (ø 50.8 mm, 173 mm long) and volumes of 6.3, 2.8, and 0.7 litres respectively. The resonators are connected to a main pipe of 76 mm diameter. Figure 7.10 from NACA [44] shows the dimensions, calculated transmission losses, and experimental results. Figure 7.11 shows WAVE modelling results of the predicted transmission losses.

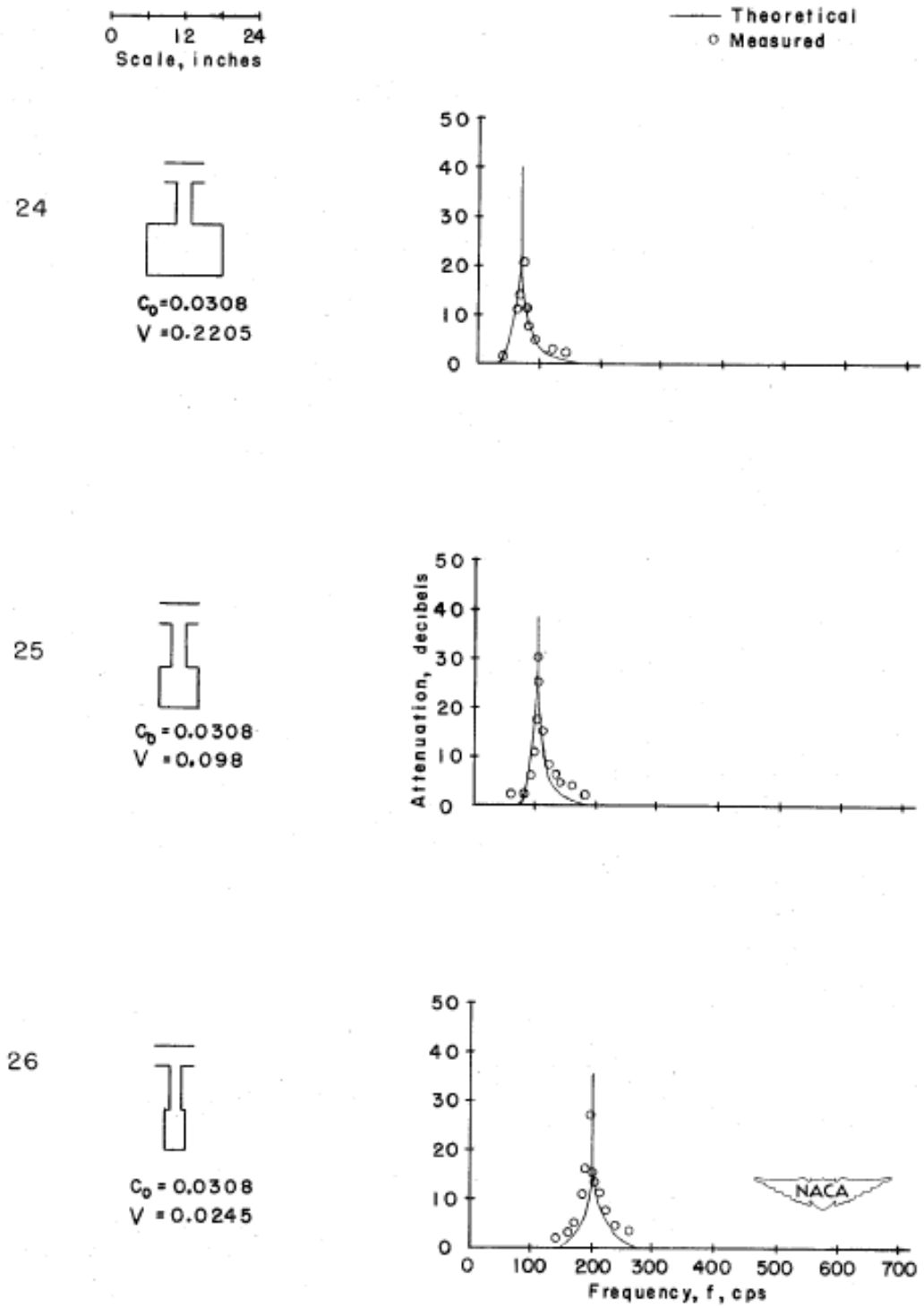

Figure 7.10 NACA Helmholtz Resonators, Effect of Volume [44]

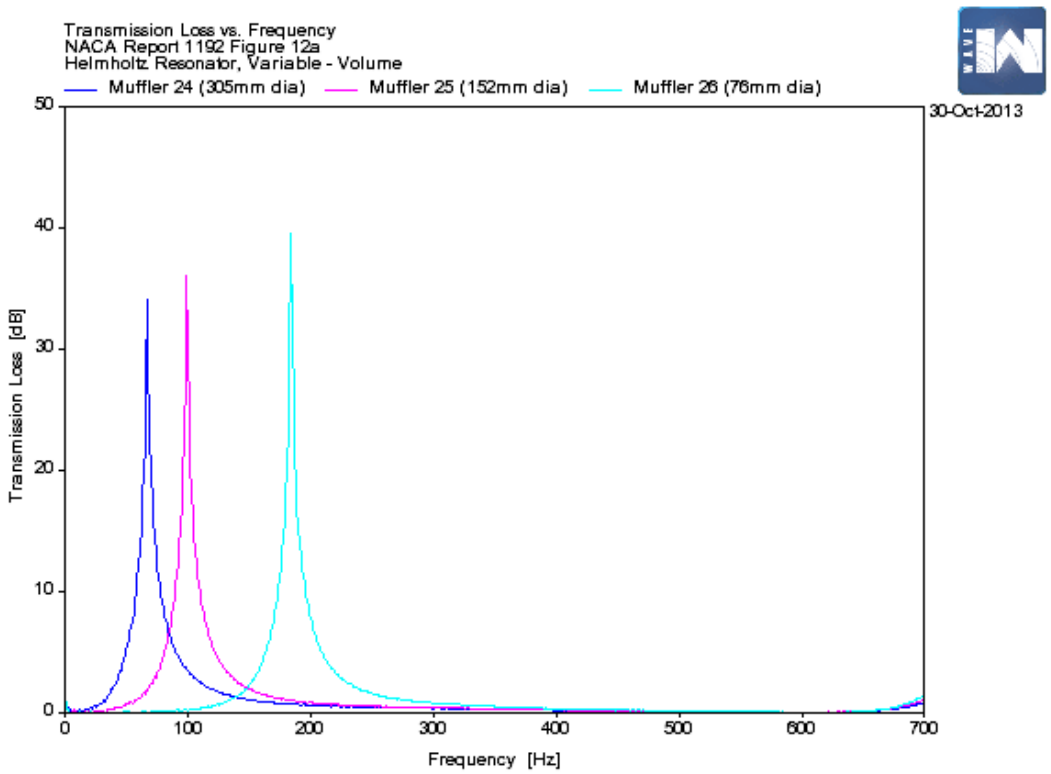

Figure 7.11 WAVE Modelling Results Equivalent to Figure 7.10

The WAVE modelling results show good agreement with NACA results. Both the NACA and WAVE results show the tuned, narrow band nature of the Helmholtz resonators with the tuned frequency corresponding to the system resonance.

7.3.5 Helmholtz Resonators with Variable Tube Area

NACA mufflers 29, 25, and 30 are Helmholtz resonators with fixed volumes (2.8 litres), fixed tube lengths (173 mm), and tube diameters of 25, 51, and 76 mm respectively. Figure 7.12 from NACA [44] shows the dimensions, calculated transmission losses, and experimental results. Figure 7.13 shows WAVE modelling results of the predicted transmission losses.

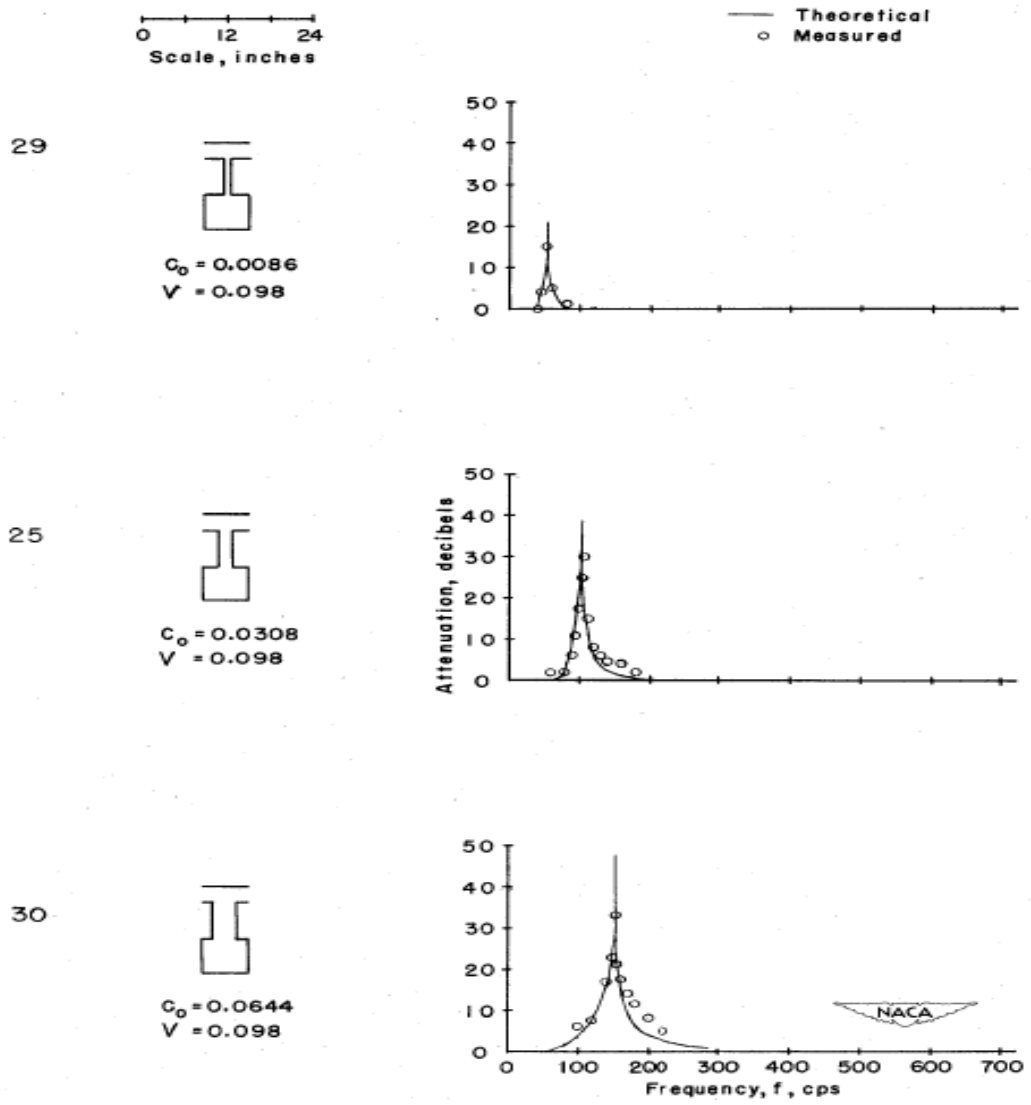

Figure 7.12 NACA Helmholtz Resonators, Effect of Tube Area [44]

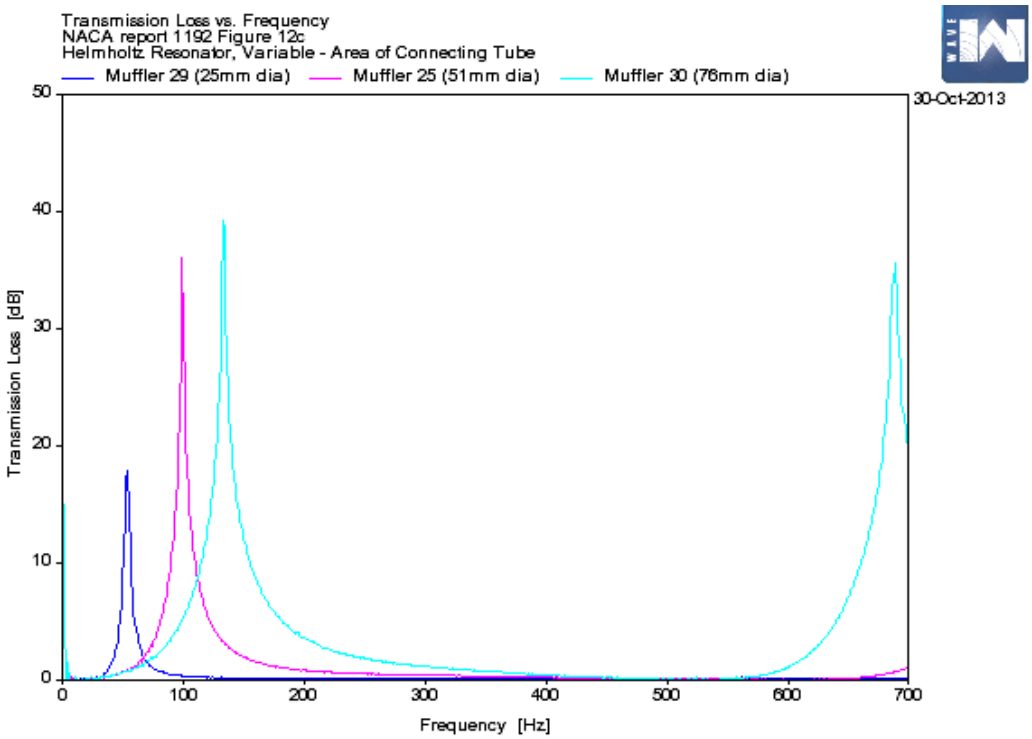

Figure 7.13 WAVE Modelling Results Equivalent to Figure 7.12

The WAVE modelling results show good agreement with NACA results. Increasing the tube area has the effect of increasing the effective stiffness of the Helmholtz resonator and thereby increases the tuned frequency as shown in the figures despite the opposite effect of the increased effective mass. The WAVE modelling's predicted second peak at 690 Hz for muffler 30 is due to a half wavelength resonance in the tube. Note that while the physical lengths of the tubes are identical, Section 9.7.2 shows that the effective lengths vary with diameter. As muffler 30 has the largest tube diameter, it has the longest effective length and the corresponding lowest half wavelength resonant frequency.

7.3.6 Helmholtz Resonators with Variable Length of Tube

NACA mufflers 31, 25, and 32 are Helmholtz resonators with fixed volumes (2.8 litres), fixed tube areas (ø 50.8 mm), and tube lengths of 11, 173, and 345 mm respectively. Figure 7.14 from NACA [44] shows the dimensions, calculated transmission losses, and experimental results. Figure 7.15 shows WAVE modelling results of the predicted transmission losses. The WAVE modelling's predicted second peak at 450 Hz for muffler 32 is again due to a half wavelength resonance in the tube.

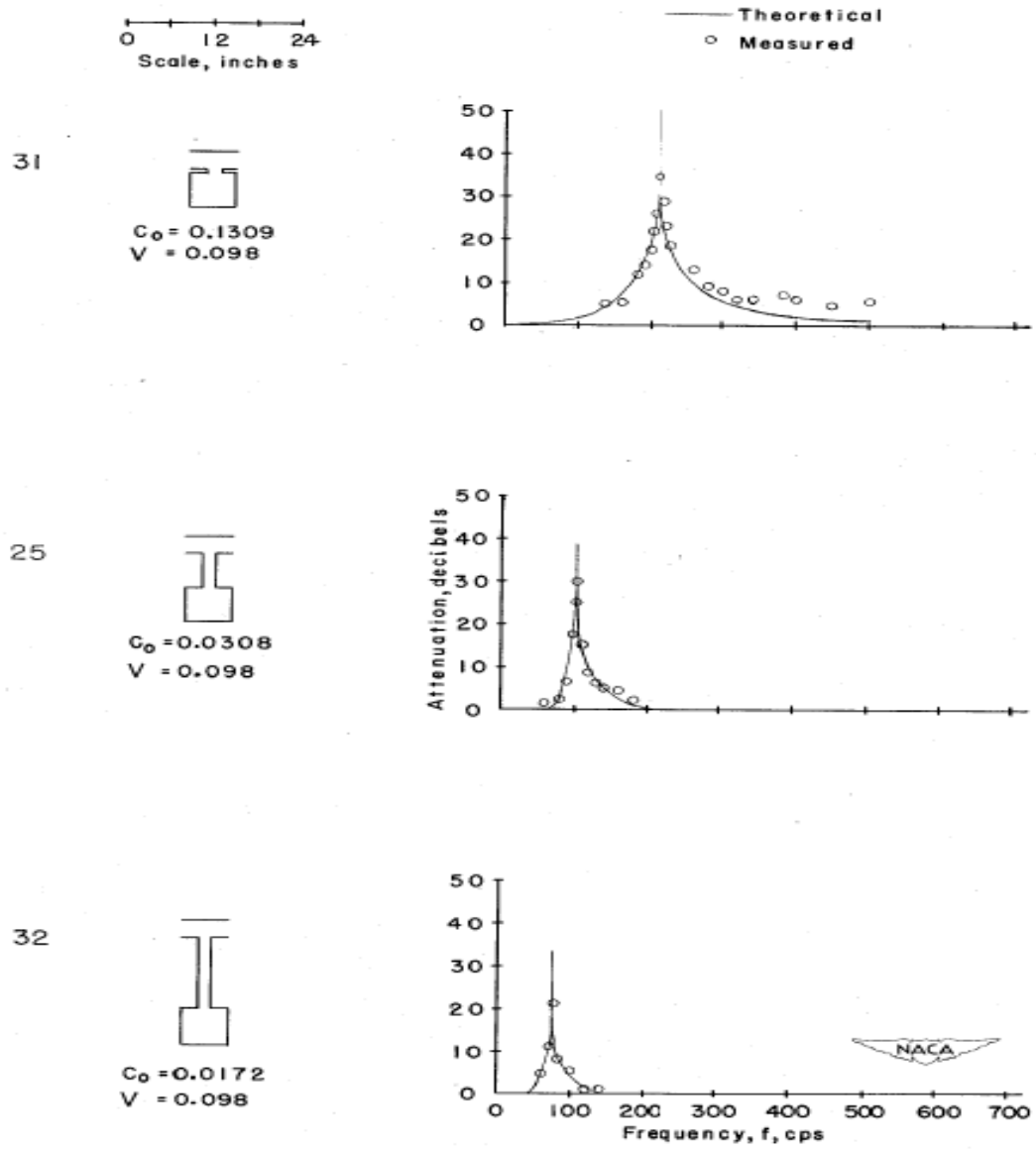

Figure 7.14 NACA Helmholtz Resonators, Effect of Tube Length [44]

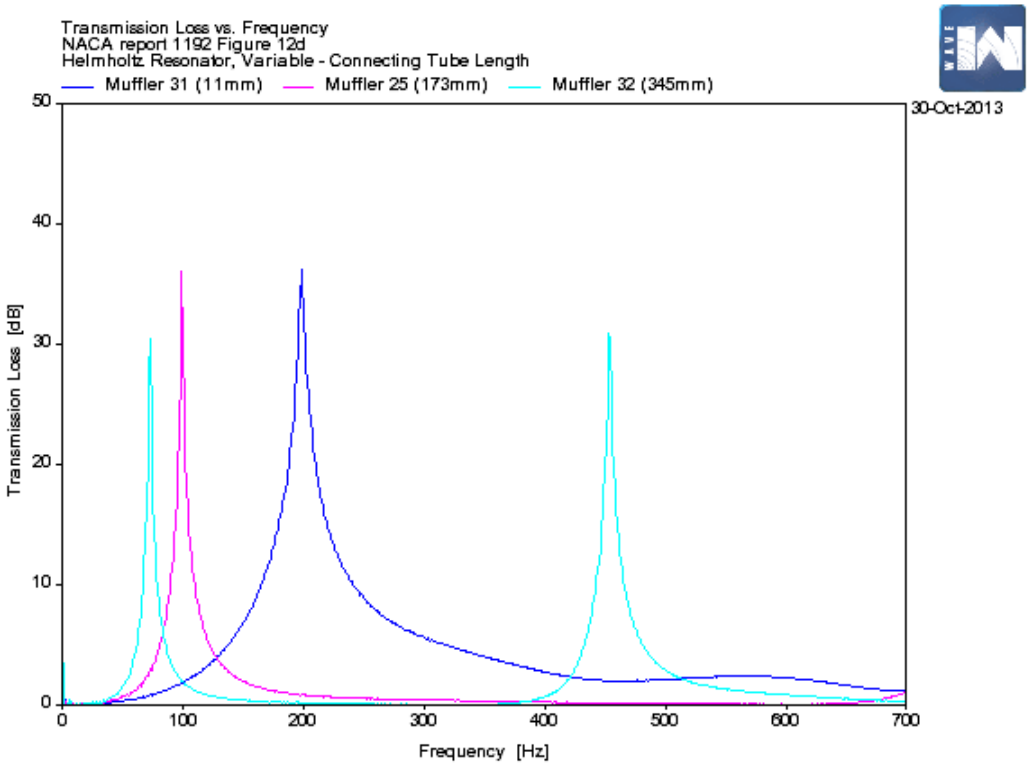

Figure 7.15 WAVE Modelling Results Equivalent to Figure 7.14

The WAVE modelling results show good agreement with NACA results for the overall shapes and magnitude of transmission losses. As expected, increasing the tube length increases the effective mass of the Helmholtz resonator and thereby reduces the tuned frequency as shown in the figures.

7.4 Complex NACA Models

This section covers a range of more complex mufflers as listed in Table 7-4 - multiple identical expansion chambers, twin expansion chambers with external interconnecting tube, and twin expansion chambers with internal interconnecting tube. NACA experimental results and WAVE modelling results are presented in the following sections for these mufflers.

Table 7-4. Summary of Complex NACA Mufflers

Description	No of Chambers	NACA Muffler No	Variable
Expansion Chamber	One, two, three	2,12,13	No of Chambers
Expansion Chamber, External Connector	Two	12,14,15,16	Length of Connector
Expansion Chamber, Internal Connector	Two	12,17,18,19,20	Length of Connector

7.4.1 Multiple Identical Expansion Chambers

The connection of two or more expansion chambers in series will lead to an increase in transmission losses by successive reflection and interference of the acoustic waves. NACA mufflers 2, 12, and 13 are expansion chambers with one, two, and three identical chambers (each 610 mm long and 305 mm diameter) respectively separated by a 1.3 mm thick baffle with 76 mm diameter inlet and exhaust pipes. Figure 7.16 from NACA [44] shows the dimensions, calculated transmission losses, and experimental results. Figure 7.17 shows WAVE modelling results of the predicted transmission losses.

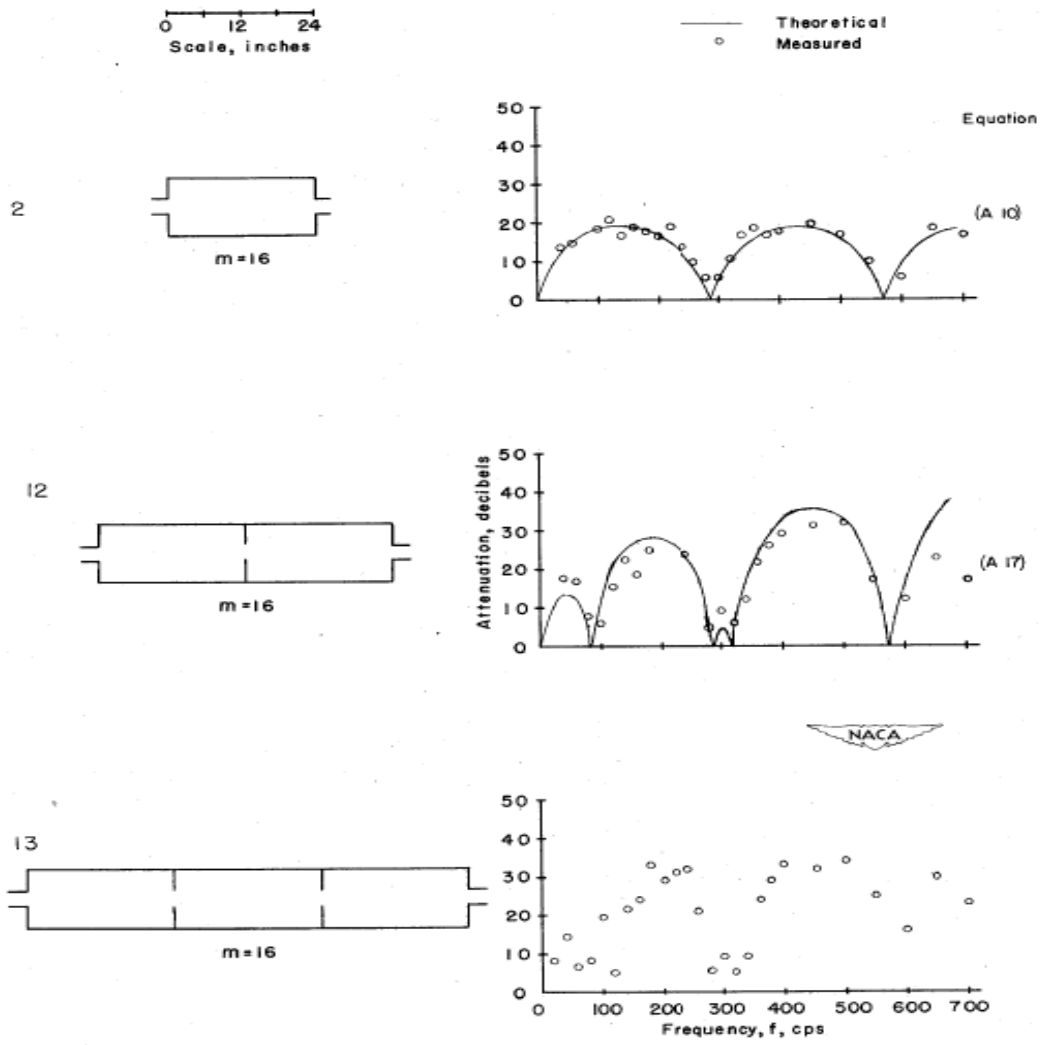

Figure 7.16 NACA Expansion Chamber Mufflers, Effect of Number of Chambers [44]

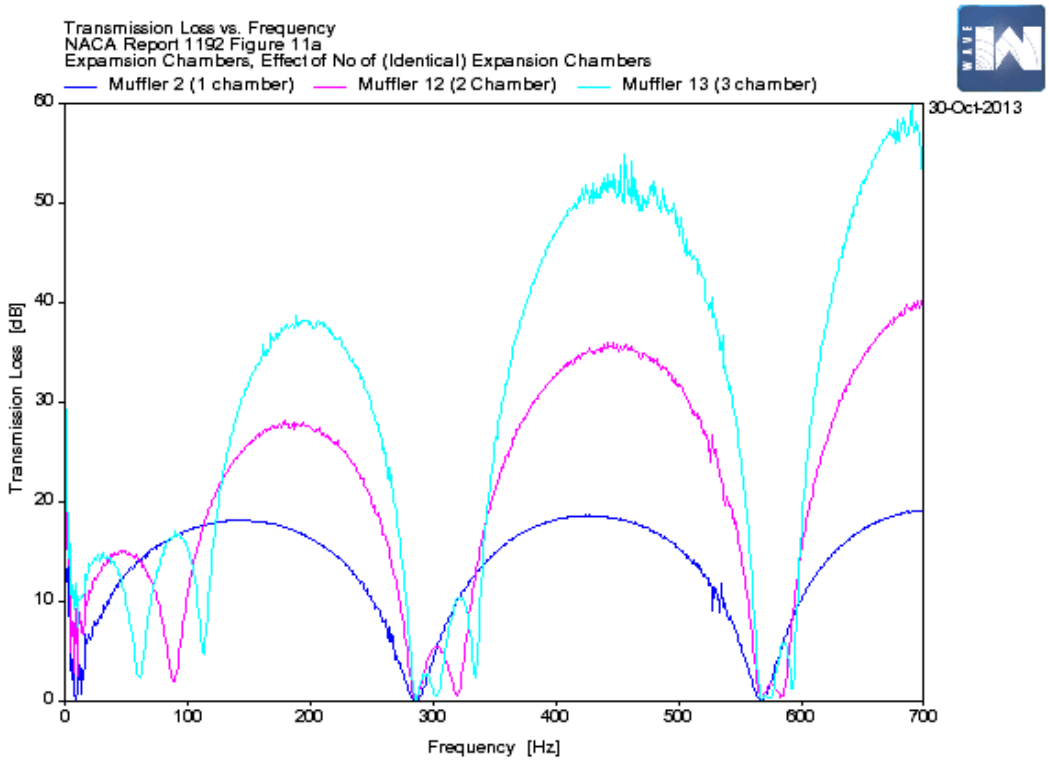

Figure 7.17 WAVE Modelling Results Equivalent to Figure 7.16

The WAVE modelling results show good agreement with NACA results for the overall shapes and magnitudes of transmission losses. As the complexity of the mufflers increase, the WAVE modelling appears to overestimate the magnitude of the transmission losses with values that seem unrealistic, e.g. 60 dB is one part in one thousand. The increase in peak transmission losses due to the addition of expansion chambers can be observed. The limited separation of the chambers results in complex interactions rather than simply acting as multiple chambers in series.

7.4.2Twin Expansion Chamber with Variable External Connecting Pipe Length

NACA mufflers 14, 15, and 16 consist of two expansion chambers (each 610 mm long and 305 mm diameter) separated by an external connecting pipe 152, 305, and 610 mm long respectively. The inlet, exhaust and connecting pipes are 76 mm diameter. Figure 7.18 from NACA [44] shows the dimensions, calculated transmission losses, and experimental results.

Figure 7.19 shows the corresponding WAVE modelling predicted transmission losses.

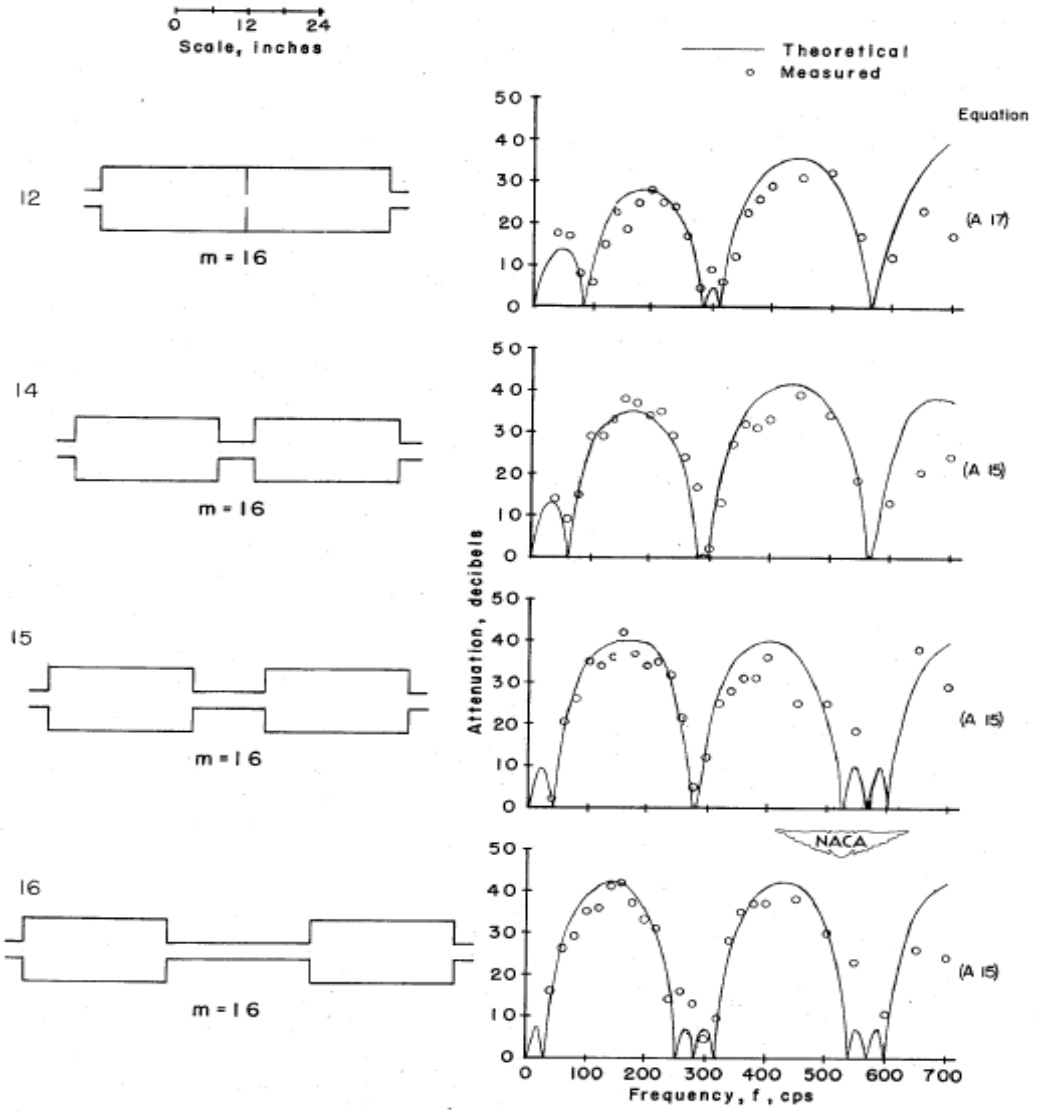

Figure 7.18 NACA Expansion Chamber Mufflers, Effect of External Connecting Tube Length [44]

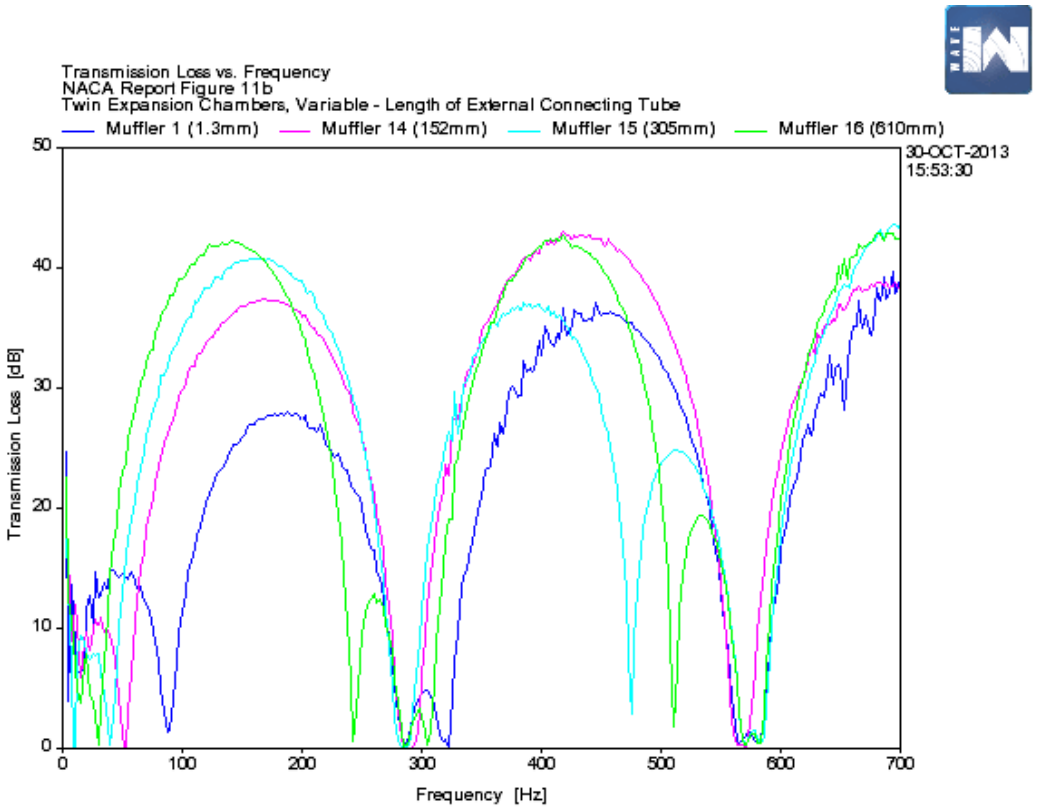

Figure 7.19 WAVE Modelling Results Equivalent to Figure 7.18

Overall, the WAVE modelling results show good agreement with NACA results. The clear separation of the chambers results in less complex interactions with the mufflers acting more like multiple chambers in series. Increasing the connecting pipe length has a small but noticeable effect on transmission losses.

7.4.3 Twin Expansion Chamber with Variable Internal Connecting Pipe Length

NACA mufflers 17, 18, 19 and 20 consist of two expansion chambers (each 610 mm long and 305 mm diameter) with an internal connecting pipe of 152, 305, 610 and 915 mm long respectively. These mufflers are considerably more complex than those previously discussed. In addition to two expansion chambers, the internal interconnecting tube forms a Helmholtz resonator with each chamber /volume – two in total. The protrusion of the connecting pipe into each expansion chambers forms a quarter wave tube – two frequencies in total. The internal tube will also have resonances at half wavelengths. Figure 7.20 from NACA [44] shows the dimensions, calculated transmission losses, and experimental results. Figure 7.21 shows WAVE modelling results of the predicted transmission losses.

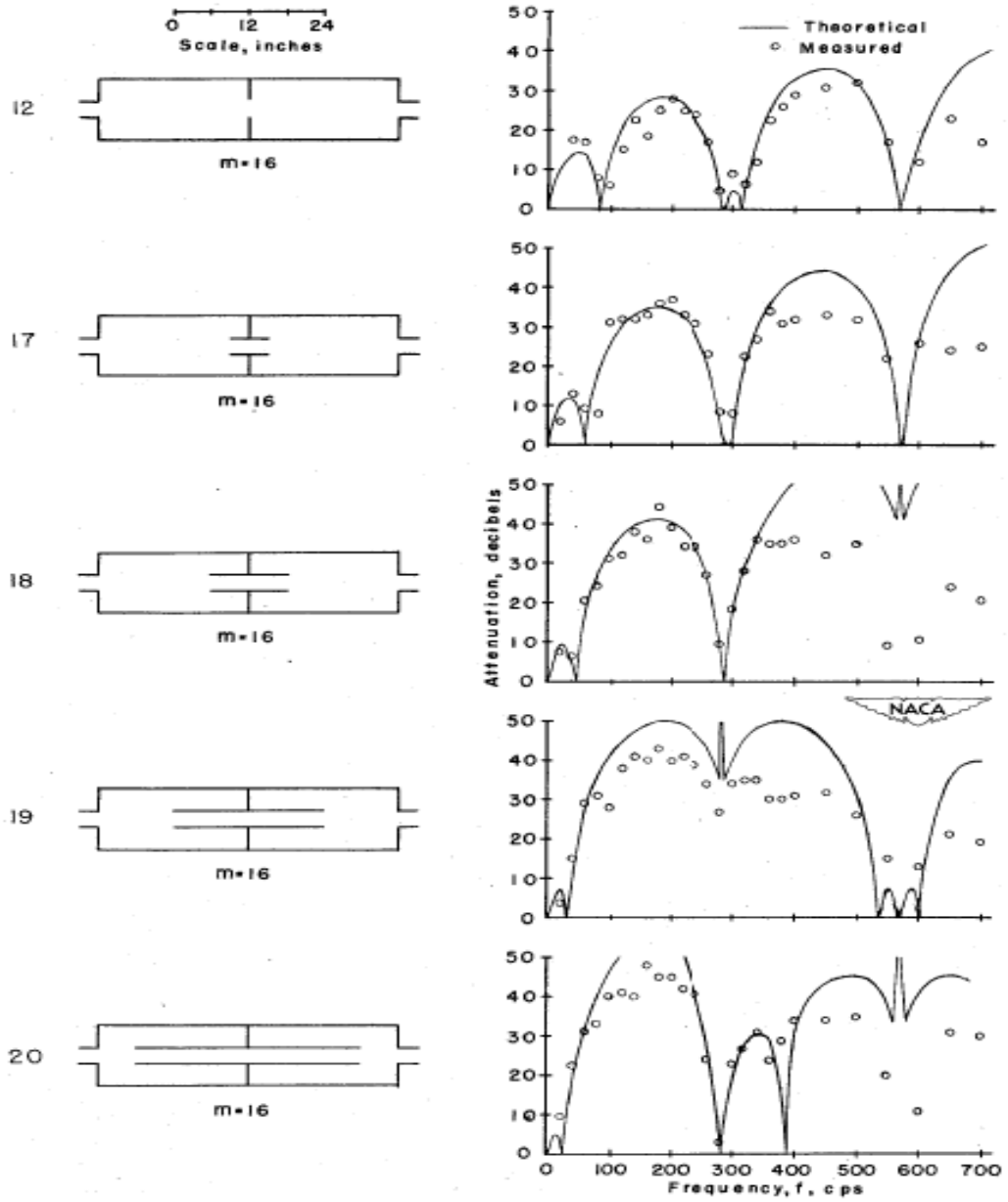

Figure 7.20 NACA Expansion Chamber Mufflers, Effect of Internal Connecting Tube Length [44]

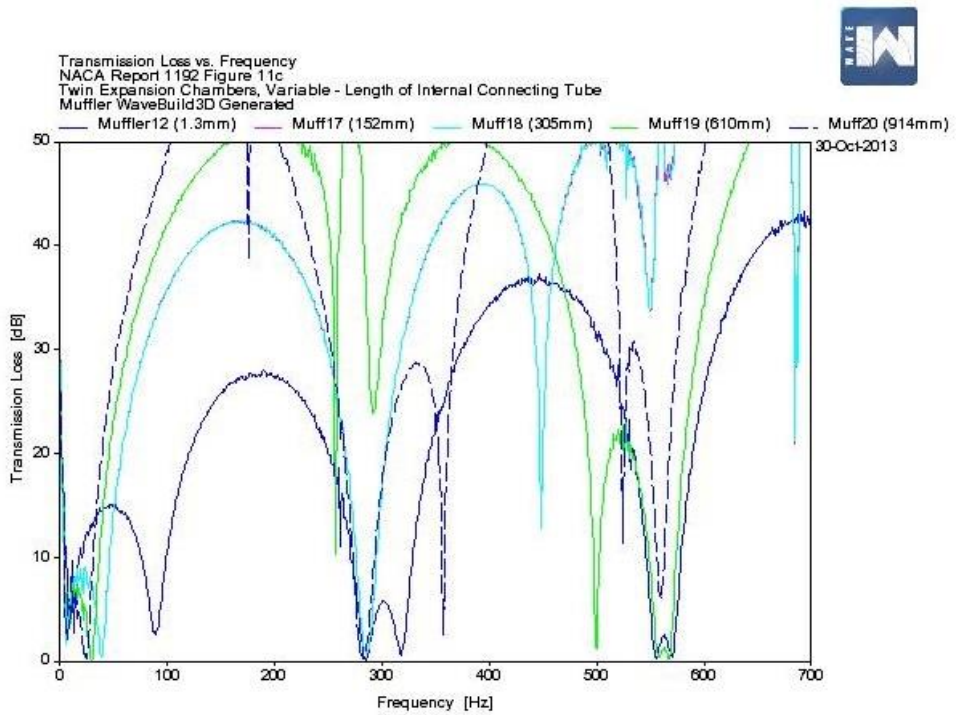

Figure 7.21 WAVE Modelling Results Equivalent to Figure 7.20

Despite the complexity of the mufflers, the WAVE modelling results show good agreement with the NACA results in regard to trends, frequencies and the shapes of the transmission loss curves. The complex geometry and interaction of the various internal devices is evident in the variation in shape and magnitude of transmission losses between the muffler variants. A variation in peak transmission loss of more than 20 dB is evident within the same external volume. It is not possible to draw a conclusion as the effect of the interconnecting tube length due to the possibly conflicting effects listed previously in this section.

7.5 Contraction / Expansion Chambers

7.5.1 Overview

To assist in validating the simulation, two acoustic devices that were simple and independently verifiable was designed and constructed by the author. While the obvious choice was a simple expansion chamber but this was discounted due to the cost and difficulty of constructing a rigid shell expansion chamber of the required size. To overcome these difficulties but retain key requirements a contraction / expansion chamber was chosen instead. The two selected contraction / expansion chambers are described further in Section 9.7.2 and shown in Figure 9.10 and are 150 mm in diameter and 432.5 mm and 1730 mm long. These lengths were selected to give a wide frequency range with peak transmission losses at multiples of approximately 200 and 50 Hz respectively. The acoustic transmission losses of these contraction / expansion chambers were measured experimentally using the experimental test bench detailed in Chapter 9.

The selected standard simulation temperature was 25 °C whereas the experimental test bench was in an uncontrolled climate laboratory with an ambient temperature on the day of testing of 20 °C. This resulted in the differences in speeds of sound for the modelling and testing of 346 and 343 m/s respectively. This 5 °C difference in test and simulation temperatures does not give a significant effect as the difference in the speed of sound is only one percent. The testing and simulation was conducted over two frequency ranges – 25 Hz to 400 Hz and 25 Hz to 800 Hz. This required two difference microphone spacings - 500 mm and 200 mm respectively. The 25 Hz lower frequency was chosen as it is the lower limit of the speaker's undistorted performance. The microphone spacing causes a divide by zero error / indeterminacy in the data processing when the microphone spacing is a half wavelength. For 500 mm and 200 mm spacings this is 346 Hz and 865 Hz respectively at 25 °C. The onset of the first lateral mode in the measurement ducts limits the experimental results to approximately 600 Hz.

The following figures compare WAVE simulation results with experimental test results for the two contraction / expansion test devices. The contraction / expansion chamber acts similar to an expansion chamber with peak attenuation being proportional to the area ratio and peak transmission loss occurs at odd multiples of quarter wavelength ($\lambda/4$) and zero transmission loss occurs at odd multiples of half wavelength ($\lambda/2$). The experimental results are in blue and the simulation results are in red.

Figure 7.22 shows the measured and modelled results for the short expansion chamber over a 400 Hz range. The correlation is excellent apart from the speaker low frequency performance effect and a 346 Hz peak due to the λ/2 microphone spacing.

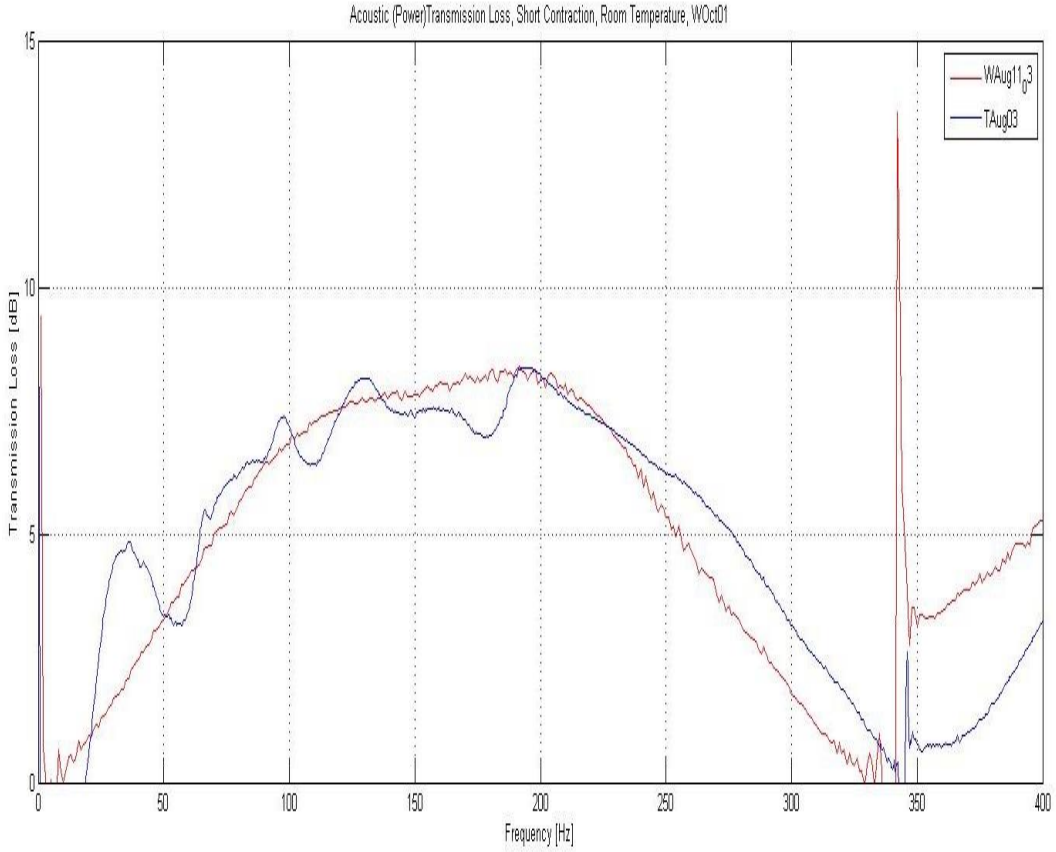

Figure 7.22 TL, Measured versus Modelling, Short (432.5 Mm Long) Contraction / Expansion Chamber, 0 to 400 Hz, (Experimental blue, Simulation red)

Figure 7.23 shows the measured and modelled results for the short contraction / expansion chamber over a 800 Hz range. The correlation is excellent apart from the speaker low frequency performance effect and the cut-on frequency limiting the measured results to below 600 Hz. There is a frequency shift in the higher frequencies that is consistent with WAVE underestimating the effective length of the contraction / expansion chamber and this will be the subject of further investigation.

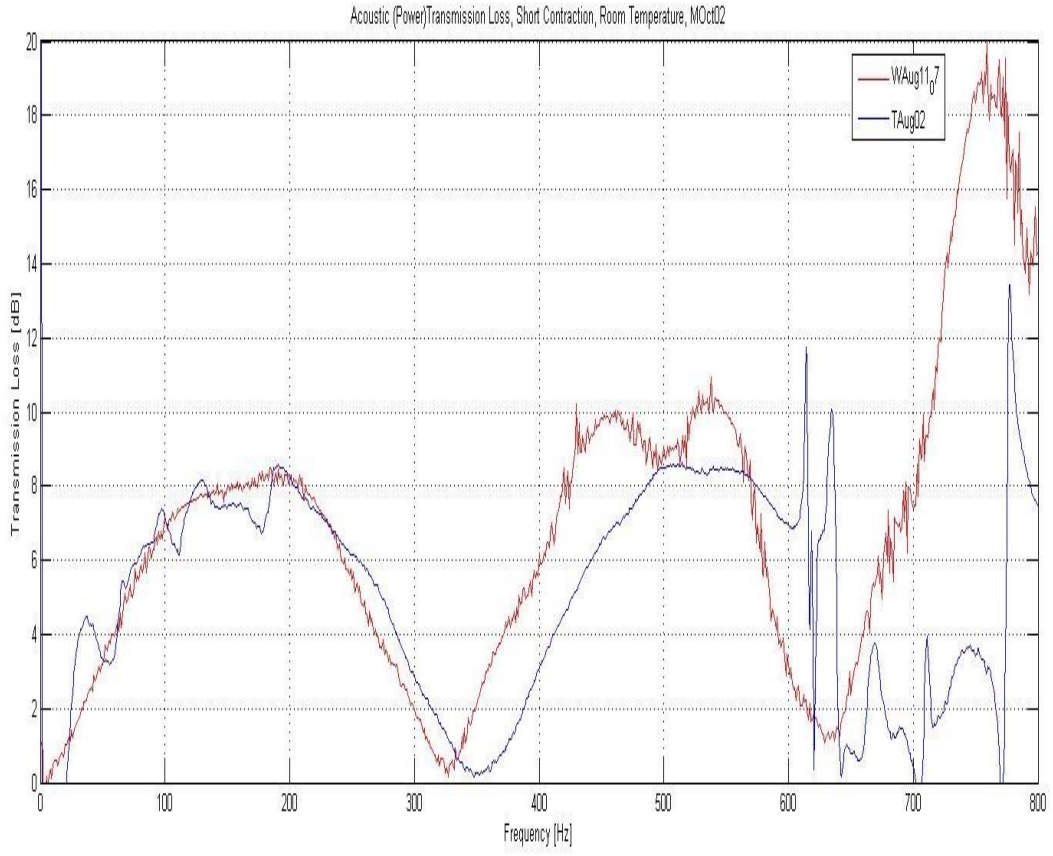

Figure 7.23 TL, Measured versus Modelling, Short (432.5 Mm Long) Contraction / Expansion Chamber, 0 to 800 Hz, (Experimental blue, Simulation red)

Figure 7.24 shows the measured and modelled results for the long expansion chamber over a 400 Hz range. The correlation is excellent apart from the speaker low frequency performance effect and a 346 Hz peak due to the λ/2 microphone spacing. Again there are frequency shifts in the higher frequencies which are consistent with WAVE underestimating the effective length of the contraction / expansion chamber.

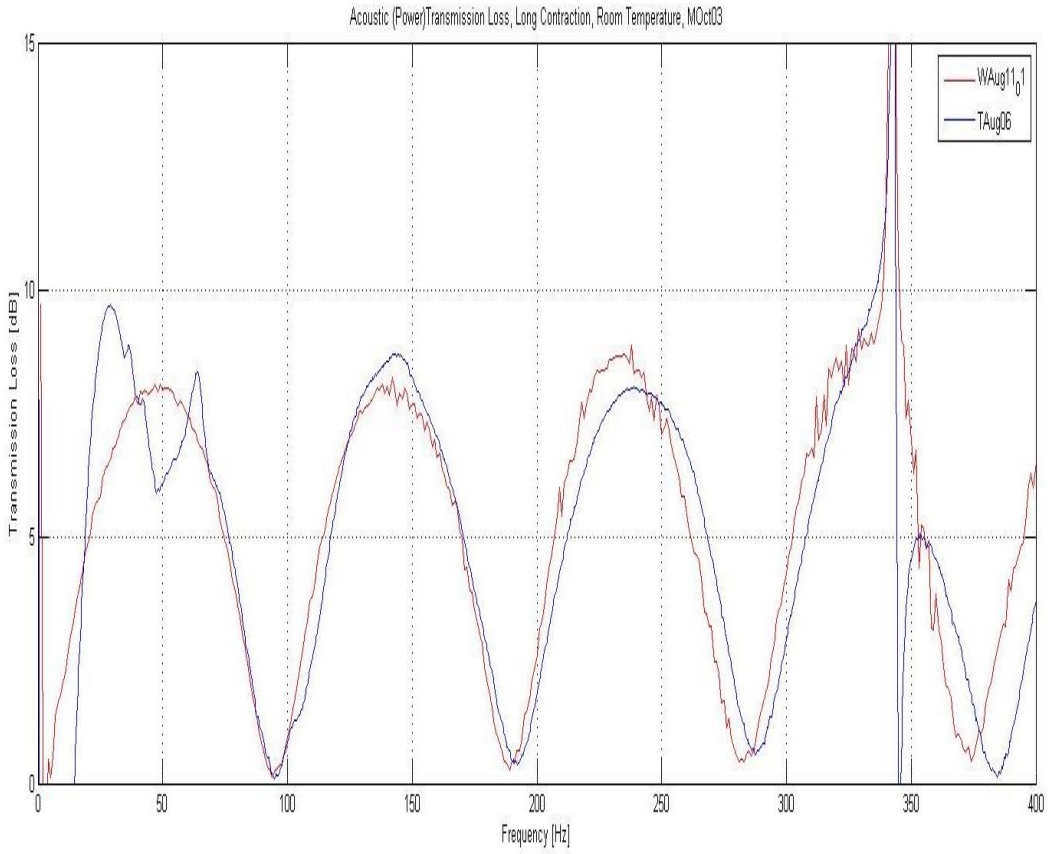

Figure 7.24 TL, Measured versus Modelling, Long (1730 Mm Long) Contraction / Expansion Chamber, 0 to 400 Hz, (Experimental blue, Simulation red)

Figure 7.25 shows the measured and modelled results for the long contraction / expansion chamber over a 800 Hz range. The correlation is excellent apart from the speaker low frequency performance effect and the cut-on frequency limiting the measured results to below 600 Hz. Again there are frequency shifts in the higher frequencies which are consistent with WAVE underestimating the effective length of the contraction / expansion chamber.

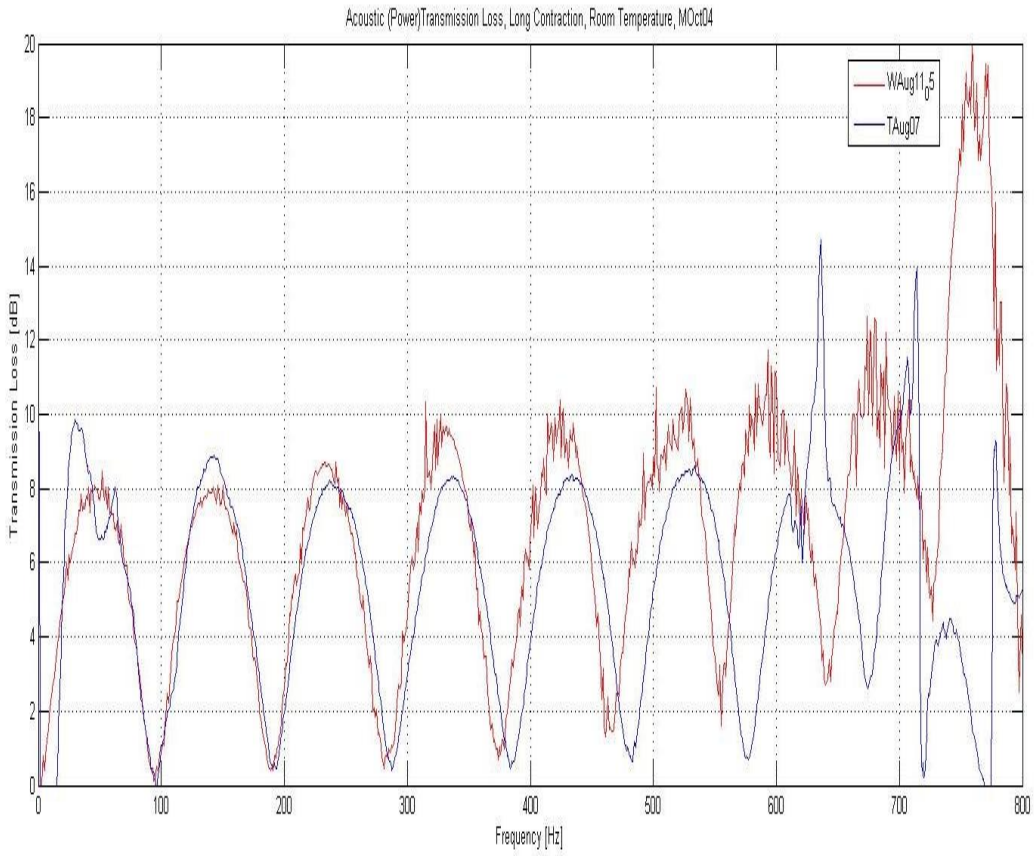

Figure 7.25 TL, Measured versus Modelling, Long (1730 Mm Long) Contraction / Expansion Chamber, 0 to 800 Hz, (Experimental blue, Simulation red)

7.6 Simplified Large Mufflers (LM)

7.6.1 Overview

These simplified large expansion chamber mufflers (Mufflers LM1 to LM10 inclusive) were described previously in Section 4.1.3 and were designed to examine possible iterations from a large single expansion chamber (LM1) to a typical large marine muffler (LM10 and LMM). These models were constructed and meshed in Wavebuild3D and the WAVE simulation for the simplified large mufflers was conducted under test bench conditions with a typical large marine diesel temperature of ≈ 430 °C. The large single expansion chamber (LM1) was also modelled using simple ducts (Muffler LM1 (ducts)).

7.6.2 Results: LM1 to LM10

The predicted acoustic transmission losses for all of the LM mufflers are shown in Figure 7.26 below.

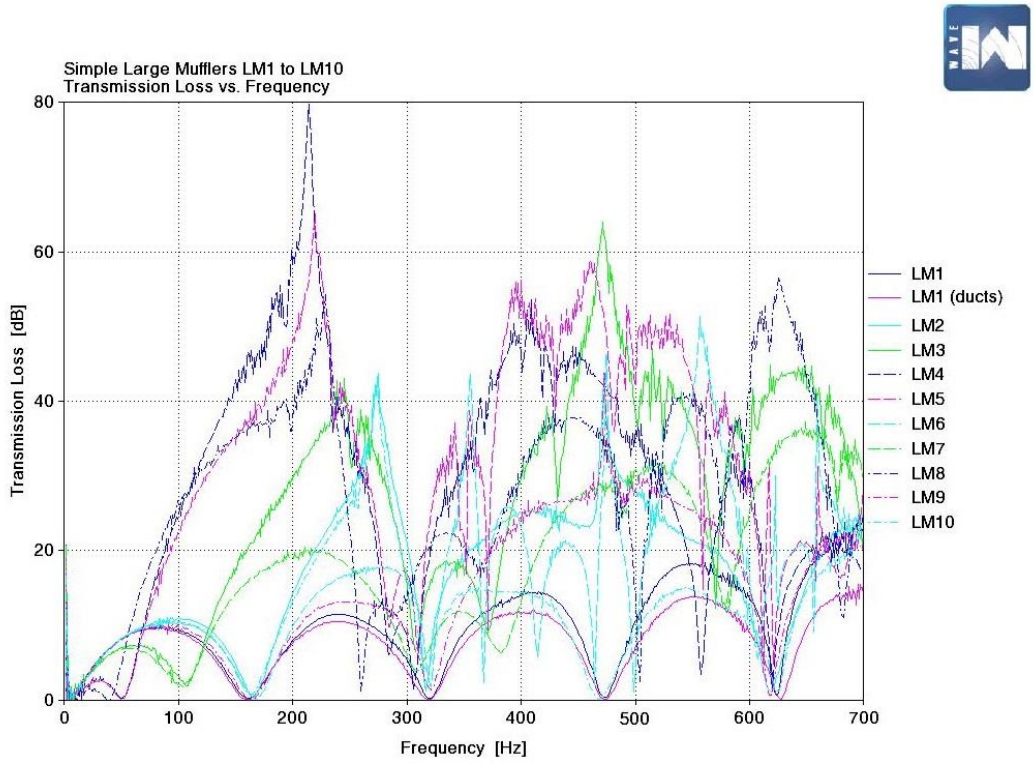

Figure 7.26 Transmission Loss of Simple Large Mufflers LM1 to LM10

It is clear that the predicted acoustic transmission loss showed high sensitivity to design changes. Muffler LM10 is complex and has twin expansion chambers, twin Helmholtz resonators (comprising the interconnecting tube and each volume), an extended inlet (quarter wave effect), extended outlet tube (quarter wave effect), the interconnecting tube (half wave resonances), and the extended section of the interconnecting tube (quarter wave effect) in each volume. The expected frequencies for each feature at 430 °C (speed of sound 530 m/s) with the exception of the Helmholtz resonators are summarised in Table 7-5 below. The Helmholtz resonator frequencies are not calculated as the volumes are not closed and the traditional formulae are not applicable. The quarter wave frequencies for the extended pipes and the half wave resonances of the interconnecting tube are for the uncorrected lengths and will be lower than that shown in the table.

Table 7-5 Expected Frequencies (Hz) for Design Elements

Muffler	Body λ/2	Chamber A, λ/2	Chamber B, λ/2	Extended Inlet λ/4	Extended Outlet λ/4	Centre Tube λ/2	Centre Tube λ/4	Centre Tube λ/4
Lengths (m)	1.675	0.75	0.925	0.4	0.185	0.61	0.13	0.48
LM1	158							
LM2	158			331	716			
LM3		353	286	331	716			
LM4		353	286	331	716	434	1019	276
LM5		353	286	331	716	434	1019	276
LM6	158			331	716			
LM7		353	286					
LM8		353	286			434	1019	276
LM9	158				716			
LM10	158			331				

To simplify the results and to show the effects of successive iterations, the ten mufflers were divided into four subsets similar to those used previously in the flow analysis.

7.6.3 Results: LM1, Meshed versus Ducts

To evaluate the effect of model meshing, a single large expansion comprised of three cylindrical ducts (LM1) was compared with the same geometry meshed into multiple 1D elements LM1 (ducts). The predicted acoustic transmission losses for each muffler are shown in Figure 7.27.

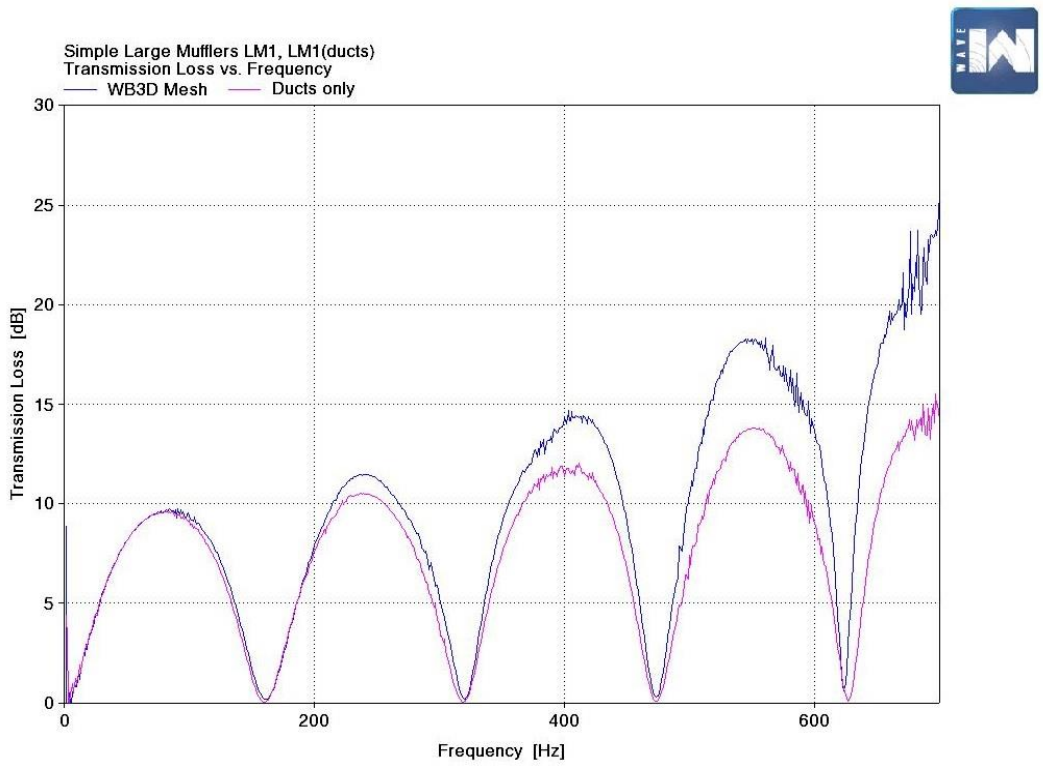

Figure 7.27 Simple Large Mufflers LM1 & LM1 (Ducts)

The null frequency of 158 Hz and its multiples are evident in both mufflers. The meshed muffler has progressively higher transmission loss than the simple ducts muffler. The reason for this is unclear and will be the subject of further investigation.

7.6.4 Results: LM1 to LM5

The progression is from a simple single expansion chamber (LM1) to a twin expansion chamber with interconnecting tube, angled extended inlet, and angled extended out let (LM5) with the intermediate steps (LM2, LM3, and LM4) included. The predicted acoustic transmission losses for each muffler are shown in Figure 7.28 below.

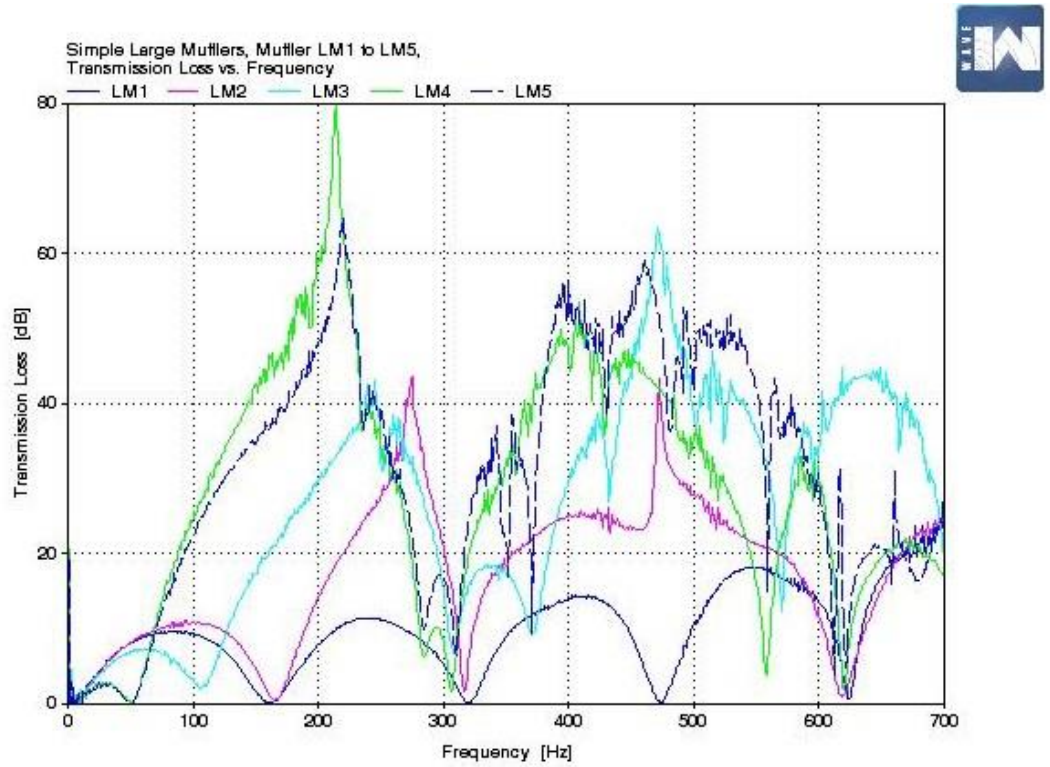

Figure 7.28 Simple Large Mufflers LM1 to LM5

Again, it is clear that the predicted acoustic transmission loss showed high sensitivity to design changes. The effectiveness of the Helmholtz resonator effect of the interconnecting tube is evident in LM4 and LM5.

7.6.5 Results: LM1 to LM2

This series consists of single expansion chamber mufflers (no centre baffle / interconnecting tube) with progression from a simple expansion chamber (LM1) to an expansion chamber with extended inlet, and extended outlet (LM2). The series splits the progression from LM1 to LM2 with LM9 which has only an extended outlet and LM10 which has only an extended inlet. The predicted transmission loss for each muffler is shown in Figure 7.29 below.

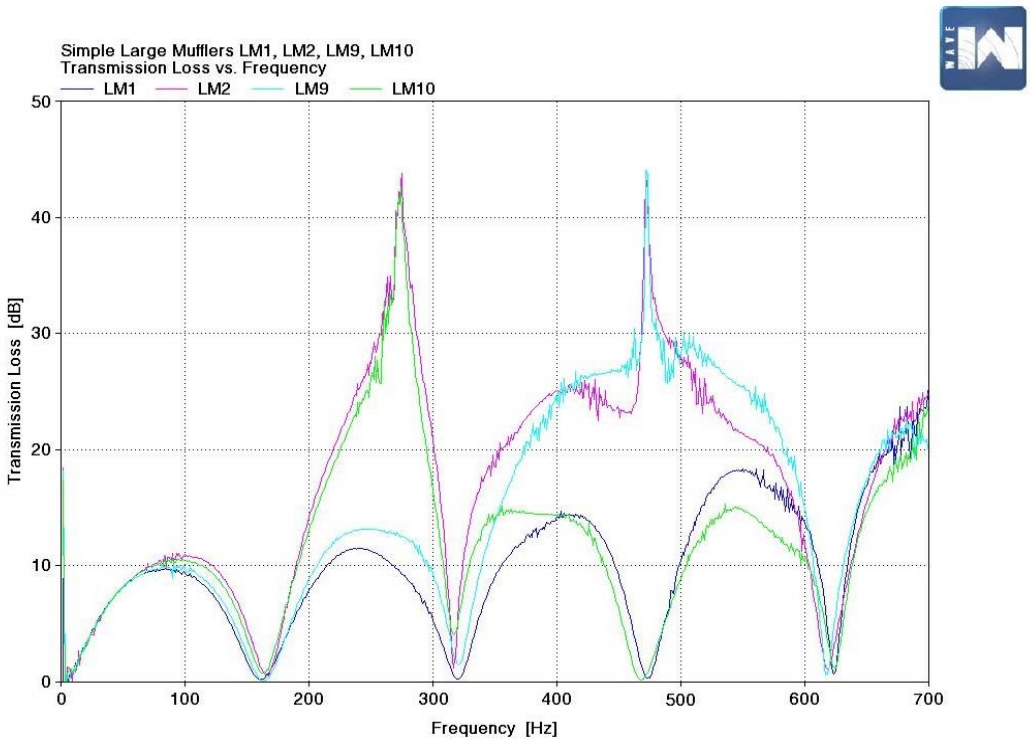

Figure 7.29 Simple Large Mufflers LM1, LM2, LM9 & LM10

The extended outlet of LM9 shows a resonance at 473 Hz which is lower as expected than the 716 Hz for the uncorrected length. The extended inlet of LM10 shows a resonance at 274 Hz which is lower as expected than the 331 Hz for the uncorrected length. The results are logical and as expected.

7.6.6 Results: LM1, LM2, LM6

This series consists of single expansion chambers with no centre baffle or interconnecting tube. The series makes the progression from LM1 to LM2 with coaxial extended elements to LM6 which has the extended inlet and extended outlet at angles to the body. The predicted acoustic transmission losses for each muffler are shown in Figure 7.30 below.

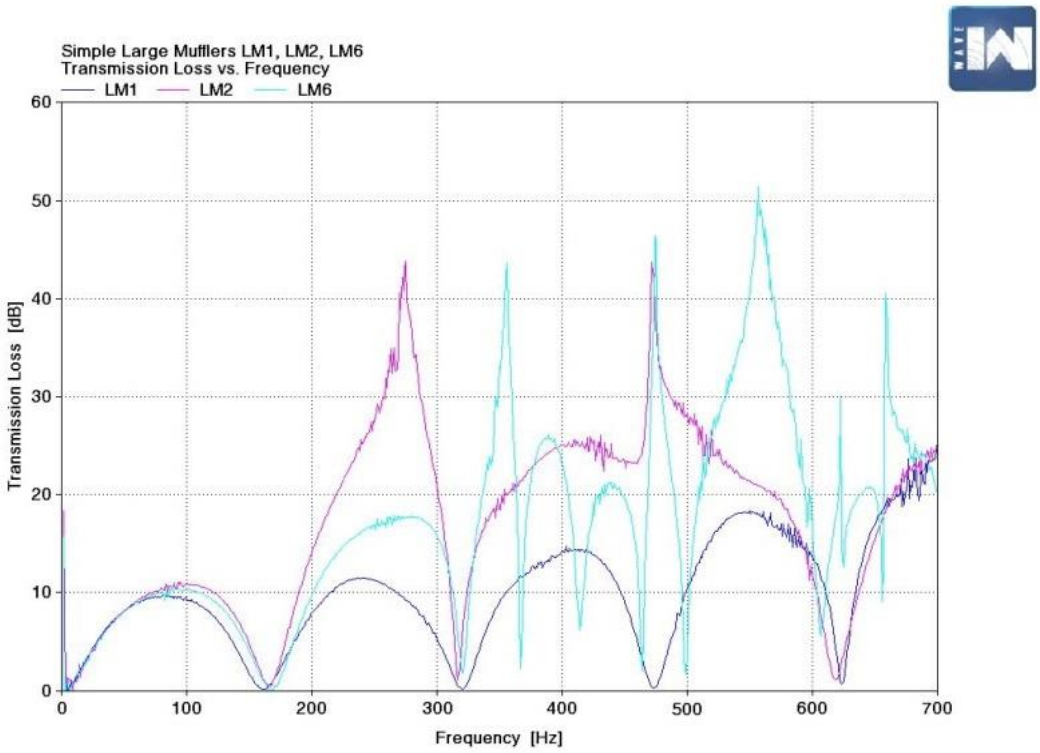

Figure 7.30 Simple Large Mufflers LM1, LM2, & LM6

The progression from LM2 to LM6 effectively reduces the lengths of the extended inlet and outlet which increases the corresponding resonant frequencies.

7.6.7 Results: LM1, LM7, LM8

The progression is from simple expansion chamber (LM1) to twin expansion chamber (LM8). This series consists of single expansion chambers with no extended inlets or extended outlets. The series makes the progression from LM1 to LM7 with a centre baffle to LM8 with centre baffle and interconnecting tube. The predicted acoustic transmission losses for each muffler are shown in Figure 7.31 below.

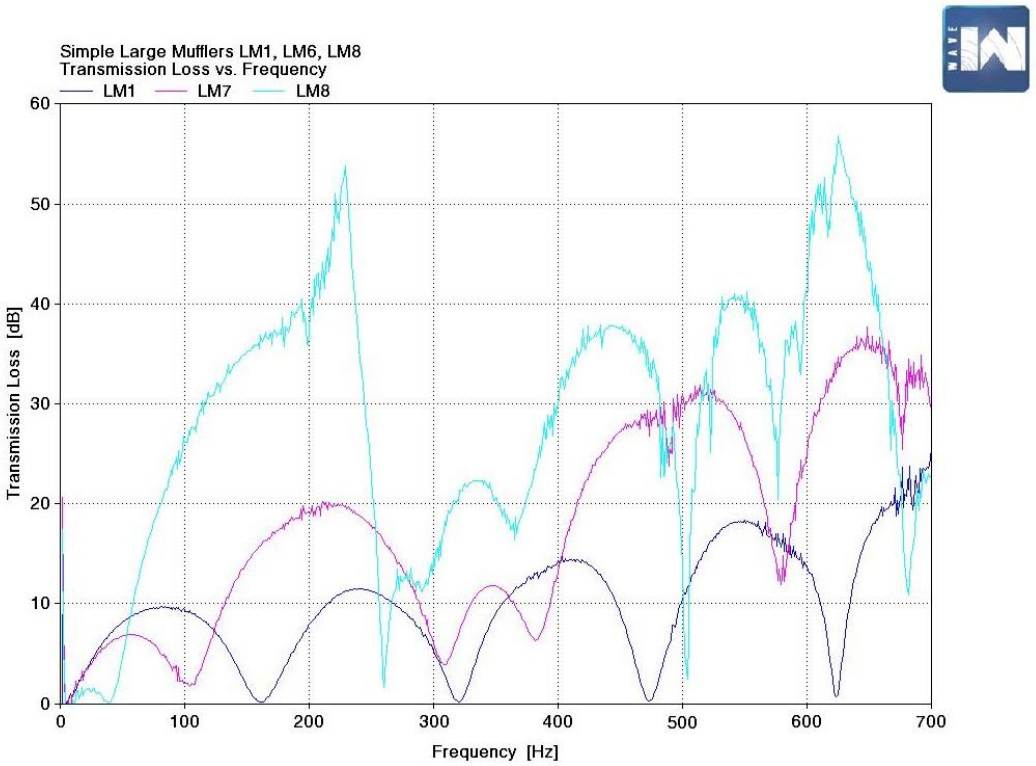

Figure 7.31 Simple Large Mufflers LM1, LM7, & LM8

The twin expansion chamber effect of LM7 is evident with increased transmission loss and a shift in the frequencies of the peaks and the nulls. The effectiveness of the Helmholtz resonator effect of the interconnecting tube is again evident in LM8.

7.6.8 Overall Result

The predicted acoustic transmission losses showed high sensitivity to design changes and expected agreement with theory.

7.7 Large Marine Muffler (LMM)

7.7.1 Overview

The large marine muffler (Mufflers LMM) was described previously and while different dimensionally to those fitted to CCSM's it is similar in concept. The model was imported from a CAD drawing and meshed in WaveBuild3D. It was modelled at an ambient temperature of 25°C to match the experimental test bench conditions with two frequency ranges – 0 to 400 Hz and 0 to 700 Hz. The discretisation size in the direction of flow (dx) was selected to break the wavelength of the highest frequency of interest into six to ten increments. During the modelling of this muffler, it was apparent that the modelling showed sensitivity to the discretisation size (dx, dy, dz, and dtube) and a mesh size sweep was attempted. Limitations on the number of elements within WAVE precluded a smaller mesh so a larger version of the software called Ricardo BIGWAVE was used. This software enables more elements but results in much longer run times. Table 7-6 shows the discretisation sizes for each of the four datasets.

Table 7-6 Muffler LMM Discretisation Sizes

Dataset	Frequency Range	dx (mm)	dy (mm)	dz (mm)	dtube (mm)	Program
WMay18_02	400 Hz	125	100	100	100	WAVE
WMay18_05	700 Hz	80	150	150	80	WAVE
WFeb17_20	400 Hz	80	80	80	80	BIGWAVE
WFeb17_21	700 Hz	80	80	80	80	BIGWAVE

Table 7-7 shows the mesh statistics and compares these to the maximum values allowable in WAVE and BIGWAVE.

Table 7-7 Muffler LMM Mesh Statistics

Dataset	Frequency Range	Cavities	Tubes	Y-junctions	Ducts	Total Y-junctions & ducts
WMay18_02	400 Hz	1	2	737	2041	2778
WMay18_05	700 Hz	1	2	626	1700	2326
WFeb17_20	400 Hz	1	2	1706	4958	6664
WFeb17_21	700 Hz	1	2	1706	4958	6664
WAVE Parameter				KMAX	LMAX	JMAX
WAVE Limit				1500	2000	3000
BIGWAVE Limit				4500	7500	11250

7.7.2 Results: Large Marine Muffler LMM

The predicted acoustic transmission losses using WAVE and BIGWAVE are shown in Figure 7.32 and Figure 7.33 and are consistent with simplified Muffler LM5. The variations in transmission loss with discretisation size are high and warranted further investigation. As shown in the previous work with the simplified mufflers, the transmission loss peak in the 150 to 250 Hz ranges is most likely due to the Helmholtz resonator effect of the interconnecting tube. The WAVE / BIGWAVE modelling may not be capturing this muffler's particular geometry correctly and thus exacerbating the sensitivity to discretisation size.

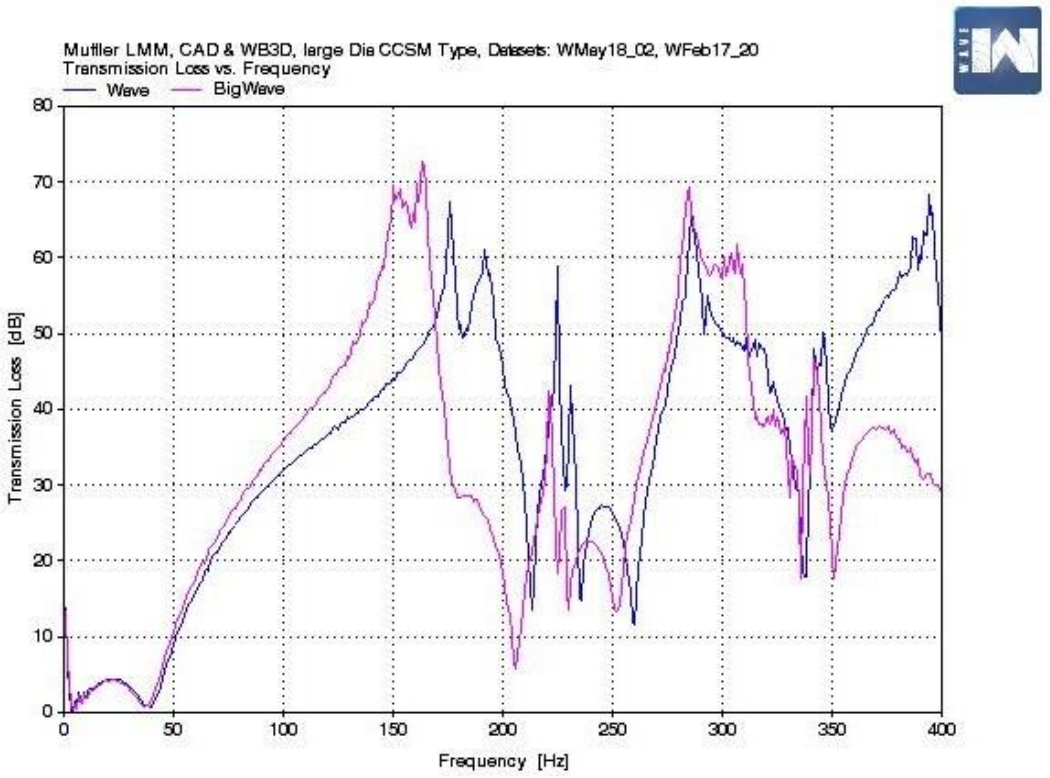

Figure 7.32 Muffler LMM, WAVE & BIGWAVE Transmission Loss, 0 to 400 Hz

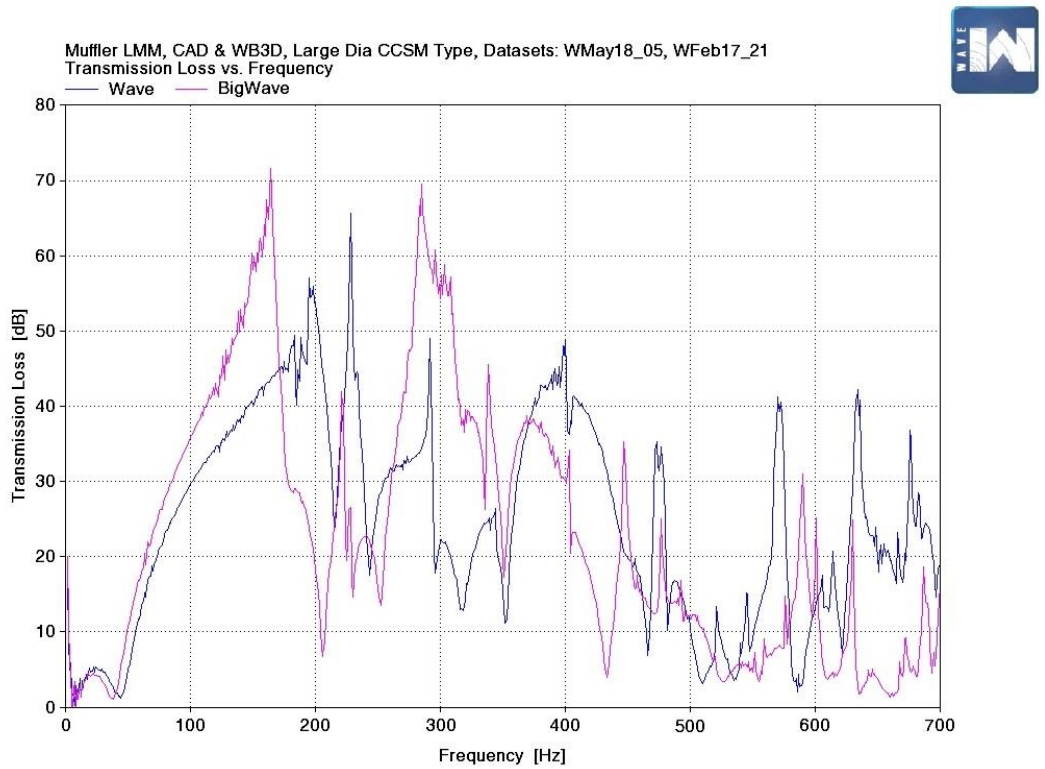

Figure 7.33 Muffler LMM, WAVE & BIGWAVE Transmission Loss, 0 to 700 Hz

7.8 Discretisation Study Muffler B, 250 Hz

7.8.1 Overview

As the modelling in Section 7.7 showed high sensitivity to the discretisation size (dx, dy, dz, and dtube), a sweep of mesh size was attempted. The transmission loss peak in the 150 to 250 Hz range was selected as it showed high variation with discretisation size and dominates the low frequency attenuation. An upper limit of 250 Hz was chosen for this study to enable a larger dx value which then permitted more elements in the lateral and vertical directions without exceeding the program limits. Again, an ambient temperature of 25 °C was selected for the modelling to match the expected experimental test bench ambient conditions. For an ambient temperature of 25 °C, the speed of sound is 346 m/s. At 250 Hz the corresponding wavelength is 1.385 m and one sixth of this is 225 mm and one tenth of this is 140 mm. So the dx values in this sensitivity study included both larger and smaller values as shown in Table 7-8 compared to the "optimum" 140 mm. This table is colour coded to highlight common parameters amongst the datasets.

Table 7-8 Discretisation Steps for Study at 250 Hz

Data set	dx (mm)	dy (mm)	dz (mm)	dtube (mm)
WJan23_05	50	200	200	100
WJan23_04	75	200	200	100
WJan23_03	100	200	200	100
WJan17_01	140	100	100	100
WJan23_01	140	100	100	100
WJan24_04	140	105	105	100
WJan24_03	140	110	110	100
WJan16_01	140	125	125	100
WJan23_02	140	200	200	100
WJan24_02	140	250	250	100
WJan24_01	140	300	300	100
WJan23_06	200	200	200	100
WJan24_05	225	80	80	100
WJan17_02	225	100	100	100
WJan16_02	225	125	125	100
WJan24_06	225	200	200	100

7.8.2 Results: dx sweep, dy & dz 200 mm

This comparison is a sweep of dx in steps from 50 mm to 255 mm while keeping dy and dz constant at 200 mm. The predicted transmission losses are shown in Figure 7.34 below. The results for each dx are relatively similar with the exception of a dx of 75 mm which exhibits a unique and unexplained peak at 167 Hz. At 167 Hz the sound wavelength is approximately two metres, so there is no obvious connection to a dx of 75 mm and warrants further investigation.

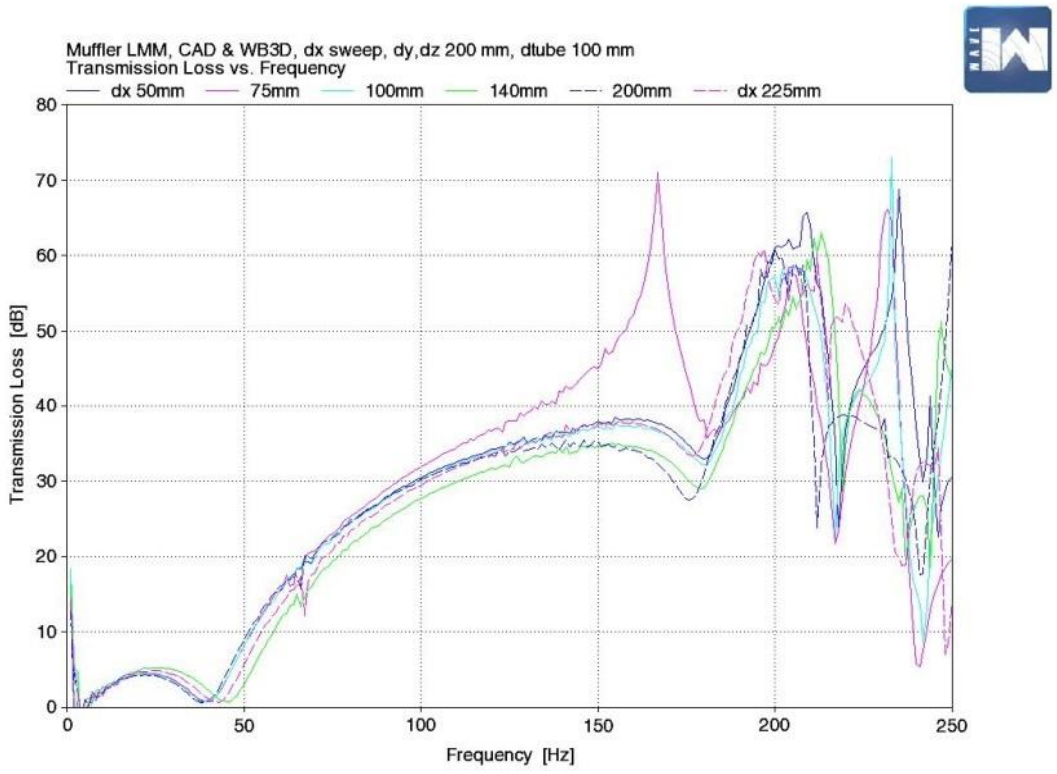

Figure 7.34 Transmission Loss Sensitivity to Mesh Size, Sweep of dx, dy & dz 200 mm

7.8.3 Results: dy & dz sweep, dx 140 mm

This comparison is a sweep of dy and dz in steps from 100 mm to 300 mm while keeping dx constant at 140 mm. The predicted transmission losses are shown in Figure 7.35 below. The results for each dy / dz step show substantial variations in the shape and magnitude of the predicted transmission loss even for small changes, e.g. 100, 105, and 110 mm.

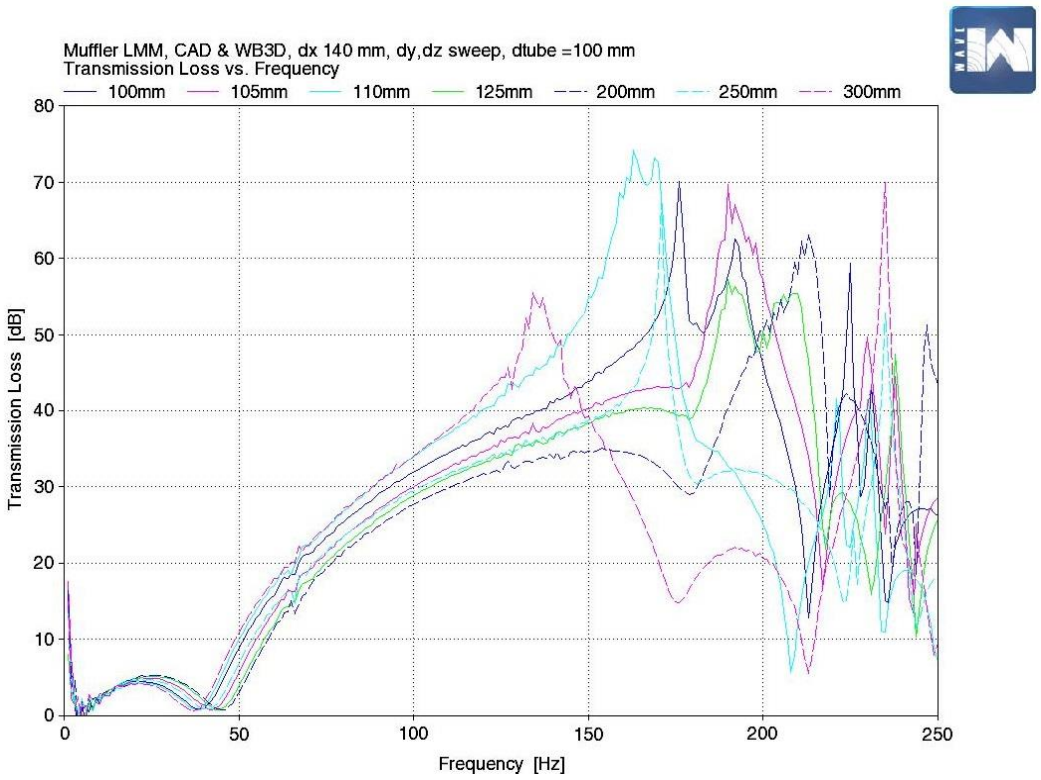

Figure 7.35 Transmission Loss Sensitivity to Mesh Size, Sweep of dy / dz, dx 140 mm

7.8.4 Results: dx 140 & 225 mm , dy & dz 100 mm

This is a comparison of dx's of 140 and 225 mm for a constant dy / dz of 100 mm. The predicted transmission losses are shown in Figure 7.36 below. The results for each dx are similar with the exception of the peak transmission loss which occurs at a higher frequency and splits into two peaks for the dx of 140 mm.

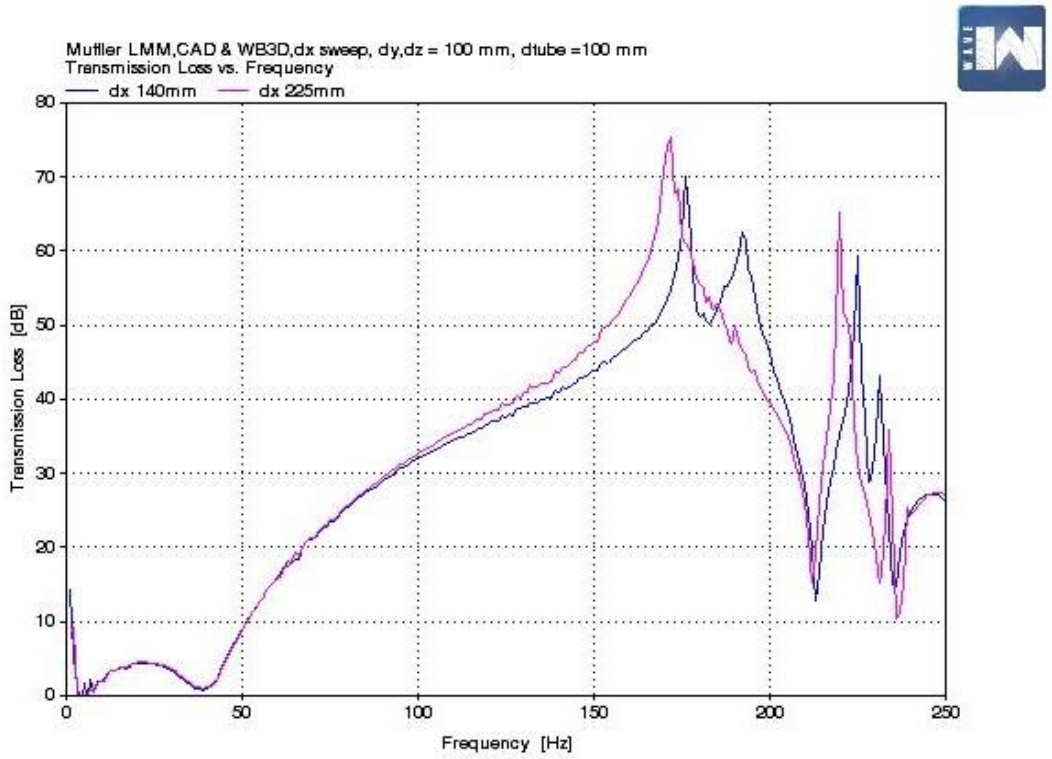

Figure 7.36 Transmission Loss Sensitivity to Mesh Size, Sweep of dx 140 & 225 mm, dy / dz 100 mm

7.8.5 Results: dy & dz sweep, dx 225 mm

This comparison is a sweep of dy and dz in steps from 80 mm to 200 mm while keeping dx constant at 225 mm. The predicted transmission losses are shown in Figure 7.37 below. The results for each dy / dz step show substantial variations in the shape and magnitude of the predicted transmission loss. The peak transmission loss occurs at increasing frequencies as dy / dz increase.

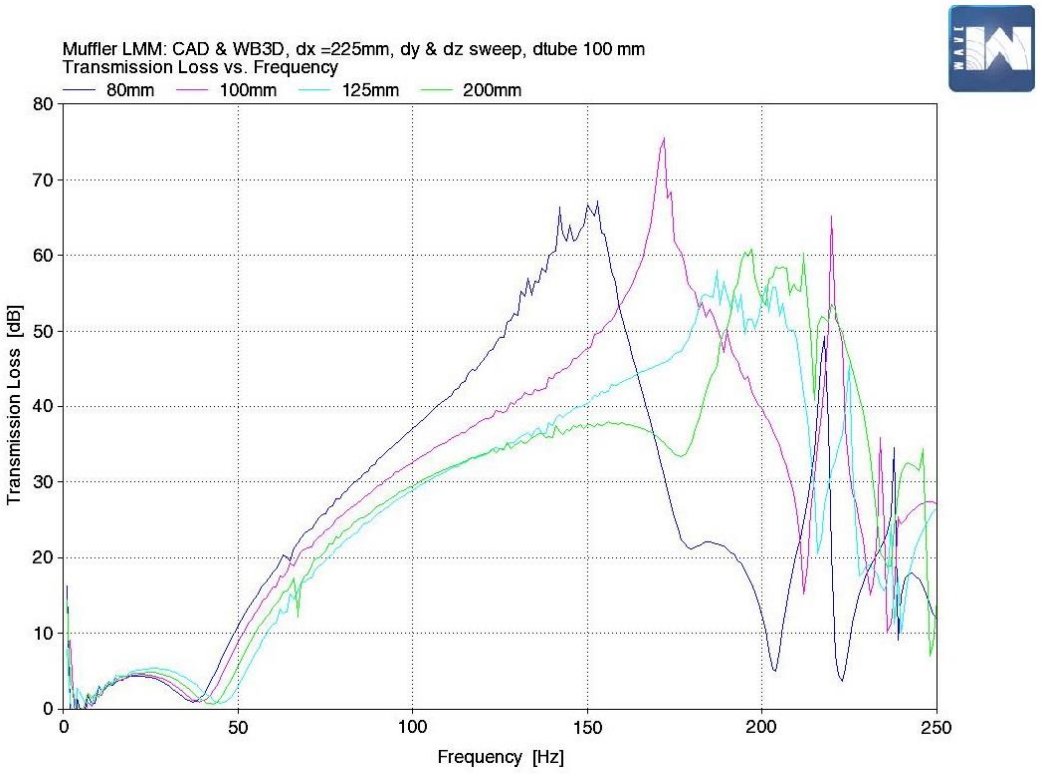

Figure 7.37 Transmission Loss Sensitivity to Mesh Size, Sweep of dy / dz, dx 225 mm

7.8.6 Results: dx 140 & 225 mm , dy & dz 125 mm

This is a comparison of dx's of 140 and 225 mm for a constant dy / dz of 125 mm. The predicted transmission losses are shown in Figure 7.38 below. The results for each dx are very similar with a slight variation in the shape of the peak transmission loss.

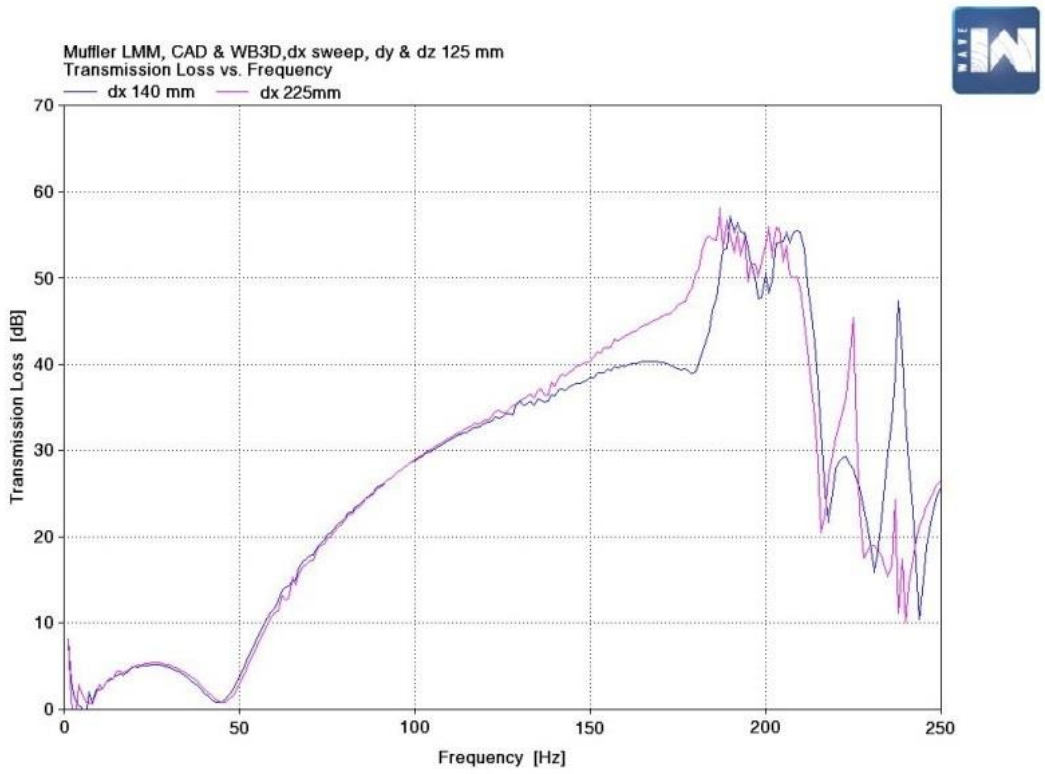

Figure 7.38 Transmission Loss Sensitivity to Mesh Size, Sweep of dx 140 & 225 mm, dy / dz 125 mm

Chapter 8 FEA Modelling of Muffler Shell

This chapter describes finite element analysis of the LMM muffler and presents and discusses results for the first 20 modes.

8.1 Overview

The WAVE modelling in this study assumes that this is no interaction between acoustic and structural modes with the shell being regarded as rigid with no coupling to the acoustic modes. This may be valid at certain frequencies but is unlikely across the frequency range of interest. At certain frequencies the acoustic energy will excite structural modes which will in turn excite acoustic cavity modes. To ascertain the structural behaviour, a three dimensional (3D) finite element analysis (FEA) of the muffler shell was undertaken using a student version of ANSYS software. ANSYS is a leading FEA software package capable of simulating fluid dynamics, structural mechanics, electromagnetics, and structures and multi-physics [78].

8.2 Modelling

The physical geometry of Muffler LMM was imported from an Autodesk Inventor CAD file and 3D meshed as shown in Figure 8.1 using tetrahedral elements. These elements called Tet10 are shown in Figure 8.2 and have nodes at their apexes and edge midpoints with the edges not necessarily being straight. In a typical application this muffler would be supported vertically by flexible isolators and rigidly bolted via flanges to many metres of heavy wall rigid pipe before and after the muffler. These pipes would also be flexibly connected axially to the engine and ship structure by metal bellows and supported vertically by a combination of the metal bellows and flexible isolators. The FEA analysis concentrated on the muffler itself rather than whole body structural modes likely to be encountered in the ship installation. Consequently the model constraints / supports chosen do not reflect the ship installation but concentrated on those modes likely to influence acoustic performance – the internal structure and the external shell. Constraints / supports for the muffler consisted of a “fixed support” on the inlet flange face and a “frictionless support” on the outlet flange face respectively as shown in Figure 8.3 and Figure 8.4 respectively.

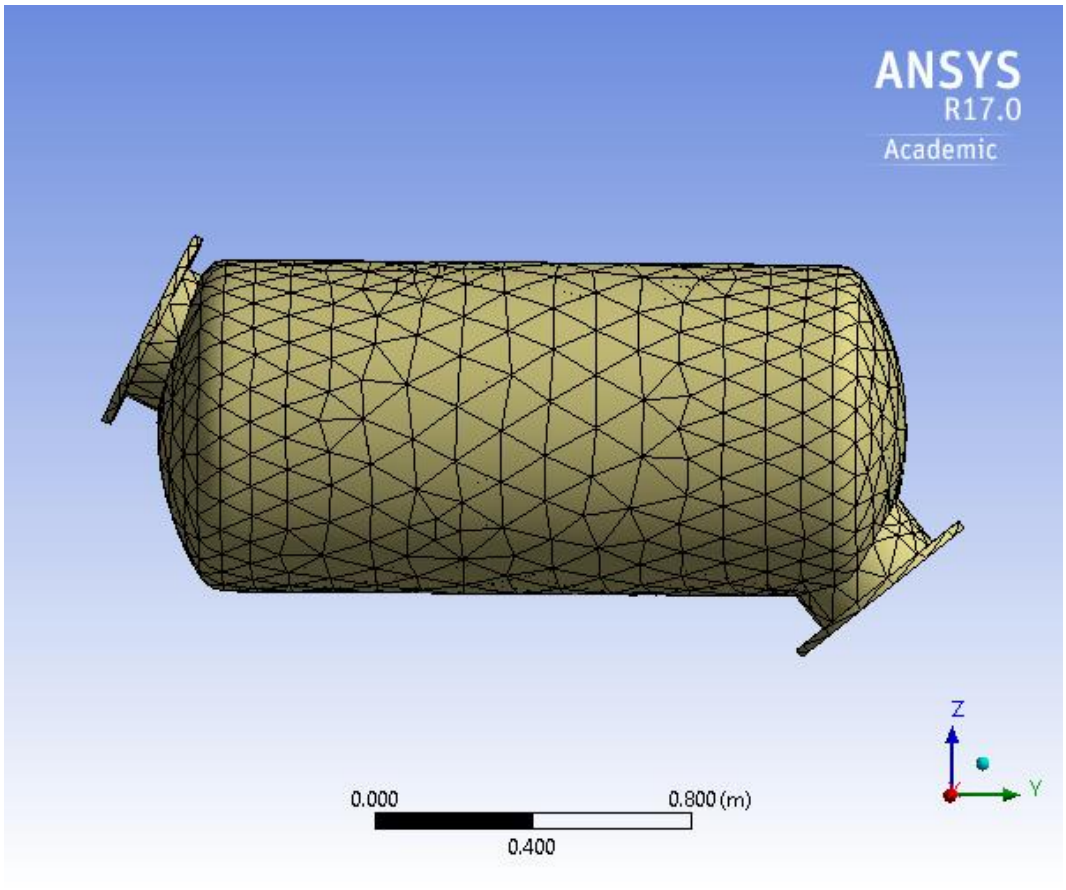

Figure 8.1 Muffler LMM Meshed in ANSYS

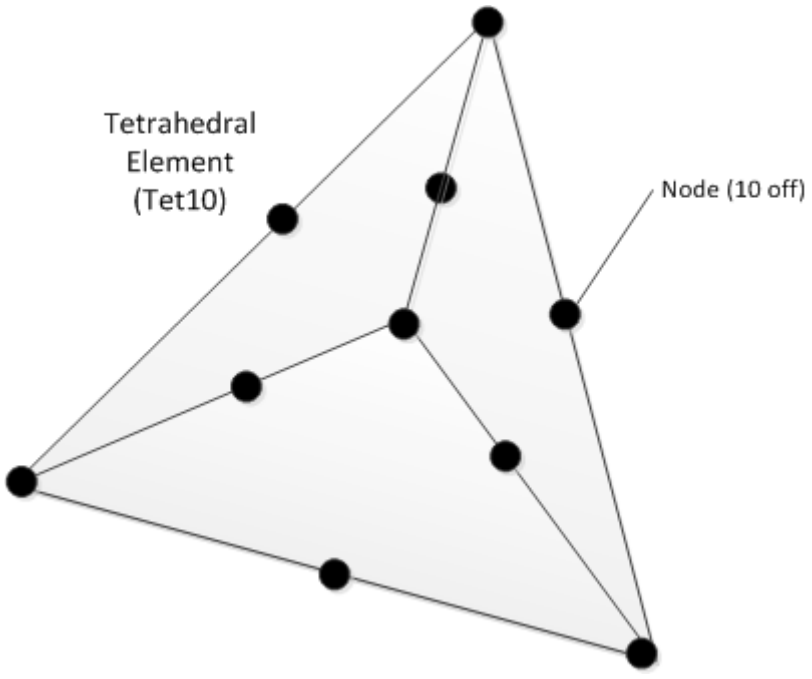

Figure 8.2 Tetrahedral Element, Ten Nodes

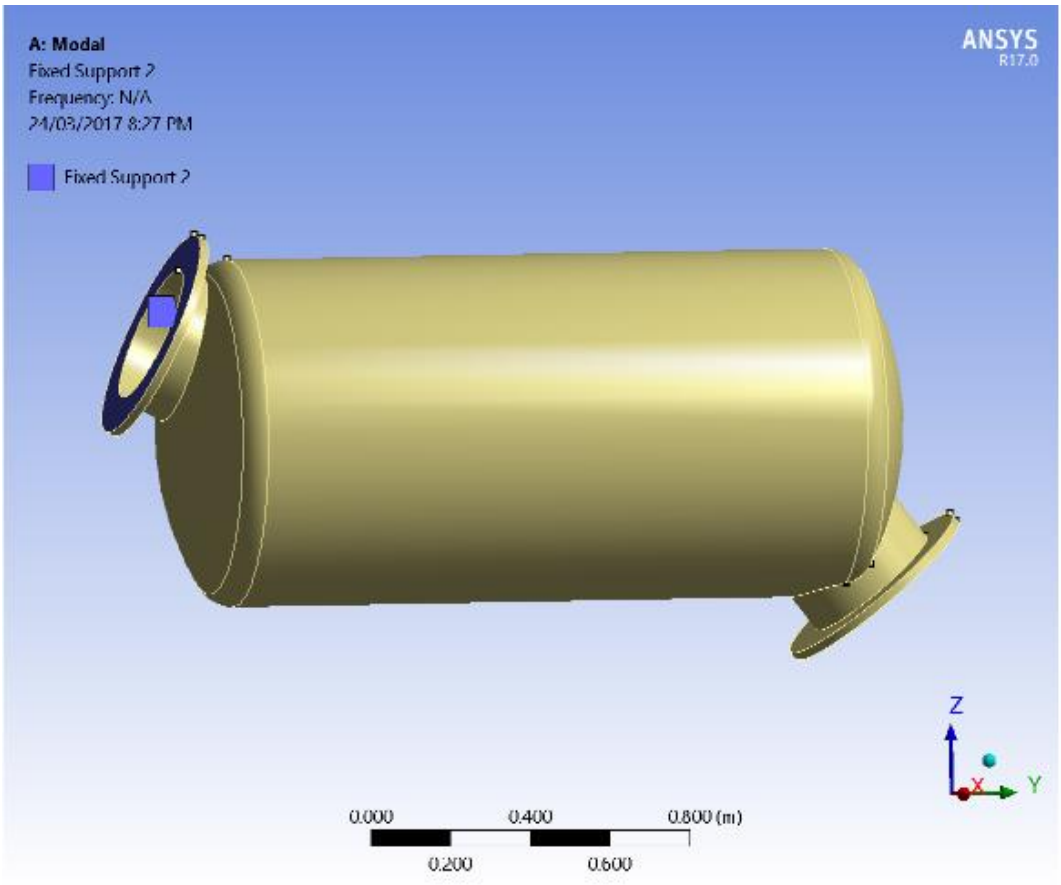

Figure 8.3 Muffler LMM, Constraint of "Fixed Support" on Inlet Flange Face

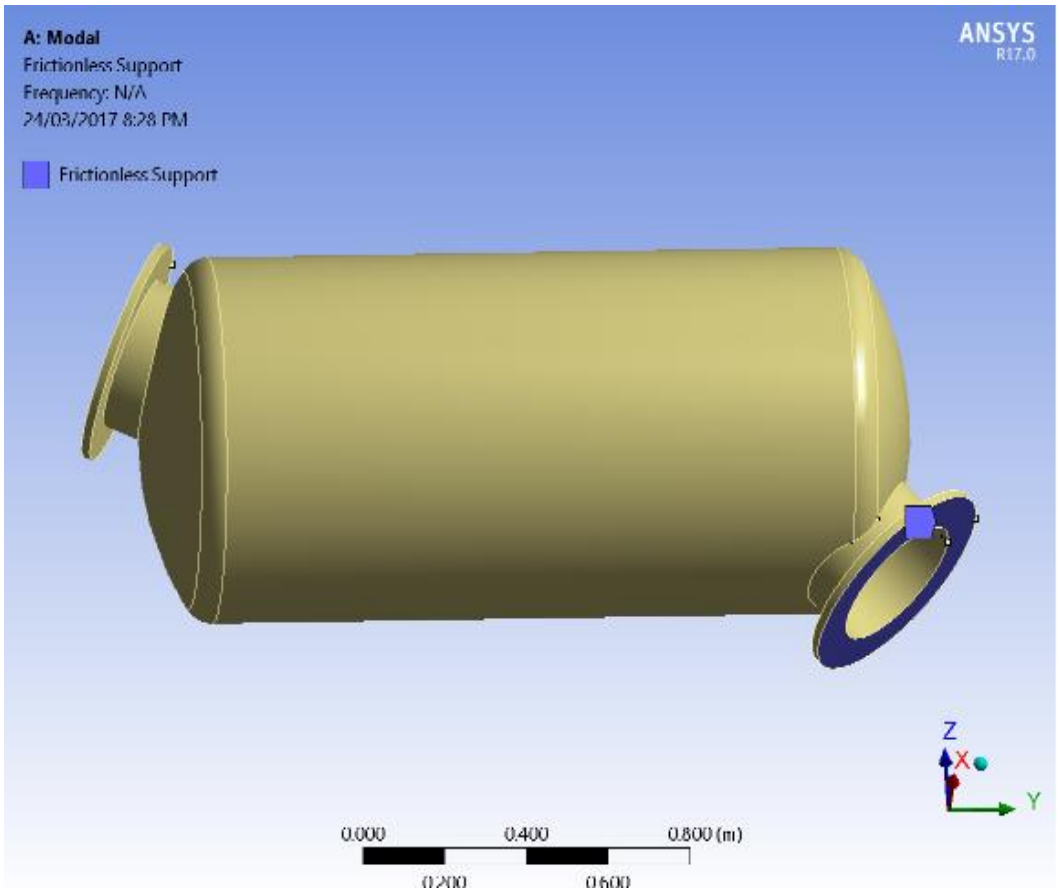

Figure 8.4 Muffler LMM, Constraint of "Frictionless Support" on Outlet Flange Face

The ANSYS meshing and analysis parameters are summarised in Table 8-1 with further detail shown in Appendix A.

Table 8-1 FEA Meshing and Analysis Parameters

ANSYS Analysis Parameters	
Analysis Type	3D, Modal
Physics Preference	Mechanical
Physics Type	Structural
Element Type	Tetrahedron, 10 nodes (Tet10)
No of Elements	8206
No of Nodes	16218
Material	Structural Steel
Material Density (kg/m^3)	7850
Material Young's Modulus (Pa)	2 E+011
Material Bulk Modulus (Pa)	1.6667 E+011
Material Shear Modulus (Pa)	7.6923 E+010
Material Poisson's Ratio	0.3
Environmental Temperature (°C)	22

The FEA modal analysis derived the first 20 structural modes with Table 8-2 summarising the mode frequencies and their descriptions. ANSYS can produce videos showing the animated mode shapes and these were used to analyse the mode shapes. The modes were grouped according to the similarity of the modes with an example of each type showing exaggerated total deformations in Figure 8.5 to Figure 8.10 inclusive. Similar figures for each of the 20 modes are included in Appendix A. The limit of 20 modes was chosen to give an upper frequency limit of 725 Hz. The analysis Project Report generated by ANSYS is also included in Appendix A.

Table 8-2 FEA Derived Modes of Muffler LMM

Mode number	Frequency (Hz)	Mode Description
1	42	Whole body lateral oscillation around inlet tube
2	128	Whole body vertical oscillation around inlet tube
3	220	Whole body rotary oscillation around inlet tube
4	266	Vertical oscillation / rotation of centre tube with flexing of internal wall
5	290	Lateral oscillation / rotation of centre tube with flexing of internal wall
6	340	Vertical oscillation / rotation of centre tube with flexing of internal wall
7	366	Vertical bending mode of body with fore / aft oscillation of centre tube with flexing of internal wall
8	407	Lateral bending mode of body with lateral oscillation of centre tube with flexing of internal wall
9	471	Ring mode on centre tube on outlet side
10	507	Ring mode on centre tube on outlet side and ring mode of body on outlet side.
11	511	Ring mode on centre tube on outlet side
12	518	Higher order ring mode on centre tube on outlet side and higher order ring mode of body on outlet and inlet side.
13	536	Higher order ring mode of body on outlet and inlet side (slight).
14	540	Ring mode on inlet tube.
15	558	Ring mode on inlet tube.
16	588	Higher order ring mode of body on outlet side and inlet side (slight).
17	617	Higher order ring mode of body on outlet side and inlet side (slight).
18	668	Higher order ring mode of body on outlet side and inlet side (slight).
19	688	Higher order ring mode of body on outlet side and inlet side (slight).
20	714	Higher order ring mode of body on inlet side and outlet side (slight).

The mode shapes were grouped and colour coded as follows:

1. Modes 1, 2 and 3 are artifices of the way the muffler was supported in the analysis and are accordingly disregarded.

2. Modes 4, 5 and 6 are oscillations / rotations of the centre tube with flexing of the centre baffle. Figure 8.5 shows Mode 4 at 266 Hz.

3. Modes 7 and 8 are bending modes of the body with flexing of the centre baffle. Figure 8.6 shows Mode 7 at 367 Hz.

4. Modes 9 and 11 are ring modes on the centre tube on the outlet side. Figure 8.7 shows Mode 11 at 511 Hz.

5. Modes 10 and 12 are ring modes on the centre tube on the outlet side and ring modes of the body. Figure 8.8 shows Mode 10 at 507 Hz.

6. Modes 14 and 15 are ring modes of the inlet tube. Figure 8.9 shows Mode 15 at 558 Hz.

7. Modes 13, 16, 17, 18, 19, and 20 are higher order ring modes of the body on the outlet and inlet side. Figure 8.10 shows Mode 19 at 688 Hz.

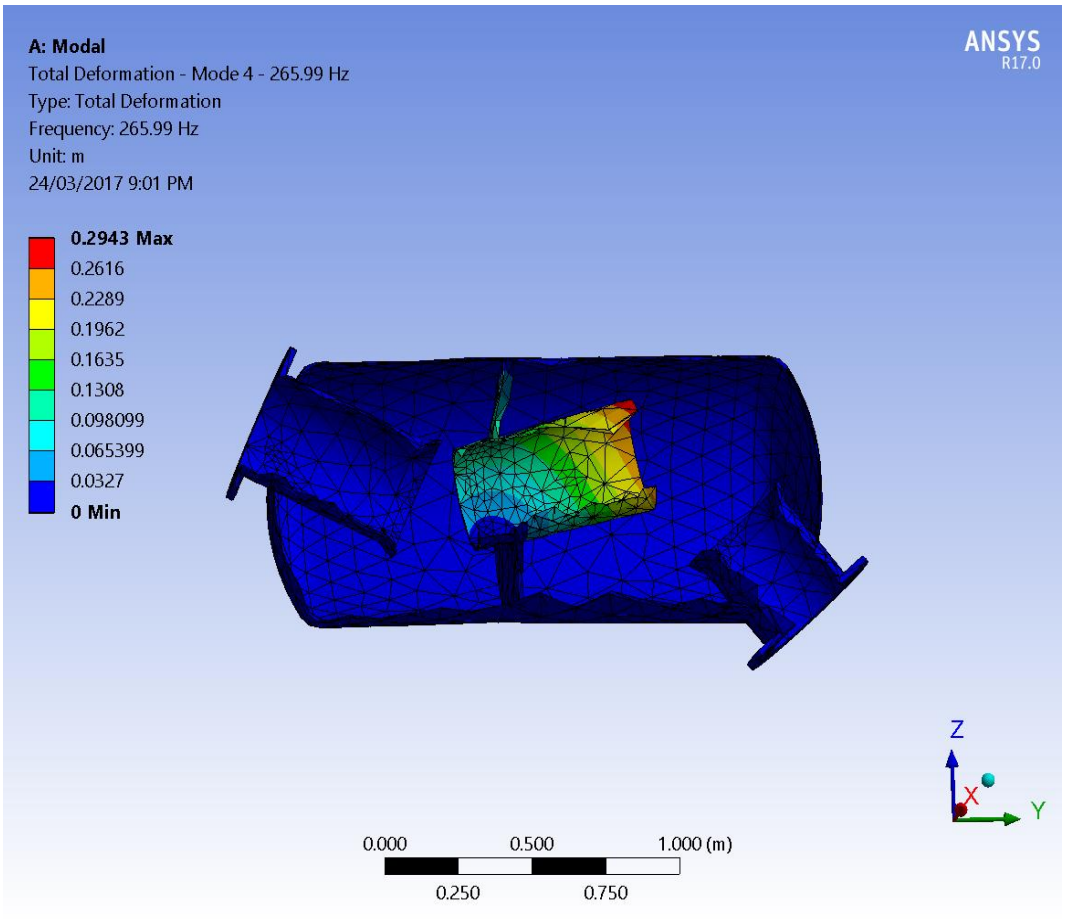

Figure 8.5 Mode 4 Total Deformation, 266 Hz

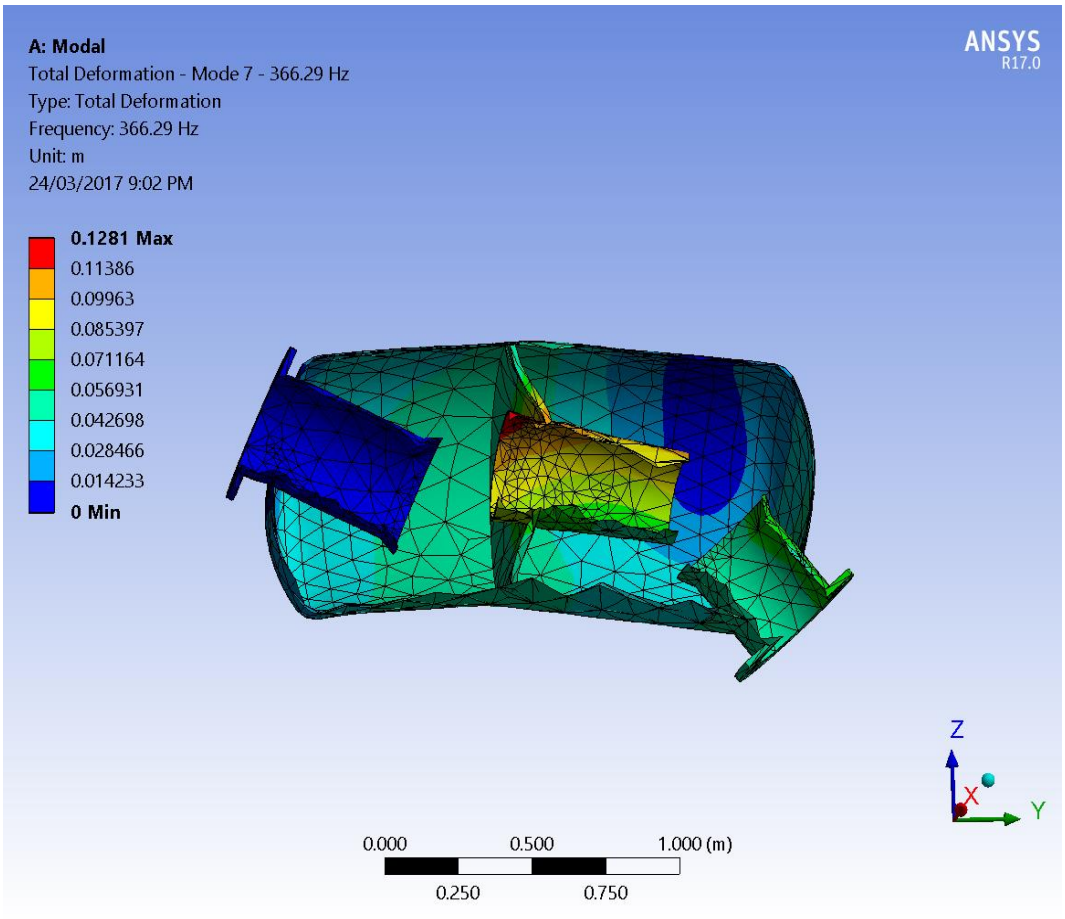

Figure 8.6 Mode 7 Total Deformation, 366 Hz

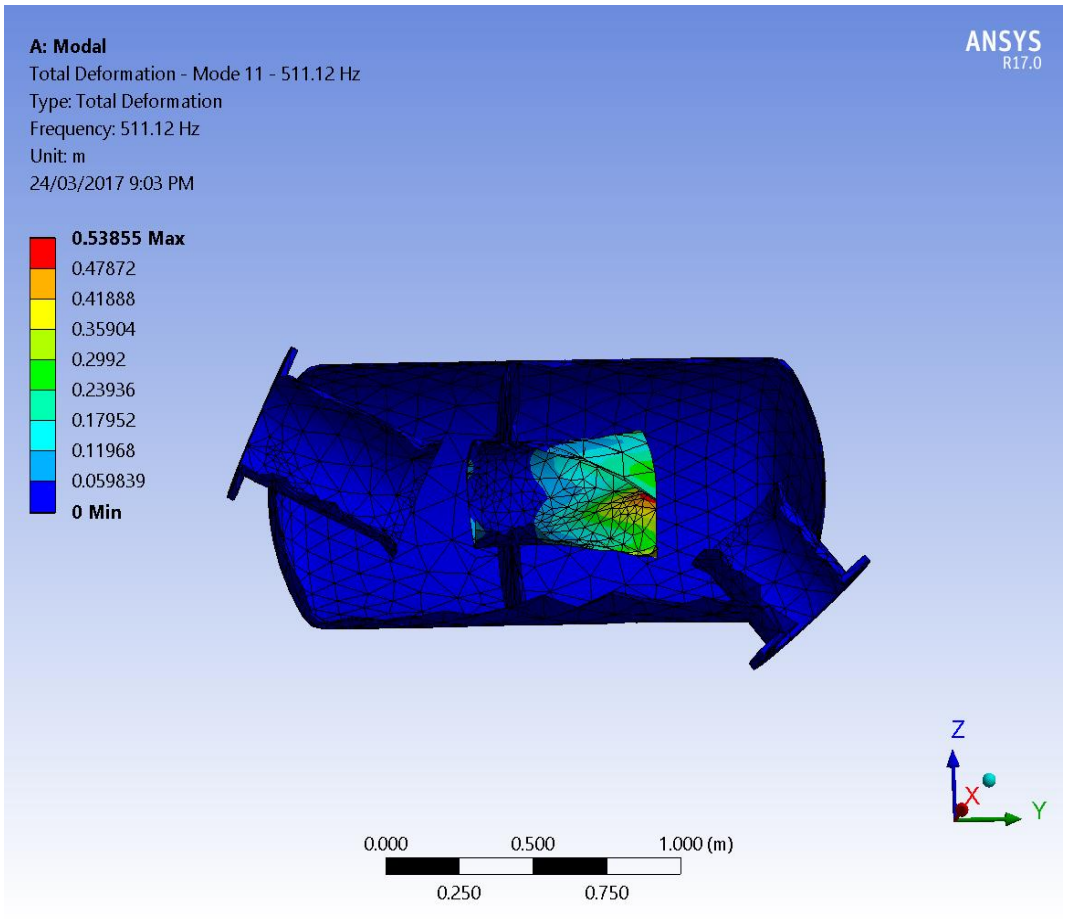

Figure 8.7 Mode 11 Total Deformation, 511 Hz

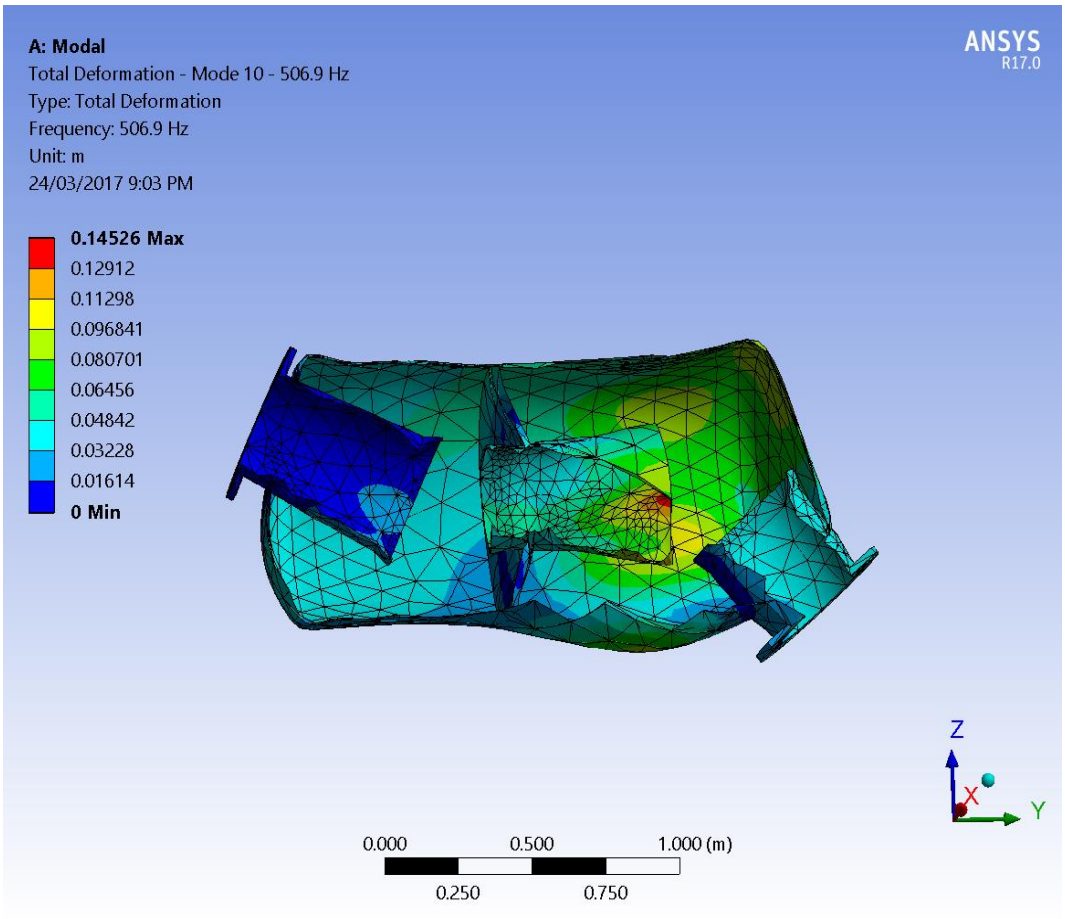

Figure 8.8 Mode 10 Total Deformation, 507 Hz

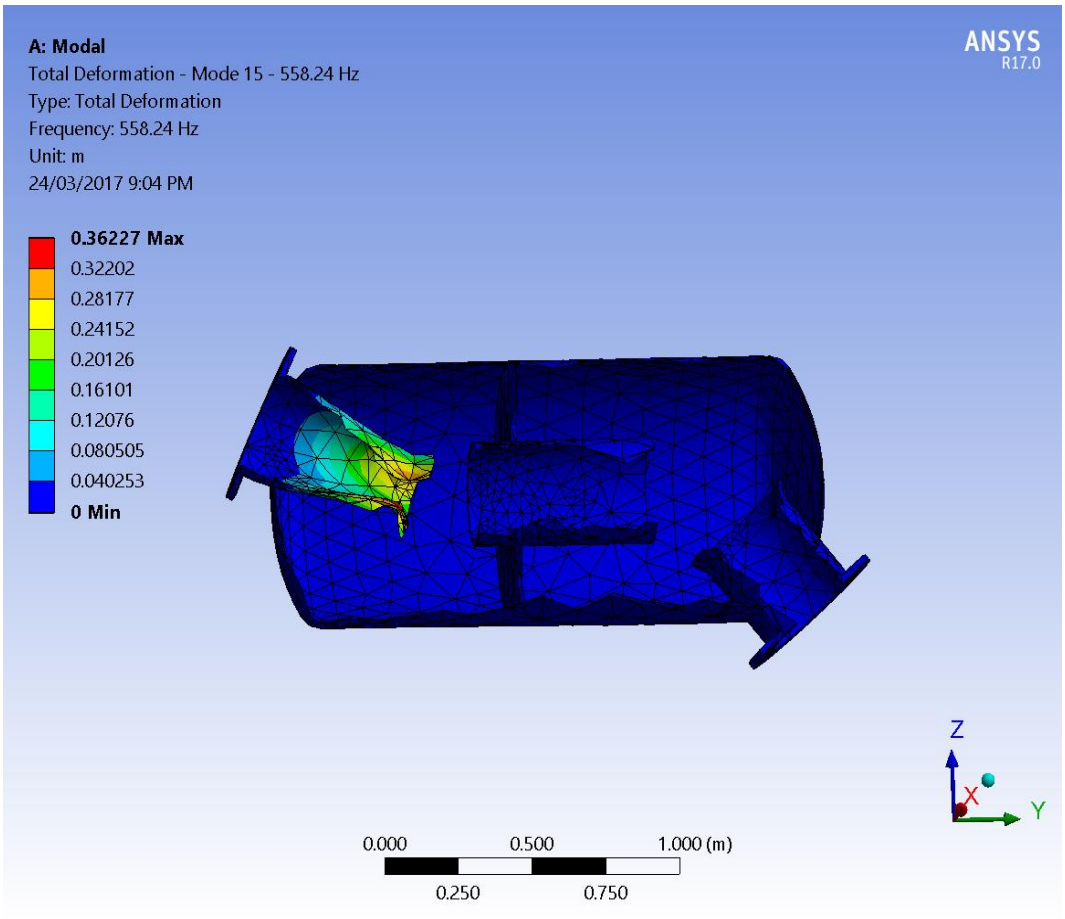

Figure 8.9 Mode 15 Total Deformation, 558 Hz

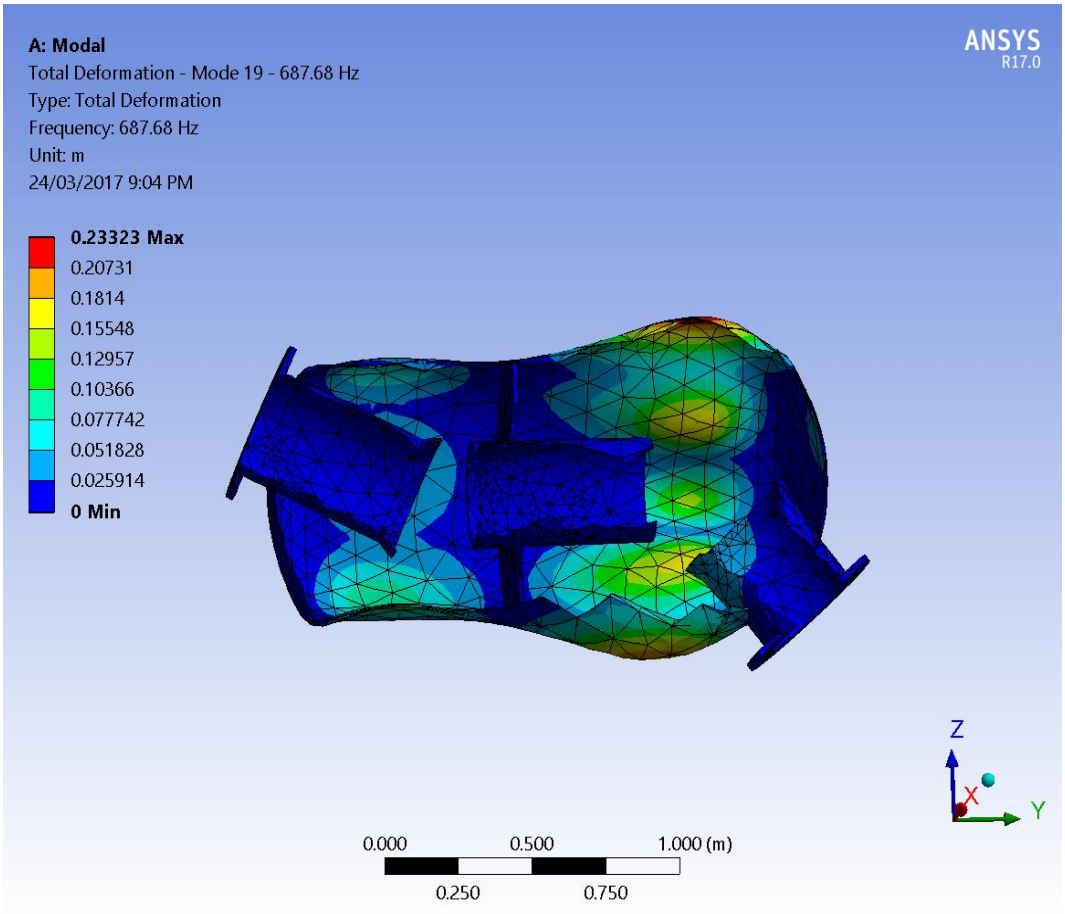

Figure 8.10 Mode 19 Total Deformation, 688 Hz

Chapter 9 Experimental Acoustic Transmission Loss Test Bench

This chapter describes the test bench, instrumentation, test parameters, sound pressure wave decomposition with and without an anechoic termination and data processing used to experimentally measure the acoustic transmission loss. Validation checks were conducted using a plain duct and simple contraction / expansion chambers. Results are presented for the test bench components.

9.1 Overview

The experimental test bench was designed and constructed by the author to measure the acoustic transmission loss at ambient temperature and pressure and zero gas flow of large marine diesel exhaust mufflers such as the one shown earlier in Figure 1.2. The test bench is approximately eight metres long (excluding speaker) and is shown schematically in Figure 9.1 and in Figure 9.2 and Figure 9.3.

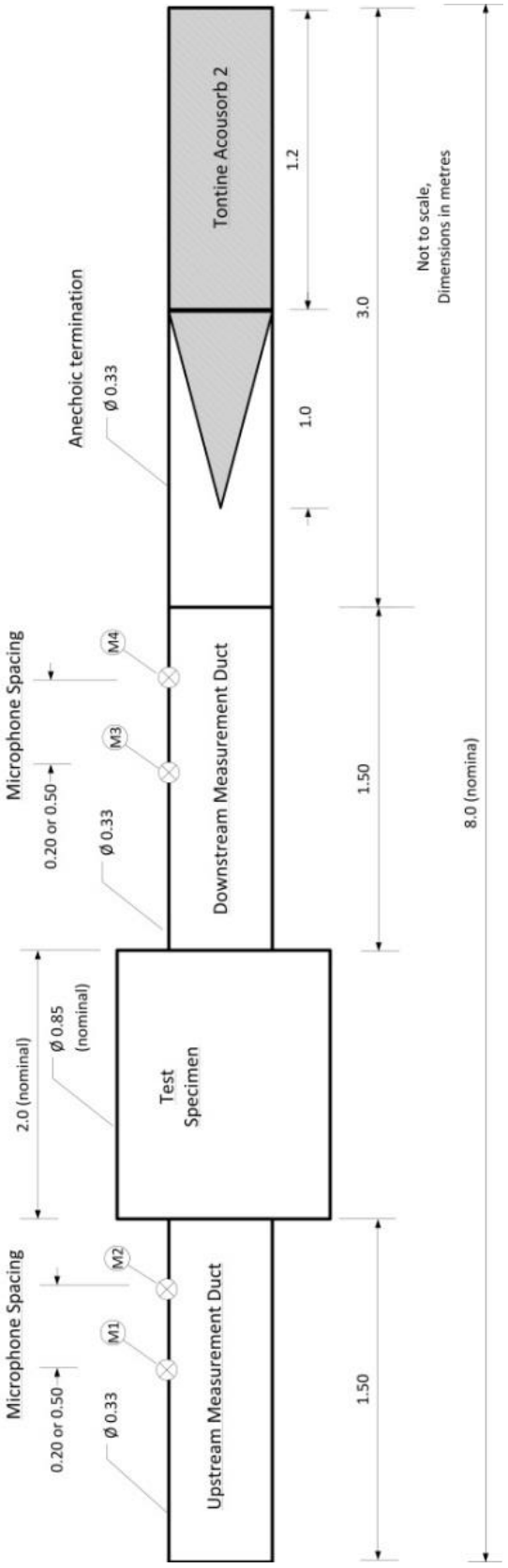

Figure 9.1 Schematic of Experimental Test Bench

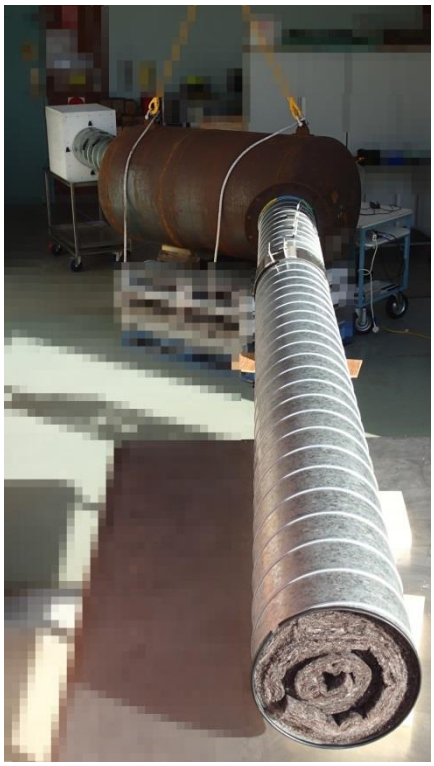

Figure 9.2 Experimental Test Bench, Termination End

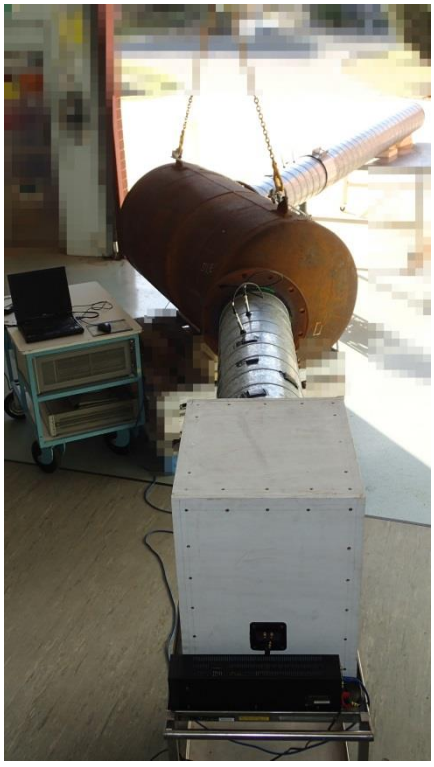

Figure 9.3 Experimental Test Bench, Source End

As the test bench has zero flow this allows the use of an effective anechoic termination which simplifies testing and data processing. Additionally the absence of flow and flow noise improves the acoustic performance signal to noise ratio. However the absence of mean gas flow does introduce the following effects which must be considered:

1. An absence of flow generated noise
2. a change to the speed of sound with a corresponding Doppler effect which depends upon the direction and speed of the gas flow
3. changes to end corrections / effective acoustic lengths
4. changes to wave propagation damping.

Details and datasheets for the test bench components are included in Appendix A. The test bench consists of:

1. a Hewlett Packard HP3567A data acquisition system and sound source
2. a Marantz mono (single channel) amplifier MA6100
3. a 305 mm (12") diameter subwoofer loudspeaker driver (Dayton Audio Model RSS315HO-44) in a custom 126 litre non-vented enclosure
4. four PCB brand half inch microphones (377B02) and preamplifiers (426E01)
5. an upstream measurement duct 1.5 metres long
6. the test muffler
7. a downstream measurement duct 1.5 metres long
8. an anechoic termination three metres long packed with Tontine Acoustisorb2 material.

The measurement ducts and anechoic termination use galvanized steel round ducting of spiral-folded-seam construction with a nominal bore of 330 mm and 1 mm wall thickness. While the spiral wrap construction provided effective damping of the ducts, the relatively thin walls may have enabled sound transmission through the walls. This would have raised the background noises levels in the test laboratory (Section 9.8.5) and increased acoustic losses along the ducts. The loudspeaker is powered by a Marantz mono amplifier with the excitation signal being provided by the sound source module in the Hewlett Packard spectrum analyser. The mono amplifier has a rated output of 125 W rms and a frequency response of 10 Hz to 70 kHz. The loudspeaker driver has a power handling rating of 700 Watts rms and a quoted usable frequency range of 20 Hz to 500 Hz.

9.2 Instrumentation

Two PCB half inch microphones with integrated PCB pre-amplifiers were installed upstream of the test element and two similar microphones were installed downstream as shown in Figure 9.1. The microphones are installed relatively flush to the inside wall using elastomeric cable grommets as shown in Figure 9.4 and Figure 9.5 . The protrusion of the microphones into the duct is determined by the height of the grommets which is five mm above the duct inside surface.

Figure 9.4 Microphone and Preamplifier in Grommet, External View

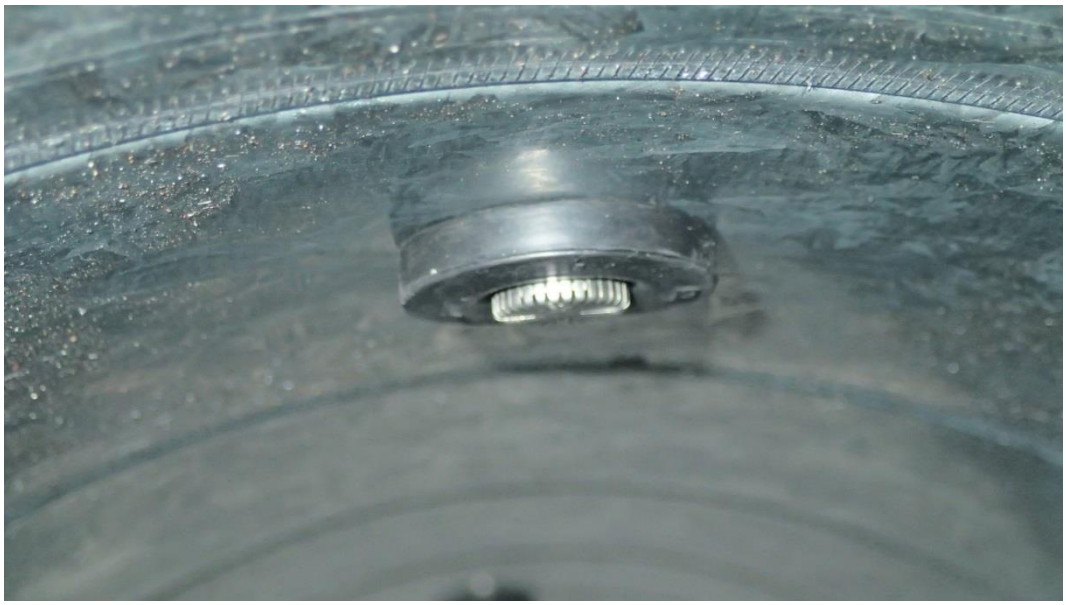

Figure 9.5 Microphone in Grommet, Internal View

The HP Spectrum Analyser Model HP3567A has four input and signal conditioning modules with 102.4 kHz bandwidth each and a sound source module. A microphone calibrator (Larson Davis CAL250) was used for amplitude calibration.

9.3 Test parameters

The nominal test conditions are zero flow, ambient atmospheric pressure and ambient temperature. Note that the ambient temperature and pressure are not controlled and variations may affect the results by changing the speed of sound. The test sound pressure level is 120 dB re 20µPa which by plane wave theory equates to 50 mm/s (rms) particle velocity. Table 9-1 summarises the test bench parameters.

Table 9-1 TL Bench Parameters, General

Parameters	TL Bench
Speed of Sound (m/s)	≈ 346
Temperature (°C)	≈ 25
Pressure (bar)	≈ 1.01
Flow	zero
Frequency Minimum (Hz)	30
Frequency Maximum (Hz)	700
Cut-on Frequency (Hz) for Ducting (ø 330 mm)	615
Cut-on Frequency (Hz) for Muffler Body (ø 820 mm)	245
Microphone Spacing (mm)	200 & 500
Input Spectra	Random
Microphone Mounting	Near flush
Measurement Duct Length (m)	1.5

9.4 Test bench design parameters

This section considers the key drivers influencing the physical layout of the test bench.

9.4.1 Frequency Range

As discussed in Section 5.3, the target range for the test facility is 30 Hz to 700 Hz.

9.4.2 Microphone Spacing

The two microphone spacings (200 mm and 500 mm) cover the required frequency range of 30 Hz to 700 Hz with microphones 2 and 4 being fixed and microphones 1 and 3 being moved to achieve the required spacings.

9.4.3 Lateral Cut-on Frequencies

While the test bench and data processing assumes plane wave propagation there are transverse / lateral modes within the frequency range of interest. As the two microphone method assumes plane wave propagation, the first lateral cut-on frequency sets an upper limit for testing. The lateral cut-on frequency for the 330 mm diameter measurement ducts is 615 Hz at 25 °C.

9.4.4 Measurement Duct Dimensions

Guidelines on the length of the measurement ducts and the microphone pair placements were available from a range of sources [47-49] and the values actually used are summarised in Table 9-2. To promote plane wave propagation the length of the measurement ducts should be five to ten times its diameter and the test sections used are at the lower end of this range at 4.5 times. To minimise the effects of attenuation along the duct, the microphone pairs should be close to the element being measured and this requirement is satisfied.

Table 9-2 TL Bench Measurement Duct Dimensions

Measurement Duct			
Length (mm)	1500		
Diameter (mm)	330		
Equivalent Duct Diameters	4.5		
Upstream Microphones			
Microphones	M1 (500)	M1 (200)	M2
Speaker to Microphone (mm)	650	950	1150
Equivalent Duct Diameters	2.0	2.9	3.5
Microphone to Muffler (mm)	850	550	350
Equivalent Duct Diameters	2.6	1.7	1.1
Downstream Microphones			
Microphones	M3 (500)	M3 (200)	M4
Muffler to Microphone (mm)	650	950	1150
Equivalent Duct Diameters	2.0	2.9	3.5
Microphone to Anechoic Termination (mm)	850	550	350
Equivalent Duct Diameters	2.6	1.7	1.1

9.5 Data Flow and Processing

A HP 3567A Spectrum Analyser was used for data acquisition and frequency analysis. The microphones' signals were averaged (25 samples) and processed in the frequency domain to give auto (power) spectra, cross (power) spectra and third octave results. HP software (HP35639A Data Viewer) was used to convert HP Standard Data Format (SDF) files (*.dat) to MATLAB data files (*.mat). Table 9-3 summarises the HP analyser instrumentation settings. Note that HP file names must be a maximum of 6 characters as "Batch convert" adds two more numbers giving a maximum of 8 characters. MATLAB scripts were then used to calculate wave decomposition, transmission loss and power reflection coefficient.

Table 9-3 TL Bench HP Analyser Parameters

Parameters	TL Bench
Input Spectra	Random
Speaker Output Amplitude - Sound pressure Level, dB ref 20 µPa	≈120
Input Amplitude to Amplifier, 400 Hz Range, Volts rms	1
Input Amplitude to Amplifier, 800 Hz Range, Volts rms	2
Input Amplitude to Amplifier, 1/3rd Octave 630 Hz Range, Volts rms	1
Input Amplitude to Amplifier, 1/3rd Octave 1.25 kHz Range, Volts rms	2
Input Amplitude to Amplifier, 1/3rd Octave 1.6 kHz Range, Volts rms	2.5
Microphone Signal Conditioning	ICP
FFT Window	Flat top
Measurement Type, FRF, 1600 frequency lines	FRF 400 & 800 Hz
Measurement Type, 1/3rd Octave	1/3rd Octave 630 and 1.25 kHz

9.6 Wave Decomposition

As described in Chapter 5, each of the four microphones can each only measure the total acoustic pressure at their respective locations. This total pressure is a summation of forward and backward travelling waves as discussed earlier. This is especially so before the test element (microphones 1 and 2) due to the reflection of sound back towards the source. The loudspeaker output is assumed to be stationary with any reflections from the loudspeaker being considered to be addition sources / speakers [52] as shown in Figure 9.6.

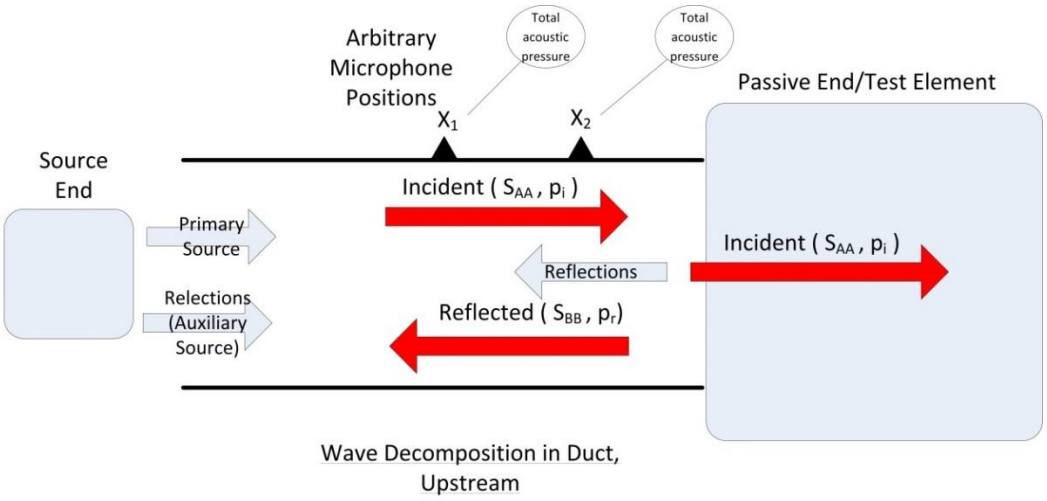

Figure 9.6 Wave Decomposition, Upstream

After the test element, wave decomposition of the two microphone signals (microphones 3 and 4) gives the forward and backwards travelling sounds. However any reflections back towards the test element are undesirable in that the resulting forward travelling sound is not that exiting the test element as shown in Figure 9.7.

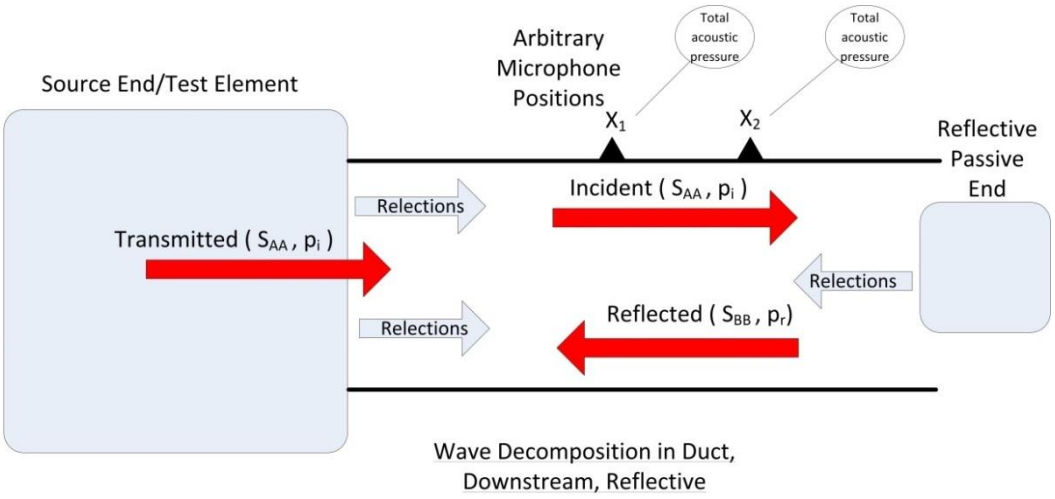

Figure 9.7 Wave Decomposition, Downstream, Reflective Termination

In contrast use of an anechoic termination eliminates any reflection after the test element as shown in Figure 9.8 with the result that wave decomposition derived forward travelling sound is purely due to that exiting the test element as

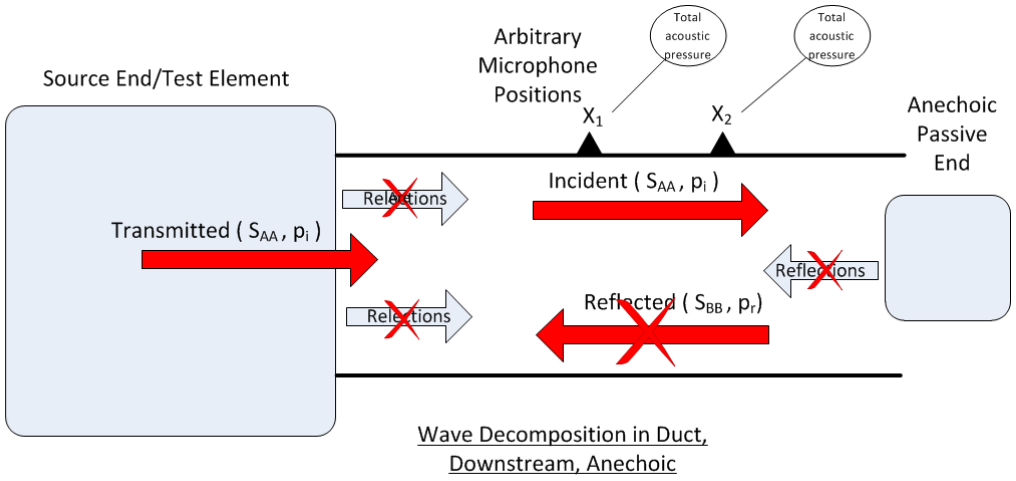

Figure 9.8 Wave Decomposition, Downstream, Anechoic Termination

If the anechoic termination is truly effective, then microphones 3 and 4 will have identical amplitude signals and so only one microphone is necessary after the test element and no wave decomposition is required as shown in Figure 9.9 . With an effective anechoic termination, the incident spectra after the test element can be derived directly from either microphone 3 or 4.

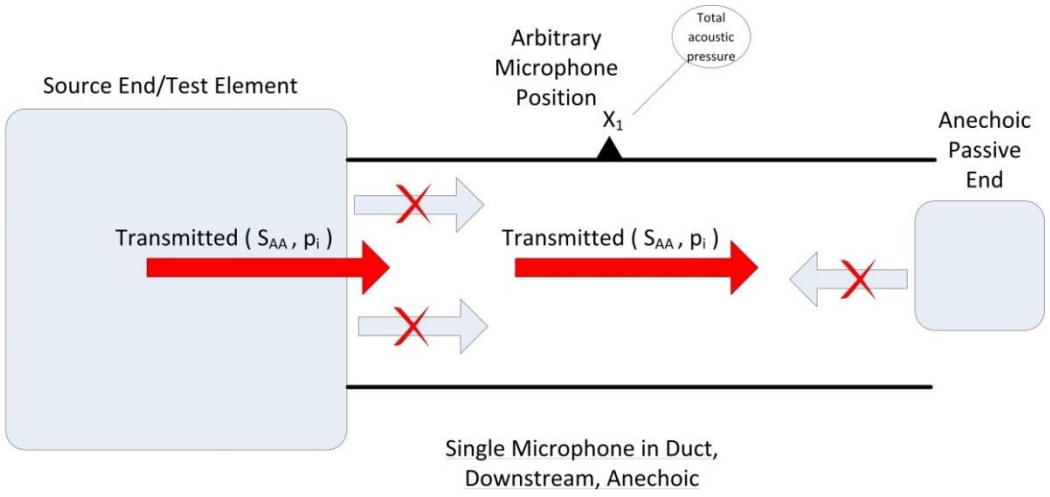

Figure 9.9 Wave Decomposition, Downstream, Anechoic Termination, Single Microphone

However with two microphones after the test element, the ratio of the incident and reflected spectra can be used to evaluate the effectiveness of the anechoic termination. Note that the higher the transmission loss of the muffler, the less there is to be absorbed by the anechoic termination. This means that the apparent performance of the anechoic termination will vary according to the muffler performance.

9.7 Validation

9.7.1 Initial

Initial validation was achieved by feeding a single signal from one microphone on an acoustic microphone calibrator to all four channels with the calibrations manipulated to give an artificial transmission loss across a "virtual" muffler. The data flow and processing was then validated by using a plain duct in lieu of a muffler. While these steps gave confidence in the data acquisition and data processing, the plain duct in particular with its predicted and measured zero transmission loss was not conclusive. This was due to the possibility of the sound power before and after the duct being incorrect but their ratio being correct and giving the correct transmission loss.

9.7.2 Contraction / Expansion

Mufflers like the large marine muffler (LMM) are complex and not possible to verify their acoustic characteristics using classical theory. So an acoustic device that was simple and independently verifiable was designed and constructed by the author. The obvious choice was a simple expansion chamber but this was discounted due to the cost and difficulty of constructing a rigid shell expansion chamber some 2 metres long and 800 mm in diameter. To overcome these difficulties but retain key requirements a contraction / expansion chamber was chosen. The two selected contraction / expansion chambers are shown in Figure 9.10 and are 150 mm in diameter and either 432.5 mm or 1730 mm long. These lengths were selected to give a wide frequency range with peak transmission losses at multiples of approximately 200 and 50 Hz respectively.

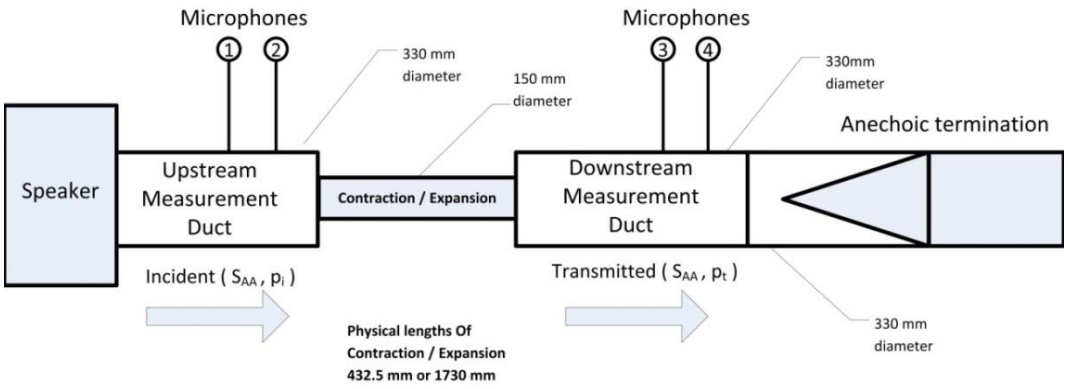

Figure 9.10 Schematic of TL Bench with Contraction / Expansion Test Element

To calculate the theoretical transmission loss versus frequency the effective or acoustic lengths must be considered. While the physical lengths were 432.5 and 1730 mm, the effective acoustic lengths include the end corrections as shown in Figure 9.11 [55].

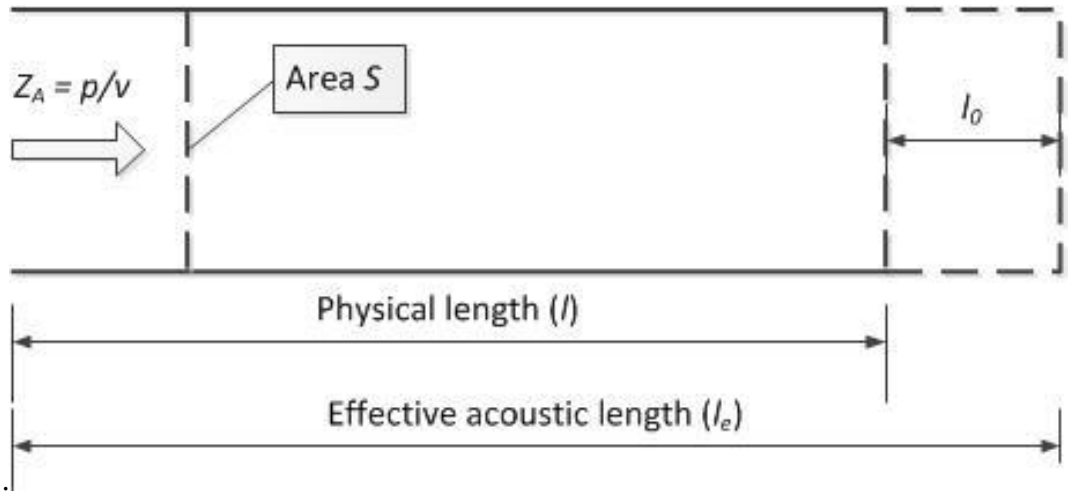

Figure 9.11 Effective Acoustic Length Showing End Correction, after [55]

The end correction to give the corrected length for the contraction can be calculated using Equation (9.1) for a pipe into a larger cylindrical space such as a Helmholtz resonator neck interfacing to a circular volume [55, 79].

$$\boldsymbol{End\ correction\ (l_0) = 0.82(1 - 1.33\xi)} \qquad (9.1)$$

where:

a is the radius of the contraction / pipe (m)

ξ is the ratio of contraction pipe diameter to expansion pipe diameter.

Note that this formula is valid when the diameter ratio ξ is less than 0.4, whereas in this case ξ is slightly larger at 0.45 (150/ 330 mm). The end correction is 24.5 mm (each end) which gives effective lengths of 481 and 1779 mm - effectively 11% and 3% longer respectively. An alternative approach is to treat each end of the contraction as a pipe exiting into open space using Equation (9.2) [55].

$$\boldsymbol{End\ correction\ (l_0) = 0.61a} \qquad (9.2)$$

The end correction is 45.8 mm (each end) which gives effective lengths of 524 and 1822 mm – effectively 21% and 5% longer respectively.

The contraction / expansion chamber acts similar to an expansion chamber with peak amplitudes being proportional to the area ratio. The peak transmission losses occur at odd multiples of λ/4 and the zero transmission losses occurring at odd multiples of λ/2. The transmission loss for each length contraction / expansion chamber can be calculated using Equation (9.3) [34] as an expansion chamber of the same area ratio and correcting for effective length using Equation (9.1) and Equation (9.2). This gives a maximum transmission loss of 8 dB for this area ratio with the transmission loss versus frequency being effective length dependent.

$$\boldsymbol{Transmission\ Loss\ (TL) = 10\log\left(\cos^2\left(2\pi\frac{l}{f}\right) + \frac{1}{4}\left(m + \frac{1}{m}\right)^2\left(\sin^2\left(2\pi\frac{l}{f}\right)\right)\right)} \quad (9.3)$$

Where:

f is the frequency in Hz

l is the length of the contraction / expansion (m)

m is the area ratio.

Figure 9.12 and Figure 9.13 show the theoretical transmission loss versus frequency for the short contraction / expansion chamber for both corrected effective lengths for 400 Hz and 800 Hz ranges respectively.

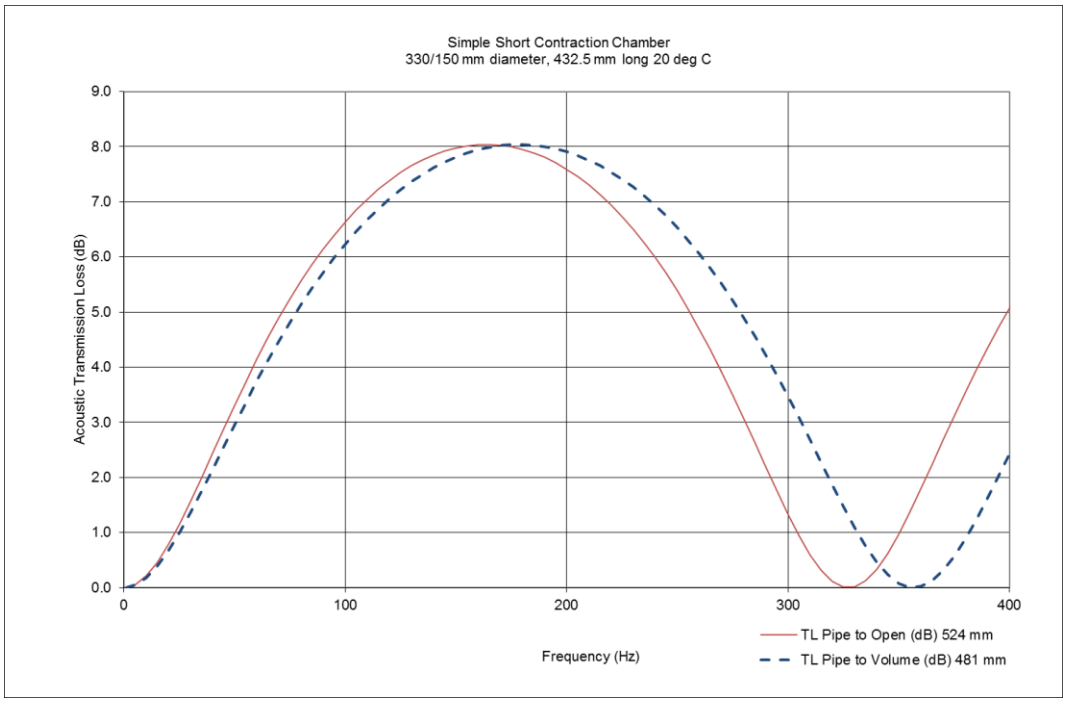

Figure 9.12 Theoretical Transmission Loss, Short Contraction / Expansion Chamber, 0 to 400 Hz

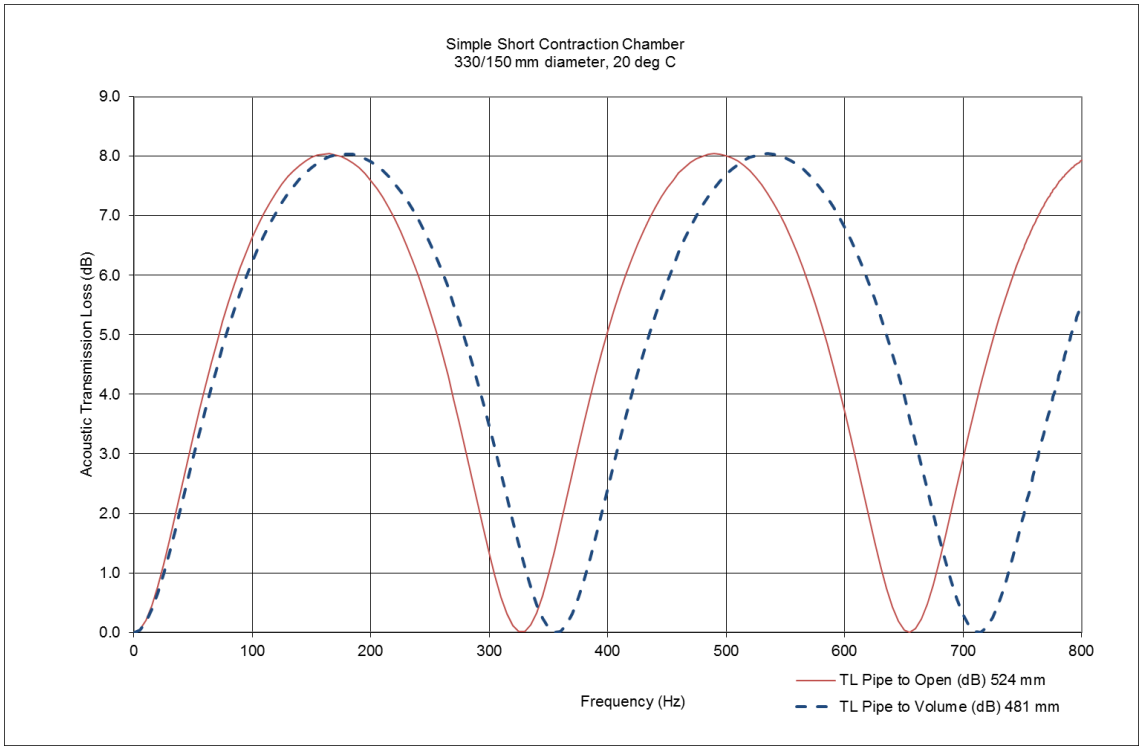

Figure 9.13 Theoretical Transmission Loss, Short Contraction / Expansion Chamber, 0 to 800 Hz

Figure 9.14 and Figure 9.15 show the theoretical transmission loss versus frequency for the long contraction / expansion chamber for both corrected effective lengths for 400 Hz and 800 Hz ranges respectively.

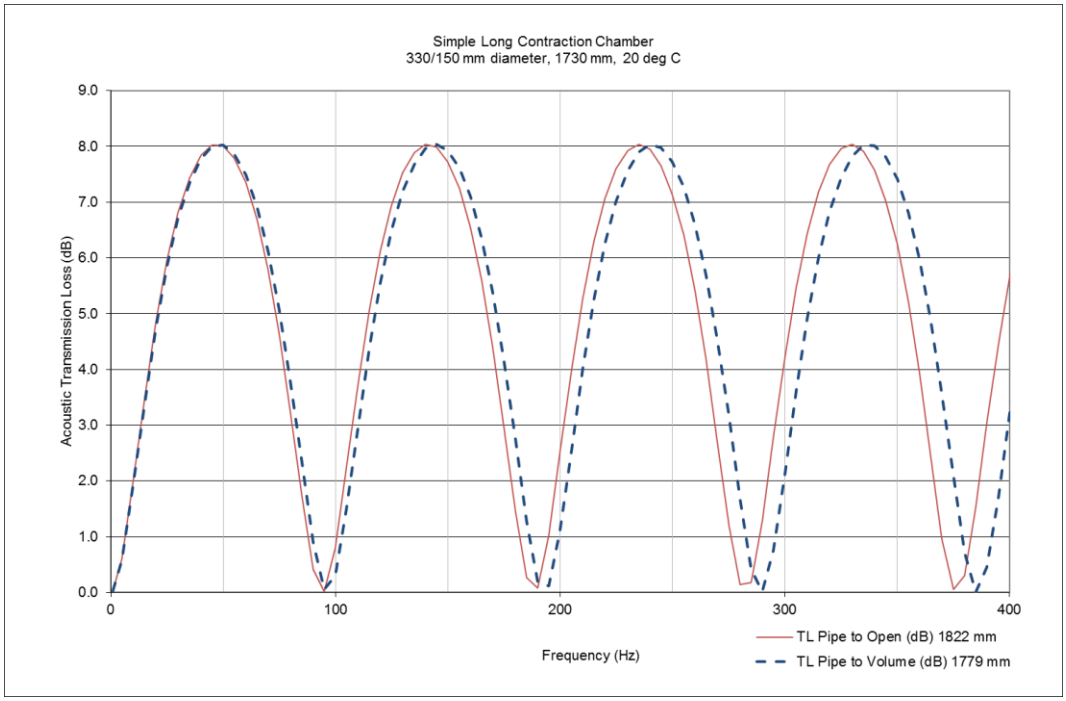

Figure 9.14 Theoretical Transmission Loss, Long Contraction / Expansion Chamber, 0 to 400 Hz

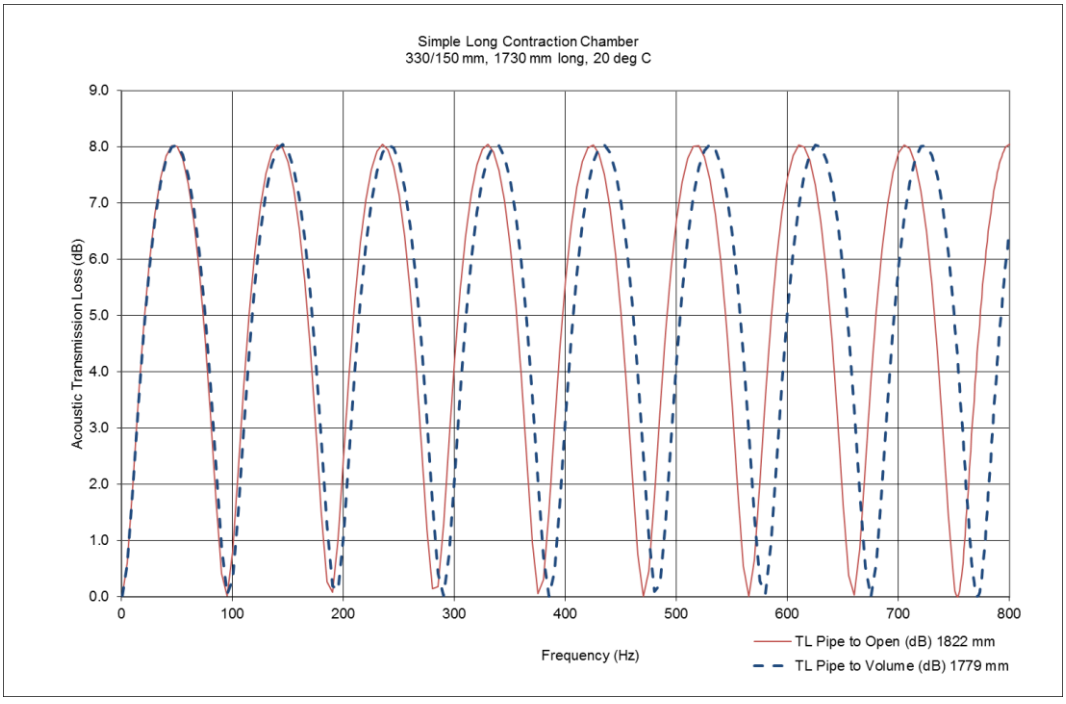

Figure 9.15 Theoretical Transmission Loss, Long Contraction / Expansion Chamber, 0 to 800 Hz

The two contraction / expansion chambers were tested on the experimental transmission loss test bench for the 400 Hz and 800 Hz ranges using four and three microphones and Figure 9.16 to Figure 9.19 show the measured transmission losses versus frequency.

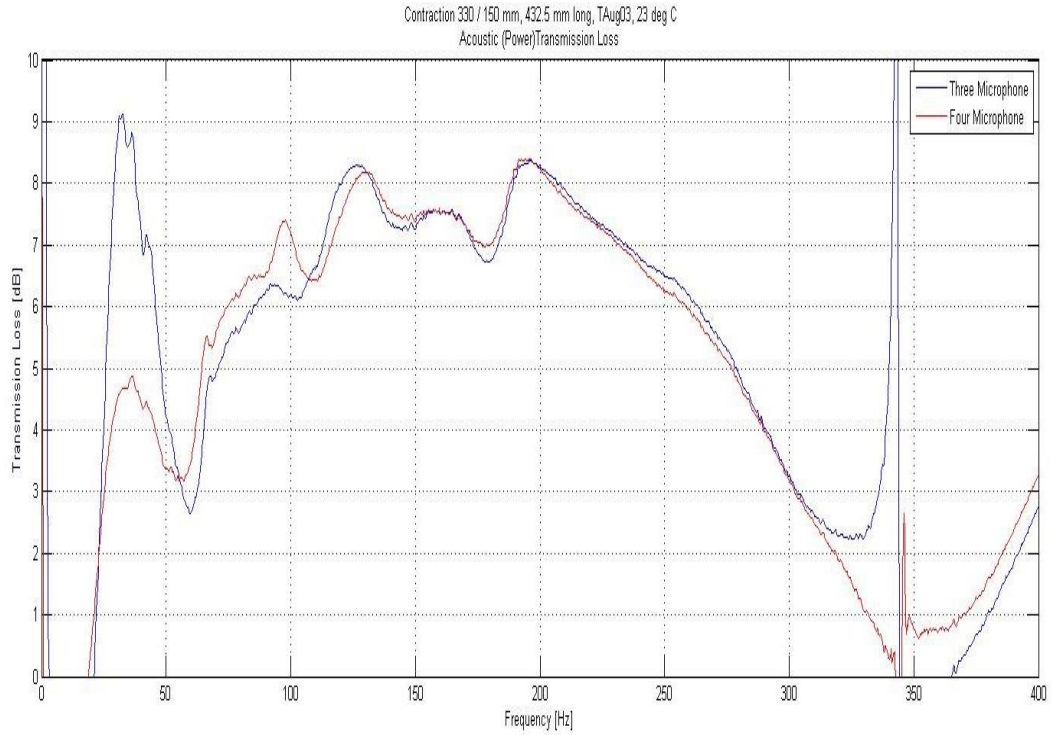

Figure 9.16 Measured Transmission Loss, Short Contraction / Expansion Chamber, 0 to 400 Hz

If we compare the measured (Figure 9.16) and theoretical results (Figure 9.12) for the short contraction / expansion chamber over a 400 Hz range, we see that the correlation is good with respect to amplitude and frequency. The deviations are due to the speaker low frequency performance effect and a 346 Hz peak due to the λ/2 microphone spacing. The 'wiggles' between 25 Hz and 200 Hz in the measured results were unexpected and will be the subject of further investigation. This could include looking at the coherence between microphones in each microphone pair.

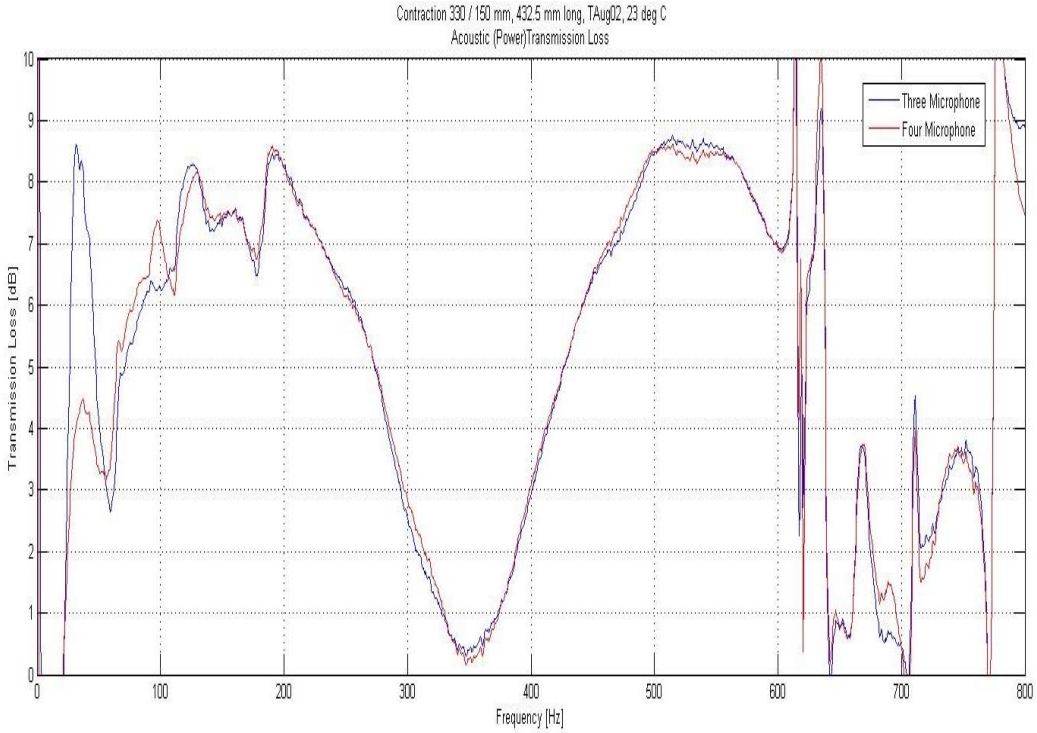

Figure 9.17 Measured Transmission Loss, Short Contraction / Expansion Chamber, 0 to 800 Hz

If we compare the measured (Figure 9.17) and theoretical results (Figure 9.13) for the short contraction / expansion chamber over a 800 Hz range, we see that the correlation is good with respect to amplitude and frequency. The deviations are due the speaker low frequency performance effect and the cut-on frequency limiting the measured results to below 600 Hz.

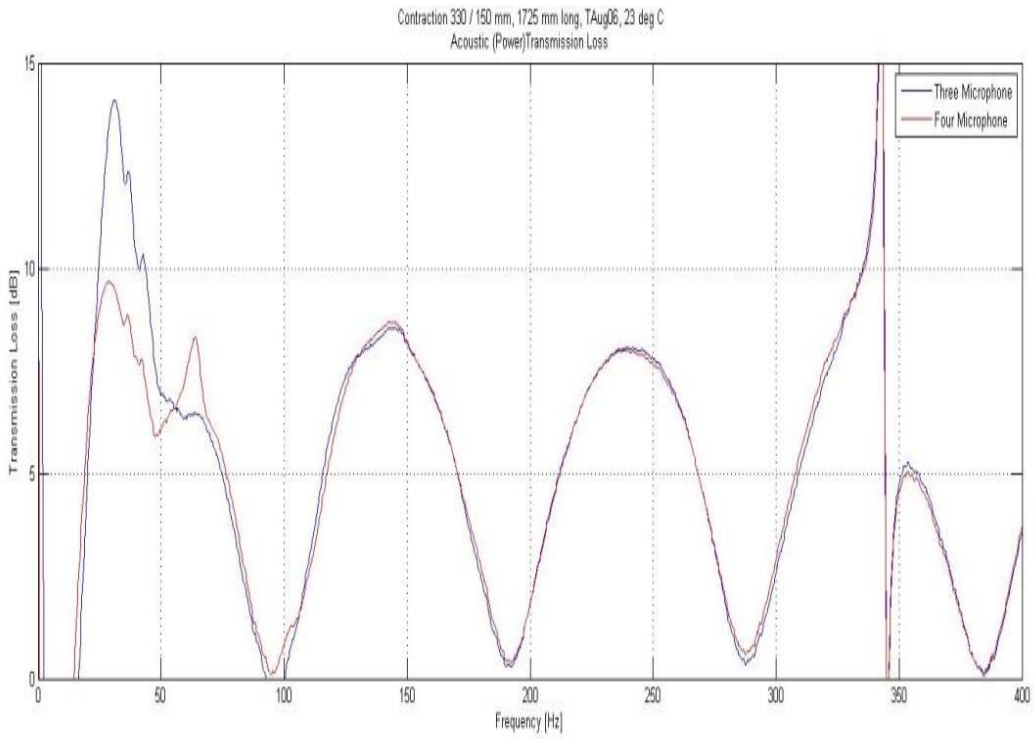

Figure 9.18 Measured Transmission Loss, Long Contraction / Expansion Chamber, 0 to 400 Hz

If we compare the measured (Figure 9.18) and theoretical results (Figure 9.14) for the long contraction / expansion chamber over a 400 Hz range, we see that the correlation is good with respect to amplitude and frequency. The deviations are due to the speaker low frequency performance effect and a 346 Hz peak due to the $\lambda/2$ microphone spacing.

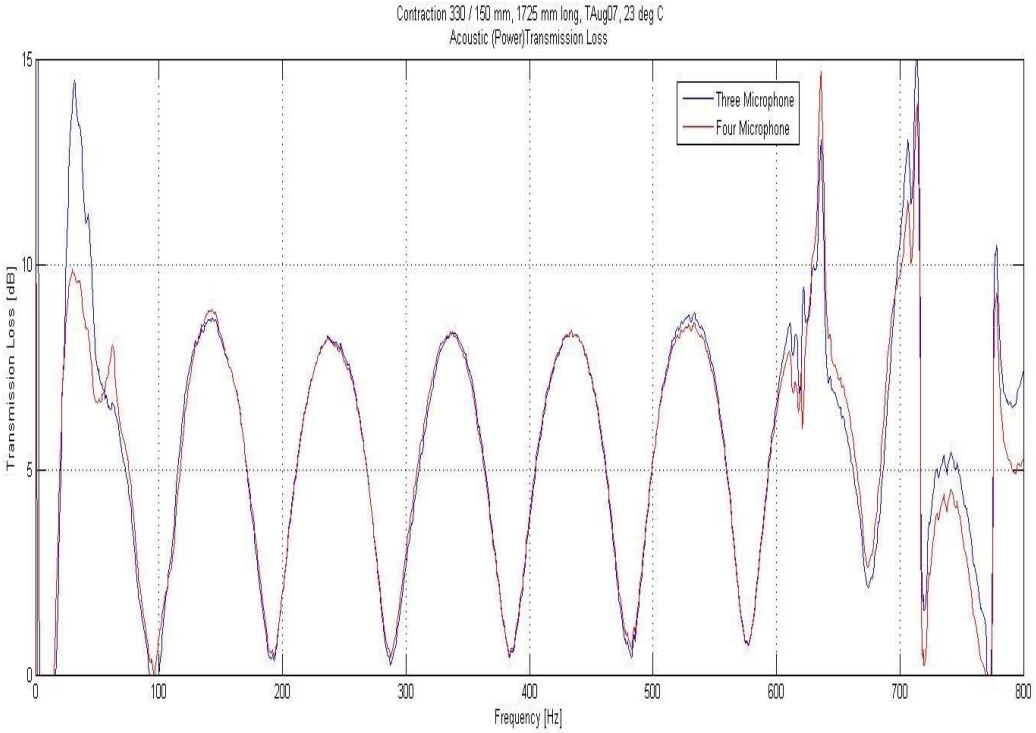

Figure 9.19 Measured Transmission Loss, Long Contraction / Expansion Chamber, 0 to 800 Hz

If we compare the measured (Figure 9.19) and theoretical results (Figure 9.15) for the long contraction / expansion chamber over a 800 Hz range, we see that the correlation is good with respect to amplitude and frequency. The deviations are due the speaker low frequency performance effect and the cut-on frequency limiting the measured results to below 600 Hz.

9.8 Results

The results from the development of the test bench are discussed under the following sub-headings.

9.8.1 Loudspeaker Performance

Two different 305 mm diameter (12”) loudspeaker drivers in a 127 litre non-vented enclosure were initially characterised with a microphone at 1.5 metres from the loudspeaker front face. In free radiation above a hard surface, the Dayton Audio driver was distortion free from 30 Hz to 1000 Hz and was therefore used in preference to the “generic” driver which had distortion below 50 Hz.

The speaker’s output spectra into a duct is more relevant for the transmission loss test bench and this was evaluated using a single measurement duct, two microphones, and an anechoic termination. The third octave spectra for microphones 1 and 2 are shown in Figure 9.20 and Figure 9.21 for 400 Hz and 1.6 kHz ranges respectively.

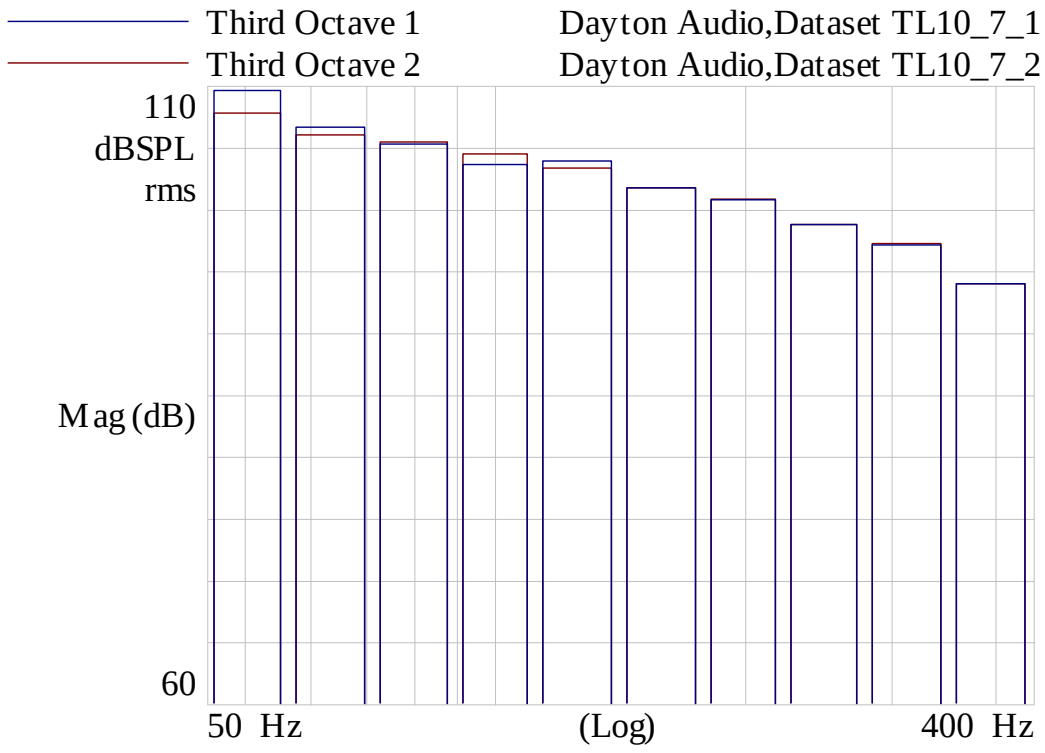

Figure 9.20 Dayton Audio In-Duct Output Third Octave Spectra, Microphones 1 & 2, 0 to 400 Hz

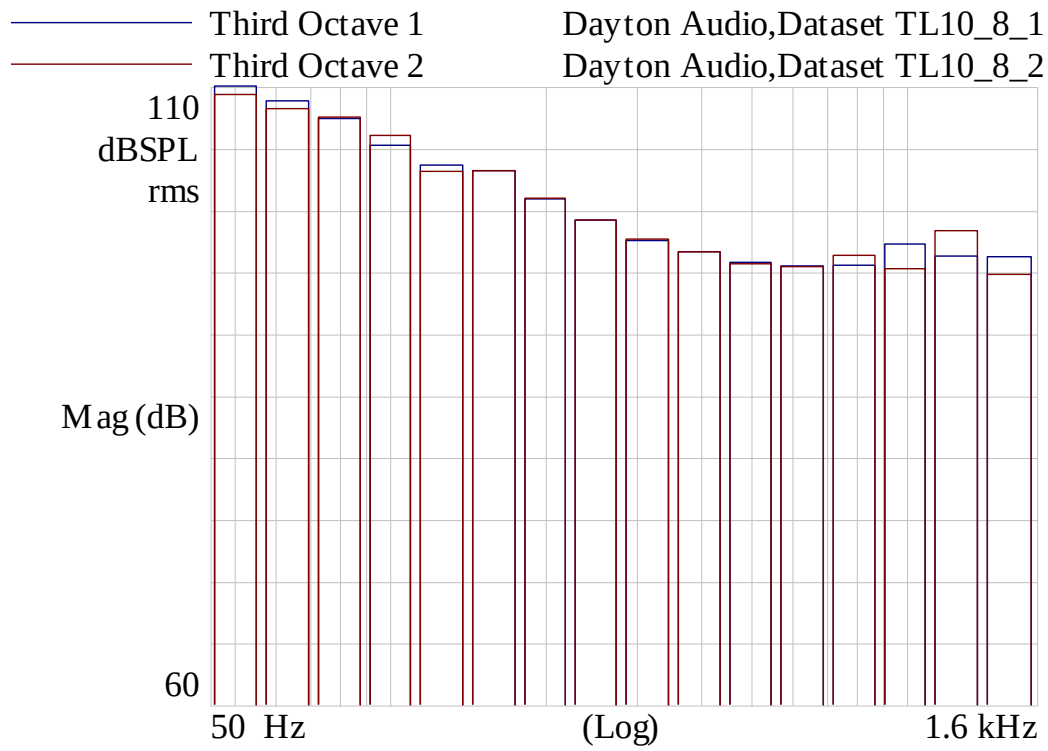

Figure 9.21 Dayton Audio In-Duct Output Third Octave Spectra, Microphones 1 & 2, 0 to 1.6 kHz

The corresponding narrow band spectra for microphones 1 and 2 are shown in Figure 9.22 and Figure 9.23 for 400 Hz and 1000 Hz ranges respectively.

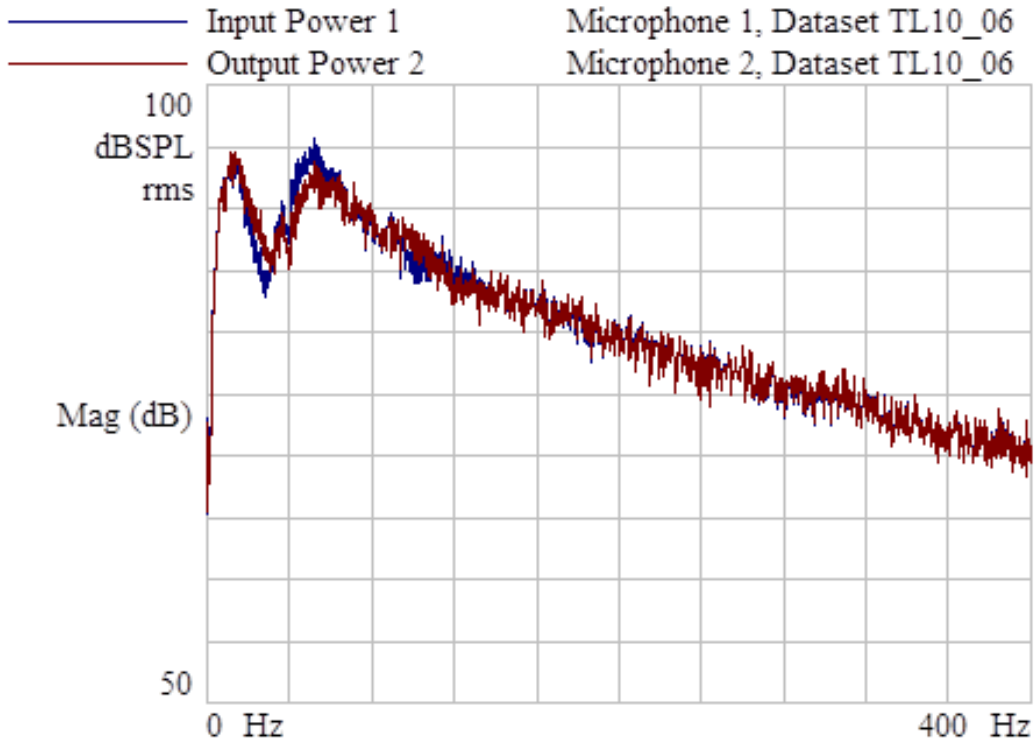

Figure 9.22 Dayton Audio In-Duct Output Spectra, SPL dB re 20µPa, Microphones 1 & 2, 0 to 400 Hz

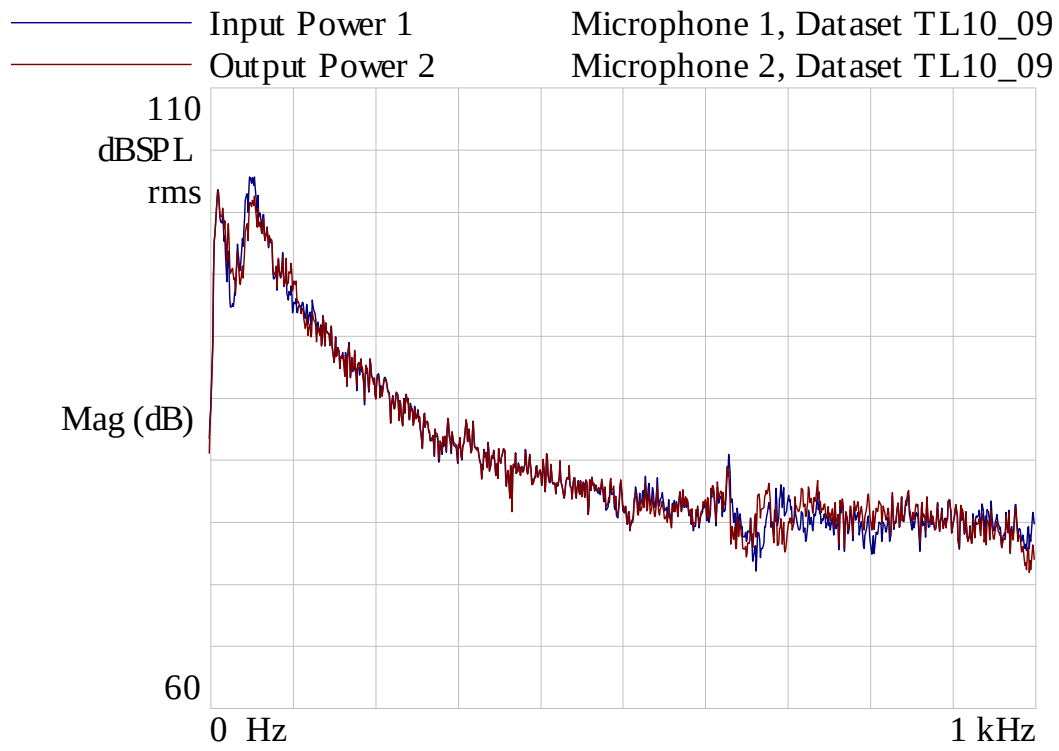

Figure 9.23 Dayton Audio In-Duct Output Spectra, SPL dB re 20µPa, Microphones 1 & 2, 0 to 1000 Hz

The sound pressures at microphones one and two over both frequency ranges are near identical as expected with an anechoic termination. While there are minimal holes in the loudspeaker output spectra, it was not linear across the full frequency range and this may be an area of potential improvement.

9.8.2 Anechoic Termination

The anechoic termination was evaluated using two plain measurement ducts in series coupled to the anechoic termination. The effectiveness of the termination is shown in Figure 9.24 with near zero reflection above 80 Hz. At the lower end target 30 Hz, the reflection is less than 15 %. The high value at 345 Hz is an aberration due to the half wavelength calculation indeterminacy discussed earlier.

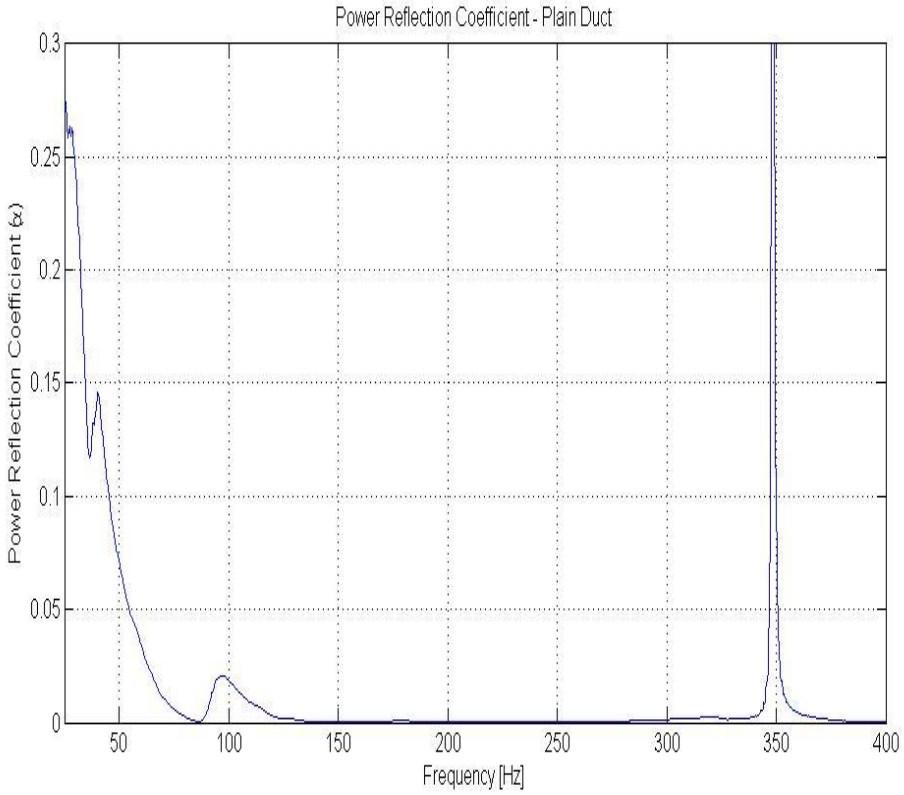

Figure 9.24 Anechoic Termination, Power Reflection Coefficient, Dataset TL12_2

9.8.3 Microphone matching

Differences in amplitude and phase between the microphones will induce errors in the calculated results and some sources recommend a measured microphone correction while others recommend interchanging of microphones [27, 30, 49, 80]. The amplitude and phase matching of the four microphones was evaluated using a single measurement duct coupled to the anechoic termination to assess the need for corrections. All microphones were located at the same distance from the loudspeaker and spaced around the circumference of the duct as shown in Figure 9.25.

Figure 9.25 TL Bench, Microphone Matching Layout

The amplitude and phase matching was excellent up to at least 550 and 600 Hz as shown in Figure 9.26 and Figure 9.27 respectively. This obviated the need to use corrections or position interchanging for this study. The variation in magnitude was less than ± 1% and the variation in phase was ±1.5 degrees using microphone 1 as a reference for the other three microphones. These are very low values as expected for the low frequency response of high quality microphones of the same model and production batch. The matching above 550 / 600 Hz could not be ascertained due to the interference of lateral modes in the measurement set-up. The actual performance can be better this with careful selection as the microphones are used in pairs and the data is processed in the same pairs.

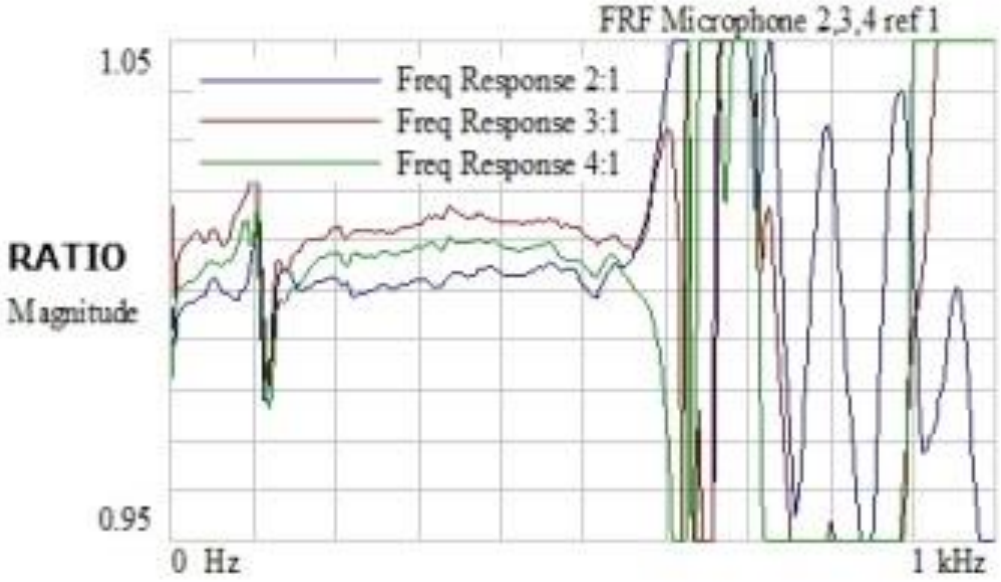

Figure 9.26 Amplitude Comparison of Microphones, FRF Relative to #1

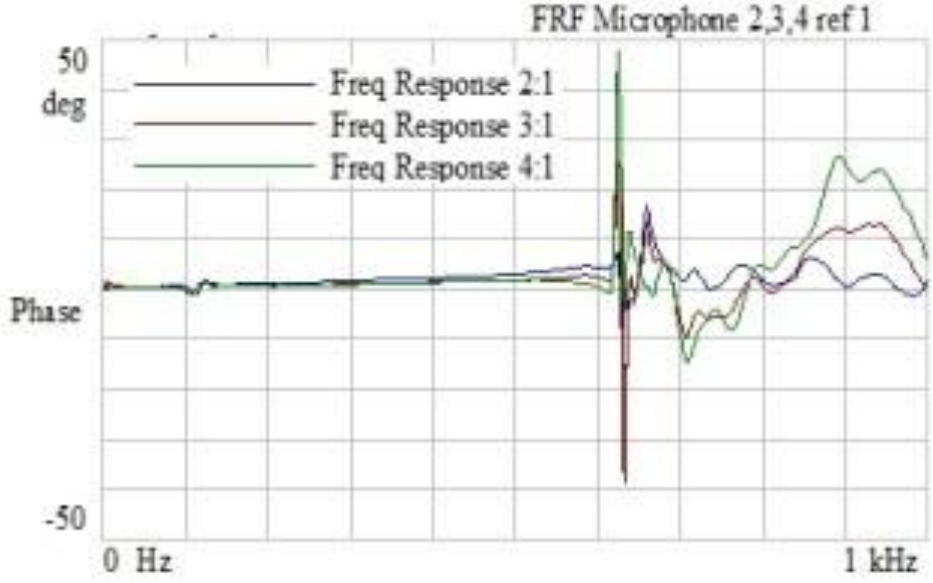

Figure 9.27 Phase Comparison of Microphones, FRF Relative to #1

9.8.4 Lateral Modes

Of particular interest were phase shifts and poor coherence at 625, 1030, 1300 and 1400 Hz indicating lateral modes. To eliminate the possibility that these were structural resonances, the measurement ducts' shell modes were measured using accelerometers and impact excitation. These measurements did not show modes at the frequencies attributed to the aforementioned lateral modes. The values of these lateral modes were confirmed using Bessel functions (Figure 9.28) for the duct diameter [81]. Note that the ambient test temperature of approximately 33 °C increased the measured lateral mode frequency to 625 Hz from the 615 Hz calculated previously at 25 °C. This lateral mode / cut-on frequency at 625 Hz effectively limits the test bench's upper frequency to 600 Hz for plane wave propagation.

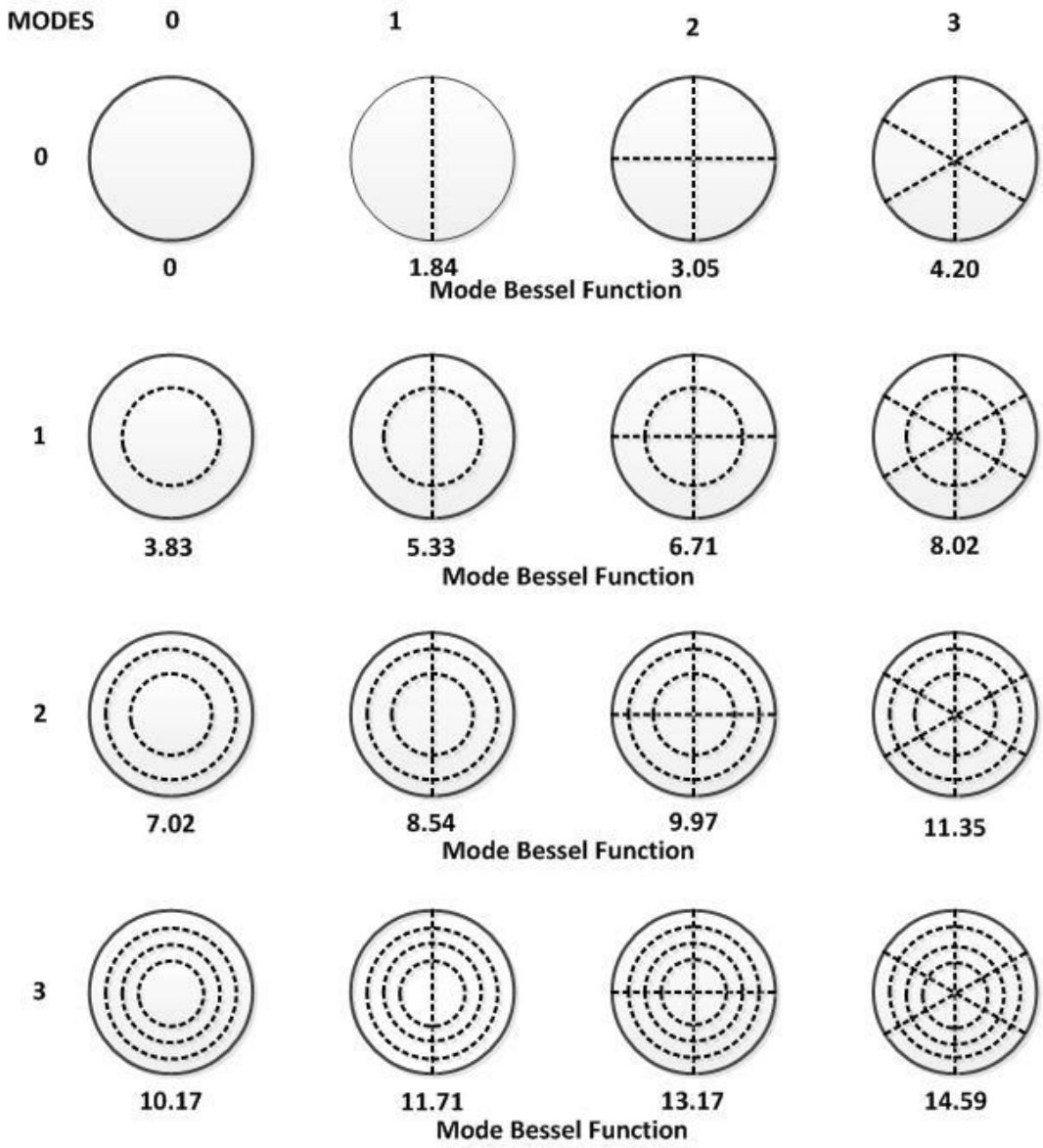

Figure 9.28 Nodal Lines For Pressure Distributions and Bessel Function Solutions Associated with Lateral Modes, after [81]

9.8.5 Background Noise Level

The test bench with the test muffler was set up and the background noise level was measured with the loudspeaker off but the microphones in place. The background noise level was 56 to 57 dB re 20µPa. This is well below the operating sound pressure levels of approximately 120 dB re 20µPa and 107 dB re 20µPa before and after the test muffler respectively.

Chapter 10 Muffler LMM Acoustic Measurements

This chapter describes the experimental validation of the large marine muffler (LMM) using air jet excitation and the experimental transmission loss test bench.

10.1 Air jet excitation of cavity modes

The acoustic resonant modes of the LMM cavities and internal features were experimentally determined using a close microphone and air jet excitation as shown in Figure 10.1. Similar in principle to a woodwind musical instrument, the air jet produced a broadband excitation and excited the muffler cavities to resonance at ambient temperature.

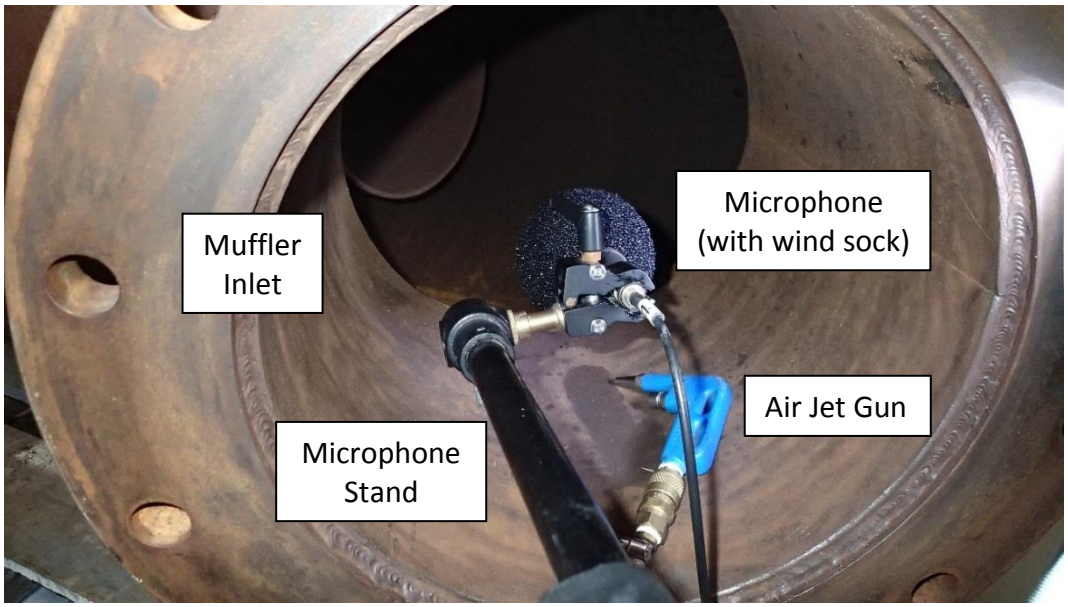

Figure 10.1 Muffler LMM Cavity Mode Determination, Microphone and Air Jet Gun, Inlet Side

The broadband frequency content of the air jet is shown in Figure 10.2.

The air jet was directed at the following locations in order to excite the cavity and internal feature modes.

1. Excitation - Inlet Side
    a. Chamber Inlet Edge
    b. Inlet chamber / centre tube
    c. Axial on centre tube
    d. Chamber inlet edge-lateral & longitudinal modes.
2. Excitation - Outlet Side
    a. Chamber Outlet Edge
    b. Outlet chamber / centre tube
    c. Axial on centre tube.

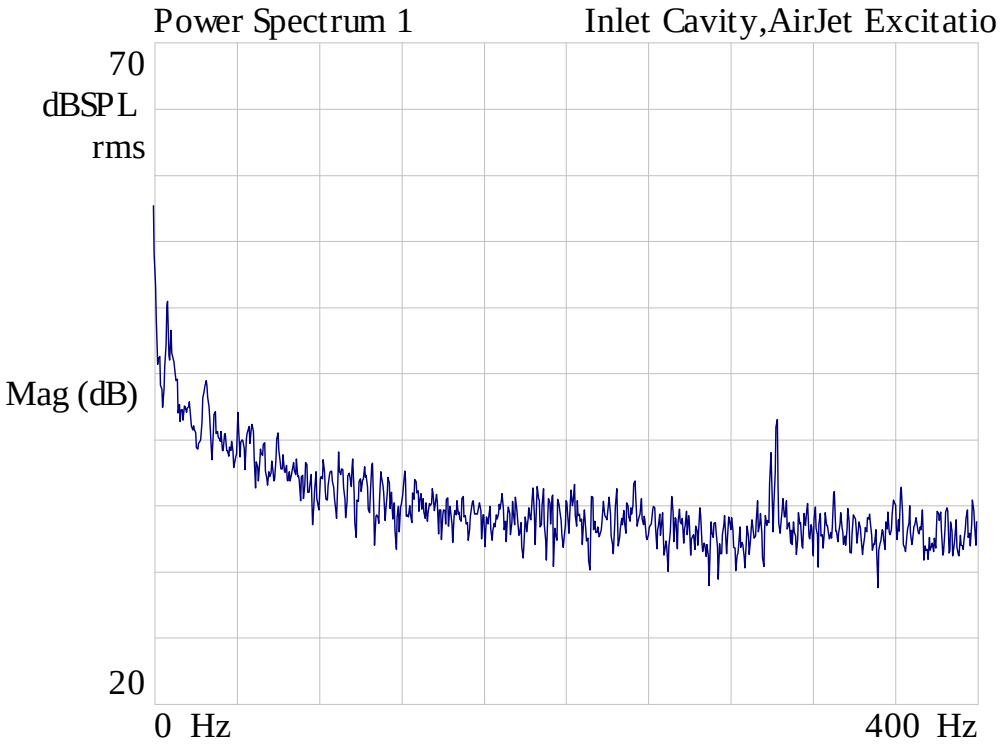

Figure 10.2 Air Jet Broadband Excitation Auto (Power) Spectrum, delta frequency 0.25 Hz, Dataset TJun33

The responses are summarised in Table 10-1 and the auto (power) spectra responses of the inlet chamber and the outlet chamber are shown in Figure 10.3 and Figure 10.4 respectively.

Table 10-1 Summary of the Natural Frequencies of the Muffler LMM Cavity Modes

Excitation Site	Frequency (Hz)					Data Set
	1st Peak	2nd Peak	3rd Peak	4th Peak	5th Peak	
Excitation - Inlet Side						
Chamber Inlet Edge	201.5	49	30.5	230	245	TJun30
Inlet chamber/centre tube	49	30.5	201.5	233	256	TJun31
Axial on centre tube	49	30.5	255	202	336	TJun32
Chamber inlet edge, lateral & longitudinal modes	202.5	49	30.5	229.5	245	TJun37
Excitation - Outlet Side						
Chamber Outlet Edge	30.5	176	49	281	221	TJun34
Outlet chamber / centre tube	49	30.5	176	221		TJun35
Axial on centre tube	49	30.5	176	221	343	TJun36

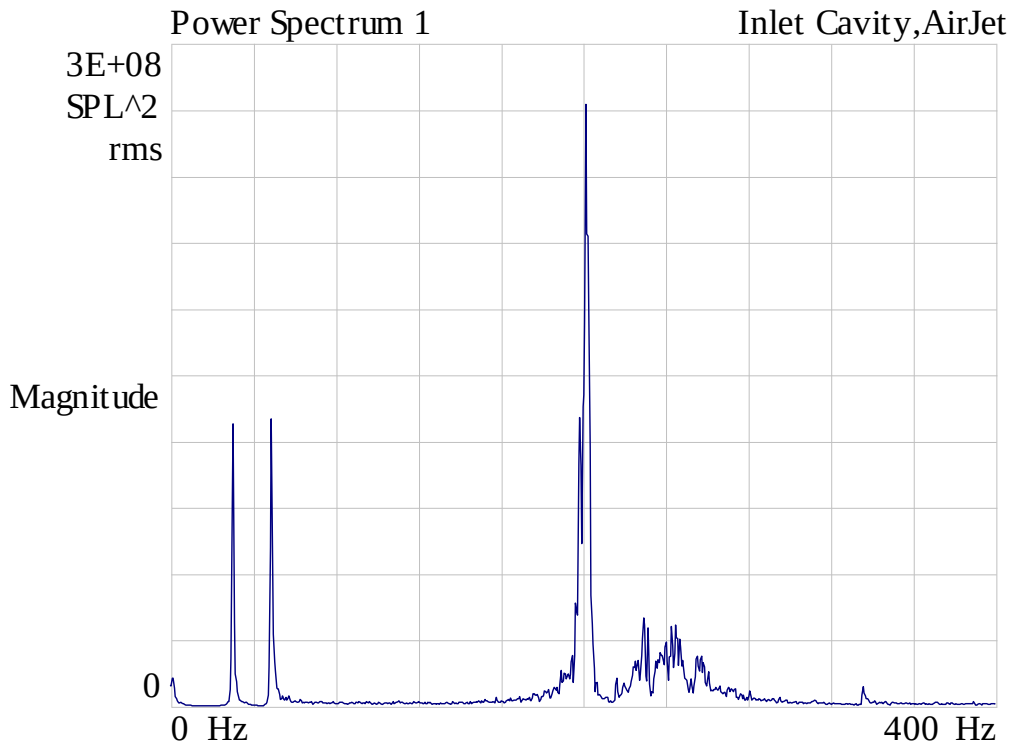

Figure 10.3 Muffler LMM, Inlet Cavity Response, delta frequency 0.25 Hz, Dataset TJun30

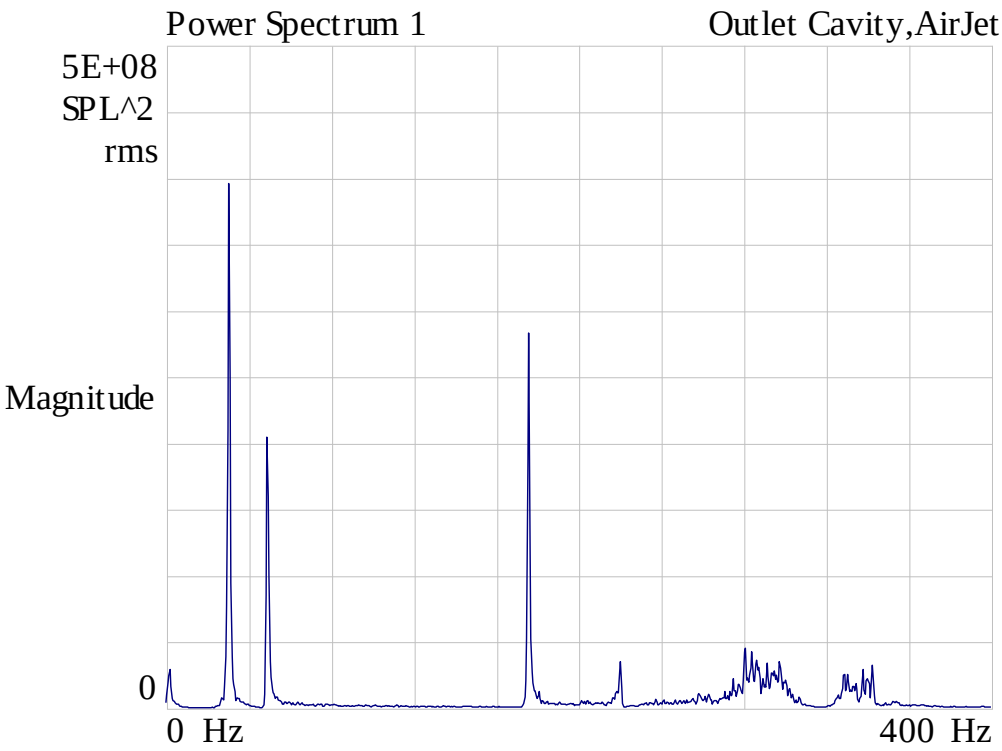

Figure 10.4 Muffler LMM, Outlet Cavity Response, delta frequency 0.25 Hz, Dataset TJun34

As can be seen from Table 10-1 , the 30.5 and 49 Hz resonant responses are common to both chambers. These frequencies have corresponding wavelengths at 25 ºC and 347 m/s speed of sound of 11.4 and 7.1 metres respectively. As these wavelengths and half wavelengths are far larger than the longitudinal dimensions of the muffler, these are most likely associated with the Helmholtz resonator / low pass filter characteristics of the muffler. The inlet side's 202 Hz resonance has an equivalent half wavelength of 0.85 metres and approximates the longitudinal length of the inlet chamber. The outlet side's 176 Hz resonance has an equivalent half wavelength of 0.99 metres and approximates the longitudinal length of the outlet chamber. The expected lateral mode at around 253 Hz for the muffler body was either not excited or not captured due to the microphone's positions.

10.2 Muffler LMM Results

The large marine muffler (LMM) was tested on the experimental acoustic transmission loss test bench across two frequency ranges using the corresponding microphone spacings. The results for Dataset TJun39 are shown in this section. The MATLAB code was used to process the data is listed in Appendix C.

Figure 10.5 shows the measured auto (power) spectra for the pair of microphones before the test muffler. The standing wave behaviour is very clear upstream of the muffler due to the reflections from both the muffler and the speaker. Reflections from the speaker end add to the noise source giving a multiple speaker effect. In contrast there is no standing wave behaviour after the muffler due to the anechoic termination as shown in Figure 10.6.

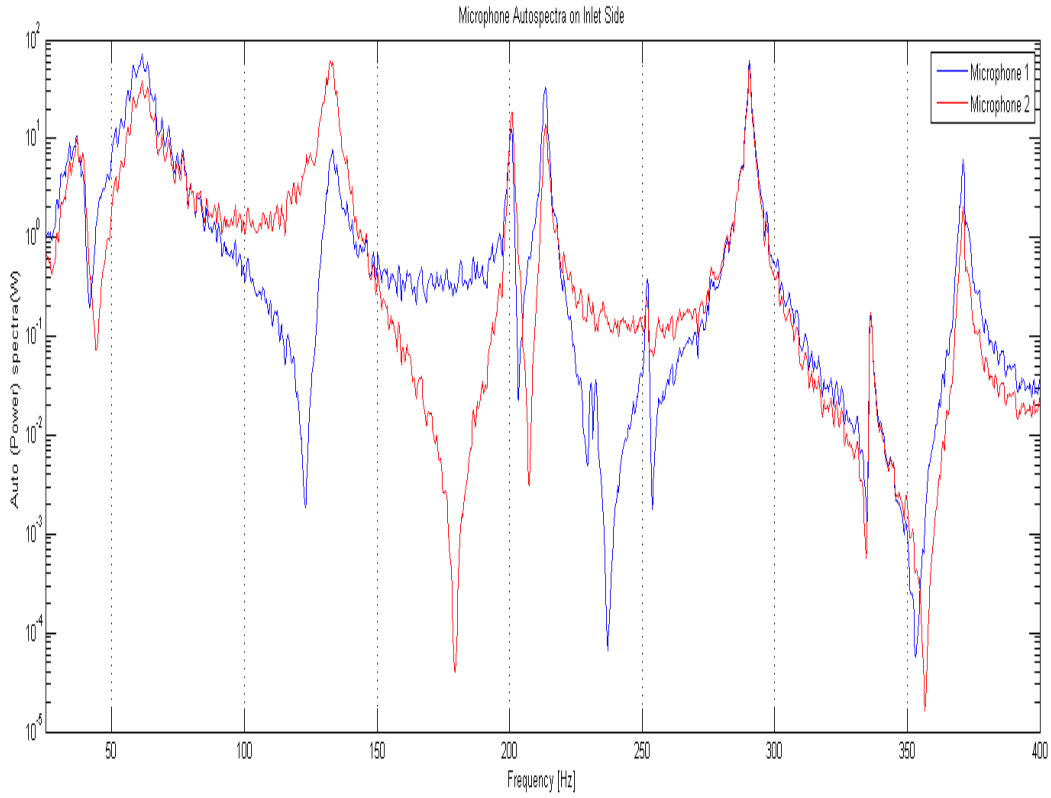

Figure 10.5 Muffler LMM, Measured Auto (Power) Spectra of Microphones 1 and 2 (Upstream)

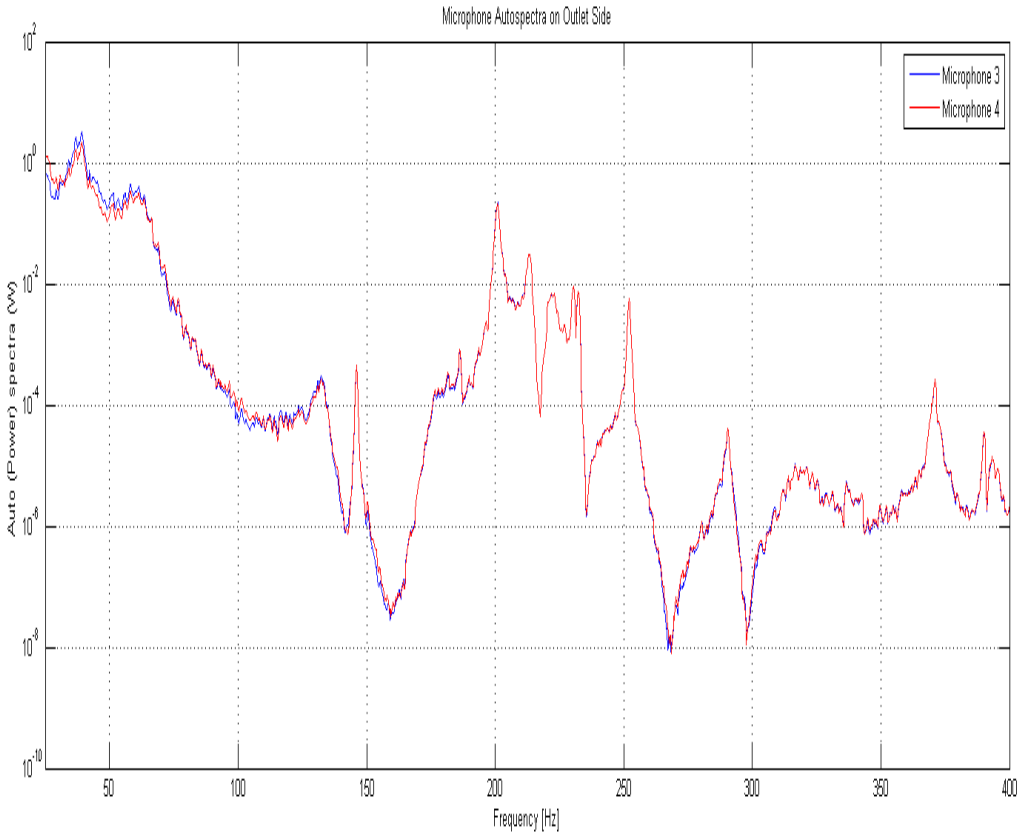

Figure 10.6 Muffler LMM, Measured Auto (Power) Spectra of Microphones 3 and 4 (Downstream)

Figure 10.7 shows the calculated incident and reflected auto (power) spectra before the test muffler. The incident auto (power) spectrum and the reflected auto (power) spectrum are essentially identical as expected due to the lack of absorption.

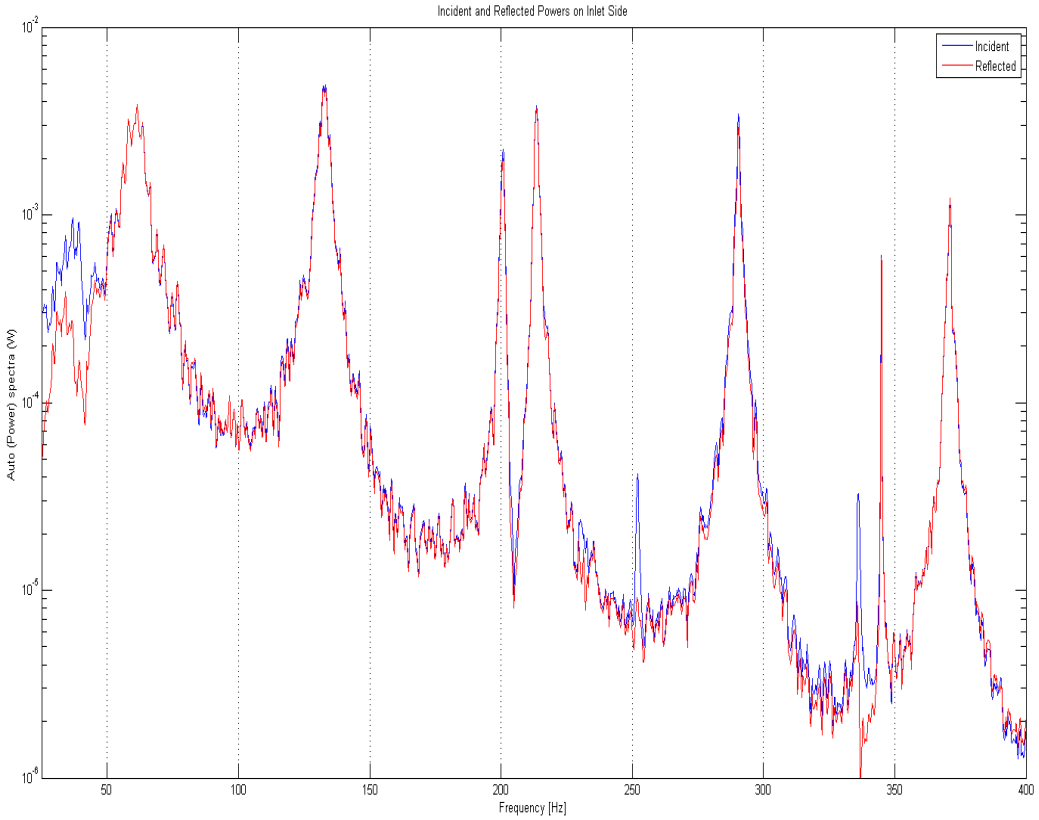

Figure 10.7 Muffler LMM, Incident and Reflected Auto (Power) Spectra - Upstream

Figure 10.8 shows the calculated incident and reflected auto (power) spectra after the test muffler. The incident auto (power) spectrum is greater than the reflected auto (power) spectrum as expected with the difference being due to the anechoic termination. The peak near 350 Hz is the microphone λ/2 spacing effect.

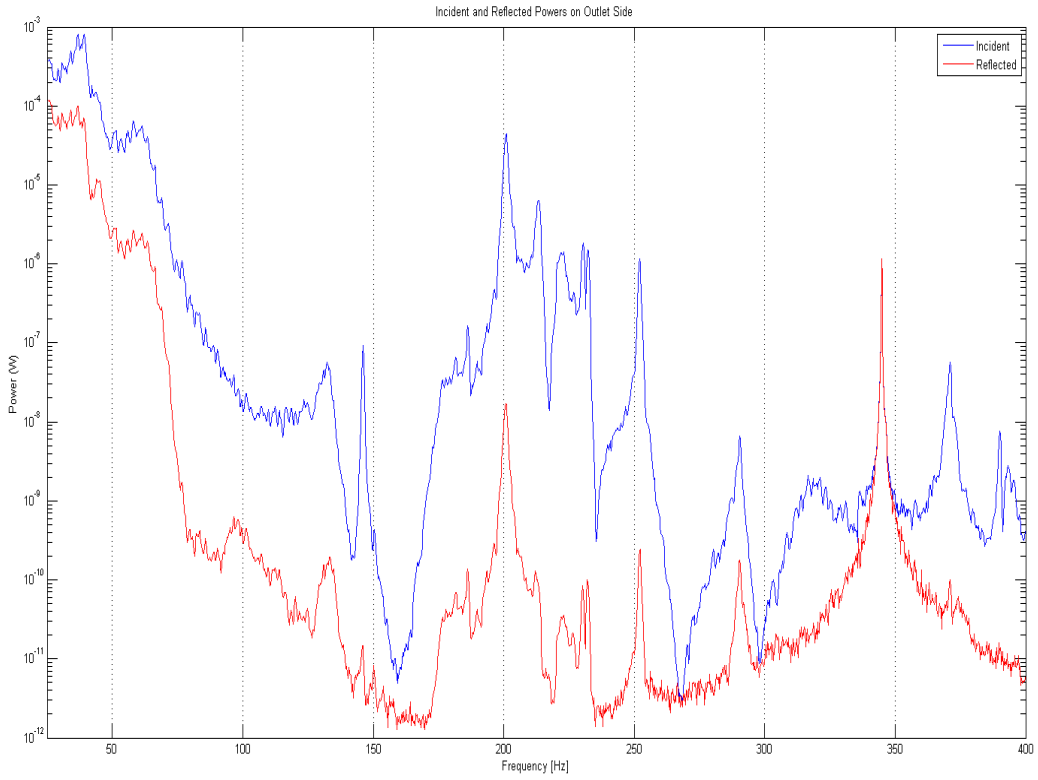

Figure 10.8 Muffler LMM, Incident and Reflected Auto (Power) Spectra - Downstream

Figure 10.9 shows the calculated acoustic transmission loss for the low frequency range. The transmission loss was also calculated using only one microphone after the muffler and this result is also included, labelled as the “three microphone” result. There is little difference between using two microphones or one after the muffler as expected with an effective anechoic termination except below 50 Hz where the anechoic termination is less effective.

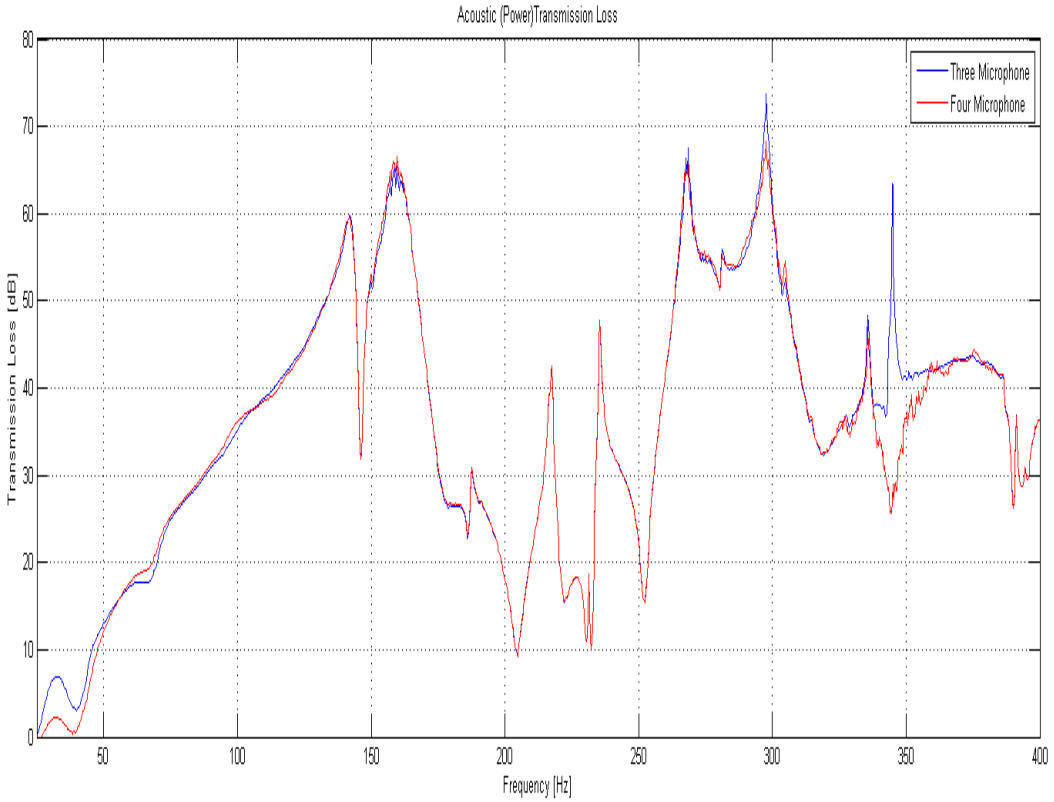

Figure 10.9 Muffler LMM, Acoustic Transmission Loss, Three and Four Microphone Measurements

Chapter 11 Measured Structural Responses – LMM Muffler

This chapter describes the experimental measurement of the dynamic structural behaviour of the LMM muffler shell and internal structures. Resonant frequency results are presented for the shell ring modes and for modes of the interconnecting tube and centre baffle.

11.1 Overview

To assess the veracity of the FEA analysis of the muffler shell (Muffler LMM), the structural resonances of the muffler were measured experimentally. This was not a modal analysis but rather a limited measurement of resonances to assist with validation of the FEA analysis. The physical constraints of the muffler were as shown in Figure 11.1 and differed from the on-engine constraints and from those used in the FEA analysis. The differences in constraints made comparisons difficult and will be revisited in future work. The acoustic modes can couple with the structural modes and vice versa with the vibro-acoustic modal coupling and relative directions of the structural vibrations and sound propagation being significant. The measurements targeted the following modes as they were considered most likely to influence acoustic performance by changing the end conditions of lateral and longitudinal cavity acoustic modes:

1. ring modes of the inlet side chamber
2. ring modes of the outlet side chamber
3. modes of the interconnecting tube mounted in the centre baffle.

Figure 11.1 Muffler LMM, Chain Supports

11.2 Instrumentation

The structural resonances were measured experimentally using an impact hammer (PCB 086C01) with white impact tip (medium stiffness) and aluminium mass extender and a single accelerometer (PCB 353B33 accelerometer 100mV/g). A HP 3567A Spectrum Analyser was used for data capture and calculation of the averaged frequency response function (FRF) – acceleration relative to input force. The processing parameters were 15 averages, Hanning window, and 1600 frequency lines.

11.3 Measurements

A comprehensive set of measurements with varying locations and input and response directions was taken and these are summarised in Table 11-1. This table lists the measured resonant frequencies, accelerometer locations and directions, input impact locations and directions, and set-up photographs. The frequencies for ring modes are summarised in Table 11-2 and Figure 11.11. Similarly, the frequencies for the centre tube / baffle modes are summarised in Table 11-3 and Figure 11.12. Frequency response functions, coherence, and input force spectra are shown in Figure 11.13 and Figure 11.14 for sample measurements for a ring mode and a centre tube / baffle respectively. A full set of these measurements are attached in Appendix A for each measurement / data set.

Table 11-1 Frequency Response Function Summary - Muffler LMM

Data Set	Target	Frequency Range (Hz)	Response Accelerometer Location & Orientation	Force Input Location & Orientation	Measured Resonances (Hz)	Setup Figure
TJuly01	Body Ring Mode, Inlet side	1600	Location A1, Radial	Location H1, Radial	408, 466, 689, 714, 728, 776, 892	Figure 11.2 Figure 11.3
TJuly02	Body Ring Mode, Outlet side	1600	Location A2, Radial	Location H2, Radial	275, 323, 351, 394, 443, 570, 712, 797, 868, 876, 894	Figure 11.2 Figure 11.4
TJuly03	Centre Tube, Outlet side	800	Location A3, Vertical	Location H3, Vertical, Up	151, 200, 443	Figure 11.5
TJuly04	Centre Tube,	800	Location A3, Vertical	Location H4, Lateral	150, 151, 200, 444	Figure 11.6
TJuly05	Outlet side	800	Location A4, Lateral	Location H7, Vertical, Down	150, 151, 200, 443	Figure 11.7
TJuly06	Centre Tube,	800	Location A4, Lateral	Location H5, Lateral	150, 200, 443	Figure 11.8
TJuly07	Outlet side	800	Location A5, Axial	Location H6, Axial	145, 151, 200	Figure 11.9
TJuly08	Centre Tube, Outlet side	800	Location A5, Axial	Location H5, Lateral	150, 200, 445	Figure 11.10

Figure 11.2 Muffler LMM, Ring Mode Locations, Data Sets TJuly01 and TJuly02

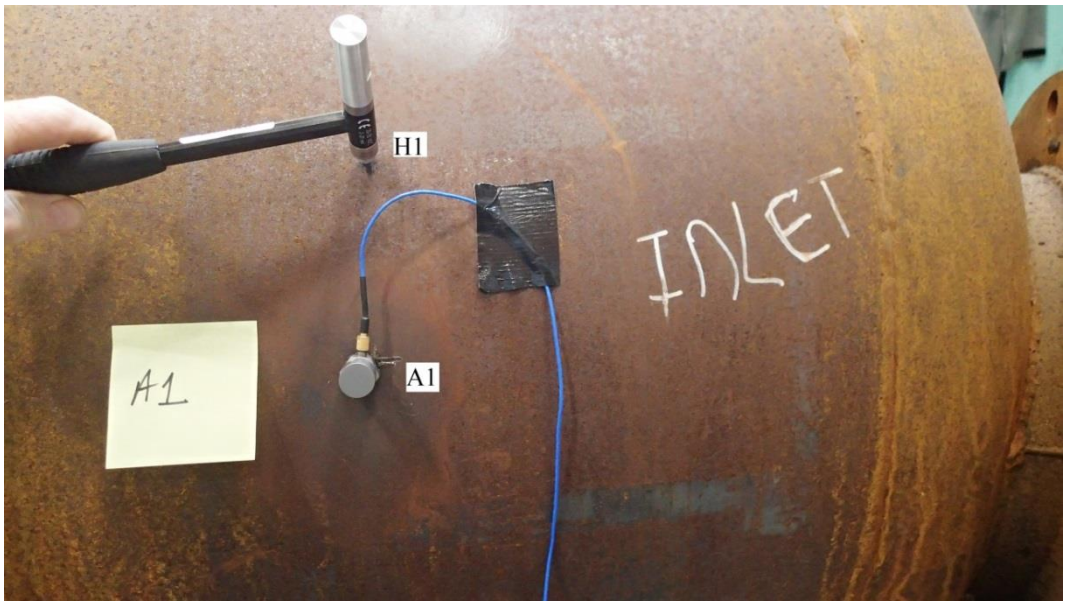

Figure 11.3 Muffler LMM, Ring Mode Locations, Inlet Side, Data Set TJuly01

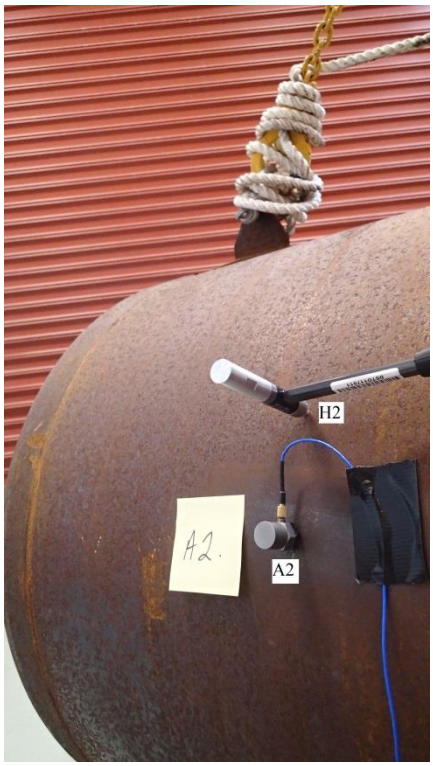

Figure 11.4 Muffler LMM, Ring Mode Locations, Outlet Side, Data Set TJuly02

Figure 11.5 Muffler LMM, Centre Tube Modes, Data Set TJuly03

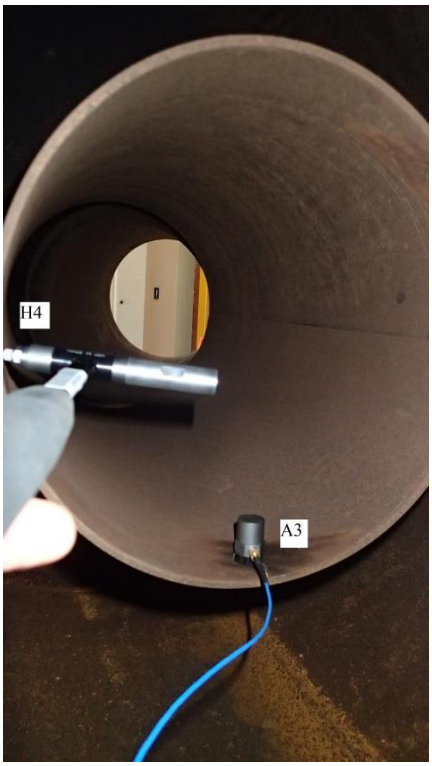

Figure 11.6 Muffler LMM, Centre Tube Modes, Data Set TJuly04

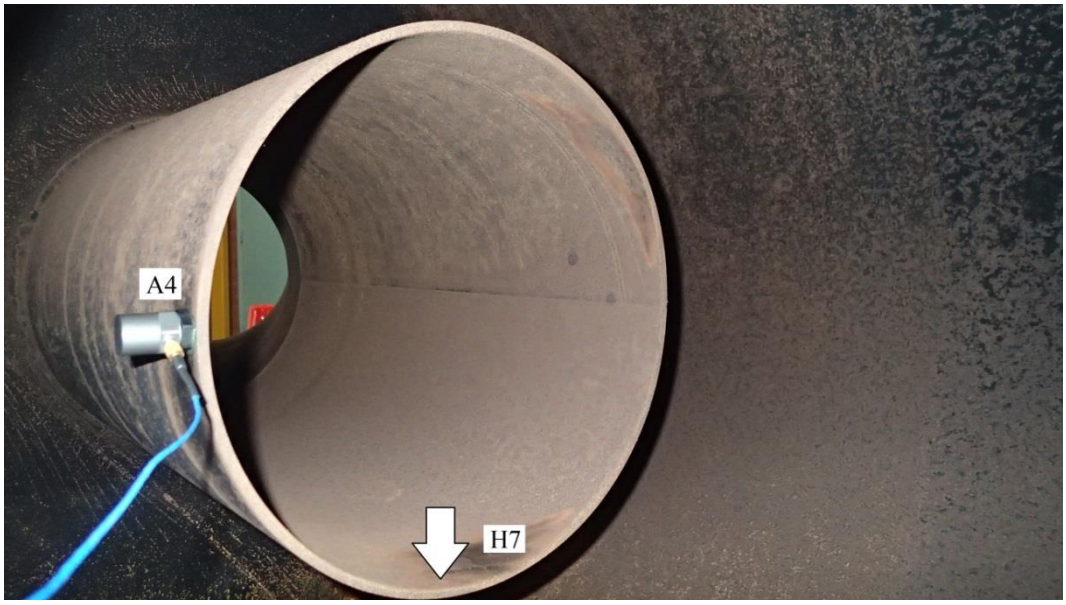

Figure 11.7 Muffler LMM, Centre Tube Modes, Data Set TJuly05

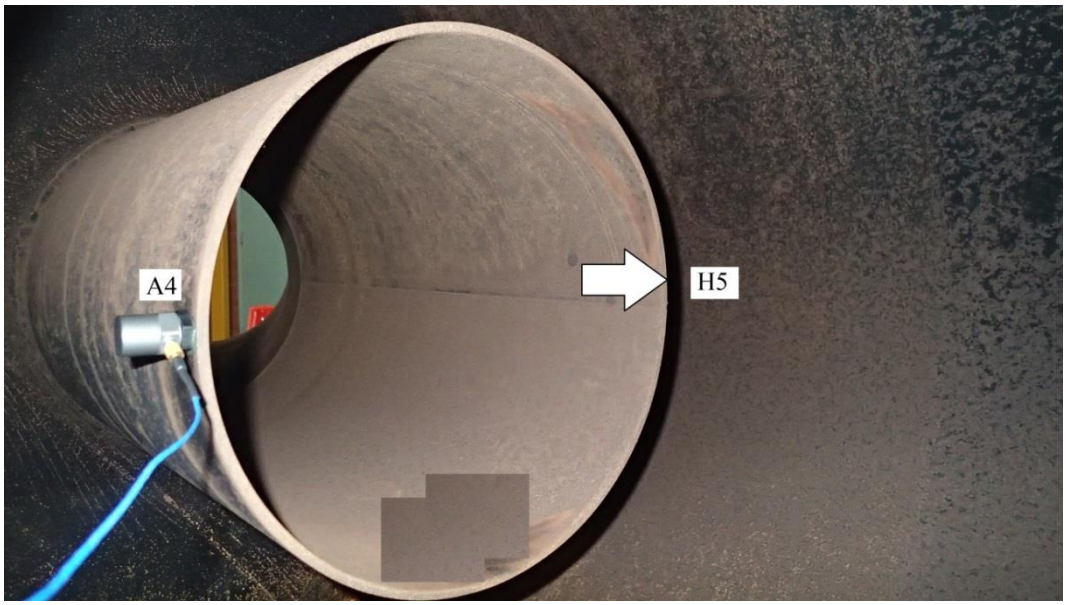

Figure 11.8 Muffler LMM, Centre Tube Modes, Data Set TJuly06

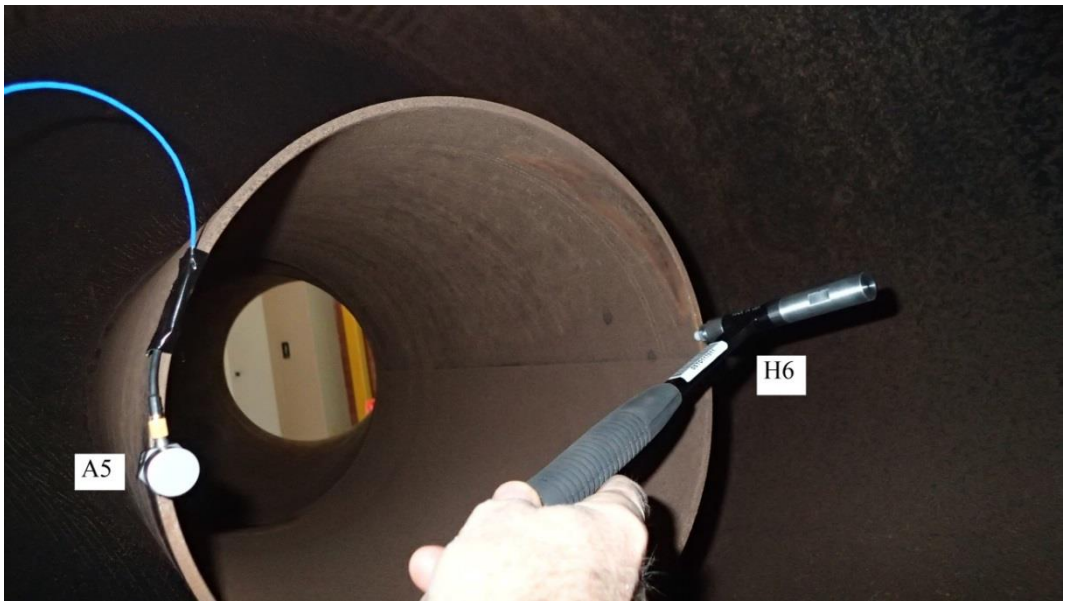

Figure 11.9 Muffler LMM, Centre Tube Modes, Data Set TJuly07

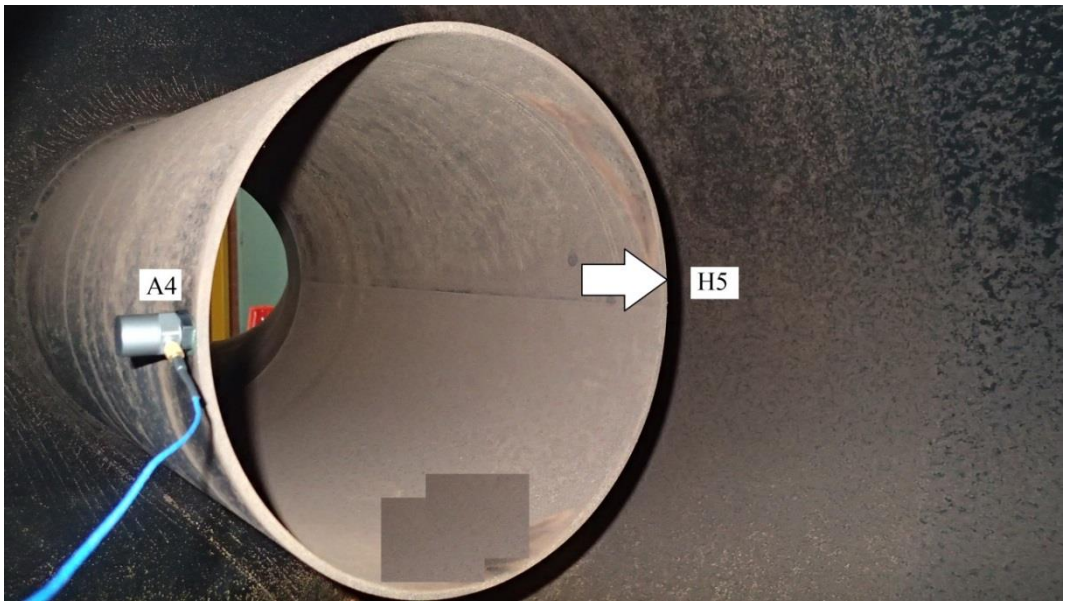

Figure 11.10 Muffler LMM, Centre Tube Modes, Data Set TJuly08

Table 11-2 Ring Mode Frequencies

Data Set	Body Ring Modes Frequencies (Hz)															
Inlet Side					408		466		689	714	728	776				892
Outlet Side	275	323	351	394		443		570		712			797	868	876	894

Table 11-3 Centre Tube Frequencies

Data Set	Centre Tube, Outlet Side, Frequencies (Hz)				
TJuly03			151	200	443
TJuly04		150	151	200	443
TJuly05		150	151	200	443
TJuly06		150		200	443
TJuly07	145		151	200	443
TJuly08		150		200	445

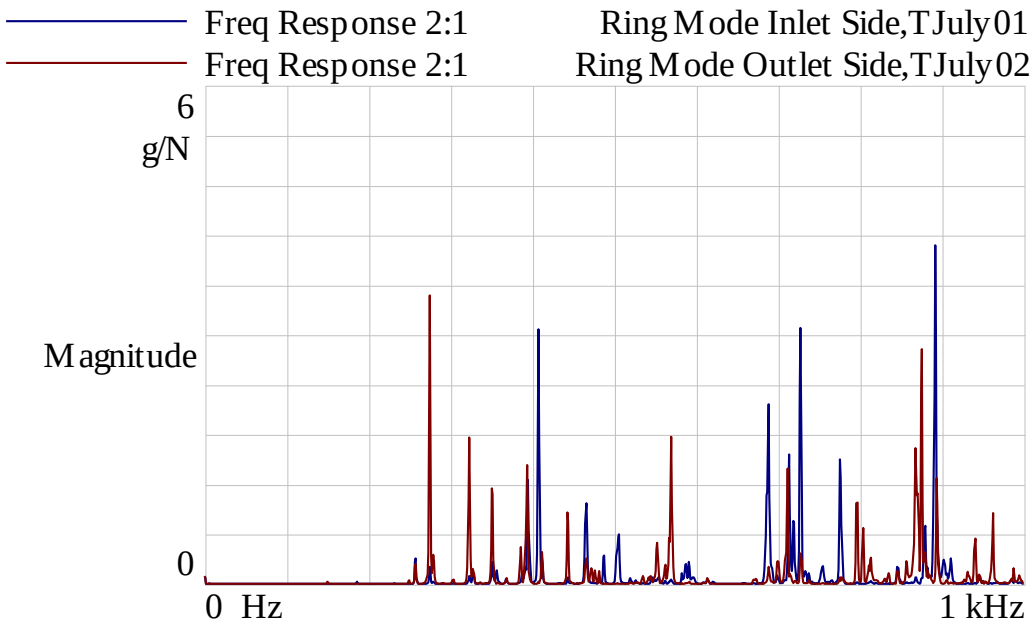

Figure 11.11 Frequency Response Function, Ring Modes

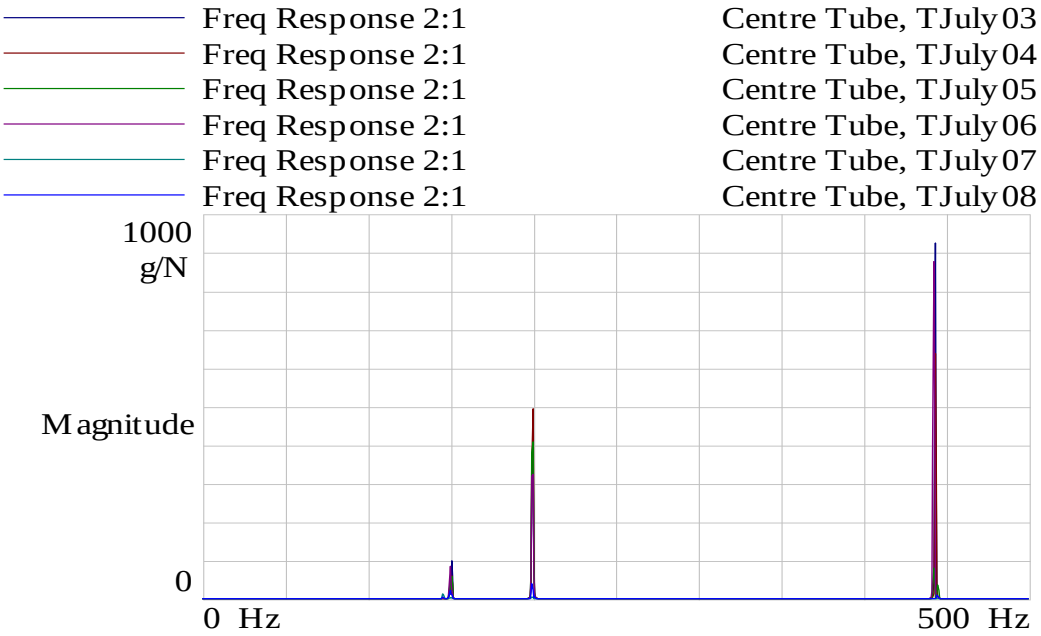

Figure 11.12 Frequency Response Function, Centre Tube Modes

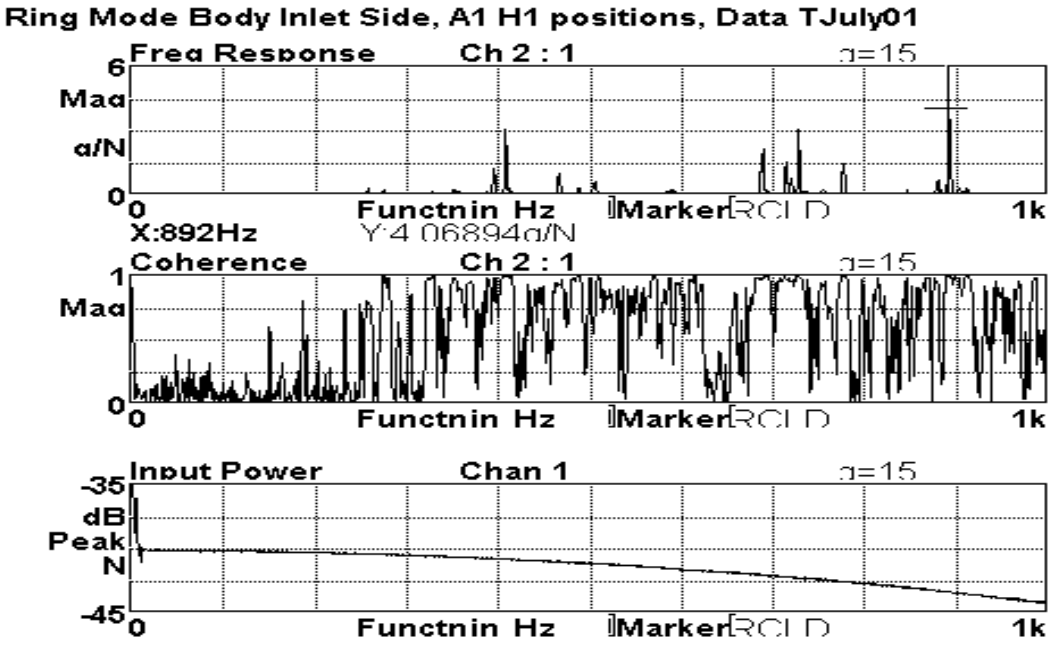

Figure 11.13 Frequency Response Function, Ring Modes, Data Set TJuly01

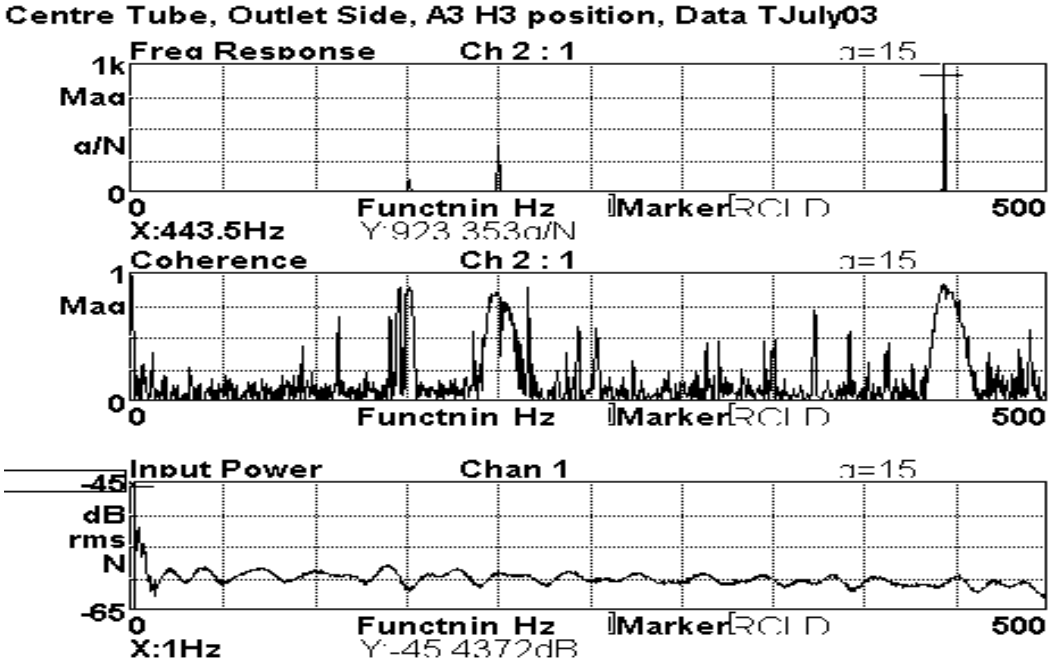

Figure 11.14 Frequency Response Function, Centre Tube Modes, Data Set TJuly03

Chapter 12 Discussion

12.1 Flow Modelling

12.1.1 Simplified Large Mufflers (LM)

The WAVE modelling results show sensitivity of flow rate to design changes and the calculated flow rate characteristics are consistent with the level of complexity and expected flow restriction of the mufflers with the exception of muffler LM2.

12.1.2 Large Marine Muffler (LMM)

For the large marine type muffler (LMM), the calculated flow rate was sensible but lower for a given pressure difference than the on-engine test data with similar mufflers suggests. The discretization study showed an 8% (minimum to maximum) flow range which highlighted the modelling sensitivity and resulting poor confidence level in the simulated absolute value.

12.2 Finite Element Analysis

The FEA analysis showed many structural modes in the frequency range of interest which are likely to influence the acoustic performance. This is particularly so where the vibro-acoustic coupling is significant and when the direction of wall motion is in the direction of propagation of the acoustic mode and / or sound wave. For example shell ring modes are more likely to interact with lateral acoustic modes than longitudinal acoustic modes. The multiple low frequency structural modes involving the centre baffle and the interconnecting tube were unexpected and any longitudinal motion of the centre baffle will influence the longitudinal waves. Additionally there is the possibility of metal fatigue failures if run at resonance and high stress amplitudes due to the lack of structural damping.

The experimental structural measurements confirmed that there are low frequency modes of the centre tube and centre baffle though at lower frequencies than predicted by the FEA analysis as shown in Figure 12.1. The measurements confirmed the existence of ring modes in the frequency range predicted by the FEA analysis but with a wider range as shown in Figure 12.2. As this was not a modal analysis but rather a limited measurement of resonances with differences in how the muffler was constrained, the correlation with the FEA analysis is acceptable for the purposes of this thesis and should be the subject of future work.

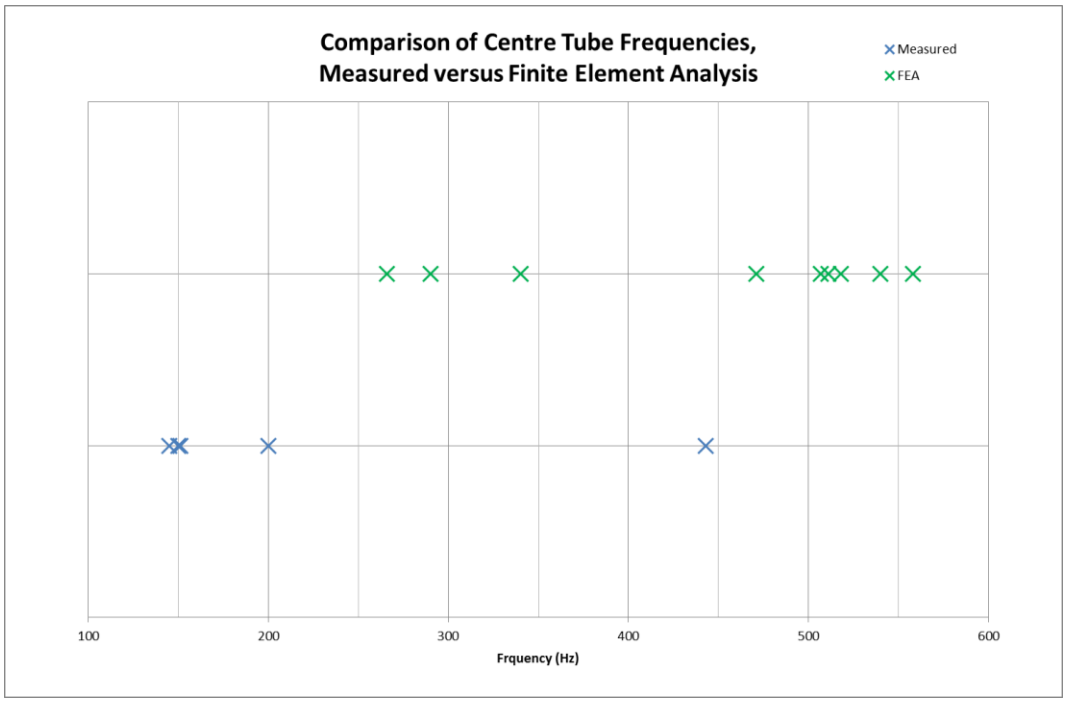

Figure 12.1 Muffler Centre Tube Modes, Measured versus FEA

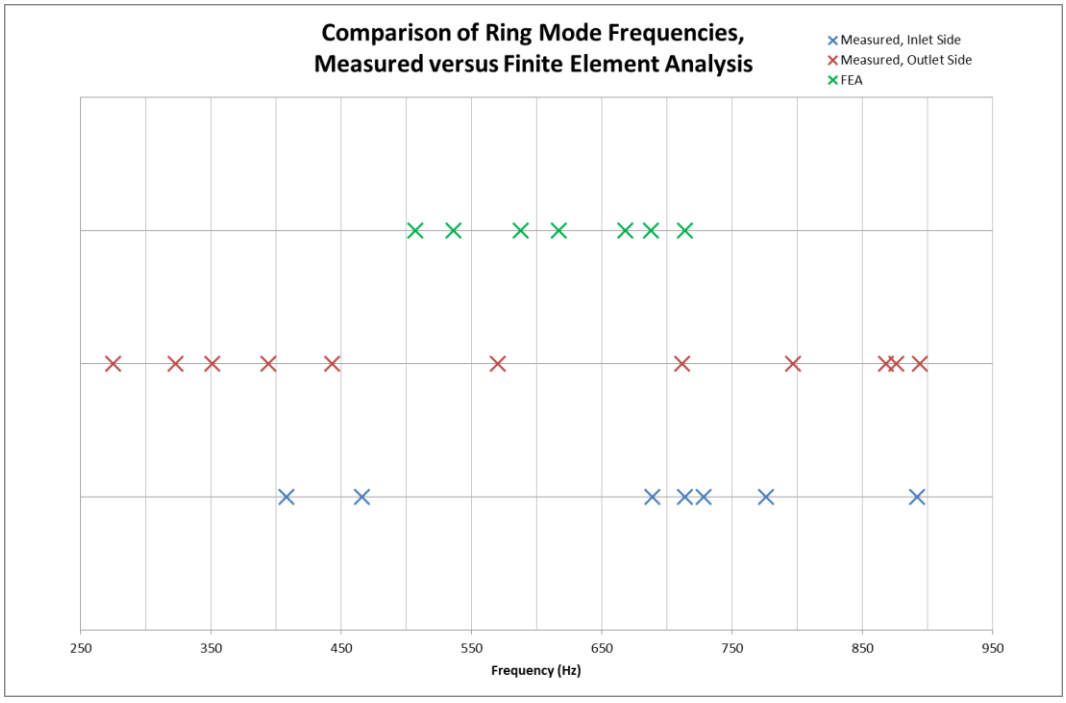

Figure 12.2 Muffler Body Ring Modes, Measured versus FEA

12.3 Acoustic TL Bench

The experimental acoustic transmission loss test bench designed, constructed and used in this study operates with zero flow at ambient conditions of temperature and pressure unlike an on-engine application. The effects of these temperature and flow differences were discussed in Sections 2.5 and 2.6 respectively and temperature can be corrected for by a ratio of the respective speeds of sound. If the flow is less than Mach 0.1, there should be minimal effect on acoustic attenuation though the local effects of turbulent flow including flow generated noise can be significant. One benefit of zero flow for the experimental bench is an improved acoustic signal to noise ratio in the absence of flow generated noise. A second and more important benefit is the ability to have an effective anechoic termination as there is no need for flow through the termination.

The performance of this facility has been compared with computer simulations and theoretical calculations. For simple components such as the contraction / expansion chambers the correlation is excellent. For the large marine muffler (LMM) there is reasonable agreement in the variation of the magnitudes of the transmission losses but frequency shifts are evident. The effective frequency range of the facility at room temperature is currently 30 Hz to 600 Hz. The lower value is limited by the speaker / driver performance and the upper value is due to the measurement duct's first cut-on frequency being at approximately 615 Hz.

12.4 Acoustic Modelling

The WAVE virtual acoustic transmission loss test bench is internally constrained by the software to operate at zero flow and Section 12.3 covers the effects of this.

12.4.1 NACA Mufflers

Modelling and experimental results from the NACA muffler research program were used to benchmark WAVE's capabilities at test bench conditions. Seven single chamber expansion chambers, nine multi-chamber expansion chambers, three quarter-wave tubes and seven Helmholtz resonators were compared. The WAVE modelling results showed good agreement with NACA results for the overall shapes and magnitude of transmission losses. As the complexity of the mufflers increase, the WAVE simulation appears to overestimate the magnitude of the transmission losses. This may be due to an absence of losses in the simulation resulting in unrealistic estimates of transmission loss, e.g. a 60 dB reduction is a reduction to one part in one thousand.

12.4.2 Simplified Large Mufflers (LM)

The WAVE modelling results for the large mufflers showed high sensitivity to design changes and the transmission loss characteristics were consistent with the findings for the NACA muffler models.

12.4.3 Large Marine Muffler (LMM)

The air jet excitation of the muffler cavities and internal features confirmed that the muffler is not simply two expansion chambers in series but rather a much more complex Helmholtz filter / low pass filter with interactions between the centre tube and the two chambers. The WAVE modelling results (at 25 ºC) and the experimental test bench results are shown in Figure 12.3. The modelling results show reasonable agreement with test results with respect to overall shape, frequencies, and amplitudes of the noise spectrum.

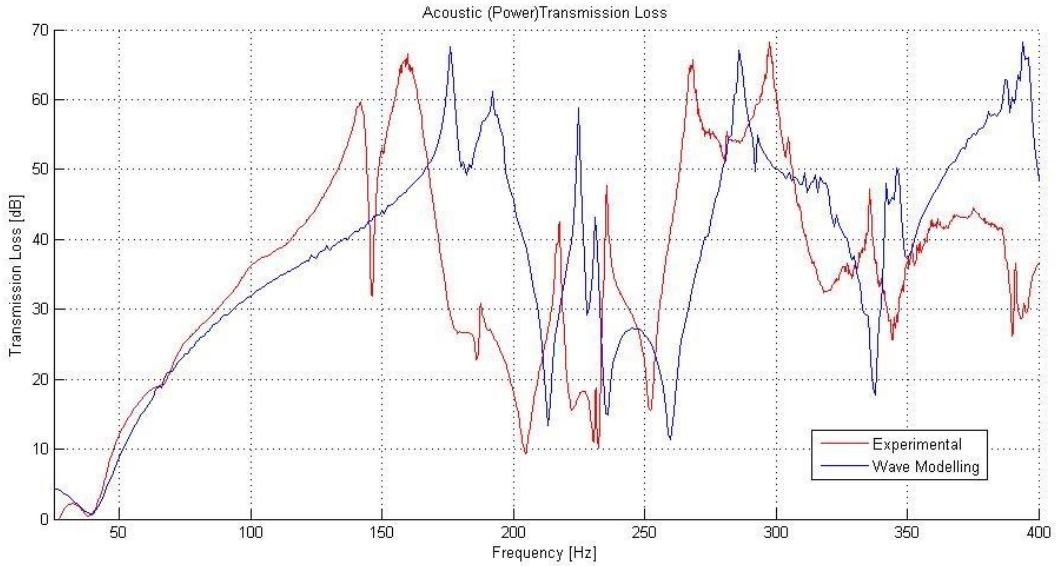

Figure 12.3 Muffler LMM, Modelling and Experimental Test Results, 0 to 400 Hz

12.4.4 Large Marine Muffler (LMM) Discretization Study

It was apparent that the predicted transmission loss of the subject muffler (LMM) is sensitive to the discretisation size in all three directions - dx, dy, and dz. In particular there doesn't appear to be an optimum size or clear trends as the mesh increases or decreases from this optimum. This may be a function of the size and complexity of the subject muffler. This appears to be an area of possible error as evidenced by Ricardo issuing guidelines for automotive sized mufflers in "Special Topics: Acoustic Benchmark & Recommended Discretization Techniques" [68]. This recommends:

1. Use the minimum number of elements possible so to minimise run times
2. Use ducts to model chambers and ducts where possible
3. Use a dx which gives at least six pieces per wavelength at maximum frequency of interest
4. In a general volume use a dx / dy / dz of 50 mm where possible.

The modelling in this thesis follows guidelines 1, 2, and 3. Guideline 4 is applicable to automotive sized mufflers but not achievable with the size of the subject mufflers. The approach taken in this thesis was to select the discretisation size in the direction of flow (dx) as one tenth of the wavelength at the highest frequency of interest and use this in the lateral directions (dy) and vertical (dz) directions where the software element number limits permit.

Chapter 13 Conclusions

13.1 Flow Analysis

The conclusions with respect to the flow simulation can be summarised as:

1. WAVE virtual test bench modelling gave sensible results for simple mufflers and design iterations with the exception of large muffler LM2.
2. WAVE virtual test bench modelling gave only fair agreement for a complex large marine muffler (LMM).
3. Accordingly, the technique is currently useful for design trend predictions but for a typical large marine muffler does not give absolute results with high confidence limits.

13.2 Finite Element Analysis

The conclusions with respect to the structural behaviour of the muffler shell as investigated using FEA and experimental measurements can be summarised as:

1. The FEA analysis showed many structural modes in the frequency range of interest which are likely to influence the acoustic performance.
2. There are multiple low frequency modes involving the centre baffle and the interconnecting tube.
3. Shell ring modes were identified for both cavities.
4. The experimental measurements confirmed that there are low frequency modes of the centre tube and centre baffle and ring modes of the muffler shell.

13.3 Experimental Acoustic TL Bench

The conclusions with respect to the experimental transmission loss test bench designed, constructed and used in this study can be summarised as:

1. An experimental facility capable of measuring the acoustic transmission loss of exhaust and intake system components representative of a large marine diesel has been designed, constructed and validated using simple and complex acoustic devices.
2. The differences between measured and simulated transmission loss results for complex mufflers need to be further investigated and the reasons identified.

3. It is expected that the experimental facility's performance can be further improved with development and optimisation of parameters including measurement duct lengths, measurement duct diameters, duct wall thicknesses, absorption on source side, microphone locations, data processing error analysis and tailored input spectra.
4. Future work could include an assessment of benefits of correcting microphone phase and magnitude differences.

13.4 Acoustic Analysis and Verification

The conclusions with respect to the acoustic behaviour of the muffler as investigated using 1D simulation and experimental measurements can be summarised as:

1. This study has developed an effective computer simulation capability based on WAVE software capable of modelling the acoustic response of an intake or exhaust system representative of a large marine diesel.
5. WAVE virtual test bench modelling results showed excellent agreement with:
    a. published NACA results
    b. theoretical results for the simplified large mufflers (LM1 to LM10)
    c. theoretical results for the contraction / expansion chambers
    d. experimentally derived results for the contraction / expansion chambers.
6. The virtual test bench modelling results showed only reasonable agreement for the large marine type muffler (LMM) perhaps due to some modelling issue with the muffler's internal geometry. The discretization study highlighted this sensitivity.
7. The computer models developed can be used for exhaust system components, complete exhaust systems or full engine-exhaust systems. The modelling flexibility permits assessment and development of systems with or without engine source data.

13.5 Overall

In summary the following overall conclusions were drawn from this study:

1. The study has shown that a commercial one-dimensional (1D) software suite targeted at automotive applications can be successfully used for modelling the acoustic performance for the intake systems and exhaust systems of medium and large diesels.
2. The study has shown that a commercial one-dimensional (1D) software suite targeted at automotive applications can be used for modelling the flow restriction for the intake systems and exhaust systems of medium and large diesels but with reservations on the absolute values obtained.

3. The study identified and catered for the acoustic, gas flow, and modelling differences between automotive scale intake systems and exhaust systems and those of medium and large diesels.
4. The study identified the most promising method for accurate characterization of the acoustic performance of intake and exhaust systems and system components in a laboratory test facility. This information was then used to design and construct the zero flow ambient conditions experimental acoustic transmission loss test bench used in this study. This test bench was validated using simple verifiable large acoustic devices such as the contraction / expansion chambers.

References

1. Taylor, C. F. (1985) *The Internal-Combustion Engine in Theory and Practice - Volume 1: Thermodynamics, Fluid Flow, Performance*. Second ed. USA, The M.I.T. Press
2. Yule, P. and Woolner, D. (2008) *The Collins Class Submarine Story - Steel,Spies and Spin*, Cambridge University Press
3. Blair, G. P. (1999) *Design and Simulation of Four-Stroke Engines*. Warrendale, Society of Automotive Engineers, Inc
4. Martyr, A. J. and Plint, M. A. (2012) *Engine Testing Theory and Practice*, Butterworth Heinemann
5. *Gamma Technologies Inc.* [Accessed 2/10/2013]; Available from: http://www.gtisoft.com/.
6. *Lotus Engineering*. [Accessed 2/10/2013]; Available from: http://www.lotuscars.com/au/engineering/about-lotus-engineering.
7. *Optimum Power Technology*. [Accessed 2/10/2013]; Available from: http://www.optimum-power.com/.
8. *AVL Powertrain Engineering Inc.* [Accessed 2/10/2013]; Available from: https://www.avl.com/home.
9. Amphlett, S., et al. (2011) Linear Acoustic Modelling using 1-D Systems which represent Complex 3-D Components. *SAE Technical Paper Series* (2011-01-1524)
10. Munjal, M. L. (1998) Analysis and Design of Mufflers —An Overview of Research at the Indian Institue of Science. *Journal of Sound and Vibration* 211 (3) 425-433
11. Munjal, M. L. (2013) Recent Advances in Muffler Acoustics. *International Journal of Acoustics and Vibration* 18 (2) 15
12. Ricardo, S. *Ricardo plc*. (2016) [Accessed 2/10/2013]; Available from: http://www.ricardo.com/.
13. Tao, Z. and Seybert, A. F. (2003) A Review of Current Techniques for Measuring Muffler Transmission Loss. *SAE Technical Paper Series* (2003-01-1653)
14. Williamson, P. S. and Chuter, R. J. (2002) Modelling Exhaust Systems Using One-Dimensional Methods. In: *SAE 2002 World Congress & Exhibition,* Detroit, MI, USA, SAE International
15. Randall, R. B. (1987) *Frequency Analysis*. 3 ed. Denmark, Bruel & Kjaer
16. MTU (2002) *Airborne Noise Analysis, MTU 16V 4000 M70*. MTU Friedrickshafen GmbH.
17. Bowden, D. and Forrest, J. (2015) Refinement of Exhaust System Noise from Large Diesel Engines Using One dimensional (1D) Simulation. In: *Acoustics 2015,* Hunter Valley, Australia: November 2015
18. Bowden, D. (2016) Development of a large experimental acoustic transmission loss test bench suitable for large marine diesel exhaust system components. In: *Acoustics 2016,* Brisbane, Australia, Australian Acoustical Society
19. Alfredson, R. J. and Davies, P. O. A. L. (1970) The Radiation of Sound from an Engine Exhaust. *Journal of Sound and Vibration* 13 (4) 389-408
20. Alfredson, R. J. and Davies, P. O. A. L. (1971) Performance of exhaust silencer components. *Journal of Sound and Vibration* 15 (2) 175-196
21. Davies, P. O. A. L. (1964) The design of silencers for internal combustion engines. *Journal of Sound and Vibration* 1 (2) 185-201
22. Davies, P. O. A. L. (1992) *Practical flow duct acoustic modelling*. Institute of Sound and Vibration Research technical report. Southampton, University of Southampton
23. Davies, P. O. A. L. (1993) Piston Engine Intake and Exhaust System System Design. In: *Vehicle Vibration Noise & Vibration Course Notes*. UK, ISVR, Southampton University
24. Davies, P. O. A. L. and Harrison, M. F. (1996) *Predictive acoustic modelling applied to the control of intake/exhaust noise of internal combustion engines*. Institute of Sound and Vibration Research technical report. Southampton, University of Southampton.

25. Chung, J. Y. and Blaser, D. A. (1980) Transfer function method of measuring acoustic intensity in a duct system with flow. *Journal of the Acoustical Society of America* **68** (6) 1570-1577
26. Chung, J. Y. and Blaser, D. A. (1980) Transfer function method of measuring in-duct acoustic properties. I. Theory. *Journal of the Acoustical Society of America* 68 (3) 907-913
27. Chung, J. Y. and Blaser, D. A. (1980) Transfer function method of measuring in-duct acoustic properties. II. Experiment. *Journal of the Acoustical Society of America* 68 (3) 914-921
28. Seybert, A. F. (1984) A review of the in-duct method for measuring acoustic intensity and acoustic properties of materials and systems. *Journal of the Acoustical Society of America* 75 (S1) S55-S55
29. Seybert, A. F. (1988) Two-sensor methods for the measurement of sound intensity and acoustic properties in ducts. *Journal of the Acoustical Society of America* 83 (6) 2233-2239
30. Seybert, A. F. and Ross, D. F. (1977) Experimental determination of acoustic properties using a two-microphone random-excitation. *Journal of the Acoustical Society of America* 61 (5) 1362-1370
31. Seybert, A. F. and Soenarko, B. (1980) In-duct measurement of acoustic properties using a two-microphone technique with random and pure tone excitation. *Journal of the Acoustical Society of America* 67 (S1) S73-S73
32. Munjal, M. L. (2013) *Noise and Vibration Control*. IISc Lecture Notes Series. Vol. 3. Singapore, World Scientific
33. Munjal, M. L. (1987) *Acoustics of ducts and mufflers with application to exhaust and ventilation system design*. New York, Wiley
34. Munjal, M. L. (2014) *Acoustics of Ducts and Mufflers*. Second ed. United Kingdom, WILEY
35. Munjal, M. L. and Doige, A. G. (1990) Theory of a two source-location method for direct experimental evaluation of the four-pole parameters of an aeroacoustic element. *Journal of Sound and Vibration* 141 (2) 323-333
36. Winterbone, D. E. and Pearson, R. J. (1999) *Design Techniques for IC Engines Wave Action Methods for IC Engines*, Professional Engineering Publishing Limited
37. Winterbone, D. E. and Pearson, R. J. (2000) *Theory of Engine Manifold Design Wave Actions for IC Engines*, Professional Engineering Publishing
38. Harrison, M. F. and Stanev, P. T. (2004) Measuring wave dynamics in IC engine intake systems. *Journal of Sound and Vibration* 269 (1–2) 389-408
39. Harrison, M. F. and Stanev, P. T. (2004) A linear acoustic model for intake wave dynamics in IC engines. *Journal of Sound and Vibration* 269 (1–2) 361-387
40. Blair, G. P. (1999) *Design and Simulation of Engines: A Century of Progress*. USA, SAE International
41. Torregrosa, A. J., et al. (2012) Analysis of acoustic networks including cavities by means of a linear finite volume method. *Journal of Sound and Vibration* 331 (20) 4575-4586
42. Montenegro, G., et al. (2007) *Integrated -D-MultiD Fluid Dynamic Models for the Simulation of I.C.E. Intake and Exhaust Systems*. USA, SAE International
43. Onarati, A., Montenegro, G. and D'Errico, G. (2006) *Prediction of the Attenuation Characteristics of I.C. Engine Silencers by 1-D and Multi-D Simulation Models*. USA, SAE International
44. Davis, D. D., et al. (1953) *Theoretical and Measured Attenuation of Mufflers at Room Temperature without Flow, with Comments on Engine-Exhaust Muffler Design*. Washington,USA, NACA
45. Davis, D. D., et al. (1954) *Theoretical and Experimental Investigation of Mufflers with Comments on Engine-Exhaust Muffler Design*. 1192, Washington, D.C., National Advisory Committee for Aeronautics
46. Abom, M. and Boden, H. (1988) Error analysis of two-microphone measurements in ducts with flow. *Journal of the Acoustical Society of America* 83 (6) 2429-2438
47. Bodén, H. and Åbom, M. (1986) Influence of errors on the two-microphone method for measuring acoustic properties in ducts. *Journal of the Acoustical Society of America* 79 (2) 541-549

48. E2611-09 (2009) *Standard Test Method for Measurement of Normal Incidence Sound Transmission of Acoustical Materials based on the Transfer Matrix Method*. USA, ASTM
49. E1050-12 (2012) *Standard Test Method for Impedance and Absorption of Acoustical materials Using a Tube, Two Microphones and a Digital Frequency Analysis System*. USA, ASTM
50. Bendat, J. S. and Piersol, A. G. (1993) *Engineering Applications of Correlation and Spectral Analysis*. Second ed. USA, Wiley
51. Spectronics (2013) *BEST PRACTICES: A Guide to Making Effective Measurements of Sound Absorption Coefficient*. USA, Spectronics Inc.
52. Seybert, A. F. (2016) *Email - Anechoic termination and wave decomposition*. To: Bowden, D.,
53. Buzbuchi, N. and Stan, L. C. (2010) NOISE MARINE DIESEL ENGINES AND THE ENVIRONMENT - PART II*. Universitatii Maritime Constanta. Analele* 13 59-62
54. Buzbuchi, N. and Stan, L. C. (2010) NOISE MARINE DIESEL ENGINES AND THE ENVIRONMENT - PART I*. Universitatii Maritime Constanta. Analele* 13 55-58
55. Bies, D. A. and Hansen, C. H. (2009) *Engineering Noise Control,Theory and Practice*. Fourth ed. Abingdon, UK, Spon Press
56. Ricardo.com (2013) *Email: Acoustic Modelling of of Large Non-automotive Diesels*. To: Bowden, D., Email, 27th August 2013
57. Johansson, C.-G., et al. (2005) Silencer measurements in the manufactory hall, Acoustical Society of Finland
58. Johansson, C.-G., et al. (2005) Exhaust noise - a new measurement technology in duct, Acoustical Society of Finland
59. Ji, Z. and Wang, X. (2008) Application of dual reciprocity boundary element method to predict acoustic attenuation characteristics of marine engine exhaust silencers*. Journal of Marine Science and Application* 7 102-110
60. Beranek, L. L. and Ver, I. L. (eds.) (1992) *Noise and Vibration Control Engineering Principles and Applications*. John Wiley & Sons
61. Eriksson, L. J. and Thawani, P. T. (1985) Theory and Practice in Exhaust System Design*. Society of Automotive Engineers* (850989)
62. Green, A. J. and Smith, P. N. (1988) *Gas Flow Noise and Pressure Loss in Heavy Vehicle Exhaust Systems*. Berkshire, UK, Department of Transport
63. Howard, C. Q. and Cazzolato, B. S. (2015) *Acoustic Analyses Using MATLAB and ANSYS*. USA, CRC Press
64. Davies, M. E. and Johnson, O. (1990) An investigation into advanced acoustic models of exhaust and intake systems*. Institution of Mechanical Engineers* C240/026 1990
65. Crocker, M. J. (1998) *Handbook of Acoustics*. USA, John Wiley & Sons, Inc
66. Allam, S. and Boden, H. (2005) Methods for Accurate Determination of Acoustic Two-port Data in Flow Ducts. In: *Twelfth International Conference on Sound and Vibration,* Lisbon, Spain
67. Howard, C. Q. and Craig, R. A. (2014) Noise Reduction Using a Quarter Wave Tube with Different Orifice Geometries*. Applied Acoustics* 76 February 2014 180-186
68. Ricardo_Software (2015) *Wave 2015.1 Help System*
69. Åbom, M. (1989) Modal decomposition in ducts based on transfer function measurements between microphone pairs*. Journal of Sound and Vibration* 135 (1) 95-114
70. Singh, S., Hansen, C. and Howard, C. (2008) A detailed tutorial for evaluating in-duct net acoustic power transmission in a circular duct with an attached cylindrical Helmholtz resonator In: *ACOUSTICS 2008,* Geelong, Australia: November 2008
71. Winterbone, D. E. and Pearson, R. J. D. (1999) *Design techniques for engine manifolds, wave action methods for IC engines*. London, Professional Engineering Publishing
72. Winterbone, D. E. and Pearson, R. J. D. (2000) *Theory of engine manifold design, wave action methods for IC engines*. London, Professional Engineering Pub.
73. RAN (1990) *NCSM Project, Prototype Test Program, Engine Type V18B*.
74. ASHRAE (2013) *ASHRAE Handbook Fundamentals*. Atlanta, USA, ASHRAE
75. Herrin, D. (2016) *Email: Anechoic Termination and Wave Decomposition*. To: Bowden, D., University of Kentucky, 13th October 2016

76. Hua, X. and Herrin, D. W. (2013) Practical Considerations when using the Two-Load Method to Determine the Transmission Loss of Mufflers and Silencers. *SAE International Technical Paper Series*
77. Bowden, D. and Tso, Y. (2015) *Development of a Computer Model for the Acoustic Response of a Submarine Diesel Exhaust System*. DSTO-TR-3077, Melbourne, Victoria, Defence Science Technology Group
78. ANSYS Inc. *ANSYS Multiphysics*. (2017) [Accessed 29/6/2017]; Available from: www.ansys.com.
79. Selamet, A. and Ji, Z. L. (2000) Circular asymetric Helmholtz resonators. *Acoustical Society of America* 107 (5) 2360-2369
80. Narayana, T. S. S. and Munjal, M. L. (2005) Comparison of Different Calibration Techniques for Estimation of Transfer Function Using the Two-microphone Method. *Acoustical Society of India* **33** 454-469
81. Eriksson, L. J. (1980) Higher order mode effects in circular ducts and expansion chambers. *Journal of the Acoustical Society of America* 68 (2) 545-550

Appendix A Muffler Shell FEA Analysis

This appendix presents the mode shapes for all 20 modes and the ANSYS generated analysis report.

A.1 FEA Analysis Mode Shapes

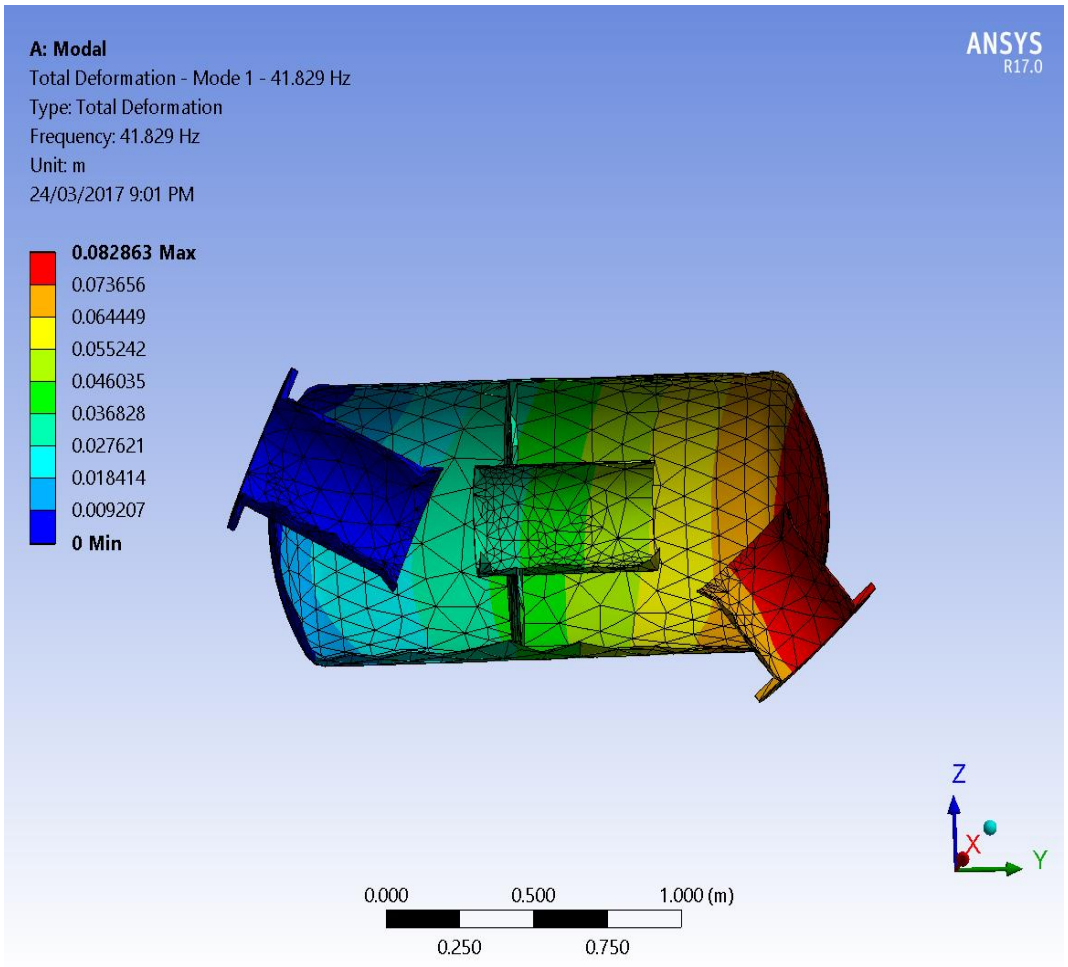

Figure App A.1 Mode 1, 42 Hz

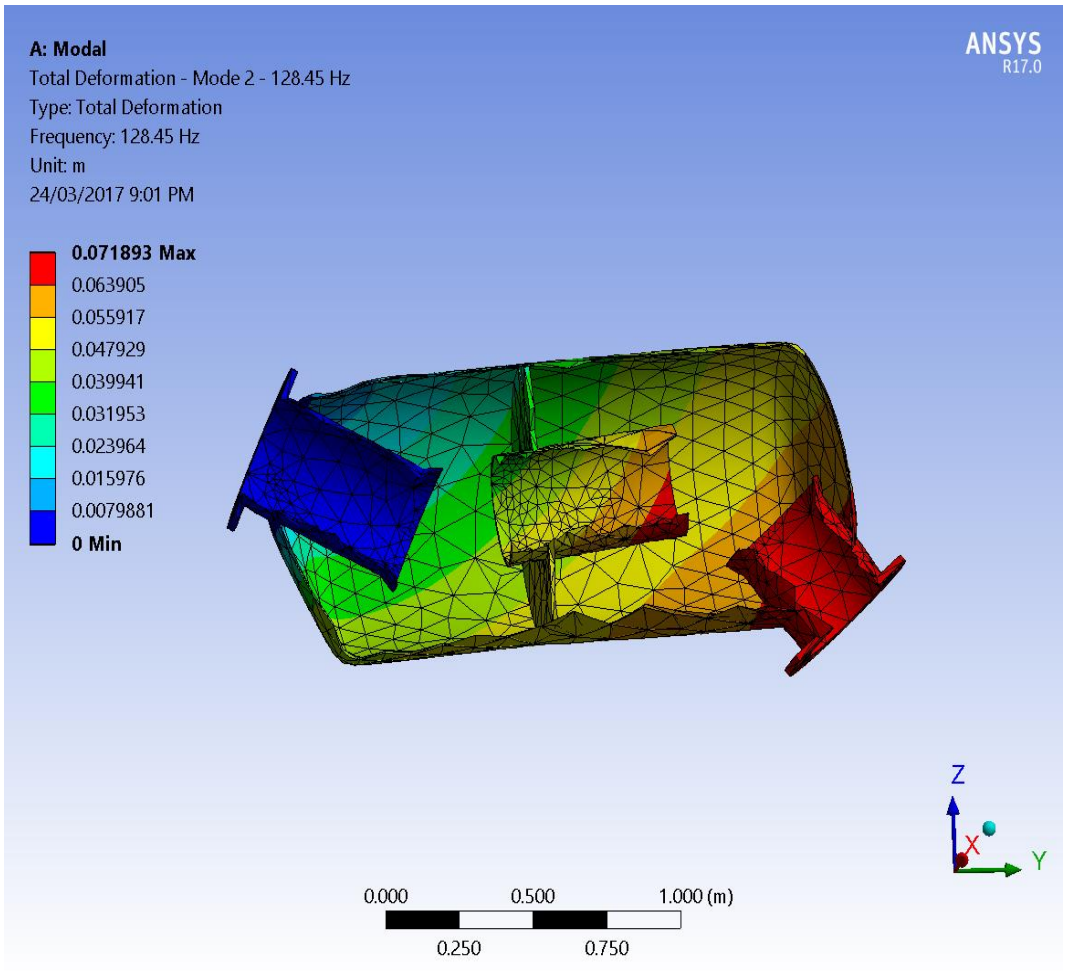

Figure App A.2 Mode 2, 128 Hz

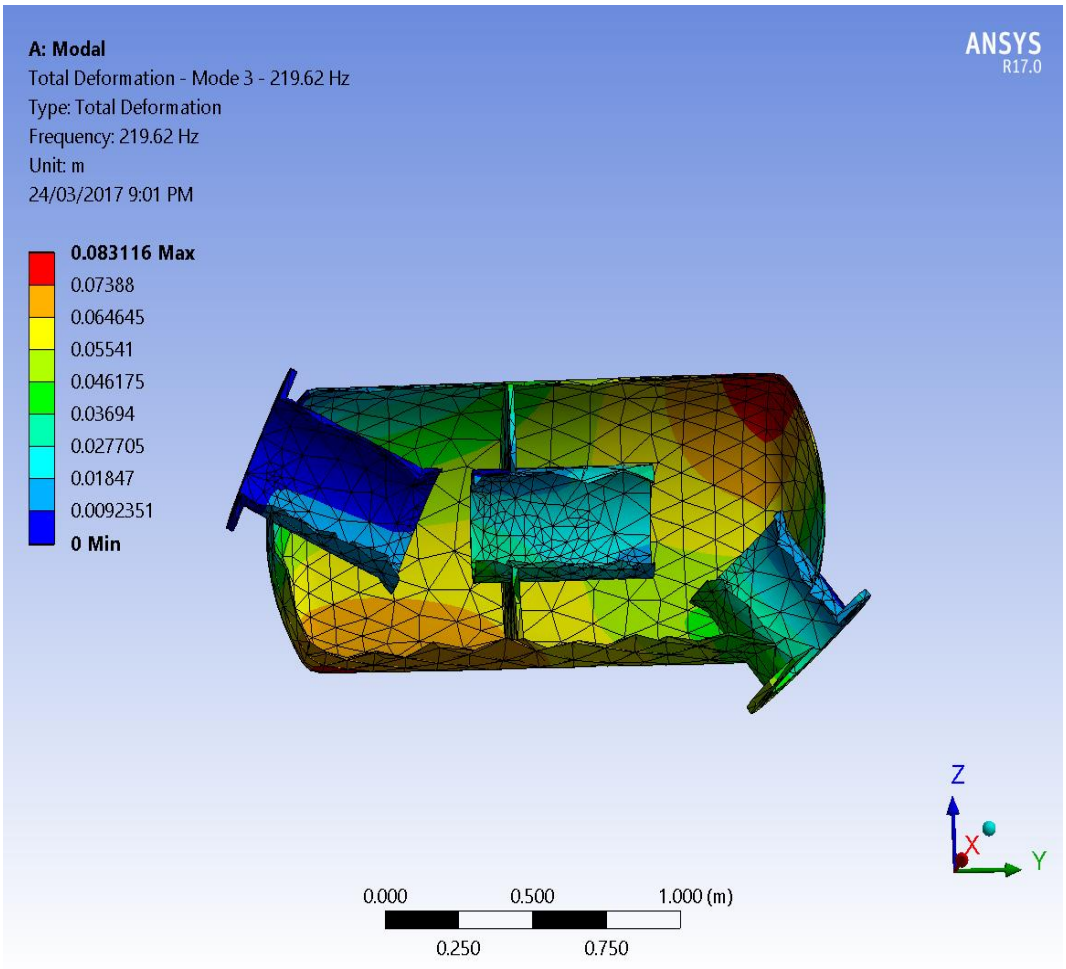

Figure App A.3 Mode 3, 220 Hz

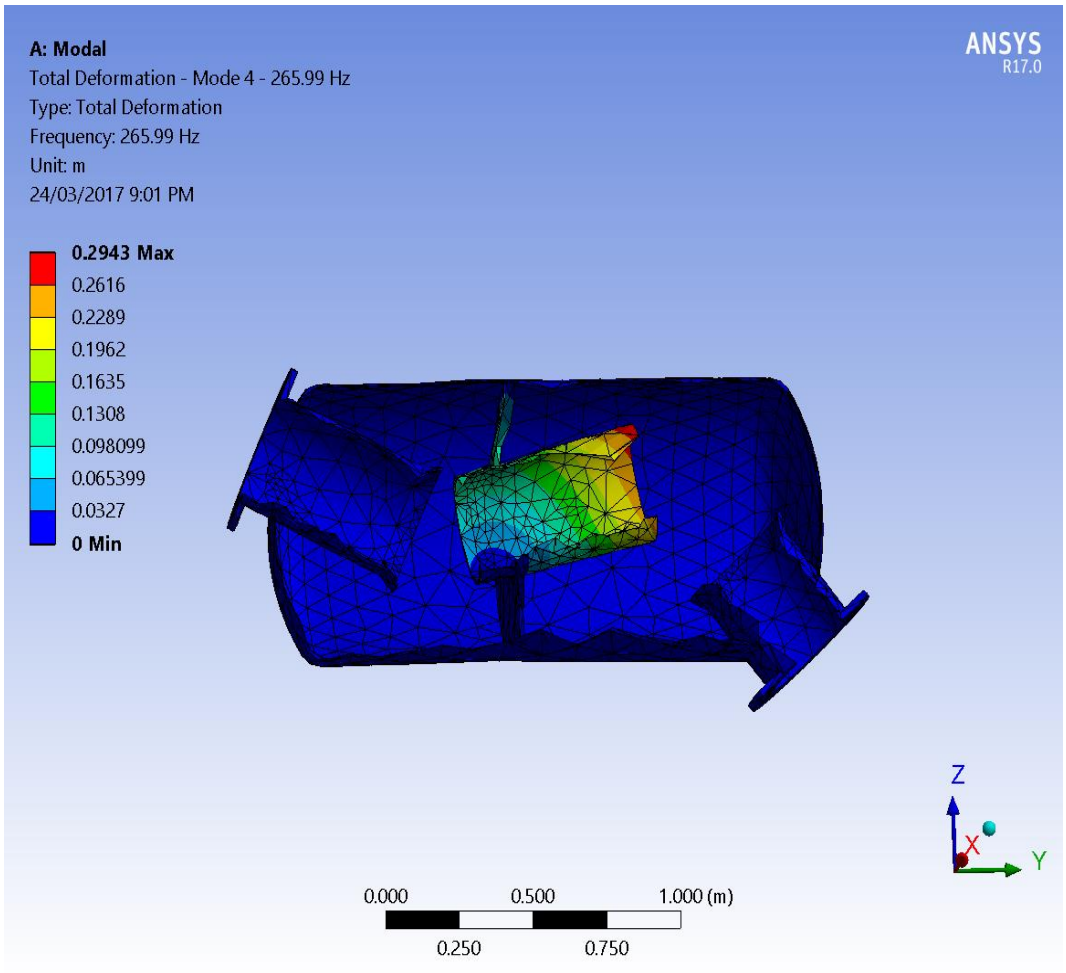

Figure App A.4 Mode 4, 266 Hz

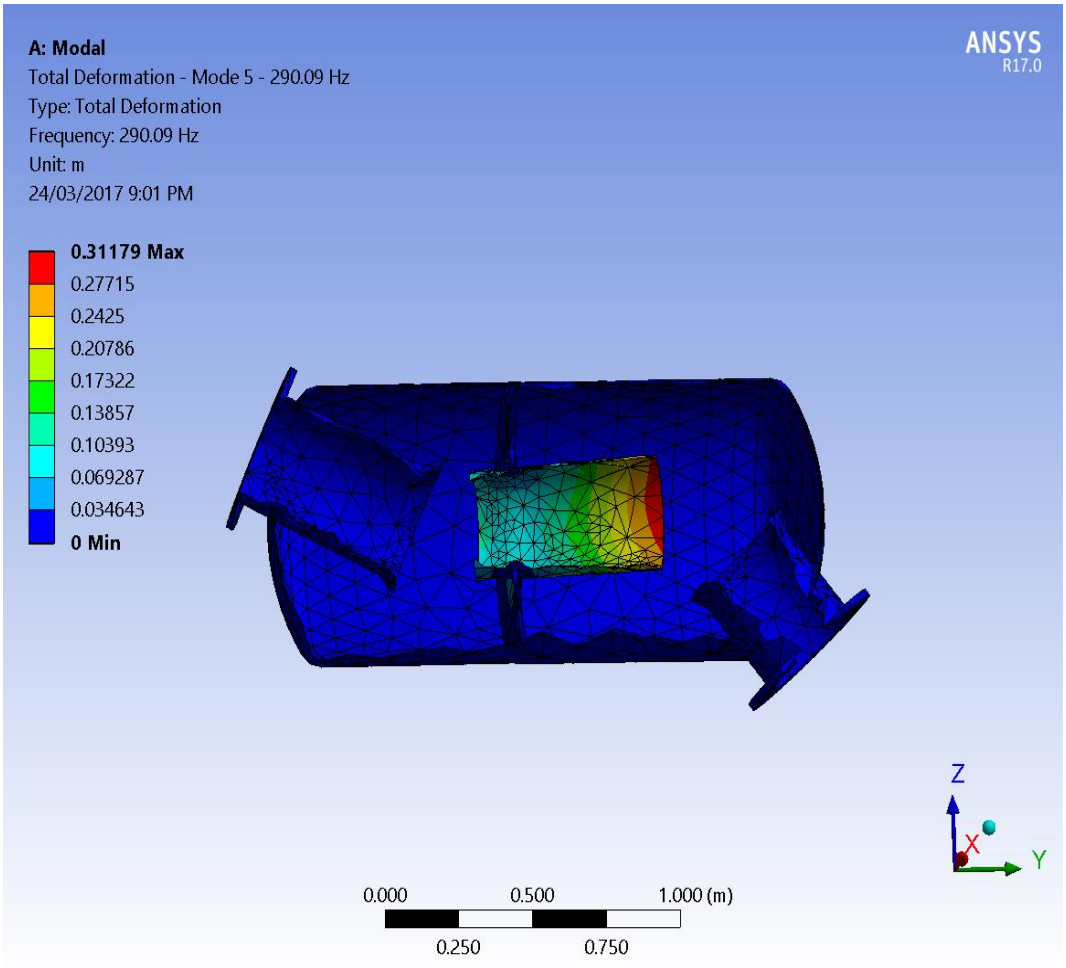

Figure App A.5 Mode 5, 290 Hz

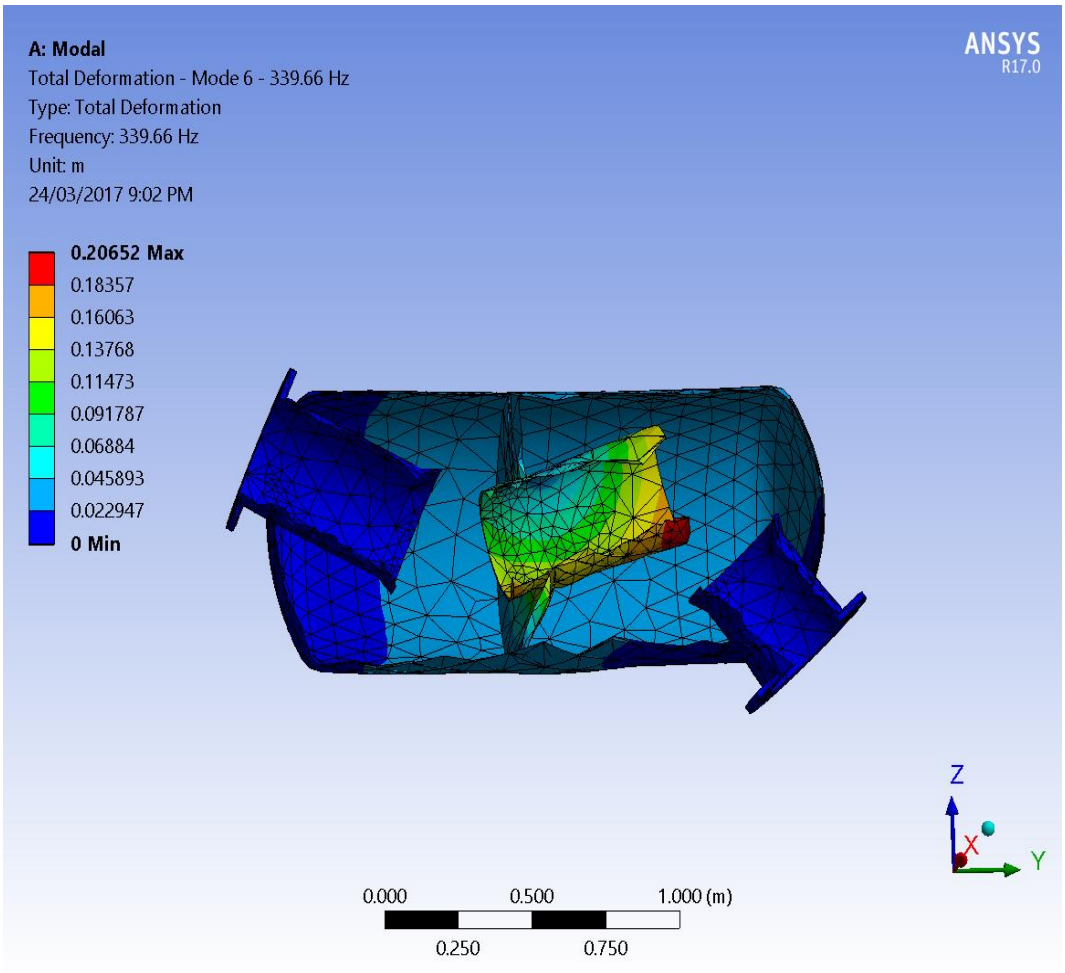

Figure App A.6 Mode 6, 340 Hz

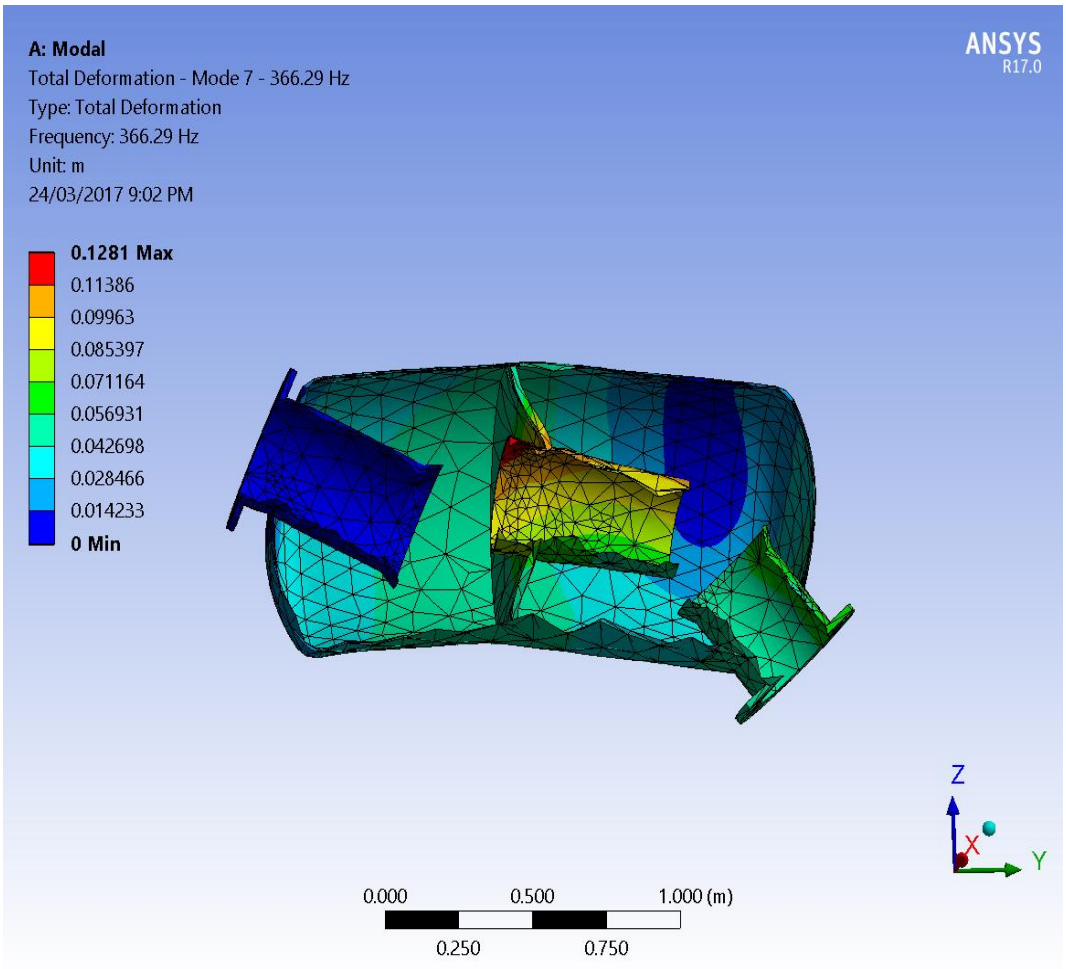

Figure App A.7 Mode 7, 366 Hz

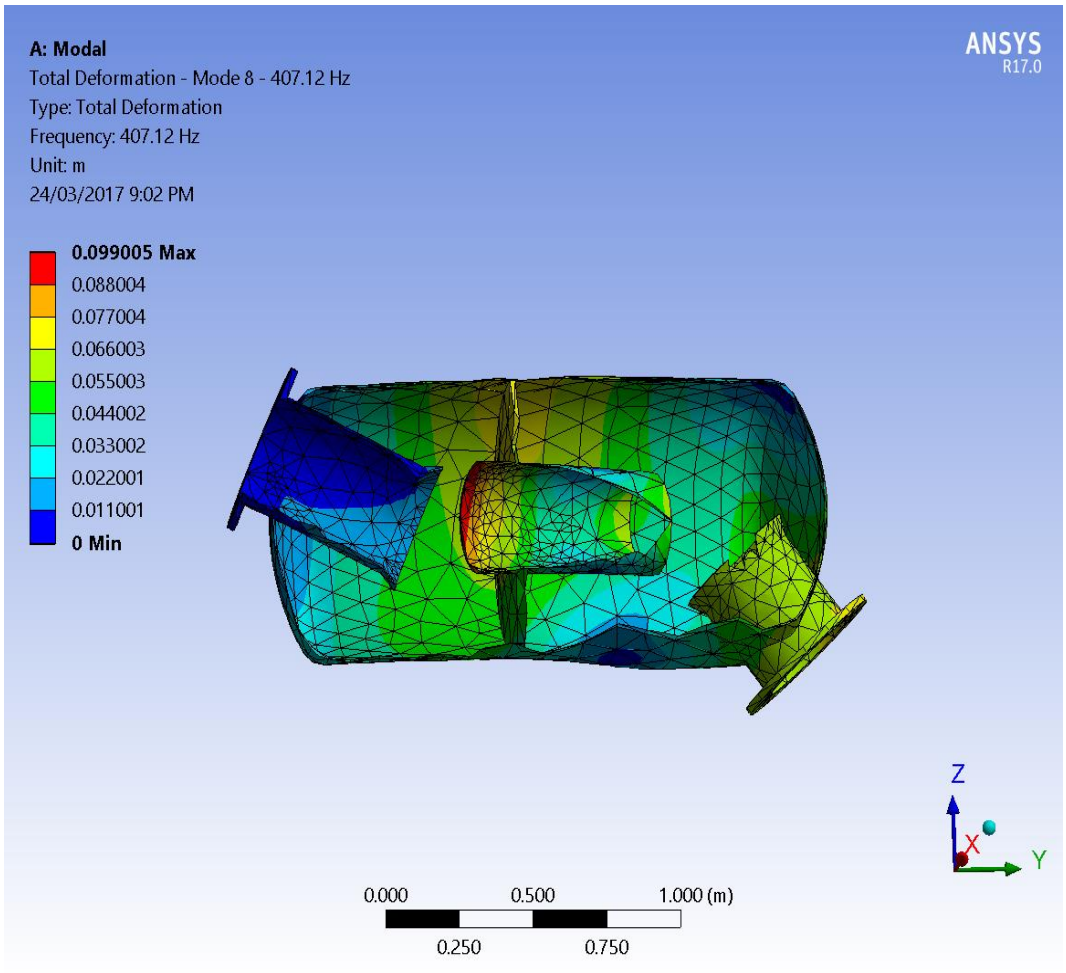

Figure App A.8 Mode 8, 407 Hz

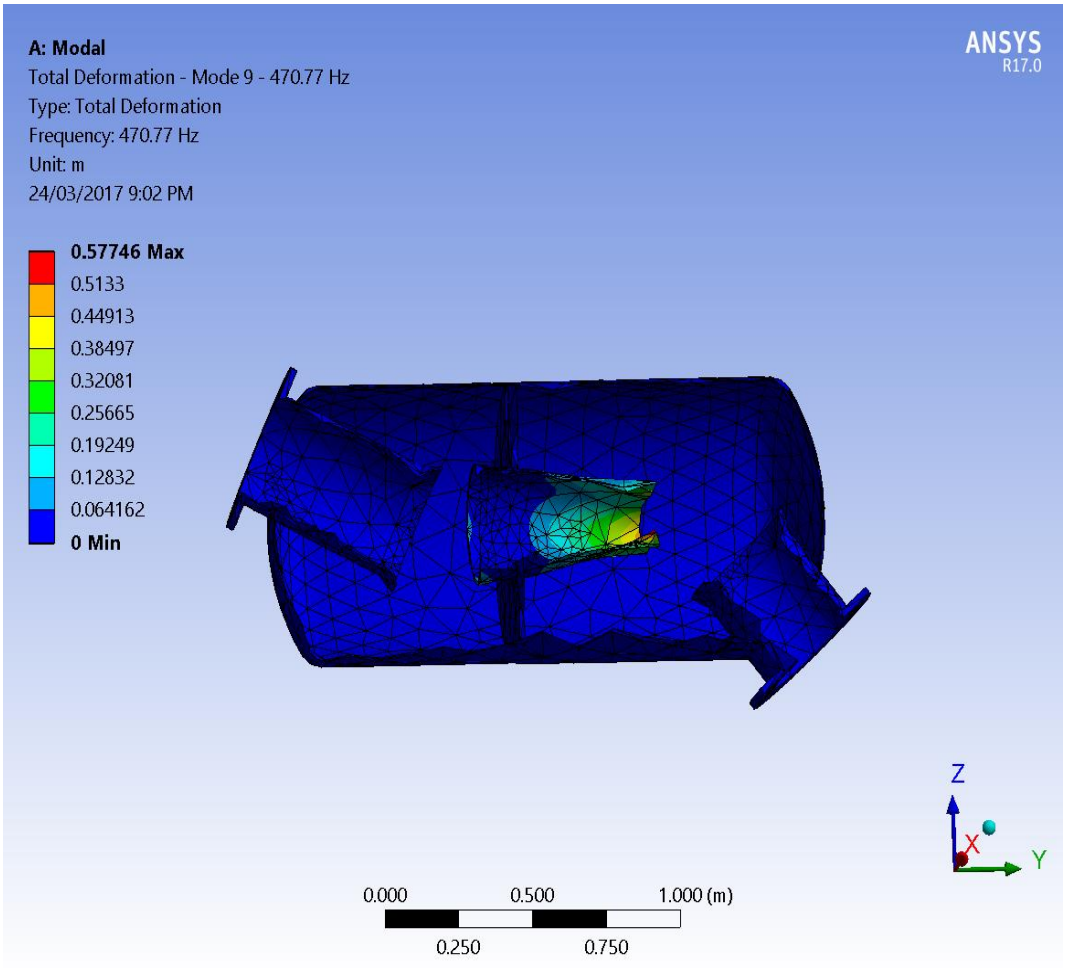

Figure App A.9 Mode 9, 471 Hz

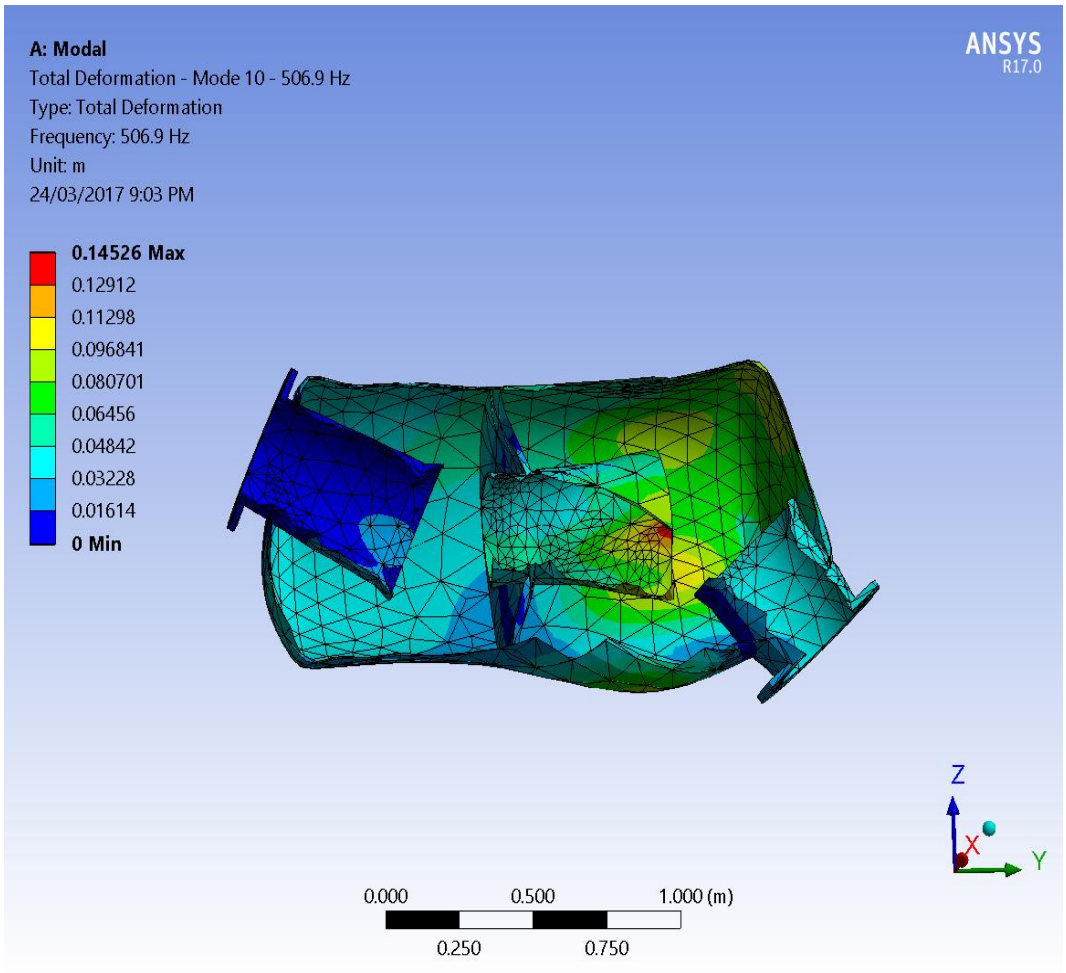

Figure App A.10 Mode 10 507 Hz

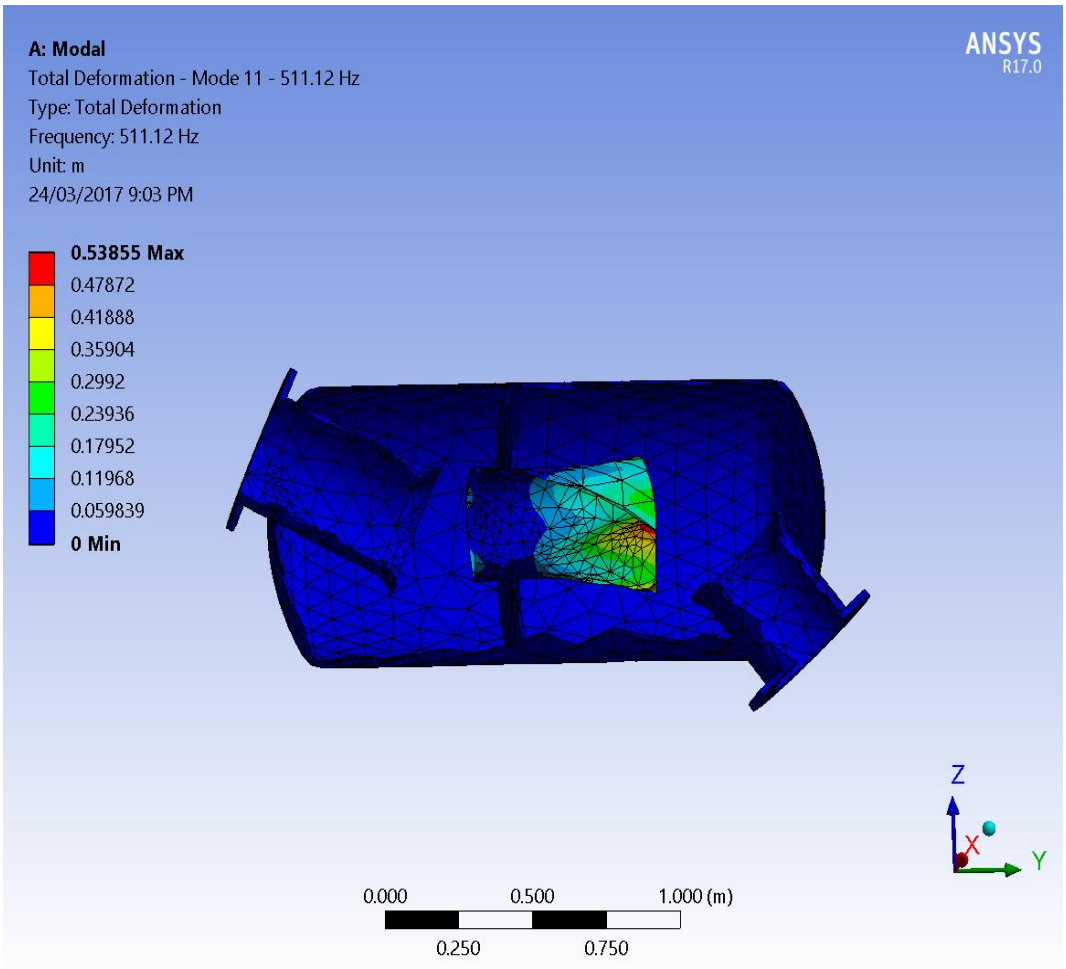

Figure App A.11 Mode 11, 511 Hz

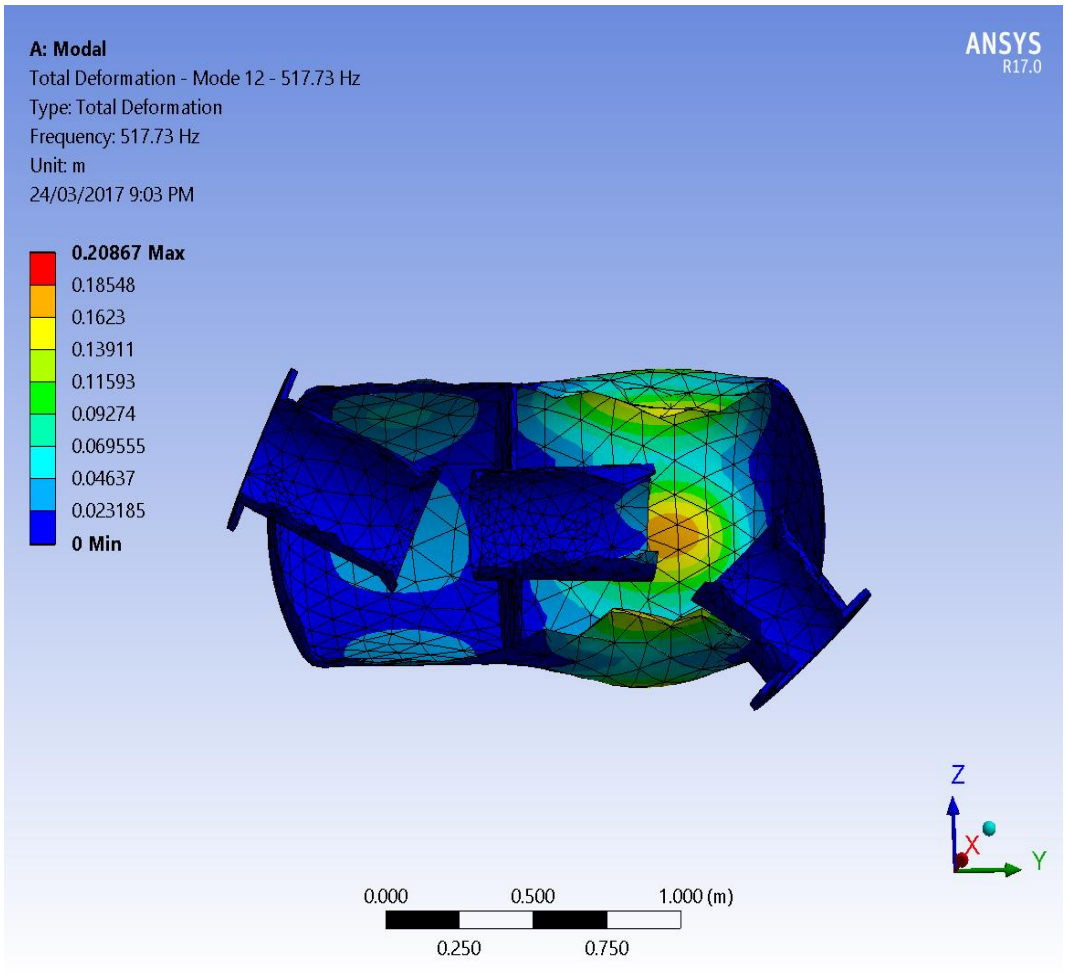

Figure App A.12 Mode 12, 518 Hz

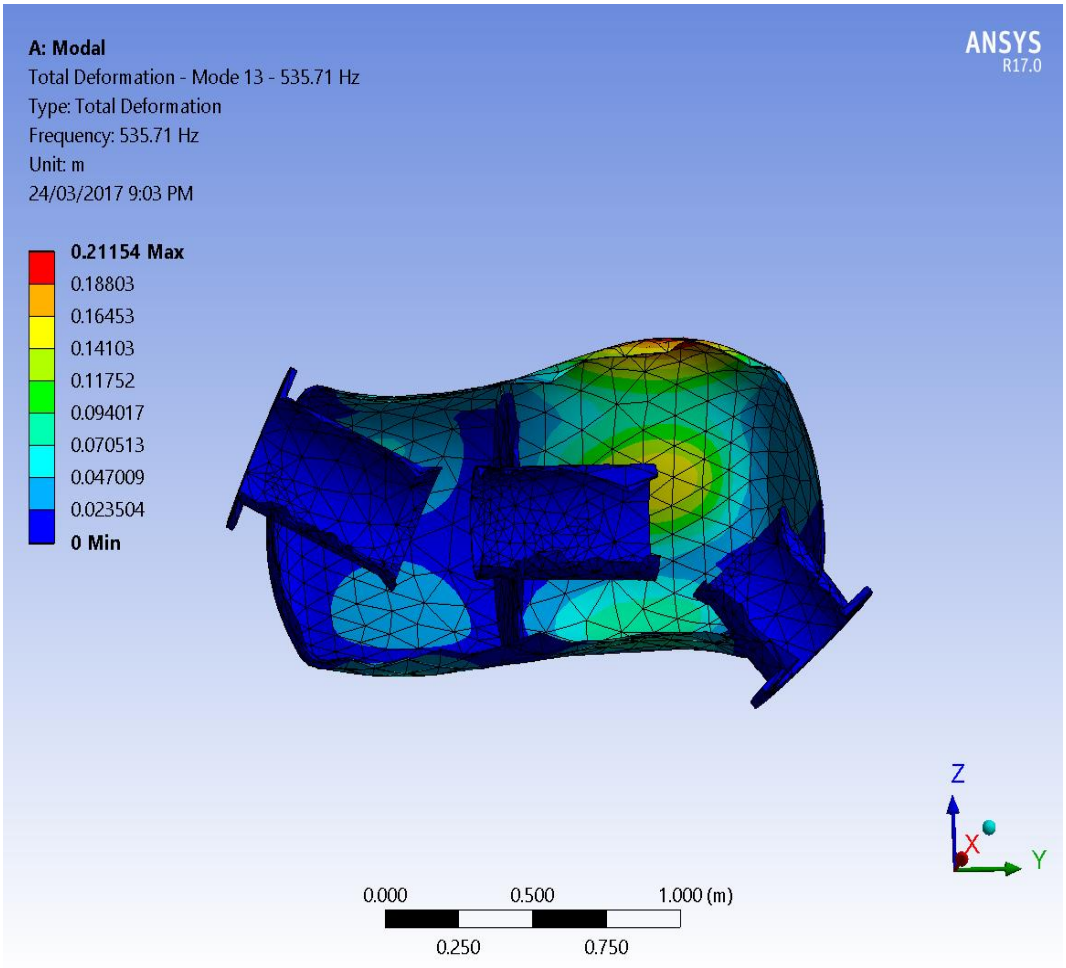

Figure App A.13 Mode 13, 536 Hz

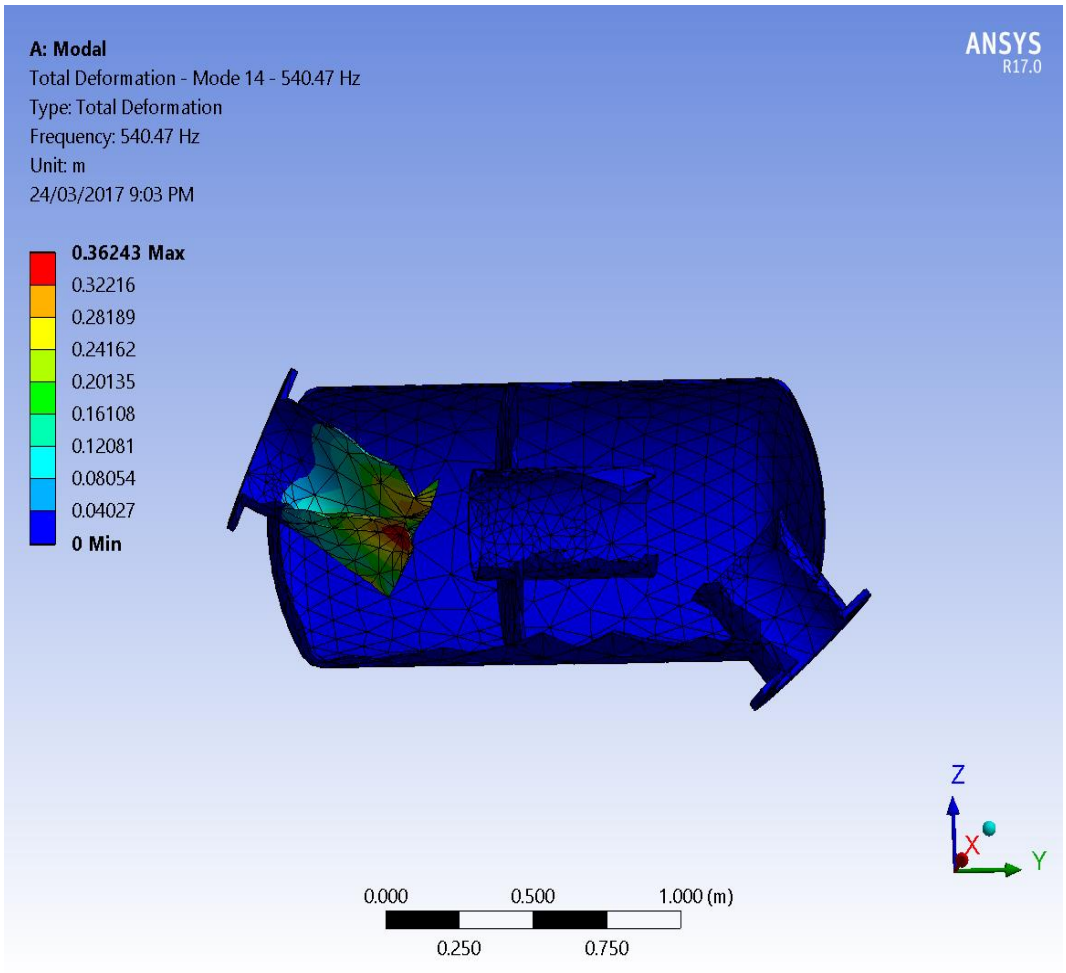

Figure App A.14 Mode 14, 540 Hz

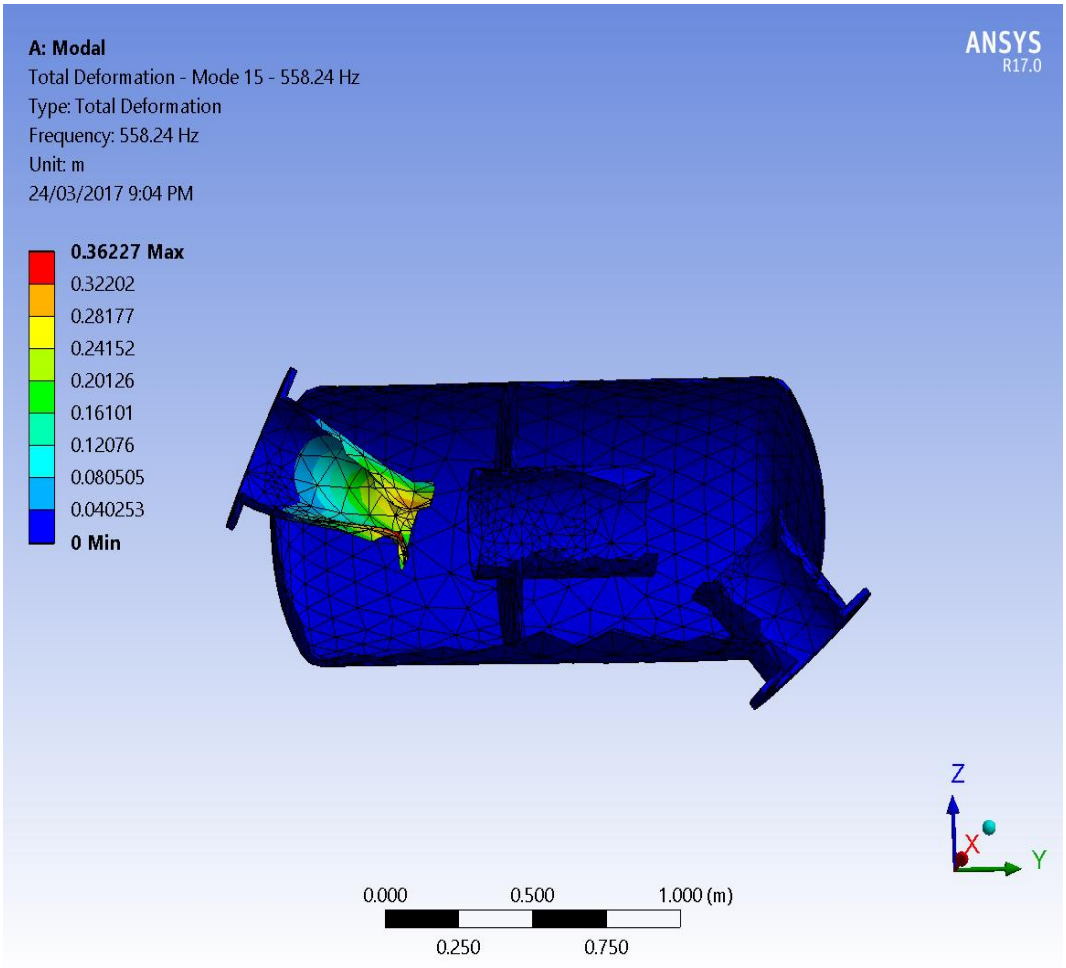

Figure App A.15 Mode 15, 558 Hz

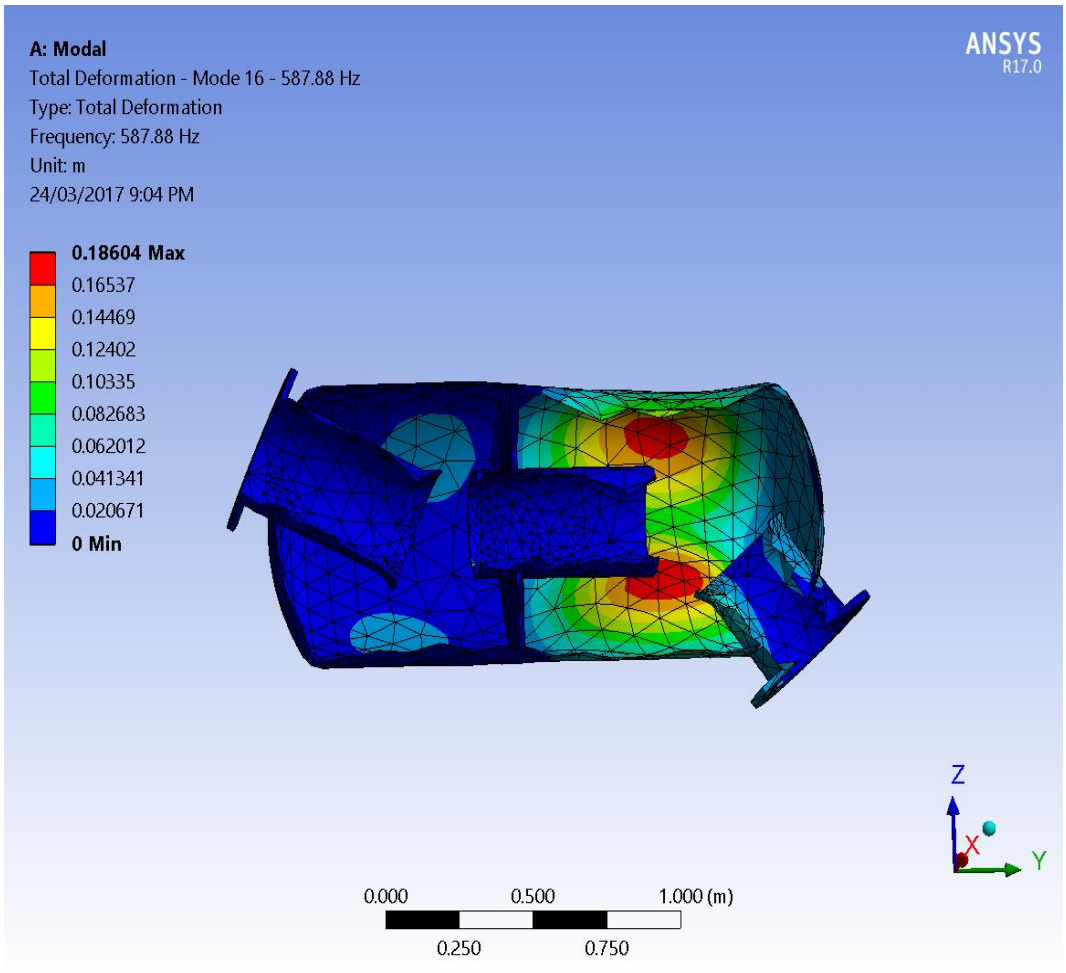

Figure App A.16 Mode 16, 588 Hz

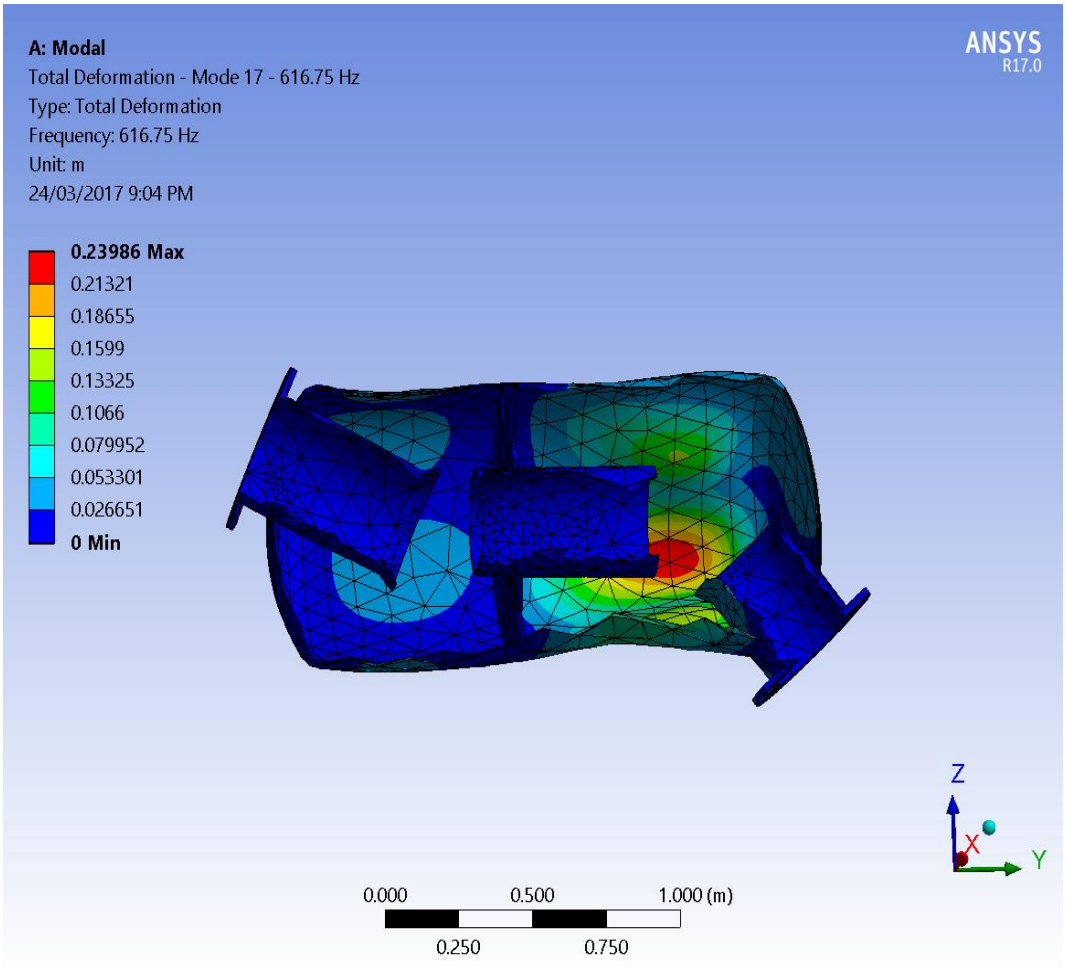

Figure App A.17 Mode 17, 617 Hz

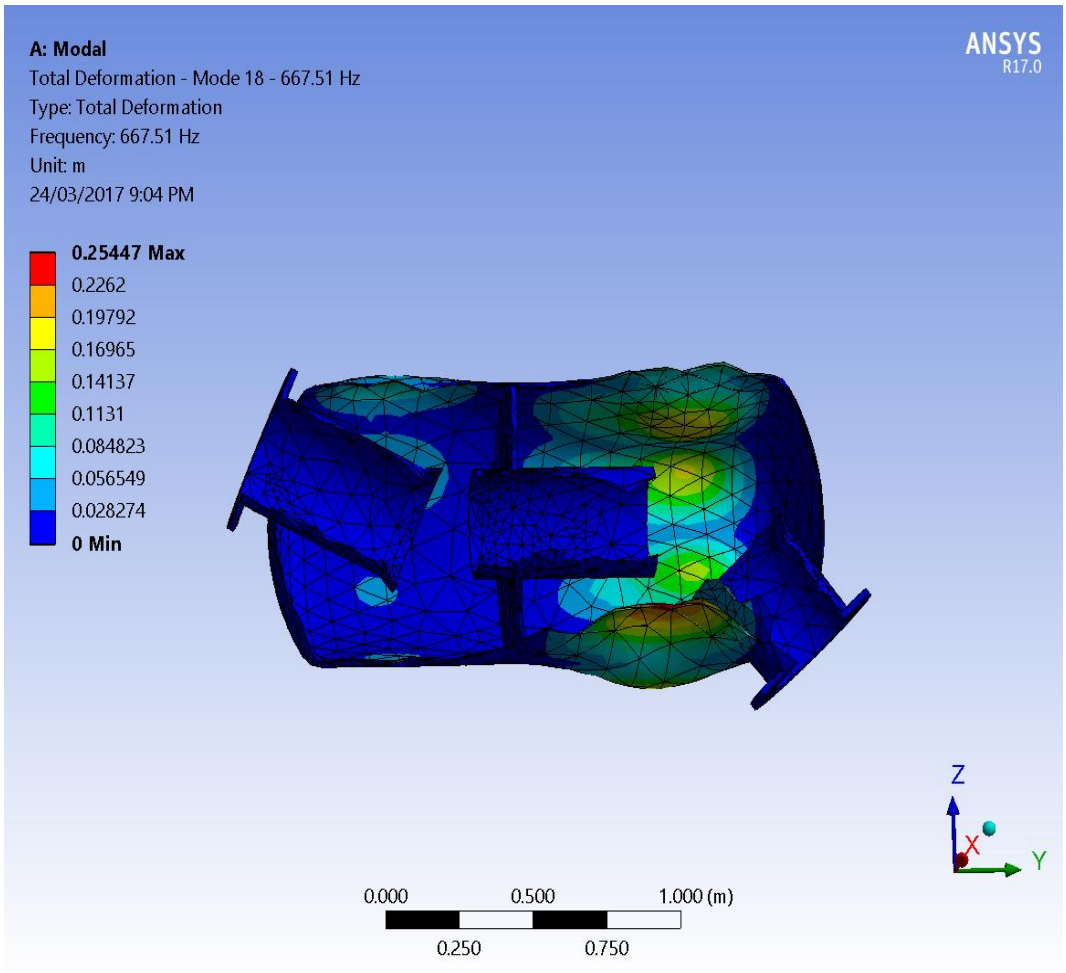

Figure App A.18 Mode 18, 668 Hz

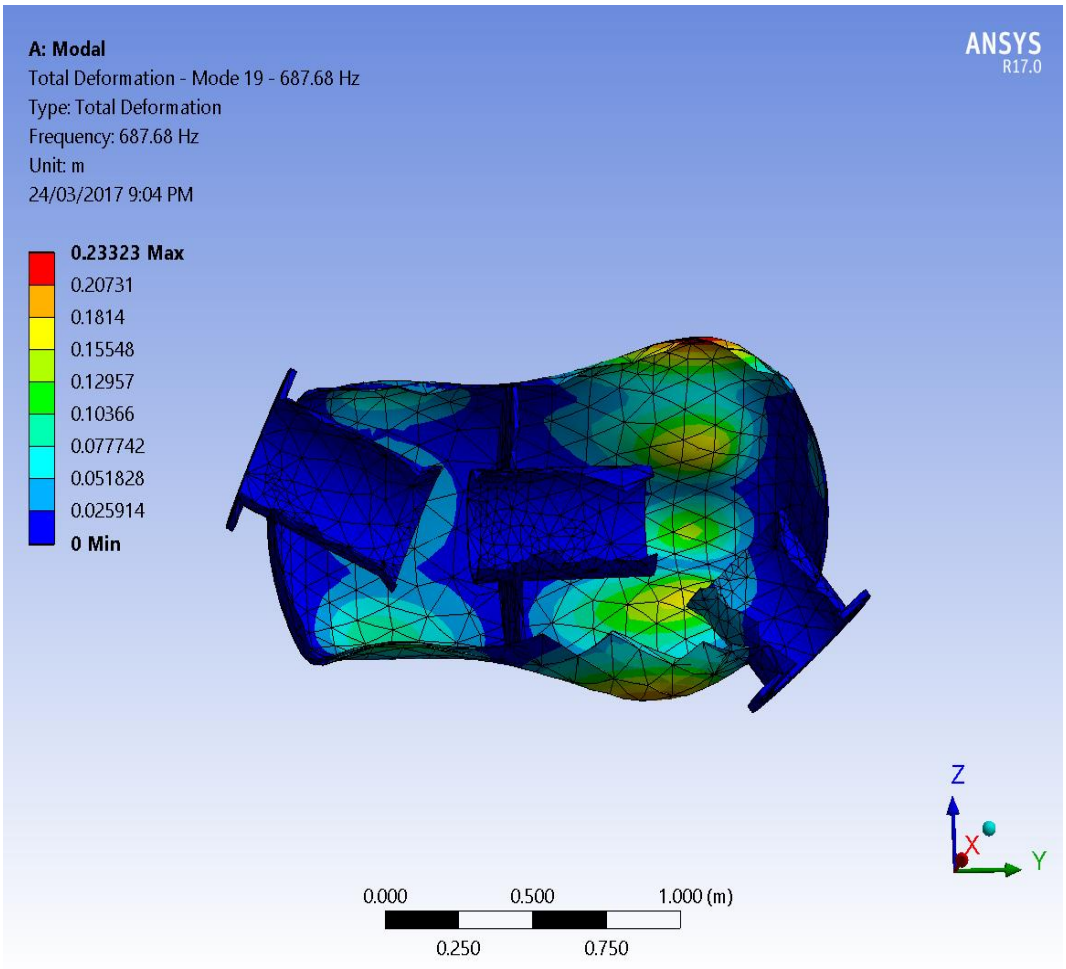

Figure App A.19 Mode 19, 688 Hz

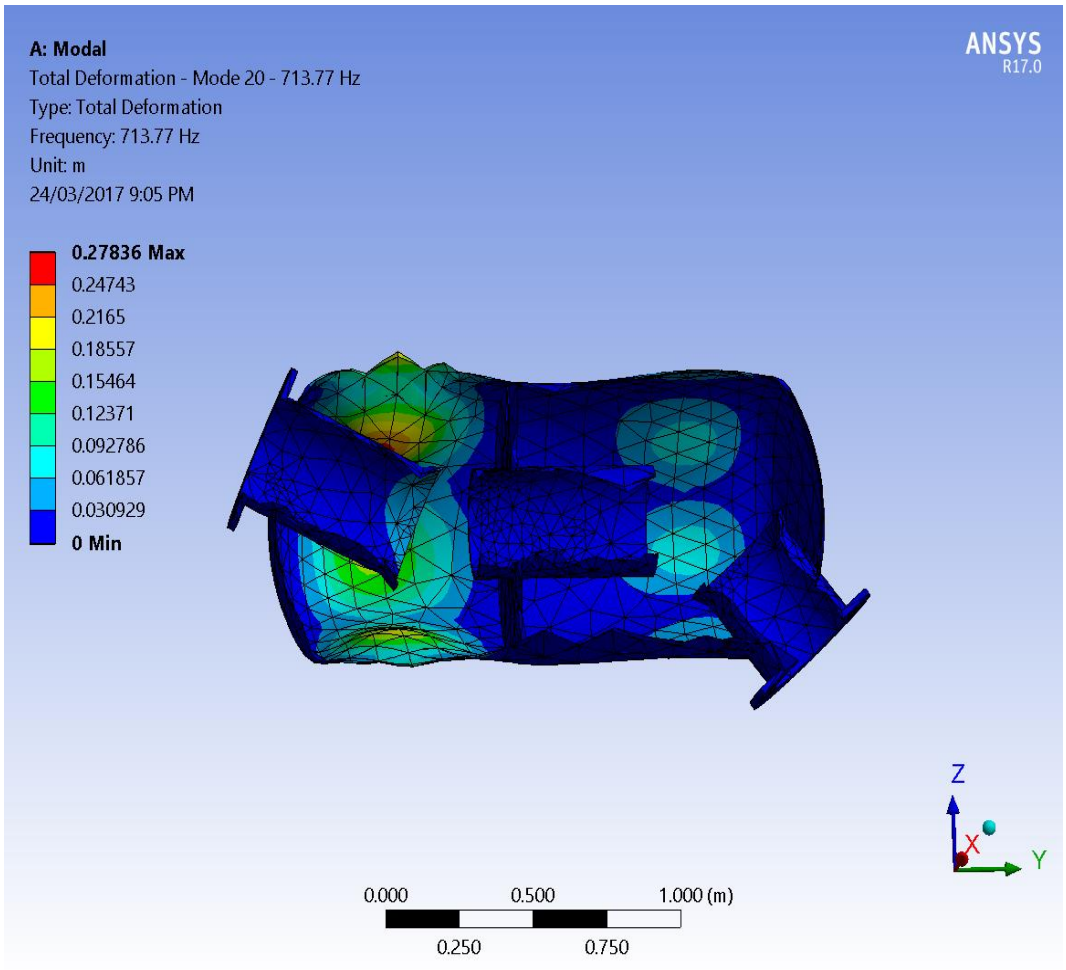

Figure App A.20 Mode 20, 714 Hz

A.2 ANSYS Analysis Report

A.2.1 Project

First Saved	Saturday, June 25, 2016
Last Saved	Tuesday, June 28, 2016
Product Version	17.0 Release
Save Project Before Solution	No
Save Project After Solution	No

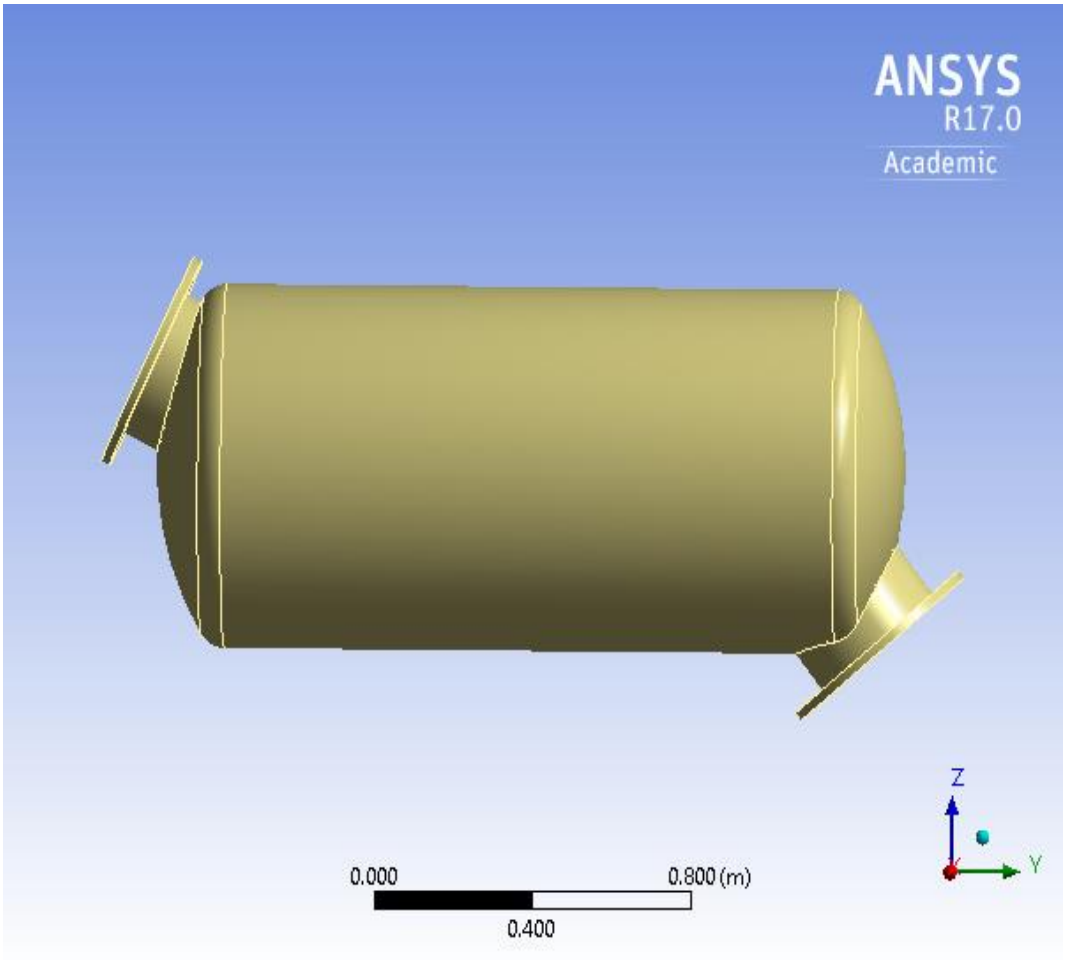

A.2.2 Contents

A.2.3 Units

TABLE 1

Unit System	Metric (m, kg, N, s, V, A) Degrees rad/s Celsius
Angle	Degrees
Rotational Velocity	rad/s
Temperature	Celsius

A.2.4 Model (A4) Geometry

TABLE 2
Model (A4) > Geometry

Object Name	*Geometry*
State	Fully Defined
Definition	
Source	C:\Users\David\Documents\Muffler B ansys_files\dp0\SYS\DM\SYS.agdb
Type	DesignModeler
Length Unit	Meters
Element Control	Program Controlled
Display Style	Body Color
Bounding Box	
Length X	0.838 m
Length Y	2.1815 m
Length Z	1.0519 m
Properties	
Volume	5.7365e-002 m³
Mass	450.31 kg
Scale Factor Value	1.
Statistics	
Bodies	1
Active Bodies	1
Nodes	16218
Elements	8206
Mesh Metric	None
Basic Geometry Options	
Solid Bodies	Yes
Surface Bodies	Yes
Line Bodies	Yes
Parameters	Yes
Parameter Key	
Attributes	Yes
Attribute Key	
Named Selections	Yes
Named Selection Key	
Material Properties	Yes
Advanced Geometry Options	
Use Associativity	Yes
Coordinate Systems	Yes
Reader Mode Saves Updated File	No
Use Instances	Yes
Smart CAD Update	Yes
Compare Parts On Update	No
Attach File Via Temp File	Yes
Temporary Directory	C:\Users\David\AppData\Local\Temp
Analysis Type	3-D
Mixed Import Resolution	None
Decompose Disjoint Geometry	Yes

Enclosure and Symmetry Processing	Yes

TABLE 3
Model (A4) > Geometry > Parts

Object Name	*Muffler B*
State	Meshed
Graphics Properties	
Visible	Yes
Transparency	1
Definition	
Suppressed	No
Stiffness Behavior	Flexible
Coordinate System	Default Coordinate System
Reference Temperature	By Environment
Behavior	None
Material	
Assignment	Structural Steel
Nonlinear Effects	Yes
Thermal Strain Effects	Yes
Bounding Box	
Length X	0.838 m
Length Y	2.1815 m
Length Z	1.0519 m
Properties	
Volume	5.7365e-002 m³
Mass	450.31 kg
Centroid X	-6.6181e-004 m
Centroid Y	-3.6377e-002 m
Centroid Z	-1.0519e-002 m
Moment of Inertia Ip1	181.53 kg·m²
Moment of Inertia Ip2	53.289 kg·m²
Moment of Inertia Ip3	178.49 kg·m²
Statistics	
Nodes	16218
Elements	8206
Mesh Metric	None

Coordinate Systems

TABLE 4
Model (A4) > Coordinate Systems > Coordinate System

Object Name	*Global Coordinate System*
State	Fully Defined
Definition	
Type	Cartesian
Coordinate System ID	0.
Origin	
Origin X	0. m
Origin Y	0. m
Origin Z	0. m
Directional Vectors	
X Axis Data	[1. 0. 0.]
Y Axis Data	[0. 1. 0.]
Z Axis Data	[0. 0. 1.]

Connections

TABLE 5
Model (A4) > Connections

Object Name	*Connections*
State	Fully Defined
Auto Detection	
Generate Automatic Connection On Refresh	Yes
Transparency	
Enabled	Yes

Mesh

TABLE 6
Model (A4) > Mesh

Object Name	*Mesh*
State	Solved
Display	
Display Style	Body Color
Defaults	
Physics Preference	Mechanical
Relevance	0
Shape Checking	Standard Mechanical
Element Midside Nodes	Program Controlled
Sizing	
Size Function	Curvature
Relevance Center	Coarse
Initial Size Seed	Active Assembly
Smoothing	Medium
Transition	Fast
Span Angle Center	Coarse
Curvature Normal Angle	Default (70.3950 °)
Min Size	Default (1.2774e-003 m)
Max Face Size	Default (0.127740 m)
Max Tet Size	Default (0.255470 m)
Growth Rate	Default (1.850)
Automatic Mesh Based Defeaturing	On
Defeaturing Tolerance	Default (6.3868e-004 m)
Minimum Edge Length	7.1343e-002 m
Inflation	
Use Automatic Inflation	None
Inflation Option	Smooth Transition
Transition Ratio	0.272
Maximum Layers	2
Growth Rate	1.2
Inflation Algorithm	Pre
View Advanced Options	No
Advanced	
Number of CPUs for Parallel Part Meshing	Program Controlled
Straight Sided Elements	No
Number of Retries	0
Extra Retries For Assembly	No
Rigid Body Behavior	Dimensionally Reduced
Mesh Morphing	Disabled
Triangle Surface Mesher	Program Controlled
Topology Checking	No
Pinch Tolerance	Default (1.1496e-003 m)
Generate Pinch on Refresh	No
Statistics	
Nodes	16218
Elements	8206
Mesh Metric	None

A.2.5 Modal (A5) Analysis

TABLE 7
Model (A4) > Analysis

Object Name	*Modal (A5)*
State	Solved
Definition	
Physics Type	Structural
Analysis Type	Modal
Solver Target	Mechanical APDL
Options	
Environment Temperature	22. °C
Generate Input Only	No

TABLE 8
Model (A4) > Modal (A5) > Initial Condition

Object Name	*Pre-Stress (None)*
State	Fully Defined
Definition	
Pre-Stress Environment	None

TABLE 9
Model (A4) > Modal (A5) > Analysis Settings

Object Name	*Analysis Settings*
State	Fully Defined
Options	
Max Modes to Find	20
Limit Search to Range	No
Solver Controls	
Damped	No
Solver Type	Program Controlled
Rotordynamics Controls	
Coriolis Effect	Off
Campbell Diagram	Off
Output Controls	
Stress	No
Strain	No
Nodal Forces	No
Calculate Reactions	No
General Miscellaneous	No
Analysis Data Management	
Solver Files Directory	C:\Users\David\Documents\Muffler B ansys_files\dp0\SYS\MECH\
Future Analysis	None
Scratch Solver Files Directory	
Save MAPDL db	No
Delete Unneeded Files	Yes
Solver Units	Active System
Solver Unit System	mks

TABLE 10
Model (A4) > Modal (A5) > Loads

Object Name	*Fixed Support 2*	*Frictionless Support*
State	Fully Defined	
Scope		
Scoping Method	Geometry Selection	
Geometry	1 Face	
Definition		
Type	Fixed Support	Frictionless Support
Suppressed	No	

A.2.6 Solution (A6)

TABLE 11
Model (A4) > Modal (A5) > Solution

Object Name	*Solution (A6)*
State	Solved
Adaptive Mesh Refinement	
Max Refinement Loops	1.
Refinement Depth	2.
Information	
Status	Done
MAPDL Elapsed Time	8. s
MAPDL Memory Used	415. MB
MAPDL Result File Size	10.938 MB
Post Processing	
Calculate Beam Section Results	No

The following bar chart indicates the frequency at each calculated mode.

FIGURE 1
Model (A4) > Modal (A5) > Solution (A6)

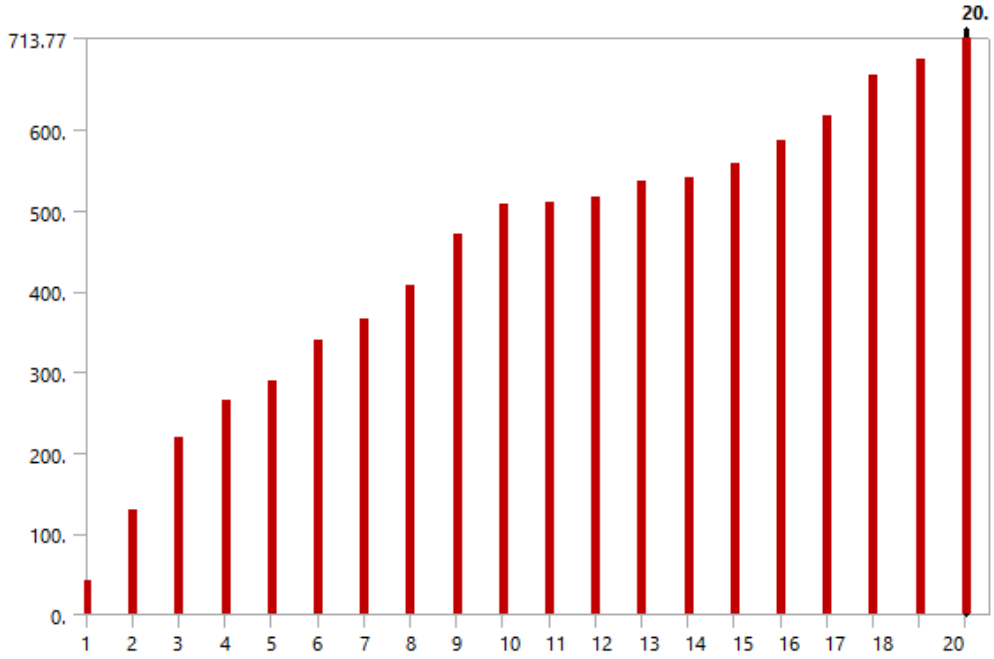

TABLE 12
Model (A4) > Modal (A5) > Solution (A6)

Mode	Frequency [Hz]
1.	41.829
2.	128.45
3.	219.62
4.	265.99
5.	290.09
6.	339.66
7.	366.29
8.	407.12
9.	470.77
10.	506.9
11.	511.12
12.	517.73
13.	535.71
14.	540.47
15.	558.24
16.	587.88
17.	616.75
18.	667.51
19.	687.68
20.	713.77

TABLE 13
Model (A4) > Modal (A5) > Solution (A6) > Solution Information

Object Name	*Solution Information*
State	Solved
Solution Information	
Solution Output	Solver Output
Newton-Raphson Residuals	0
Identify Element Violations	0
Update Interval	2.5 s
Display Points	All
FE Connection Visibility	
Activate Visibility	Yes
Display	All FE Connectors
Draw Connections Attached To	All Nodes
Line Color	Connection Type
Visible on Results	No
Line Thickness	Single
Display Type	Lines

Model (A4) > Modal (A5) > Solution (A6) > Comment

TABLE 14
Model (A4) > Modal (A5) > Solution (A6) > Results

Object Name	*Total Deformation*
State	Solved
Scope	
Scoping Method	Geometry Selection
Geometry	All Bodies
Definition	
Type	Total Deformation
Mode	9.
Identifier	
Suppressed	No
Results	
Minimum	0. m
Maximum	0.57746 m
Minimum Occurs On	Muffler B
Maximum Occurs On	Muffler B
Information	
Frequency	470.77 Hz

TABLE 15
Model (A4) > Modal (A5) > Solution (A6) > Total Deformation

Mode	Frequency [Hz]
1.	41.829
2.	128.45
3.	219.62
4.	265.99
5.	290.09
6.	339.66
7.	366.29
8.	407.12
9.	470.77
10.	506.9
11.	511.12
12.	517.73
13.	535.71
14.	540.47
15.	558.24
16.	587.88
17.	616.75
18.	667.51
19.	687.68
20.	713.77

A.2.7 Material Data

Structural Steel

TABLE 16
Structural Steel > Constants

Density	7850 kg m^-3
Coefficient of Thermal Expansion	1.2e-005 C^-1
Specific Heat	434 J kg^-1 C^-1
Thermal Conductivity	60.5 W m^-1 C^-1
Resistivity	1.7e-007 ohm m

TABLE 17
Structural Steel > Color

Red	Green	Blue
132	139	179

TABLE 18
Structural Steel > Compressive Ultimate Strength

Compressive Ultimate Strength Pa
0

TABLE 19
Structural Steel > Compressive Yield Strength

Compressive Yield Strength Pa
2.5e+008

TABLE 20
Structural Steel > Tensile Yield Strength

Tensile Yield Strength Pa
2.5e+008

TABLE 21
Structural Steel > Tensile Ultimate Strength

Tensile Ultimate Strength Pa
4.6e+008

TABLE 22
Structural Steel > Isotropic Secant Coefficient of Thermal Expansion

Zero-Thermal-Strain Reference Temperature C
22

TABLE 23
Structural Steel > Alternating Stress Mean Stress

Alternating Stress Pa	Cycles	Mean Stress Pa
3.999e+009	10	0
2.827e+009	20	0
1.896e+009	50	0
1.413e+009	100	0
1.069e+009	200	0
4.41e+008	2000	0
2.62e+008	10000	0
2.14e+008	20000	0
1.38e+008	1.e+005	0
1.14e+008	2.e+005	0
8.62e+007	1.e+006	0

TABLE 24
Structural Steel > Strain-Life Parameters

Strength Coefficient Pa	Strength Exponent	Ductility Coefficient	Ductility Exponent	Cyclic Strength Coefficient Pa	Cyclic Strain Hardening Exponent
9.2e+008	-0.106	0.213	-0.47	1.e+009	0.2

TABLE 25
Structural Steel > Isotropic Elasticity

Temperature C	Young's Modulus Pa	Poisson's Ratio	Bulk Modulus Pa	Shear Modulus Pa
	2.e+011	0.3	1.6667e+011	7.6923e+010

TABLE 26
Structural Steel > Isotropic Relative Permeability

Relative Permeability
10000

Appendix B Transmission Loss Test Bench - Experimental

B.1 Construction

This appendix covers the physical construction, instrumentation and data sheets for the experimental acoustic transmission loss test bench. The measurement ducts and the anechoic termination shell were constructed using galvanized steel round ducting of spiral-folded-seam construction with a nominal bore of 330 mm and one mm wall thickness. The anechoic termination was three metres long and packed with Tontine Acoustisorb2 material in a one metre long cone (Figure App B.1) followed by a 1.2 metre long parallel section (Figure App B.2). The upstream and downstream measurement ducts were each 1.5 metres long.

Figure App B.1 Anechoic Termination, Cone Section

Figure App B.2 Anechoic Termination, Parallel Section

The transmission loss test bench used the following instrumentation:

1. Marantz brand Model MA6100 mono amplifier.
2. HP 3567A Spectrum Analyser with
    a. four HP 35652B input modules
    b. HP 35653C sound source module
3. Dayton Audio brand Model RSS315HO-44, subwoofer loudspeaker driver, ø 12 inch (305 mm)
4. Custom non-vented speaker enclosure, 126 litre, 18 mm plywood, lined with Tontine Acoustisorb2 material 25 mm thick
5. PCB brand Model 378B02 half inch microphones (four)
6. PCB Model 426E01 preamplifiers (four)
7. Microphone holder, cable grommet, TST Rutaseal Light, Part Number T_14 583 32
8. Larson Davis Model CAL250 microphone calibrator, 114 dB re 20µPa at 251.2 Hz

B.2 Data Sheets

B.2.1 Mono (single channel) Amplifier

Table App B.1 Marantz MA6100 Specification Summary

Mono Amplifier Specification	
Model	Marantz MA6100
Rated Output	125 W 8 ohms rms
Distortion	0.02%
Rated Input Level	1 V rms
Frequency Response (-1 dB)	10 Hz to 70 kHz
Signal / Noise Ratio (A weighted)	110 dB
Damping Factor (1 kHz)	60

B.2.2 HP Spectrum Analyser HP3576A

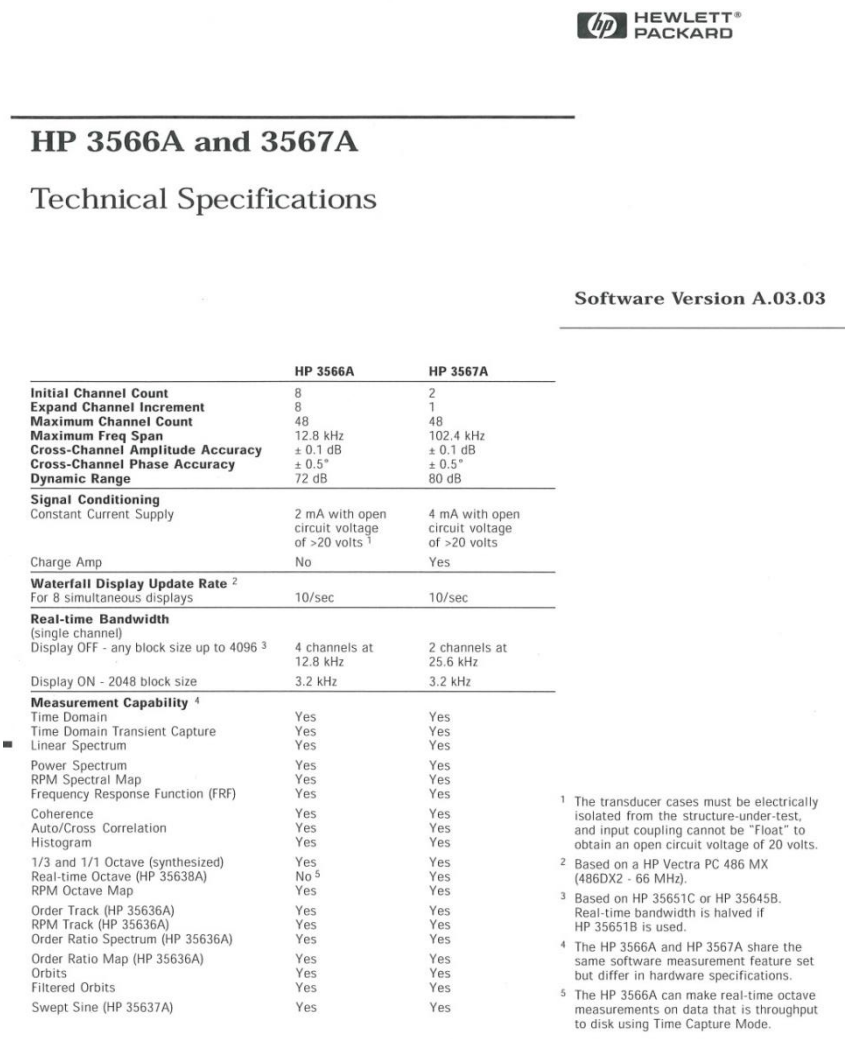

HEWLETT® PACKARD

HP 3566A and 3567A

Technical Specifications

Software Version A.03.03

	HP 3566A	HP 3567A
Initial Channel Count	8	2
Expand Channel Increment	8	1
Maximum Channel Count	48	48
Maximum Freq Span	12.8 kHz	102.4 kHz
Cross-Channel Amplitude Accuracy	± 0.1 dB	± 0.1 dB
Cross-Channel Phase Accuracy	± 0.5°	± 0.5°
Dynamic Range	72 dB	80 dB
Signal Conditioning		
Constant Current Supply	2 mA with open circuit voltage of >20 volts [1]	4 mA with open circuit voltage of >20 volts
Charge Amp	No	Yes
Waterfall Display Update Rate [2]		
For 8 simultaneous displays	10/sec	10/sec
Real-time Bandwidth (single channel)		
Display OFF - any block size up to 4096 [3]	4 channels at 12.8 kHz	2 channels at 25.6 kHz
Display ON - 2048 block size	3.2 kHz	3.2 kHz
Measurement Capability [4]		
Time Domain	Yes	Yes
Time Domain Transient Capture	Yes	Yes
Linear Spectrum	Yes	Yes
Power Spectrum	Yes	Yes
RPM Spectral Map	Yes	Yes
Frequency Response Function (FRF)	Yes	Yes
Coherence	Yes	Yes
Auto/Cross Correlation	Yes	Yes
Histogram	Yes	Yes
1/3 and 1/1 Octave (synthesized)	Yes	Yes
Real-time Octave (HP 35638A)	No [5]	Yes
RPM Octave Map	Yes	Yes
Order Track (HP 35636A)	Yes	Yes
RPM Track (HP 35636A)	Yes	Yes
Order Ratio Spectrum (HP 35636A)	Yes	Yes
Order Ratio Map (HP 35636A)	Yes	Yes
Orbits	Yes	Yes
Filtered Orbits	Yes	Yes
Swept Sine (HP 35637A)	Yes	Yes

[1] The transducer cases must be electrically isolated from the structure-under-test, and input coupling cannot be "Float" to obtain an open circuit voltage of 20 volts.

[2] Based on a HP Vectra PC 486 MX (486DX2 - 66 MHz).

[3] Based on HP 35651C or HP 35645B. Real-time bandwidth is halved if HP 35651B is used.

[4] The HP 3566A and HP 3567A share the same software measurement feature set but differ in hardware specifications.

[5] The HP 3566A can make real-time octave measurements on data that is throughput to disk using Time Capture Mode.

Figure App B.3 HP3566 / 67A Specification Sheet Page 1

Specifications

Amplitude

	HP 3566A	HP 3567A
Input Range	5 mVpk to 10 Vpk in 2 dB steps	1.26 mVpk to 39.8 Vpk in 2 dB steps
Dynamic Range	72 dB (75 dB typical)*	80 dB <51.2 kHz (85 dB typical)* 75 dB >51.2 kHz (80 dB typical)*
Noise (Rs=50 Ω, 16 RMS avgs., flat top window measured on most sensitive range)		
20 to 1000 Hz (frequency dependent)	$<2260/\sqrt{(f)}$ nVrms $\sqrt{(Hz)}$	
>1000 Hz (frequency independent)	<70 nVrms/ $\sqrt{(Hz)}$	
20 to 200 Hz (frequency dependent)		$<(565/\sqrt{(f)}$ nVrms/$\sqrt{(Hz)}$
Above 200 Hz (frequency independent)		<40 nVrms $\sqrt{(Hz)}$
Single Channel Amplitude Accuracy (0.1 Hz to 100 kHz)	± 0.15 dB	1.26 to 3.16 mVpk ± 0.25 dB
		3.98 mVpk to 39.8 Vpk
	± 0.15 dB	

Time Capture

Transient Capture Rates (Time Capture to Memory/DOS or HP 35659A with option AT3 internal disk)	HP 3566A	HP 3567A
Max Rate per Channel (samples/sec)	32,768	262,144
Max Aggregate Rate (samples/sec)	1.3 million	1.3 million
Max Time Samples to RAM	1.5 million 7.5 million (opt. 116)	1.5 million 7.5 million (opt. 116)
Max Time Samples To Disk (HP 35659A with option AT3 internal disk)	500 million	500 million

Maximum Frequency Spans for Time Capture to HP 35659A SCSI Module Option AT3 Internal Disk (typical)*	*Number of Channels*	*Maximum Frequency Span (kHz)*[6]	*Aggregate Transfer Rate (Mbytes/sec)*
	5	*102.4 (80)*	*2.62*
	10	*51.2 (40)*	*2.62*
	20	*25.6 (20)*	*2.62*
	40	*12.8 (10)*	*2.62*
	48	*6.4 (5)*	*1.57*

[6] Value in parenthesis is for offline real-time 1/3-octave measurements. Online real-time 1/3-octave measurements require smaller frequency spans. See the Real-time Octave Analysis section for online performance.

* Specifications designated as "typical" reflect supplemental, non-warranted characteristics.

Figure App B.4 HP3566 / 67A Specification Sheet Page 2

Frequency

	HP 3566A	HP 3567A
Measurement Range	64 µHz to 12.8 kHz	64 µHz to 102.4 kHz
Accuracy	± 8 ppm	± 8 ppm
Sample Rate	32,768 samples/sec	262,144 samples/sec
Resolution	25, 50, 100, 200, 400, 800, 1600, or 3200 lines	25, 50, 100, 200, 400, 800, 1600, or 3200 lines
Spans		
102.4 kHz	—	X [7]
51.2 kHz	—	X
25.6 kHz	—	X
12.8 kHz	X	X
6.4 kHz	X	X
3.2 kHz	X	X
1.6 kHz	X	X
800 Hz	X	X
400 Hz	X	X
200 Hz	X	X
100 Hz	X	X
50 Hz	X	X
25 Hz	X	X
12.5 Hz	X	X
6.25 Hz	X	X
3.125 Hz	X	X
1.562 Hz	X	X
781 mHz	X	X
390 mHz	X	X
195 mHz	X	X
Center Frequency Resolution	0.25 Hz	0.25 Hz
Real-time Bandwidth (Fast averaging, display off)	4 channels at 12.8 kHz [8]	2 channels at 25.6 kHz [8]

Frequency Response (Gain/Phase)

	HP 3566A	HP 3567A
Cross Channel Accuracy		
Gain	± 0.1 dB	± 0.1 dB (0.1 Hz to 100 kHz)
Phase	± 0.5°	± 0.5° (0.1 Hz to 100 kHz)
Charge Input Accuracy		
Gain (at 1 kHz)	n/a	± 0.3 dB
Flatness (to 51.2 kHz)	n/a	± 0.1 dB
Phase (to 51.2 kHz)	n/a	± 0.5°

[7] Extendible to 110 kHz by making a zoom measurement. (Specifications are not guaranteed >102.4 kHz).

[8] Based on HP 35651C or HP 35654B. Real-time bandwidth is halved if HP 35651B is used.

Figure App B.5 HP3566 / 67A Specification Sheet Page 3

Order Tracking

Amplitude Accuracy	± 1.0 dB			
Phase Accuracy	***RPM Range***	***1st Order***	***Orders 2-5***	***Orders >5***
	10 to 10,000	± 0.5°	± 1.0°	± 5°
	10,000 to 120,000	± 1.0°		
	HP 3566A	**HP 3567A**		
Ramp Rates	3000 RPM/sec	3000 RPM/sec		

(4 input channels 600-6000 RPM. Δ order = 0.1, 30 RPM step, pulses/revs = 4.0)

Inputs

	HP 3566A	HP 3567A
Connection	Grounded or Floating	Grounded or Floating
Input Impedance	1 MΩ ± 5%	1 MΩ ± 5%
Input Coupling	ac or dc ac roll-off is <3 dB at 1 Hz	ac or dc ac roll-off is <3 dB at 1 Hz
IEPE Input		
Constant Current Source	2 mA [14]	4 mA
Open Circuit Voltage	>20 V	>20 V
Charging Amplifier	grounded and floating	grounded and floating

Source

Max Output Level	10 V
Max Current	50 mA
Max Capacitive Load	0.01 µF
Min Frequency Resolution	15.6 mHz
Max Frequency	102.4 kHz (HP 35653C) 51.2 kHz (HP 35653A)

DAC

Max Output Level	10 V
Max Current	50 mA
Max Capacitave Load	0.01µF
Max Frequency Clock	131,072 Hz, set in 2x steps
Anti-Alias Filter Setability	200 Hz - 51.2 kHz (200 Hz steps)
Amplitude Resolution	16 bits
Harmonics and Sub-Harmonies	-68 dBc (<2 kHz) -48 dBc (<10 kHz)
Max Buffer Length	1.5 M samples 7.5 M samples (with opt.116)

Trigger

Internal	Positive or negative slope
Trigger Level Resolution	± 0.031% of full scale range TTL, positive or negative slope
Max Trigger Delay [15]	Post-trigger: from 0 to 104,575 samples Pre-trigger: from 0 to 8,191 samples ΔT=1/(Fspan x 2.56)

Tachometer/Trigger Level (HP 35658A)

Range	-23V to +23V
Resolution	<5V: 40mV >5V: 200mV
Input Impedance	>20 kΩ (typical)

[14] Transducers must be isolated from the structure under test and the input coupling cannot be "Float" to obtain a 20 V open-circuit voltage.

[15] HP 3566A input channels share the same trigger delay settings. Trigger delay for HP 3567A input channels may be set independently.

Figure App B.6 HP3566 / 67A Specification Sheet Page 6

General

Mainframe Power Supply	
Line	115 Vac range: 86 - 127 Vac
Voltage	230 Vac range: 195 - 253 Vac
Line Frequency	47.5 to 66 Hz
Line Current	115 Vac range: <6.0 Amps 230 Vac range: <3.0 Amps
Mainframe Dimensions	222 mm (8.75 in) high 432 mm (17.0 in) wide 584 mm (23.0 in) deep
Environmental:	
Ambient Temp	0 to 55° Celsius
Relative Humidity	Can be operated in environments with relative humidity of 95% at 40° C. Modules should be protected from temperature extremes, which may cause condensation.
HP-IB Implementation	SH1 AH1 T6 TE0 L4 LE0 SR1 RL0 PP0 DC1 DT1 C4,11 (IEEE Std 488-1978)

Abbreviations

dB	decibel
f	bin frequency in hertz
nV/√(Hz)	nano-volts rms per square root hertz
RPM	revolutions per minute
Rs	resistance of source or termination connected to an input

HP 3566A and 3567A Measurement Features

Measurements/results
Auto-correlation
Cross-correlation
Coherence
Cross-spectrum
Frequency response
Histogram
Probability density funct. (PDF)
Cumulative density funct. (CDF)
Overall power order tracking [1]
Peak order tracking [1]
Power spectrum order tracking [1]
Phase order tracking [1]
Composite power order tracking [1]
Order ratio map [1]
Order ratio spectrum [1]
Synthesized 1/3 octave (24 bands) [2]
Synthesized 1/1 octave (9 bands) [2]
Real-time 1/12 octave (144 bands) [3]
Real-time 1/3 octave (36 bands) [3]
Real-time 1/1 octave (12 bands) [3]
A, B, and C weights
Orbits
Filtered orbits
Power spectrum
Power spectral density
RPM spectral map
Instantaneous linear spectrum
Swept sine [4]
1/1, 1/3 octave RPM map
Instantaneous time record

X-axis coordinates
Linear, log, octave, Hz, rad/sec, RPM, CPM, order, sec, minute, user

Y-axis coordinates
Log magnitude, log dB, linear magnitude, phase, real data, imaginary data, Nyquist, Nichols, polar, EU, EU^2, EU^2/Hz (PSD), EU/√Hz

Engineering units (EUs) are displayed as peak, peak to peak, or RMS.

[1] Requires HP 35636A rotating machinery software.
[2] Conforms to 1976 ANSI specification.
[3] Conforms to ANSI S1.11-1986, order 3, type 1-D specification.
[4] Requires HP 35637A.

Figure App B.7 HP3566 / 67A Specification Sheet Page 7

B.2.3 Subwoofer loudspeaker driver

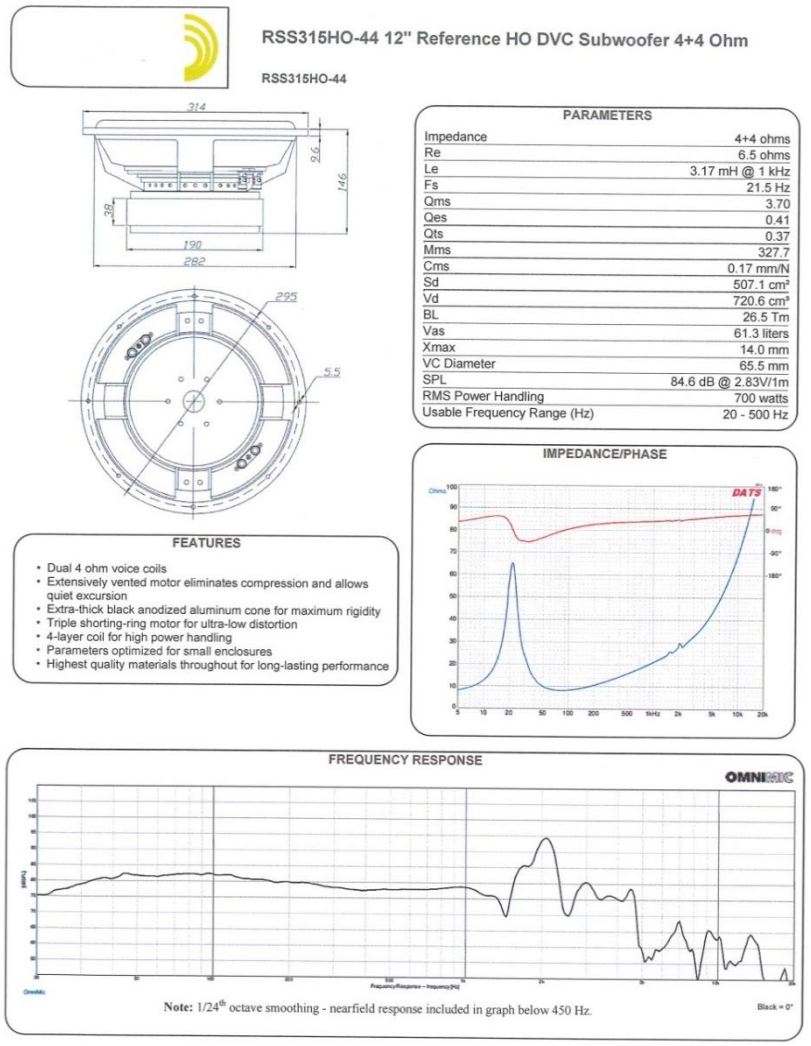

Figure App B.8 Dayton Audio RSS315HO-44 Data Sheet

B.2.4 Acoustic Absorptive Material

Product Description

Tontine Acoustisorb 2 is a medium weight flexible insulation manufactured using thermally bonded polyester fibre, with a high percentage of recycled fibres. Tontine Acoustisorb 2 provides both thermal and acoustic insulation and is manufactured to comply with AS/NZS 4859.1. For more information on physical properties and material safety data please refer to the Tontine Bonded Polyester Products Material Safety Data Sheet.

Applications

Tontine Acoustisorb 2 is a high performance acoustic sound absorber ideally to be used in areas where the control of noise is critical like recording studios, cinemas, certain wall, ceiling and baffle applications. Other recommended uses include storage tanks, process appliance cabinets and plant rooms.

Standard Sizes

ROLLS				SHEETS			
Nominal Thickness (mm)	Length (m)	Width (mm)	Number per pack	Nominal Thickness (mm)	Length (mm)	Width (mm)	Number per pack
25	15	1200	1	25	2400	1200	10
50	8	1200	1	50	2400	1200	5
				75	2400	1200	3
				100	2400	1200	3

Acoustic Performance

Acoustic results are based on tests in accordance to AS1045.

	SOUND ABSORPTION COEFFICIENTS @ FREQUENCIES					
Product	125 Hz	250Hz	500Hz	1000Hz	2000Hz	NRC
Plain 25mm	0.13	0.42	0.71	0.89	0.93	0.75
Plain 50mm	0.23	0.65	0.95	1.06	0.99	0.90
Perf Foil 50mm	0.37	0.75	1.07	1.08	0.94	0.95
Al Foil Trilam 50mm	0.26	0.68	1.10	0.92	0.60	0.80
Plain 75mm	0.38	0.95	1.03	1.09	1.05	1.05
Plain 100mm	0.67	1.08	1.16	1.11	1.12	1.10

Thermal Performance

Thermal ratings are based on testing in accordance with AS/NZS 4859.1 at 23°C mean temperature.

Product	R-Value
Acoustisorb 2 Plain 25mm	R 0.7
Acoustisorb 2 Plain 50mm	R 1.4
Acoustisorb 2 Perf Foil 50mm	R 1.4
Acoustisorb 2 Al Foil Trilam 50mm	R 1.4
Acoustisorb 2 Plain 75mm	R 2.1
Acoustisorb 2 Plain 100mm	R2.7

Technical Data Sheet 1 of 2

Figure App B.9 Tontine Acoutisorb 2 Data Sheet

B.2.5 Microphones

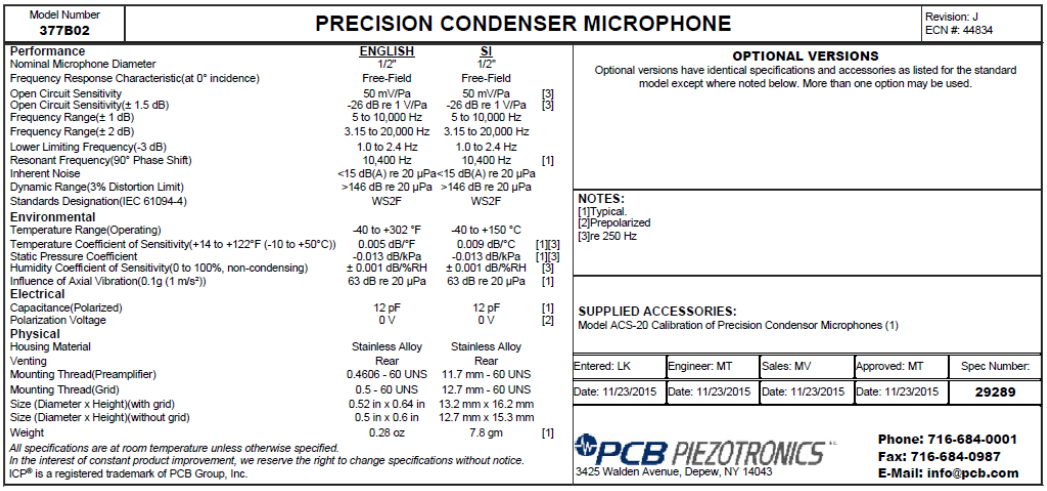

Model Number 377B02	PRECISION CONDENSER MICROPHONE	Revision: J ECN #: 44834

Performance	ENGLISH	SI	
Nominal Microphone Diameter	1/2"	1/2"	
Frequency Response Characteristic(at 0° incidence)	Free-Field	Free-Field	
Open Circuit Sensitivity	50 mV/Pa	50 mV/Pa	[3]
Open Circuit Sensitivity(± 1.5 dB)	-26 dB re 1 V/Pa	-26 dB re 1 V/Pa	[3]
Frequency Range(± 1 dB)	5 to 10,000 Hz	5 to 10,000 Hz	
Frequency Range(± 2 dB)	3.15 to 20,000 Hz	3.15 to 20,000 Hz	
Lower Limiting Frequency(-3 dB)	1.0 to 2.4 Hz	1.0 to 2.4 Hz	
Resonant Frequency(90° Phase Shift)	10,400 Hz	10,400 Hz	[1]
Inherent Noise	<15 dB(A) re 20 µPa	<15 dB(A) re 20 µPa	
Dynamic Range(3% Distortion Limit)	>146 dB re 20 µPa	>146 dB re 20 µPa	
Standards Designation(IEC 61094-4)	WS2F	WS2F	
Environmental			
Temperature Range(Operating)	-40 to +302 °F	-40 to +150 °C	
Temperature Coefficient of Sensitivity(+14 to +122°F (-10 to +50°C))	0.005 dB/°F	0.009 dB/°C	[1][3]
Static Pressure Coefficient	-0.013 dB/kPa	-0.013 dB/kPa	[1][3]
Humidity Coefficient of Sensitivity(0 to 100%, non-condensing)	± 0.001 dB/%RH	± 0.001 dB/%RH	[3]
Influence of Axial Vibration(0.1g (1 m/s²))	63 dB re 20 µPa	63 dB re 20 µPa	[1]
Electrical			
Capacitance(Polarized)	12 pF	12 pF	[1]
Polarization Voltage	0 V	0 V	[2]
Physical			
Housing Material	Stainless Alloy	Stainless Alloy	
Venting	Rear	Rear	
Mounting Thread(Preamplifier)	0.4606 - 60 UNS	11.7 mm - 60 UNS	
Mounting Thread(Grid)	0.5 - 60 UNS	12.7 mm - 60 UNS	
Size (Diameter x Height)(with grid)	0.52 in x 0.64 in	13.2 mm x 16.2 mm	
Size (Diameter x Height)(without grid)	0.5 in x 0.6 in	12.7 mm x 15.3 mm	
Weight	0.28 oz	7.8 gm	[1]

All specifications are at room temperature unless otherwise specified.
In the interest of constant product improvement, we reserve the right to change specifications without notice.
ICP® is a registered trademark of PCB Group, Inc.

OPTIONAL VERSIONS
Optional versions have identical specifications and accessories as listed for the standard model except where noted below. More than one option may be used.

NOTES:
[1]Typical.
[2]Prepolarized
[3]re 250 Hz

SUPPLIED ACCESSORIES:
Model ACS-20 Calibration of Precision Condensor Microphones (1)

Entered: LK	Engineer: MT	Sales: MV	Approved: MT	Spec Number:
Date: 11/23/2015	Date: 11/23/2015	Date: 11/23/2015	Date: 11/23/2015	29289

PCB PIEZOTRONICS
3425 Walden Avenue, Depew, NY 14043
Phone: 716-684-0001
Fax: 716-684-0987
E-Mail: info@pcb.com

Figure App B.10 PCB Model 377B02 Data Sheet

B.2.6 Microphone Preamplifiers

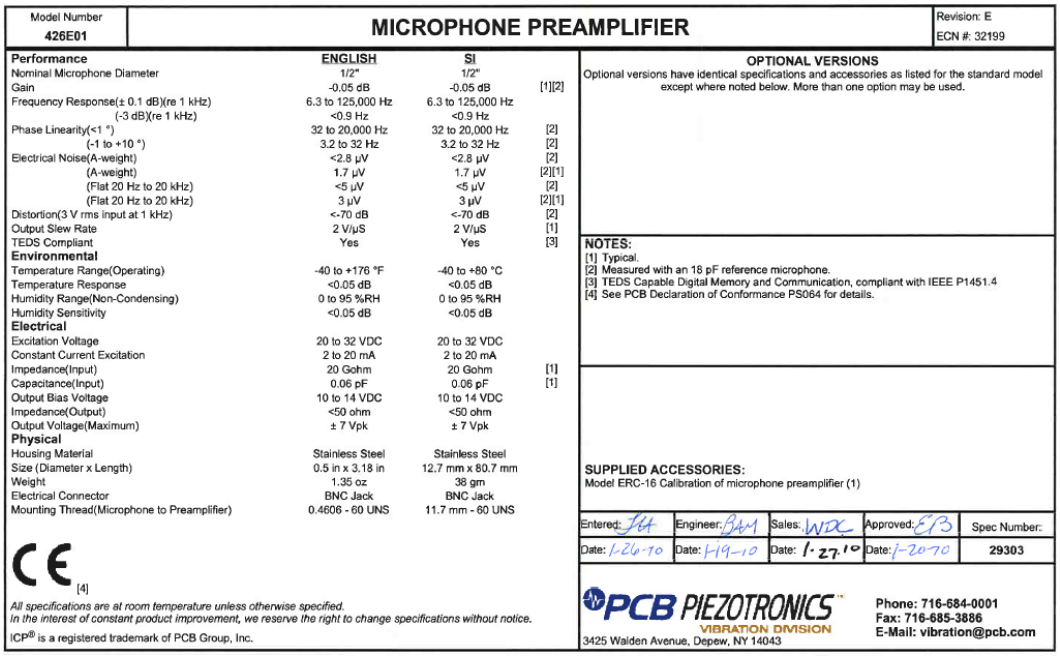

Model Number 426E01	MICROPHONE PREAMPLIFIER	Revision: E ECN #: 32199

Performance	ENGLISH	SI	
Nominal Microphone Diameter	1/2"	1/2"	
Gain	-0.05 dB	-0.05 dB	[1][2]
Frequency Response(± 0.1 dB)(re 1 kHz)	6.3 to 125,000 Hz	6.3 to 125,000 Hz	
(-3 dB)(re 1 kHz)	<0.9 Hz	<0.9 Hz	
Phase Linearity(<1 °)	32 to 20,000 Hz	32 to 20,000 Hz	[2]
(-1 to +10 °)	3.2 to 32 Hz	3.2 to 32 Hz	[2]
Electrical Noise(A-weight)	<2.8 µV	<2.8 µV	[2]
(A-weight)	1.7 µV	1.7 µV	[2][1]
(Flat 20 Hz to 20 kHz)	<5 µV	<5 µV	[2]
(Flat 20 Hz to 20 kHz)	3 µV	3 µV	[2][1]
Distortion(3 V rms input at 1 kHz)	<-70 dB	<-70 dB	[2]
Output Slew Rate	2 V/µS	2 V/µS	[1]
TEDS Compliant	Yes	Yes	[3]
Environmental			
Temperature Range(Operating)	-40 to +176 °F	-40 to +80 °C	
Temperature Response	<0.05 dB	<0.05 dB	
Humidity Range(Non-Condensing)	0 to 95 %RH	0 to 95 %RH	
Humidity Sensitivity	<0.05 dB	<0.05 dB	
Electrical			
Excitation Voltage	20 to 32 VDC	20 to 32 VDC	
Constant Current Excitation	2 to 20 mA	2 to 20 mA	
Impedance(Input)	20 Gohm	20 Gohm	[1]
Capacitance(Input)	0.06 pF	0.06 pF	[1]
Output Bias Voltage	10 to 14 VDC	10 to 14 VDC	
Impedance(Output)	<50 ohm	<50 ohm	
Output Voltage(Maximum)	± 7 Vpk	± 7 Vpk	
Physical			
Housing Material	Stainless Steel	Stainless Steel	
Size (Diameter x Length)	0.5 in x 3.18 in	12.7 mm x 80.7 mm	
Weight	1.35 oz	38 gm	
Electrical Connector	BNC Jack	BNC Jack	
Mounting Thread(Microphone to Preamplifier)	0.4606 - 60 UNS	11.7 mm - 60 UNS	

CE [4]

All specifications are at room temperature unless otherwise specified.
In the interest of constant product improvement, we reserve the right to change specifications without notice.
ICP® is a registered trademark of PCB Group, Inc.

OPTIONAL VERSIONS
Optional versions have identical specifications and accessories as listed for the standard model except where noted below. More than one option may be used.

NOTES:
[1] Typical.
[2] Measured with an 18 pF reference microphone.
[3] TEDS Capable Digital Memory and Communication, compliant with IEEE P1451.4
[4] See PCB Declaration of Conformance PS064 for details.

SUPPLIED ACCESSORIES:
Model ERC-16 Calibration of microphone preamplifier (1)

Entered: JH	Engineer: BM	Sales: WDL	Approved: EB	Spec Number:
Date: 1-26-10	Date: 1-19-10	Date: 1-27-10	Date: 1-20-10	29303

PCB PIEZOTRONICS
VIBRATION DIVISION
3425 Walden Avenue, Depew, NY 14043
Phone: 716-684-0001
Fax: 716-685-3886
E-Mail: vibration@pcb.com

Figure App B.11 PCB Model 426E01 Data Sheet

B.2.7 Microphone holder

RUTASEAL LIGHT® EPDM Metric




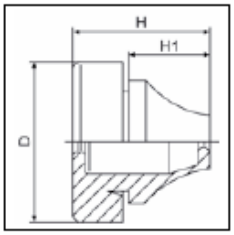

Material	EPDM - Halogen Free Resistant to chemicals and weatherproof.
Mode of protection	IP67
Temperature range	-40°C....+110°C (5)
Test standard	EN 60670-1:2005+A1:2013
Semko report	1313520

- Quick and simple assembly without the use of tools
- Can be assembled from either end depedning on application
- Less material makes it easier to install, as well as pull out
- "Pushout" membrane

Product number	Size	For cable/ pipe Ø mm	A mm	B mm	D mm	H mm	H1 mm	Pcs pack	
RAL 7001									
T_14 583 26	M16	5 - 9	16,5	1 - 4	21	18	11	50	4000
T_14 583 27	M20	8 - 12	20,5	1 - 4	25,5	20	13,4	50	2000
T_14 583 28	M25	11 - 16	25,5	1 - 4	30,5	21,6	15,3	50	1500
RAL 9005									
T_14 583 30	M16	5 - 9	16,5	1 - 4	21	18	11	50	4000
T_14 583 31	M20	8 - 12	20,5	1 - 4	25,5	20	13,4	50	2000
T_14 583 32	M25	11 - 16	25,5	1 - 4	30,5	21,6	15,3	50	1500
RAL 7035									
T_14 583 34	M16	5 - 9	16,5	1 - 4	21	18	11	50	4000
T_14 583 35	M20	8 - 12	20,5	1 - 4	25,5	20	13,4	50	2000
T_14 583 36	M25	11 - 16	25,5	1 - 4	30,5	21,6	15,3	50	1500

RUTASEAL® RUTASEAL LIGHT®

Figure App B.12 TST Rutaseal T_14 583 32 Data Sheet

B.2.8 Microphone Calibrator

Model CAL250

CAL250
Precision Acoustic Calibrator

IEC 60942 Class 1 Handheld Sound Level Calibrator for 1" microphones at 251.2 Hz
Used for Sound Level Meters and Other Sound Measuring Equipment

Highlights

- Output level: 114 dB
- Output frequency: 251.2 Hz
- Standard: 1" microphone
- IEC 60942-1:2003 compliant
- Internal battery
- Output level independent of battery condition
- Adaptors: 1/2", 1/4", 3/8", 1/8" microphones
- Array adaptor for 8 microphones simultaneously

Applications

Field calibration or laboratory calibration of:

- Sound level meters
- Noise dosimeters
- Noise monitoring stations
- Microphone arrays

CAL250 Portable Sound Calibrator

079A31

ADP021

ADP019

The Larson Davis Model CAL250 is a battery operated precision microphone calibrator used for the calibration of sound level meters and other sound measurement equipment. The CAL250 delivers a full 114.0 dB level output signal @ 251.2 Hz.

It has been designed for field or laboratory use and its accuracy has been calibrated to a reference traceable to the National Institute of Standards and Technology (NIST).

The Larson Davis CAL250 features a stable sound pressure independent of the battery condition. In addition, the CAL250 will turn off automatically to preserve battery and guarantee a stable output.

LARSON DAVIS
A PCB PIEZOTRONICS DIV.

Larson Davis ☎ Toll-Free in USA 888-258-3222 ☎ 716-926-8243 www.larsondavis.com

Figure App B.13 Larson Davis CAL250 Data Sheet Page 1

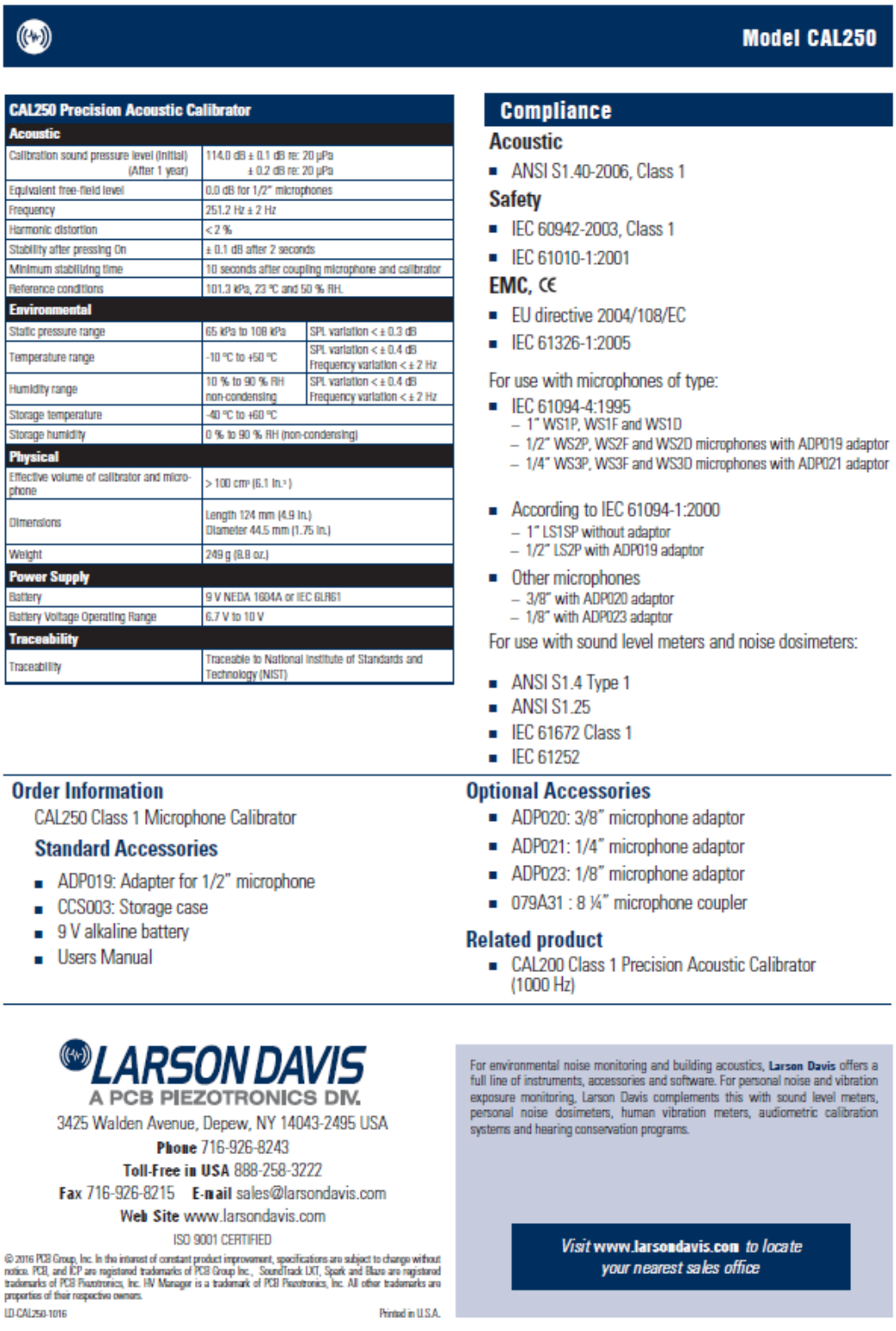

Model CAL250

CAL250 Precision Acoustic Calibrator

Acoustic		
Calibration sound pressure level (Initial) (After 1 year)	114.0 dB ± 0.1 dB re: 20 µPa ± 0.2 dB re: 20 µPa	
Equivalent free-field level	0.0 dB for 1/2" microphones	
Frequency	251.2 Hz ± 2 Hz	
Harmonic distortion	< 2 %	
Stability after pressing On	± 0.1 dB after 2 seconds	
Minimum stabilizing time	10 seconds after coupling microphone and calibrator	
Reference conditions	101.3 kPa, 23 °C and 50 % RH.	
Environmental		
Static pressure range	65 kPa to 108 kPa	SPL variation < ± 0.3 dB
Temperature range	-10 °C to +50 °C	SPL variation < ± 0.4 dB Frequency variation < ± 2 Hz
Humidity range	10 % to 90 % RH non-condensing	SPL variation < ± 0.4 dB Frequency variation < ± 2 Hz
Storage temperature	-40 °C to +60 °C	
Storage humidity	0 % to 90 % RH (non-condensing)	
Physical		
Effective volume of calibrator and microphone	> 100 cm³ (6.1 in.³)	
Dimensions	Length 124 mm (4.9 in.) Diameter 44.5 mm (1.75 in.)	
Weight	249 g (8.8 oz.)	
Power Supply		
Battery	9 V NEDA 1604A or IEC 6LR61	
Battery Voltage Operating Range	6.7 V to 10 V	
Traceability		
Traceability	Traceable to National Institute of Standards and Technology (NIST)	

Compliance

Acoustic

- ANSI S1.40-2006, Class 1

Safety

- IEC 60942-2003, Class 1
- IEC 61010-1:2001

EMC, CE

- EU directive 2004/108/EC
- IEC 61326-1:2005

For use with microphones of type:

- IEC 61094-4:1995
  - 1" WS1P, WS1F and WS1D
  - 1/2" WS2P, WS2F and WS2D microphones with ADP019 adaptor
  - 1/4" WS3P, WS3F and WS3D microphones with ADP021 adaptor
- According to IEC 61094-1:2000
  - 1" LS1SP without adaptor
  - 1/2" LS2P with ADP019 adaptor
- Other microphones
  - 3/8" with ADP020 adaptor
  - 1/8" with ADP023 adaptor

For use with sound level meters and noise dosimeters:

- ANSI S1.4 Type 1
- ANSI S1.25
- IEC 61672 Class 1
- IEC 61252

Order Information

CAL250 Class 1 Microphone Calibrator

Standard Accessories

- ADP019: Adapter for 1/2" microphone
- CCS003: Storage case
- 9 V alkaline battery
- Users Manual

Optional Accessories

- ADP020: 3/8" microphone adaptor
- ADP021: 1/4" microphone adaptor
- ADP023: 1/8" microphone adaptor
- 079A31 : 8 ¼" microphone coupler

Related product

- CAL200 Class 1 Precision Acoustic Calibrator (1000 Hz)

LARSON DAVIS
A PCB PIEZOTRONICS DIV.
3425 Walden Avenue, Depew, NY 14043-2495 USA
Phone 716-926-8243
Toll-Free in USA 888-258-3222
Fax 716-926-8215 **E-mail** sales@larsondavis.com
Web Site www.larsondavis.com
ISO 9001 CERTIFIED

LD CAL250-1016 Printed in U.S.A.

For environmental noise monitoring and building acoustics, **Larson Davis** offers a full line of instruments, accessories and software. For personal noise and vibration exposure monitoring, Larson Davis complements this with sound level meters, personal noise dosimeters, human vibration meters, audiometric calibration systems and hearing conservation programs.

Visit **www.larsondavis.com** *to locate your nearest sales office*

Figure App B.14 Larson Davis CAL250 Data Sheet Page 2

Appendix C MATLAB Code

This appendix lists the MATLAB R2014a code used to calculate the acoustic transmission loss using the four microphone frequency domain averaged data from the HP analyser and the experimental transmission loss test bench. This has been generated using the 'Report' function in MATLAB.

Table of Contents

Wave Decomposition and Acoustic Transmission Loss

```
Author David Bowden;
Revision date 11th May 2017;
This program calculates and plots the transmission loss for
an acoustic device / silencer on an experimental test bench;
Transmission loss is calculated as the acoustic power level difference
between the incident and the transmitted waves.
```

Decomposition theory is used to separate the forward (incident)

and backwards (reflected)travelling waves Tao & Seybert,2003, SAE Technical paper Series 2003-01-1653 "A Review of Current Techniques for Measuring Muffler Transmission Loss" A.F. Seybert, 1988, Acoustical Society of America, "Two-sensor methods for the measurements of sound intensity and acoustical properties in ducts"

The test set-up comprises

```
Hewlett Packard 3567A Spectrum Analyser;
4 microphone data with 2 microphones before and
2 microphones after test device;
for FRF of Channels 1:2,  channel 1 is the reference;
for FRF of Channels 3:4,  channel 3 is the reference;
1600 frequency lines;
broad band speaker excitation to  400, 800, or 1600 Hz;
an anechoic termination;
room temperature;
ambient pressure, and
zero flow.
```

Input File Formats

```
The input files are Matlab data files - converted from
HP3566/67 analyser SDF files to Matlab files
using HP utility HP 35639A "Data Viewer" batch convert
These files are in the following format in 'peak' amplitudes
with units of SPL or SPL^2 as appropriate.
The data is now converted from SPL or SPL^2 to Pa and Pa^2
by mutiplying by 2e-5 or (2e-5)^2 as appropriate;
The HP file naming convention is as follows:
filename'00' FRF Channels 1:2,  complex, magnitude,
filename'01' FRF Channels 3:4,  complex, magnitude,
filename'10  Coherence Channels 1:2, magnitude,
filename'11' Coherence Channels 3:4, magnitude,
filename'20' Input Power Channels 1:2, peak, magnitude,
filename'21' Input Power Channels 3:4, peak, magnitude,
filename'30' Output Power Channels 1:2, peak, magnitude,
filename'31' Output Power Channels 3:4, peak, magnitude,
filename'40' Cross Power Channels 1:2,  complex, peak, magnitude,
filename'41' Cross Power Channels 3:4,  complex, peak, magnitude,
filename'50' Instantaneous Time Channels 1, magnitude,
filename'51' Instantaneous Time Channels 2, magnitude,
filename'52' Instantaneous Time Channels 3, magnitude,
filename'53' Instantaneous Time Channels 4, magnitude.
```

Algorithms

Decomposition: S(AA)=(S(11)+S(22)-2*C(12)*cos(k*x(12)) + 2*Q(12)*sin(k*x(12))) / (4*sin(k*x(12))^2; S(BB)=(S(11)+S(22)-2*C(12)*cos(k*x(12)) - 2*Q(12)*sin(k*x(12))) / (4*sin(k*x(12))^2); where S(AA)is the auto (power) spectra of the incident wave S(BB)is the auto (power) spectra of the reflected wave S(11)is the auto (power) spectra of the total acoustic pressure at point 1 S(22)is the auto (power) spectra of the total acoustic pressure at point 2 C(12) is the real part of the cross power spectrum between points 1 and 2 Q(12)is the imaginary part of the cross power spectrum between points 1 and 2 k is the wave number x(12) is the distance between the two microphones (points 1 and 2)

Wave number (k)

```
k = 2*pi*f/c, where
```

```
f is frequency
c is speed of sound
```

Speed of Sound (c)

```
c= gamma*r*T^.5,  where
    gamma is 1.4
    R is 287
    T is temperature in degrees Kelvin
```

Amplitude of incident sound wave pressure (p(incident))

```
p(incident) = sqrt(S(AA))
```

Sound Power (W(i))

W(i) = (p(i)^2)*S(i)/(rho * c) where S(i) is the tube area rho is the fluid density

Density of air (rho)

```
rho = p(air) / ( R*T)
```

Transmission Loss

```
TL = 10*log10(W(incident) / W(transmitted))
    or
TL = 20 * log10 (p(incident) / p(transmitted)) + 10 log10 (S(i) / S(o))
```

initialize Matlab

```
clc;
clear;
close;
```

Test Input Data

```
dataset='TJun39';           % Data Set
P_atmospheric =  101700;    % [Pa] Atmospheric pressure
T_airC =  23;               % air temperature in degrees C
x_12= 0.5;  % microphone spacing in metres between points 1&2 (400 Hz)
x_34 = 0.5; % microphone spacing in metres between points 3&4 (400 Hz)
```

Air properties at test conditions

```
gamma = 1.4;                        % ratio of specific heats
R_specific = 287;                   % Specific gas constant
```

```
T_airK =  T_airC + 273;                % Air temperature in degrees K
rho = P_atmospheric / ( R_specific* T_airK); % [kg/m^3] Density of air
c= sqrt(gamma * R_specific * T_airK);        % speed of sound m/s
```

Measurement duct physical

```
dia_inlet = 330 ;                       % inlet diameter in mm
area_inlet = pi/4*(dia_inlet/1000)^2;   % inlet area in m^2
dia_outlet = 330 ;                      % outlet diameter in mm
area_outlet = pi/4*(dia_outlet/1000)^2; % outlet area in m^2
```

Zero matrices

```
%Zero Matrices
    % Inlet measurement Duct
        S_AA = zeros(1601,1);
        S_BB = zeros(1601,1);
        S_11 = zeros(1601,1);
        S_22 = zeros(1601,1);
        C_12 = zeros(1601,1);
        Q_12 = zeros(1601,1);
        k = zeros(1601,1);
        frequency = zeros(1601,1);
        TAP1 = zeros(1601,1);
        TAP2 = zeros(1601,1);
        CS_12 = zeros(1601,1);
        pressure_i = zeros(1601,1);
        power_i = zeros(1601,1);
    % Outlet measurement Duct
        S_XX = zeros(1601,1);
        S_YY = zeros(1601,1);
        S_33 = zeros(1601,1);
        S_44 = zeros(1601,1);
        C_34 = zeros(1601,1);
        Q_34 = zeros(1601,1);
        TAP3 = zeros(1601,1);
        TAP4 = zeros(1601,1);
        CS_34 = zeros(1601,1);
        pressure_t = zeros(1601,1);
        pressure_t1 = zeros(1601,1);
        power_t = zeros(1601,1);
        power_t1 = zeros(1601,1);
    % Transmission Loss
        TL3m = zeros(1601,1);
        TL4m = zeros(1601,1);
        TL3mpower = zeros(1601,1);
        TL4mpower = zeros(1601,1);
```

Import microphone data from HP analyser

```
Note that data files  are in peak units
Load data files
```

Input Measurement Duct

```
%Input Measurement Duct
    % Total accoustic pressure at point 1
        TAP1 = load(strcat(dataset,'20'));
        S_11 = (TAP1.y) *((2e-5)^2);
    % frequency
        frequency = TAP1.x;
    % Wave Speed k
        k = 2*pi*frequency/c;
     % Total accoustic pressure at point 2
        TAP2 = load(strcat(dataset,'30'));
        S_22 = (TAP2.y) *((2e-5)^2);
    % Cross Spectrum between point1 and point 2
        % real
        CS_12 = load(strcat(dataset,'40'));
        C_12  = real(CS_12.y)*((2e-5)^2);
        % Imaginary
        Q_12 = imag(CS_12.y) *((2e-5)^2);
```

Output Measurement Duct

```
%Output Measurement Duct
    % Total accoustic pressure at point 3
        TAP3 = load(strcat(dataset,'21'));
        S_33 = (TAP3.y) *((2e-5)^2);
    % Total accoustic pressure at point 4
        TAP4 = load(strcat(dataset,'31'));
        S_44 = (TAP4.y)*((2e-5)^2);
    % Cross Spectrum between point3 and point 4
        % real
        CS_34 = load(strcat(dataset,'41'));
        C_34 = real(CS_34.y)  *((2e-5)^2);
        % Imaginary
        Q_34 = imag(CS_34.y) *((2e-5)^2);
```

Calculate the acoustic transmission loss

```
%Acoustic Transmission Loss
    % Wave Speed k
        k = 2*pi/c.*frequency;
    % Incident pressure and power calculations using two microphone method
        S_AA = (S_11 + S_22 - 2*C_12 .* cos(x_12 * k) - 2*Q_12 .* ...
            sin(x_12 * k))./ (4 * (sin(x_12 * k)) .^2);
        S_BB = (S_11 + S_22 - 2*C_12 .* cos(x_12 * k) + 2*Q_12 .* ...
            sin(x_12 * k))./ (4 * (sin(x_12 * k)) .^2);
    % S_AA and S_BB : sign of Q_12 interchanged to suit HP data convention
    % amplitude of incident sound wave pressure (p(i))
        pressure_i = sqrt(S_AA);
    % amplitude of reflected sound wave pressure (p(ir))
        pressure_ir = sqrt(S_BB);
    % Sound Power
```

```
    power_i = pressure_i.^2 * area_inlet/(rho * c);
    power_ir = pressure_ir.^2 * area_inlet/(rho * c);
% Transmitted pressure & power calculations using 2 microphone method;
    S_XX = (S_33 + S_44 - 2*C_34 .* cos(x_34 * k) - 2*Q_34 .* ...
        sin(x_34 * k))./ (4*(sin(x_34*k)).^2);
    S_YY = (S_33 + S_44 - 2*C_34 .* cos(x_34 * k) + 2*Q_34 .* ...
        sin(x_34 * k))./ (4*(sin(x_34*k)).^2);
% S_XX & S_YY :sign of Q_34 interchanged to correct HP data convention
% amplitude of transmitted sound wave pressure
    pressure_t = sqrt(S_XX);
% amplitude of reflected sound wave pressure (p(ir))
    pressure_tr = sqrt(S_YY);
% Sound Power transmitted
    power_t = pressure_t.^2 * area_outlet / (rho * c);
    power_tr = pressure_tr.^2 * area_inlet/(rho * c);
% Transmission Loss using pressure amplitudes for calculation
    TL4m = 20 * log10 (pressure_i./pressure_t) + 10 * ...
        log10 (area_inlet / area_outlet);
% Transmission Loss using power for calculation
    TL4mpower = 10*log10( power_i ./ power_t);
```

Transmitted pressure and power calculations

using one microphone after silencer

```
%One Microphone
    % amplitude of transmitted sound wave pressure
        pressure_t1 = sqrt(S_44);
    % Sound Power transmitted
        power_t1 = pressure_t1.^2 * area_outlet / (rho * c);
    % Transmission Loss using pressure amplitudes for calculation
        TL3m = 20 * log10 (pressure_i./pressure_t1) + 10 * ...
            log10 (area_inlet / area_outlet);
    % Transmission Loss using power for calculation
        TL3mpower = 10*log10( power_i ./ power_t1);
```

Save Data and Results

```
    save(strcat(dataset,'_results'));
```

Plot the results

```
%Results
    % Plot the Transmission Loss
        figure(1);
    % Three Microphone Method
        plot(frequency,TL3m,'b');
        grid on;
        title('Acoustic (Power)Transmission Loss');
        xlabel('Frequency [Hz]');
        ylabel('Transmission Loss [dB]');
        hold on;
    % Four Microphone Method
```

```
plot(frequency,TL4m,'r');
legend('Three Microphone','Four Microphone');
hold off;
```

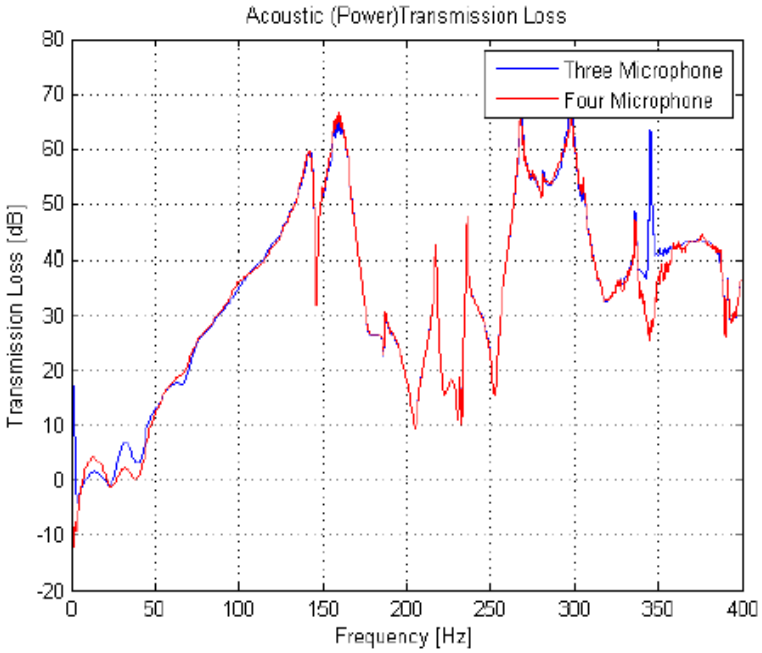

Plots of Intermediate Calculations

```
%Intermediate Calculations
% Input side of Silencer
    % Plot the Microphone Autospectras
        figure(2);
        semilogy(frequency,S_11,'b'); % Autospectra Power at Microphone 1;
        grid on;
        title('Microphone Autospectra on Inlet Side');
        xlabel('Frequency [Hz]');
        ylabel('Autospectra (Power) Pa^2');
        hold on;
        semilogy(frequency,S_22,'r'); %Autospectra Power at Microphone 2;
        legend('Microphone 1','Microphone 2');
        hold off;
    % Plot the Input Incident and Reflected
       figure(3);
       semilogy(frequency,power_i,'b'); %Incident Sound Pressure, power_i;
       grid on;
       title('Incident and Reflected Powers on Inlet Side');
       xlabel('Frequency [Hz]');
       ylabel('Power Pa^2');
```

```
        hold on;
        semilogy(frequency,power_ir,'r');%Reflected Sound Pressure,power_ir;
        legend('Incident','Reflected');
        hold off;
% Output side of Silencer
    % Plot the Microphone Autospectras
        figure(4);
        semilogy(frequency,S_33,'b'); % Autospectra Power at Microphone 3;
        grid on;
        title('Microphone Autospectra on Outlet Side');
        xlabel('Frequency [Hz]');
        ylabel('Autospectra (Power) Pa^2');
        hold on;
        semilogy(frequency,S_44,'r'); %Autospectra Power at Microphone 4;
        legend('Microphone 3','Microphone 4');
        hold off;
    % Plot the Input Incident and Reflected
        figure(5);
        semilogy(frequency,power_t,'b'); %Incident Sound Pressure, power_i;
        grid on;
        title('Incident and Reflected Powers on Outlet Side');
        xlabel('Frequency [Hz]');
        ylabel('Power Pa^2');
        hold on;
        semilogy(frequency,power_tr,'r');%Reflected Sound Pressure,power_ir;
        legend('Incident','Reflected');
        hold off;
```

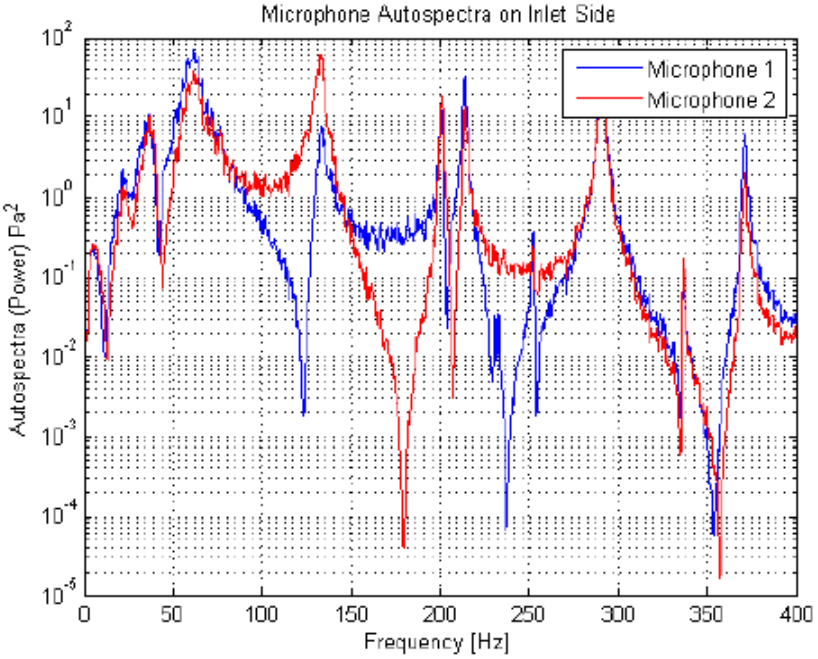
Microphone Autospectra on Inlet Side
Microphone 1
Microphone 2
Autospectra (Power) Pa2
Frequency [Hz]

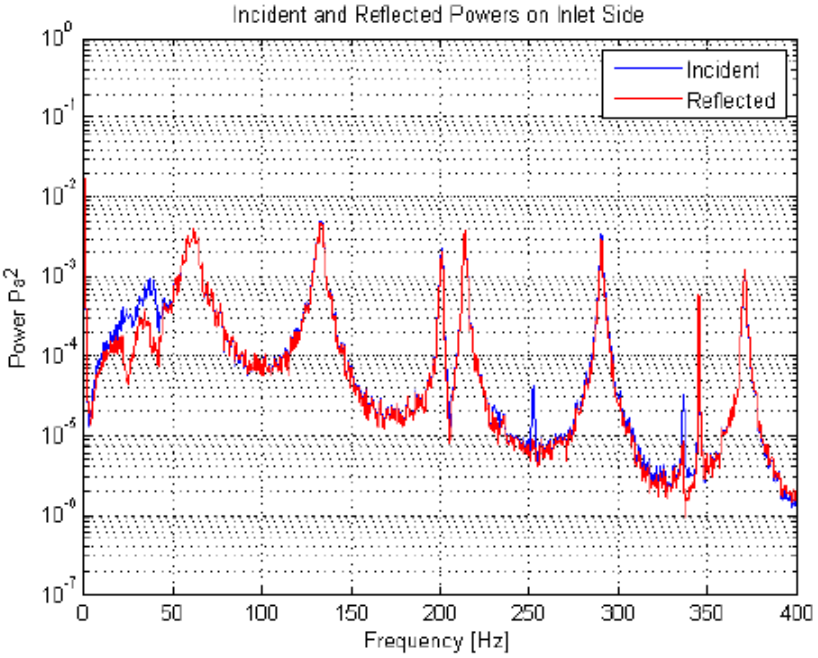
Incident and Reflected Powers on Inlet Side
Incident
Reflected
Power Pa2
Frequency [Hz]

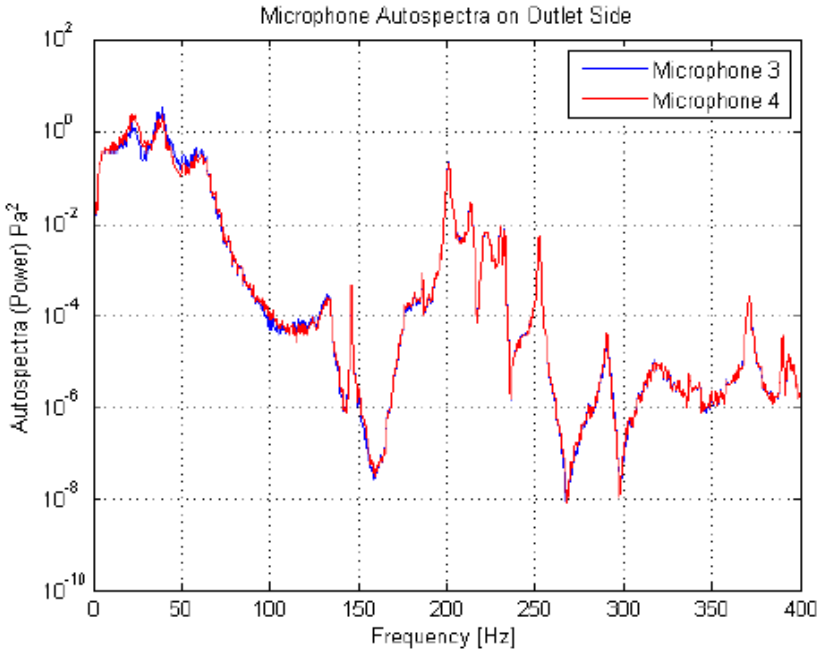
Microphone Autospectra on Outlet Side
Microphone 3
Microphone 4
Autospectra (Power) Pa2
Frequency [Hz]

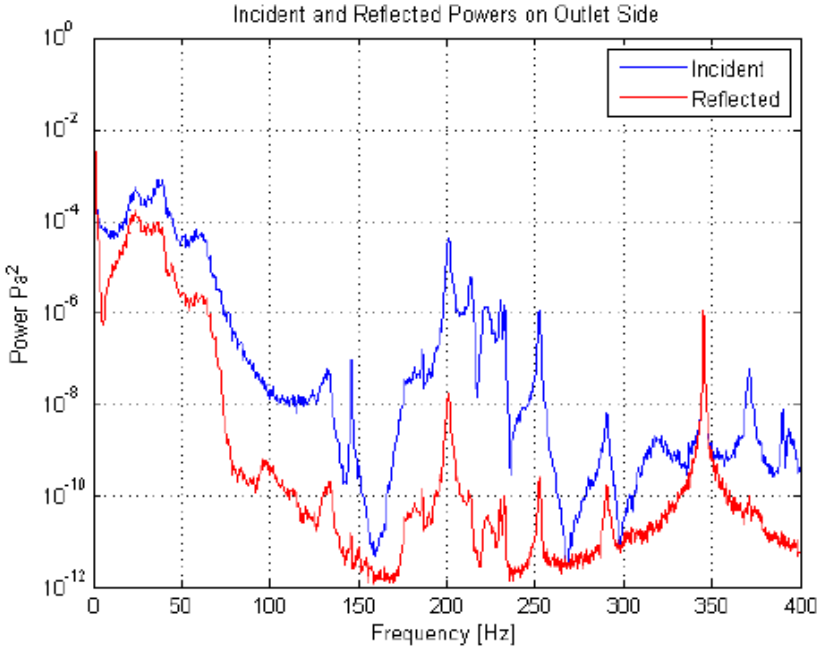
Incident and Reflected Powers on Outlet Side
Incident
Reflected
Power Pa2
Frequency [Hz]

Plot Cross Spectras

```
%Cross Spectra
    % Plot the Cross Spectrum 1;2
        figure(6);
        plot(frequency,C_12,'r');%Cross Spectrum, Real
        hold on
        plot(frequency,Q_12,'g');%Cross Spectrum, Imaginary
        title('Cross Spectrum 1:2');
        xlabel('Frequency [Hz]');
        ylabel('Cross Spectra Power Pa^2');
        legend('Real','Imaginary');
        hold off;
    % Plot the Cross Spectrum 3:4
        figure(7);
        plot(frequency,C_34,'r');%Cross Spectrum, Real
        hold on;
        plot(frequency,Q_34,'g');%Cross Spectrum, Imaginary
        title('Cross Spectrum 3:4');
        xlabel('Frequency [Hz]');
        ylabel('Cross Spectra Power Pa^2');
        legend('Real','Imaginary');
        hold off;
```

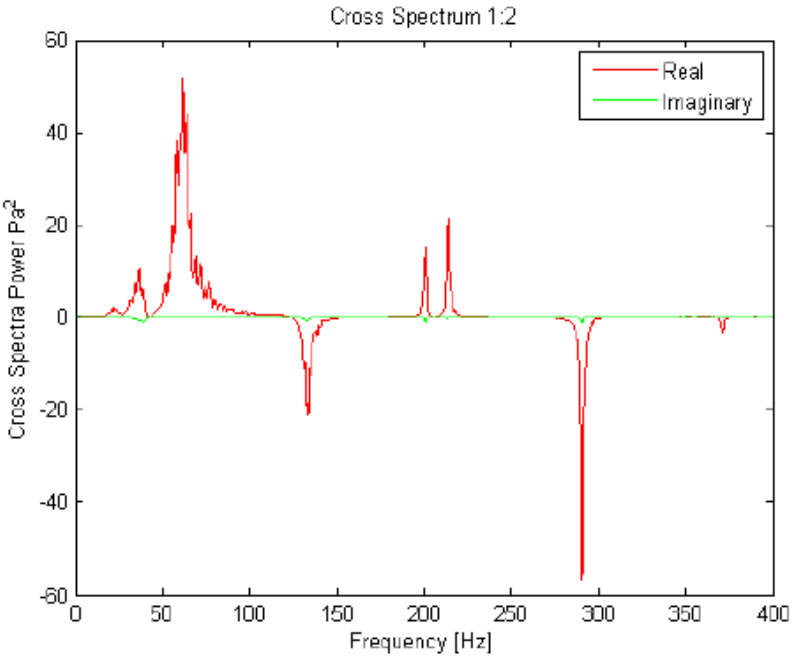

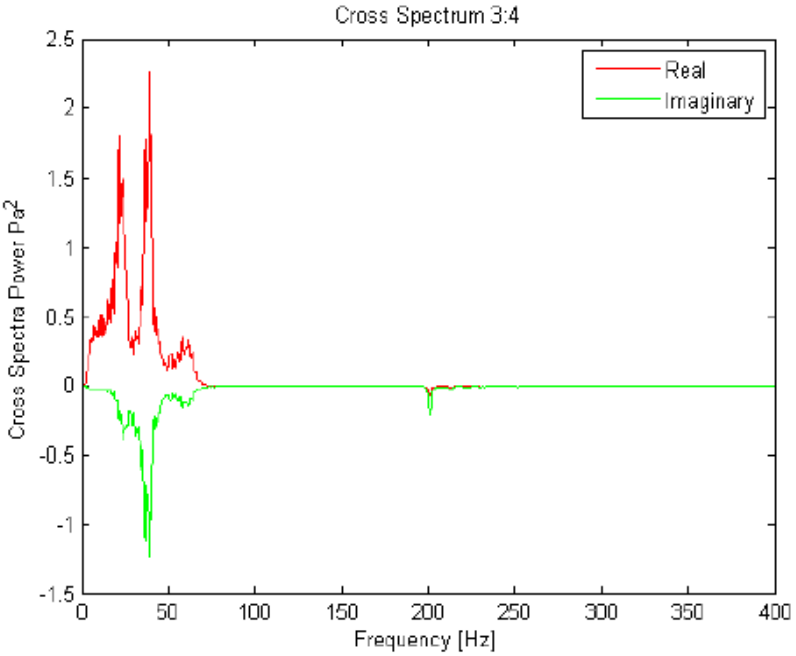

Input Parameter Check

```
disp (['Input Data set is ',(dataset)]);
disp (['Atmospheric pressure in Pa is ',num2str(P_atmospheric)]);
disp (['Air temperature in degrees C is ',num2str(T_airC)]);
disp (['Microphone spacing in metres between points 1 and 2 is ' ...
    ,num2str(x_12)]);
disp (['Microphone spacing in metres between points 3 and 4 is ' ...
    ,num2str(x_34)]);
disp (['Speed of sound m/s is ', num2str(c)]);
disp (['Inlet diameter in mm is ',num2str(dia_inlet)]);
disp (['Outlet diameter in mm is ',num2str(dia_outlet)]);
```

```
Input Data set is TJun39
Atmospheric pressure in Pa is 101700
Air temperature in degrees C is 23
Microphone spacing in metres between points 1 and 2 is 0.5
Microphone spacing in metres between points 3 and 4 is 0.5
Speed of sound m/s is 344.8664
Inlet diameter in mm is 330
Outlet diameter in mm is 330
```

END

The test set-up comprises

Hewlett Packard 3567A Spectrum Analyser;
4 microphone data with 2 microphones before and
2 microphones after test device;
for FRF of Channels 1:2, channel 1 is the reference;
for FRF of Channels 3:4, channel 3 is the reference;
1600 frequency lines;
broad band speaker excitation to 400, 800, or 1600 Hz;
an anechoic termination;
room temperature;
ambient pressure, and
zero flow.

Input File Formats

The input files are Matlab data files - converted from
HP3566/67 analyser SDF files to Matlab files
using HP utility HP 35639A "Data Viewer" batch convert
These files are in the following format in 'peak' amplitudes
with units of SPL or SPL^2 as appropriate.
The data is now converted from SPL or SPL^2 to Pa and Pa^2
by mutiplying by 2e-5 or (2e-5)^2 as appropriate;
The HP file naming convention is as follows:
filename'00' FRF Channels 1:2, complex, magnitude,
filename'01' FRF Channels 3:4, complex, magnitude,
filename'10 Coherence Channels 1:2, magnitude,
filename'11' Coherence Channels 3:4, magnitude,
filename'20' Input Power Channels 1:2, peak, magnitude,
filename'21' Input Power Channels 3:4, peak, magnitude,
filename'30' Output Power Channels 1:2, peak, magnitude,
filename'31' Output Power Channels 3:4, peak, magnitude,
filename'40' Cross Power Channels 1:2, complex, peak, magnitude,
filename'41' Cross Power Channels 3:4, complex, peak, magnitude,
filename'50' Instantaneous Time Channels 1, magnitude,
filename'51' Instantaneous Time Channels 2, magnitude,
filename'52' Instantaneous Time Channels 3, magnitude,
filename'53' Instantaneous Time Channels 4, magnitude.

Algorithms

Decomposition: S(AA)=(S(11)+S(22)-2*C(12)*cos(k*x(12)) + 2*Q(12)*sin(k*x(12))) / (4*sin(k*x(12))^2; S(BB)=(S(11)+S(22)-2*C(12)*cos(k*x(12)) - 2*Q(12)*sin(k*x(12))) / (4*sin(k*x(12))^2); where S(AA)is the auto (power) spectra of the incident wave S(BB)is the auto (power) spectra of the reflected wave S(11)is the auto (power) spectra of the total acoustic pressure at point 1 S(22)is the auto (power) spectra of the total acoustic pressure at point 2 C(12) is the real part of the cross power spectrum between points 1 and 2 Q(12)is the imaginary part of the cross power spectrum between points 1 and 2 k is the wave number x(12) is the distance between the two microphones (points 1 and 2)

Wave number (k)

k = 2*pi*f/c, where

```
f is frequency
c is speed of sound
```

Speed of Sound (c)

```
c= gamma*r*T^.5,  where
    gamma is 1.4
    R is 287
    T is temperature in degrees Kelvin
```

Amplitude of incident sound wave pressure (p(incident))

```
p(incident) = sqrt(S(AA))
```

Sound Power (W(i))

W(i) = (p(i)^2)*S(i)/(rho * c) where S(i) is the tube area rho is the fluid density

Density of air (rho)

```
rho = p(air) / ( R*T)
```

Transmission Loss

```
TL = 10*log10(W(incident) / W(transmitted))
    or
TL = 20 * log10 (p(incident) / p(transmitted)) + 10 log10 (S(i) / S(o))
```

initialize Matlab

```
clc;
clear;
close;
```

Test Input Data

```
dataset='TJun39';           % Data Set
P_atmospheric =  101700;    % [Pa] Atmospheric pressure
T_airC =  23;               % air temperature in degrees C
x_12= 0.5;  % microphone spacing in metres between points 1&2 (400 Hz)
x_34 = 0.5; % microphone spacing in metres between points 3&4 (400 Hz)
```

Air properties at test conditions

```
gamma = 1.4;                        % ratio of specific heats
R_specific = 287;                   % Specific gas constant
```

```
T_airK =  T_airC + 273;                % Air temperature in degrees K
rho = P_atmospheric / ( R_specific* T_airK); % [kg/m^3] Density of air
c= sqrt(gamma * R_specific * T_airK);        % speed of sound m/s
```

Measurement duct physical

```
dia_inlet = 330 ;                       % inlet diameter in mm
area_inlet = pi/4*(dia_inlet/1000)^2;   % inlet area in m^2
dia_outlet = 330 ;                      % outlet diameter in mm
area_outlet = pi/4*(dia_outlet/1000)^2; % outlet area in m^2
```

Zero matrices

```
%Zero Matrices
    % Inlet measurement Duct
        S_AA = zeros(1601,1);
        S_BB = zeros(1601,1);
        S_11 = zeros(1601,1);
        S_22 = zeros(1601,1);
        C_12 = zeros(1601,1);
        Q_12 = zeros(1601,1);
        k = zeros(1601,1);
        frequency = zeros(1601,1);
        TAP1 = zeros(1601,1);
        TAP2 = zeros(1601,1);
        CS_12 = zeros(1601,1);
        pressure_i = zeros(1601,1);
        power_i = zeros(1601,1);
    % Outlet measurement Duct
        S_XX = zeros(1601,1);
        S_YY = zeros(1601,1);
        S_33 = zeros(1601,1);
        S_44 = zeros(1601,1);
        C_34 = zeros(1601,1);
        Q_34 = zeros(1601,1);
        TAP3 = zeros(1601,1);
        TAP4 = zeros(1601,1);
        CS_34 = zeros(1601,1);
        pressure_t = zeros(1601,1);
        pressure_t1 = zeros(1601,1);
        power_t = zeros(1601,1);
        power_t1 = zeros(1601,1);
    % Transmission Loss
        TL3m = zeros(1601,1);
        TL4m = zeros(1601,1);
        TL3mpower = zeros(1601,1);
        TL4mpower = zeros(1601,1);
```

Import microphone data from HP analyser

```
Note that data files  are in peak units
Load data files
```

Input Measurement Duct

```
%Input Measurement Duct
    % Total accoustic pressure at point 1
        TAP1 = load(strcat(dataset,'20'));
        S_11 = (TAP1.y) *((2e-5)^2);
    % frequency
        frequency = TAP1.x;
    % Wave Speed k
        k = 2*pi*frequency/c;
     % Total accoustic pressure at point 2
        TAP2 = load(strcat(dataset,'30'));
        S_22 = (TAP2.y) *((2e-5)^2);
    % Cross Spectrum between point1 and point 2
        % real
        CS_12 = load(strcat(dataset,'40'));
        C_12  = real(CS_12.y)*((2e-5)^2);
        % Imaginary
        Q_12 = imag(CS_12.y) *((2e-5)^2);
```

Output Measurement Duct

```
%Output Measurement Duct
    % Total accoustic pressure at point 3
        TAP3 = load(strcat(dataset,'21'));
        S_33 = (TAP3.y) *((2e-5)^2);
    % Total accoustic pressure at point 4
        TAP4 = load(strcat(dataset,'31'));
        S_44 = (TAP4.y)*((2e-5)^2);
    % Cross Spectrum between point3 and point 4
        % real
        CS_34 = load(strcat(dataset,'41'));
        C_34 = real(CS_34.y)  *((2e-5)^2);
        % Imaginary
        Q_34 = imag(CS_34.y) *((2e-5)^2);
```

Calculate the acoustic transmission loss

```
%Acoustic Transmission Loss
    % Wave Speed k
        k = 2*pi/c.*frequency;
    % Incident pressure and power calculations using two microphone method
        S_AA = (S_11 + S_22 - 2*C_12 .* cos(x_12 * k) - 2*Q_12 .* ...
            sin(x_12 * k))./ (4 * (sin(x_12 * k)) .^2);
        S_BB = (S_11 + S_22 - 2*C_12 .* cos(x_12 * k) + 2*Q_12 .* ...
            sin(x_12 * k))./ (4 * (sin(x_12 * k)) .^2);
    % S_AA and S_BB : sign of Q_12 interchanged to suit HP data convention
    % amplitude of incident sound wave pressure (p(i))
        pressure_i = sqrt(S_AA);
    % amplitude of reflected sound wave pressure (p(ir))
        pressure_ir = sqrt(S_BB);
    % Sound Power
```

```
    power_i = pressure_i.^2 * area_inlet/(rho * c);
    power_ir = pressure_ir.^2 * area_inlet/(rho * c);
% Transmitted pressure & power calculations using 2 microphone method;
    S_XX = (S_33 + S_44 - 2*C_34 .* cos(x_34 * k) - 2*Q_34 .* ...
        sin(x_34 * k))./ (4*(sin(x_34*k)).^2);
    S_YY = (S_33 + S_44 - 2*C_34 .* cos(x_34 * k) + 2*Q_34 .* ...
        sin(x_34 * k))./ (4*(sin(x_34*k)).^2);
% S_XX & S_YY :sign of Q_34 interchanged to correct HP data convention
% amplitude of transmitted sound wave pressure
    pressure_t = sqrt(S_XX);
% amplitude of reflected sound wave pressure (p(ir))
    pressure_tr = sqrt(S_YY);
% Sound Power transmitted
    power_t = pressure_t.^2 * area_outlet / (rho * c);
    power_tr = pressure_tr.^2 * area_inlet/(rho * c);
% Transmission Loss using pressure amplitudes for calculation
    TL4m = 20 * log10 (pressure_i./pressure_t) + 10 * ...
        log10 (area_inlet / area_outlet);
% Transmission Loss using power for calculation
    TL4mpower = 10*log10( power_i ./ power_t);
```

Transmitted pressure and power calculations

using one microphone after silencer

```
%One Microphone
    % amplitude of transmitted sound wave pressure
        pressure_t1 = sqrt(S_44);
    % Sound Power transmitted
        power_t1 = pressure_t1.^2 * area_outlet / (rho * c);
    % Transmission Loss using pressure amplitudes for calculation
        TL3m = 20 * log10 (pressure_i./pressure_t1) + 10 * ...
            log10 (area_inlet / area_outlet);
    % Transmission Loss using power for calculation
        TL3mpower = 10*log10( power_i ./ power_t1);
```

Save Data and Results

```
    save(strcat(dataset,'_results'));
```

Plot the results

```
%Results
    % Plot the Transmission Loss
        figure(1);
    % Three Microphone Method
        plot(frequency,TL3m,'b');
        grid on;
        title('Acoustic (Power)Transmission Loss');
        xlabel('Frequency [Hz]');
        ylabel('Transmission Loss [dB]');
        hold on;
    % Four Microphone Method
```

```
plot(frequency,TL4m,'r');
legend('Three Microphone','Four Microphone');
hold off;
```

Plots of Intermediate Calculations

```
%Intermediate Calculations
% Input side of Silencer
    % Plot the Microphone Autospectras
        figure(2);
        semilogy(frequency,S_11,'b'); % Autospectra Power at Microphone 1;
        grid on;
        title('Microphone Autospectra on Inlet Side');
        xlabel('Frequency [Hz]');
        ylabel('Autospectra (Power) Pa^2');
        hold on;
        semilogy(frequency,S_22,'r'); %Autospectra Power at Microphone 2;
        legend('Microphone 1','Microphone 2');
        hold off;
    % Plot the Input Incident and Reflected
       figure(3);
       semilogy(frequency,power_i,'b'); %Incident Sound Pressure, power_i;
       grid on;
       title('Incident and Reflected Powers on Inlet Side');
       xlabel('Frequency [Hz]');
       ylabel('Power Pa^2');
```

```
        hold on;
        semilogy(frequency,power_ir,'r');%Reflected Sound Pressure,power_ir;
        legend('Incident','Reflected');
        hold off;
% Output side of Silencer
    % Plot the Microphone Autospectras
        figure(4);
        semilogy(frequency,S_33,'b'); % Autospectra Power at Microphone 3;
        grid on;
        title('Microphone Autospectra on Outlet Side');
        xlabel('Frequency [Hz]');
        ylabel('Autospectra (Power) Pa^2');
        hold on;
        semilogy(frequency,S_44,'r'); %Autospectra Power at Microphone 4;
        legend('Microphone 3','Microphone 4');
        hold off;
    % Plot the Input Incident and Reflected
        figure(5);
        semilogy(frequency,power_t,'b'); %Incident Sound Pressure, power_i;
        grid on;
        title('Incident and Reflected Powers on Outlet Side');
        xlabel('Frequency [Hz]');
        ylabel('Power Pa^2');
        hold on;
        semilogy(frequency,power_tr,'r');%Reflected Sound Pressure,power_ir;
        legend('Incident','Reflected');
        hold off;
```

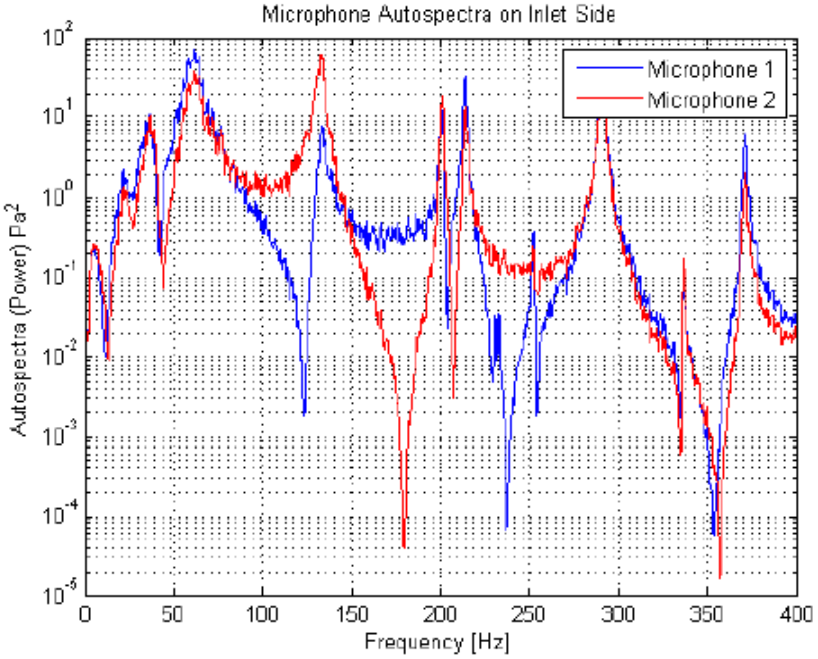
Microphone Autospectra on Inlet Side
Microphone 1
Microphone 2
Autospectra (Power) Pa2
Frequency [Hz]

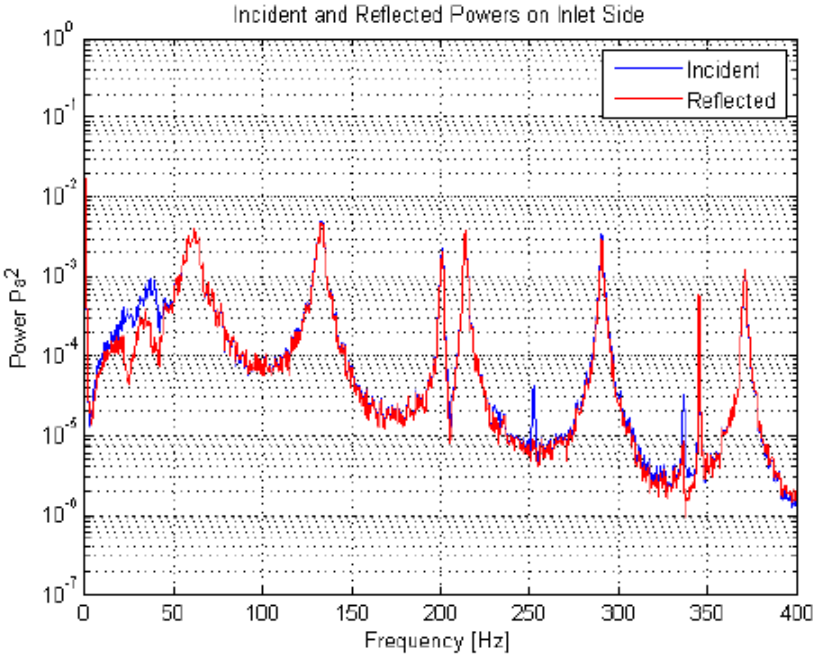
Incident and Reflected Powers on Inlet Side
Incident
Reflected
Power Pa2
Frequency [Hz]

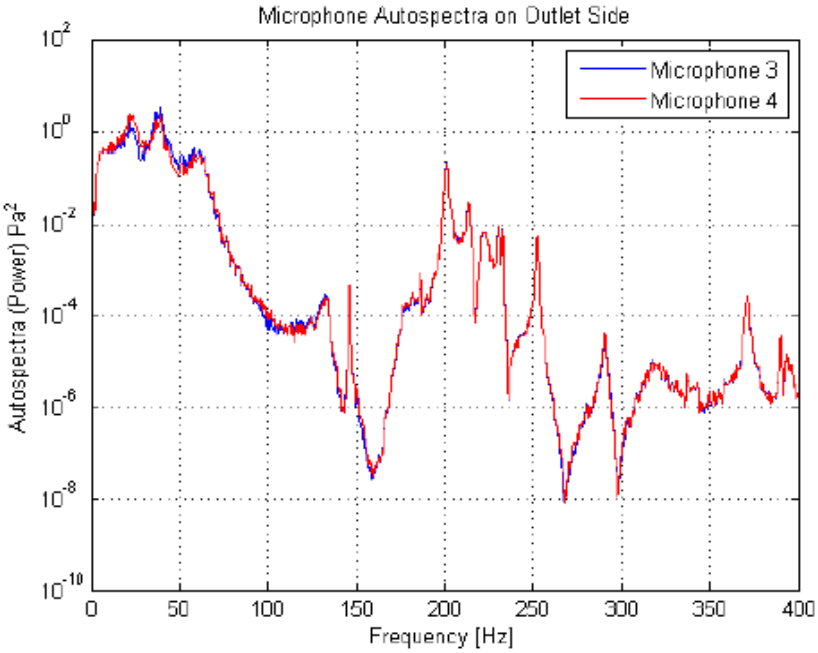
Microphone Autospectra on Outlet Side
Microphone 3
Microphone 4
Autospectra (Power) Pa²
Frequency [Hz]

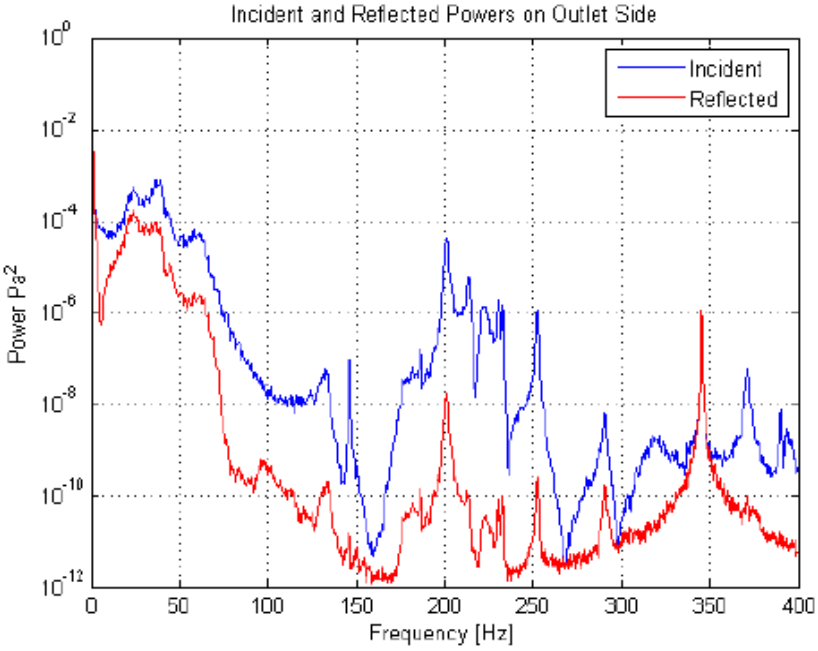
Incident and Reflected Powers on Outlet Side
Incident
Reflected
Power Pa²
Frequency [Hz]

Plot Cross Spectras

```
%Cross Spectra
    % Plot the Cross Spectrum 1;2
        figure(6);
        plot(frequency,C_12,'r');%Cross Spectrum, Real
        hold on
        plot(frequency,Q_12,'g');%Cross Spectrum, Imaginary
        title('Cross Spectrum 1:2');
        xlabel('Frequency [Hz]');
        ylabel('Cross Spectra Power Pa^2');
        legend('Real','Imaginary');
        hold off;
    % Plot the Cross Spectrum 3:4
        figure(7);
        plot(frequency,C_34,'r');%Cross Spectrum, Real
        hold on;
        plot(frequency,Q_34,'g');%Cross Spectrum, Imaginary
        title('Cross Spectrum 3:4');
        xlabel('Frequency [Hz]');
        ylabel('Cross Spectra Power Pa^2');
        legend('Real','Imaginary');
        hold off;
```

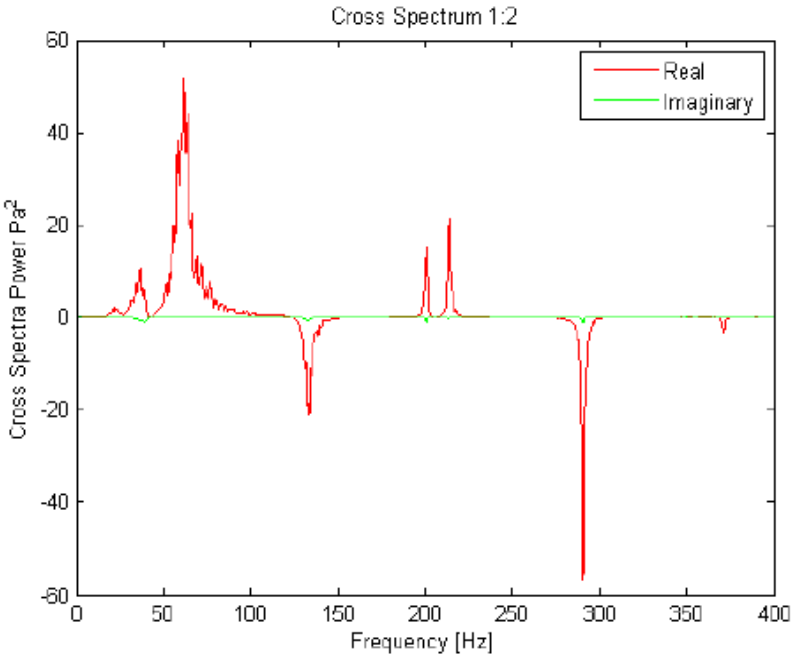

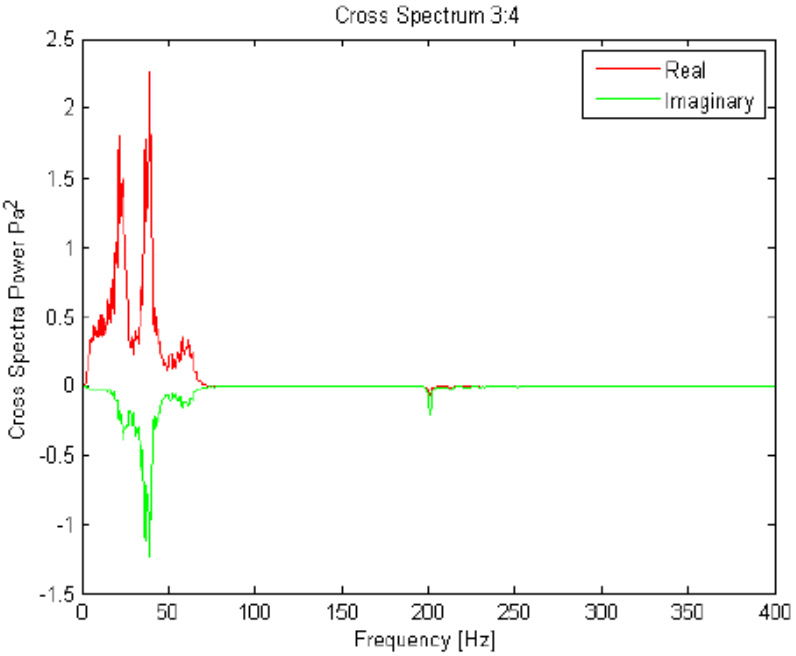

Input Parameter Check

```
disp (['Input Data set is ',(dataset)]);
disp (['Atmospheric pressure in Pa is ',num2str(P_atmospheric)]);
disp (['Air temperature in degrees C is ',num2str(T_airC)]);
disp (['Microphone spacing in metres between points 1 and 2 is ' ...
    ,num2str(x_12)]);
disp (['Microphone spacing in metres between points 3 and 4 is ' ...
    ,num2str(x_34)]);
disp (['Speed of sound m/s is ', num2str(c)]);
disp (['Inlet diameter in mm is ',num2str(dia_inlet)]);
disp (['Outlet diameter in mm is ',num2str(dia_outlet)]);
```

```
Input Data set is TJun39
Atmospheric pressure in Pa is 101700
Air temperature in degrees C is 23
Microphone spacing in metres between points 1 and 2 is 0.5
Microphone spacing in metres between points 3 and 4 is 0.5
Speed of sound m/s is 344.8664
Inlet diameter in mm is 330
Outlet diameter in mm is 330
```

END

Appendix D Muffler Shell Experimental Measurements

This appendix lists the instrumentation used for the experimental analysis of the LMM muffler shell and internal structure. The measured FRF, coherence and input power spectrum are presented for each measurement.

D.1 Instrumentation

The structural resonances were measured experimentally using:

1. PCB brand Model 086C01 impact hammer
2. PCB brand white impact tip (medium stiffness)
3. PCB aluminium mass extender
4. PCB brand Model 353B33 accelerometer (100mV/g)
5. HP 3567A Spectrum Analyser

Model Number 086C01	ICP® IMPACT HAMMER		Revision: K ECN #: 32387
Performance	**ENGLISH**	**SI**	
Sensitivity(± 15 %)	50 mV/lbf	11.2 mV/N	
Measurement Range	± 100 lbf pk	± 444 N pk	
Resonant Frequency	≥ 15 kHz	≥ 15 kHz	
Non-Linearity	≤ 1 %	≤ 1 %	
Electrical			
Excitation Voltage	20 to 30 VDC	20 to 30 VDC	
Constant Current Excitation	2 to 20 mA	2 to 20 mA	
Output Impedance	<100 ohm	<100 ohm	[1]
Output Bias Voltage	8 to 14 VDC	8 to 14 VDC	
Discharge Time Constant	≥ 500 sec	≥ 500 sec	[1]
Physical			
Sensing Element	Quartz	Quartz	
Sealing	Epoxy	Epoxy	
Hammer Mass	0.23 lb	0.10 kg	
Head Diameter	0.62 in	1.57 cm	
Tip Diameter	0.25 in	0.63 cm	
Hammer Length	8.5 in	21.6 cm	
Electrical Connection Position	Bottom of Handle	Bottom of Handle	
Extender Mass Weight	0.9 oz	25 gm	
Electrical Connector	BNC Jack	BNC Jack	

CE [2]

All specifications are at room temperature unless otherwise specified.
In the interest of constant product improvement, we reserve the right to change specifications without notice.
ICP® is a registered trademark of PCB Group, Inc.

OPTIONAL VERSIONS
Optional versions have identical specifications and accessories as listed for the standard model except where noted below. More than one option may be used.

T - TEDS Capable of Digital Memory and Communication Compliant with IEEE P1451.4

NOTES:
[1] Typical.
[2] See PCB Declaration of Conformance PS068 for details.

SUPPLIED ACCESSORIES:
Model 081B05 Mounting Stud (10-32 to 10-32) (2)
Model 084A06 Extender - aluminum, 0.6" diameter (1)
Model 084B03 Hard Tip- Hard (S.S) (1)
Model 084B04 Hammer Tip- Medium (White Plastic) (1)
Model 084C05 Hammer Tip- Soft (Black) (2)
Model 084C11 Hammer Tip- Supersoft (Red) (2)
Model 085A10 Vinyl Cover For Medium Tip (Blue) (2)
Model HCS-2 Calibration of Series 086 instrumented impact hammers (1)

Entered:	Engineer:	Sales:	Approved:	Spec Number:
Date: 2/24/10	Date: 2/18/09	Date: 2/17/10	Date: 2/17/10	9120

PCB PIEZOTRONICS™ VIBRATION DIVISION
3425 Walden Avenue, Depew, NY 14043
Phone: 716-684-0001
Fax: 716-685-3886
E-Mail: vibration@pcb.com

Figure App D.1 PCB Impact Hammer Model 086C01 Data Sheet

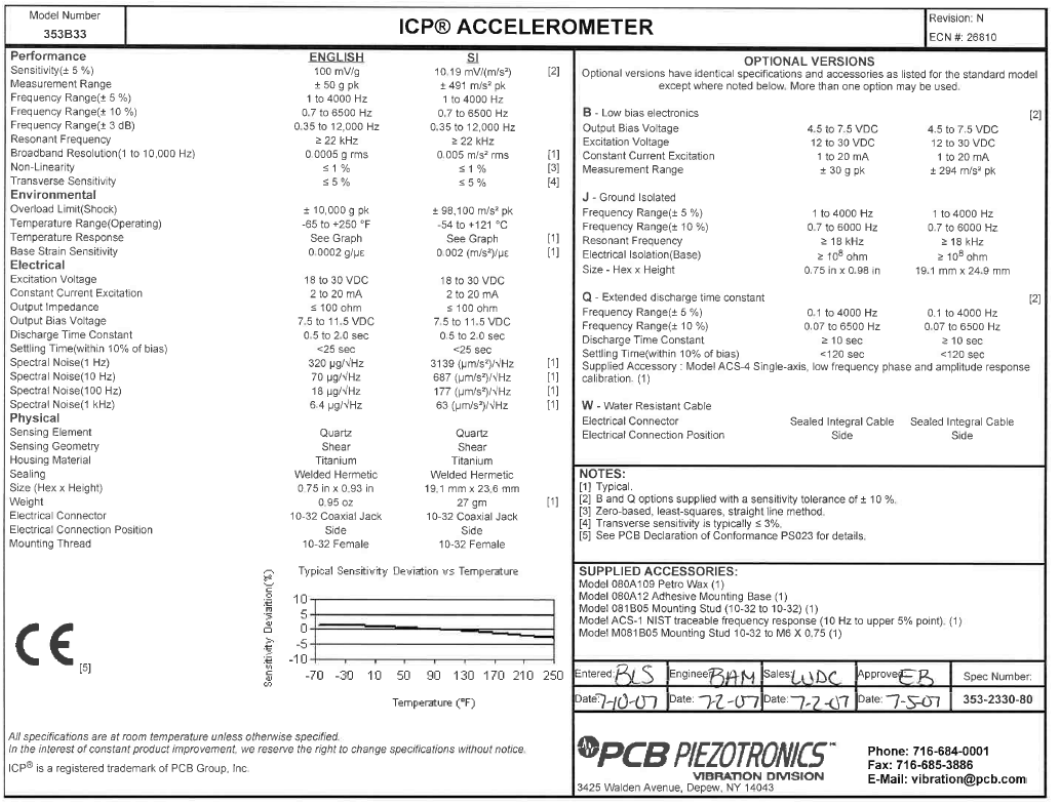

Model Number 353B33	ICP® ACCELEROMETER	Revision: N ECN #: 26810

Performance	ENGLISH	SI	
Sensitivity(± 5 %)	100 mV/g	10.19 mV/(m/s²)	[2]
Measurement Range	± 50 g pk	± 491 m/s² pk	
Frequency Range(± 5 %)	1 to 4000 Hz	1 to 4000 Hz	
Frequency Range(± 10 %)	0.7 to 6500 Hz	0.7 to 6500 Hz	
Frequency Range(± 3 dB)	0.35 to 12,000 Hz	0.35 to 12,000 Hz	
Resonant Frequency	≥ 22 kHz	≥ 22 kHz	
Broadband Resolution(1 to 10,000 Hz)	0.0005 g rms	0.005 m/s² rms	[1]
Non-Linearity	≤ 1 %	≤ 1 %	[3]
Transverse Sensitivity	≤ 5 %	≤ 5 %	[4]
Environmental			
Overload Limit(Shock)	± 10,000 g pk	± 98,100 m/s² pk	
Temperature Range(Operating)	-65 to +250 °F	-54 to +121 °C	
Temperature Response	See Graph	See Graph	[1]
Base Strain Sensitivity	0.0002 g/με	0.002 (m/s²)/με	[1]
Electrical			
Excitation Voltage	18 to 30 VDC	18 to 30 VDC	
Constant Current Excitation	2 to 20 mA	2 to 20 mA	
Output Impedance	≤ 100 ohm	≤ 100 ohm	
Output Bias Voltage	7.5 to 11.5 VDC	7.5 to 11.5 VDC	
Discharge Time Constant	0.5 to 2.0 sec	0.5 to 2.0 sec	
Settling Time(within 10% of bias)	<25 sec	<25 sec	
Spectral Noise(1 Hz)	320 μg/√Hz	3139 (μm/s²)/√Hz	[1]
Spectral Noise(10 Hz)	70 μg/√Hz	687 (μm/s²)/√Hz	[1]
Spectral Noise(100 Hz)	18 μg/√Hz	177 (μm/s²)/√Hz	[1]
Spectral Noise(1 kHz)	6.4 μg/√Hz	63 (μm/s²)/√Hz	[1]
Physical			
Sensing Element	Quartz	Quartz	
Sensing Geometry	Shear	Shear	
Housing Material	Titanium	Titanium	
Sealing	Welded Hermetic	Welded Hermetic	
Size (Hex x Height)	0.75 in x 0.93 in	19.1 mm x 23.6 mm	
Weight	0.95 oz	27 gm	[1]
Electrical Connector	10-32 Coaxial Jack	10-32 Coaxial Jack	
Electrical Connection Position	Side	Side	
Mounting Thread	10-32 Female	10-32 Female	

CE [5]

Typical Sensitivity Deviation vs Temperature

All specifications are at room temperature unless otherwise specified.
In the interest of constant product improvement, we reserve the right to change specifications without notice.

ICP® is a registered trademark of PCB Group, Inc.

OPTIONAL VERSIONS

Optional versions have identical specifications and accessories as listed for the standard model except where noted below. More than one option may be used.

B - Low bias electronics			[2]
Output Bias Voltage	4.5 to 7.5 VDC	4.5 to 7.5 VDC	
Excitation Voltage	12 to 30 VDC	12 to 30 VDC	
Constant Current Excitation	1 to 20 mA	1 to 20 mA	
Measurement Range	± 30 g pk	± 294 m/s² pk	

J - Ground Isolated		
Frequency Range(± 5 %)	1 to 4000 Hz	1 to 4000 Hz
Frequency Range(± 10 %)	0.7 to 6000 Hz	0.7 to 6000 Hz
Resonant Frequency	≥ 18 kHz	≥ 18 kHz
Electrical Isolation(Base)	≥ 10^8 ohm	≥ 10^8 ohm
Size - Hex x Height	0.75 in x 0.98 in	19.1 mm x 24.9 mm

Q - Extended discharge time constant			[2]
Frequency Range(± 5 %)	0.1 to 4000 Hz	0.1 to 4000 Hz	
Frequency Range(± 10 %)	0.07 to 6500 Hz	0.07 to 6500 Hz	
Discharge Time Constant	≥ 10 sec	≥ 10 sec	
Settling Time(within 10% of bias)	<120 sec	<120 sec	

Supplied Accessory : Model ACS-4 Single-axis, low frequency phase and amplitude response calibration. (1)

W - Water Resistant Cable		
Electrical Connector	Sealed Integral Cable	Sealed Integral Cable
Electrical Connection Position	Side	Side

NOTES:
[1] Typical.
[2] B and Q options supplied with a sensitivity tolerance of ± 10 %.
[3] Zero-based, least-squares, straight line method.
[4] Transverse sensitivity is typically ≤ 3%.
[5] See PCB Declaration of Conformance PS023 for details.

SUPPLIED ACCESSORIES:
Model 080A109 Petro Wax (1)
Model 080A12 Adhesive Mounting Base (1)
Model 081B05 Mounting Stud (10-32 to 10-32) (1)
Model ACS-1 NIST traceable frequency response (10 Hz to upper 5% point). (1)
Model M081B05 Mounting Stud 10-32 to M6 X 0.75 (1)

Entered: BLS	Engineer: BAM	Sales: WDC	Approved: EB	Spec Number:
Date: 7-10-07	Date: 7-2-07	Date: 7-2-07	Date: 7-5-07	353-2330-80

PCB PIEZOTRONICS™
VIBRATION DIVISION
3425 Walden Avenue, Depew, NY 14043
Phone: 716-684-0001
Fax: 716-685-3886
E-Mail: vibration@pcb.com

Figure App D.2 PCB Accelerometer Model 353B33 Data Sheet

D.2 Measured FRF's

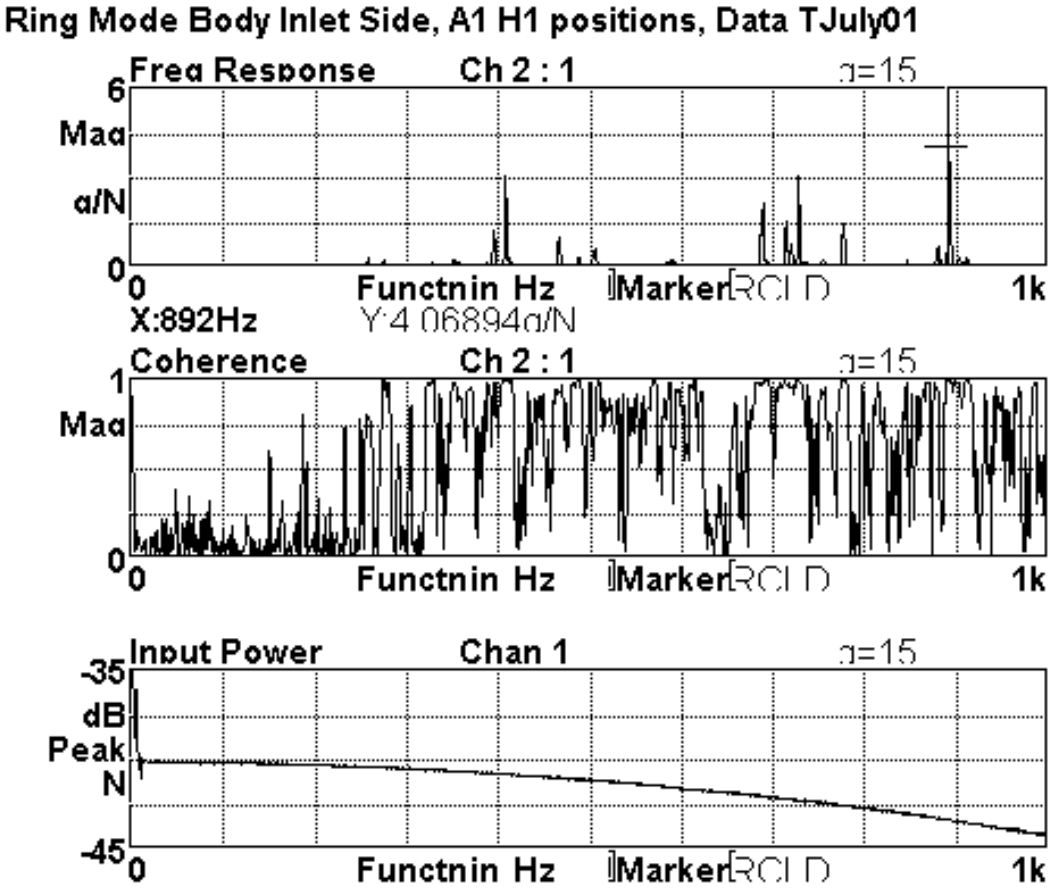

Figure App D.3 FRF, Body Ring Mode, A1 H1, Data Set TJuly01

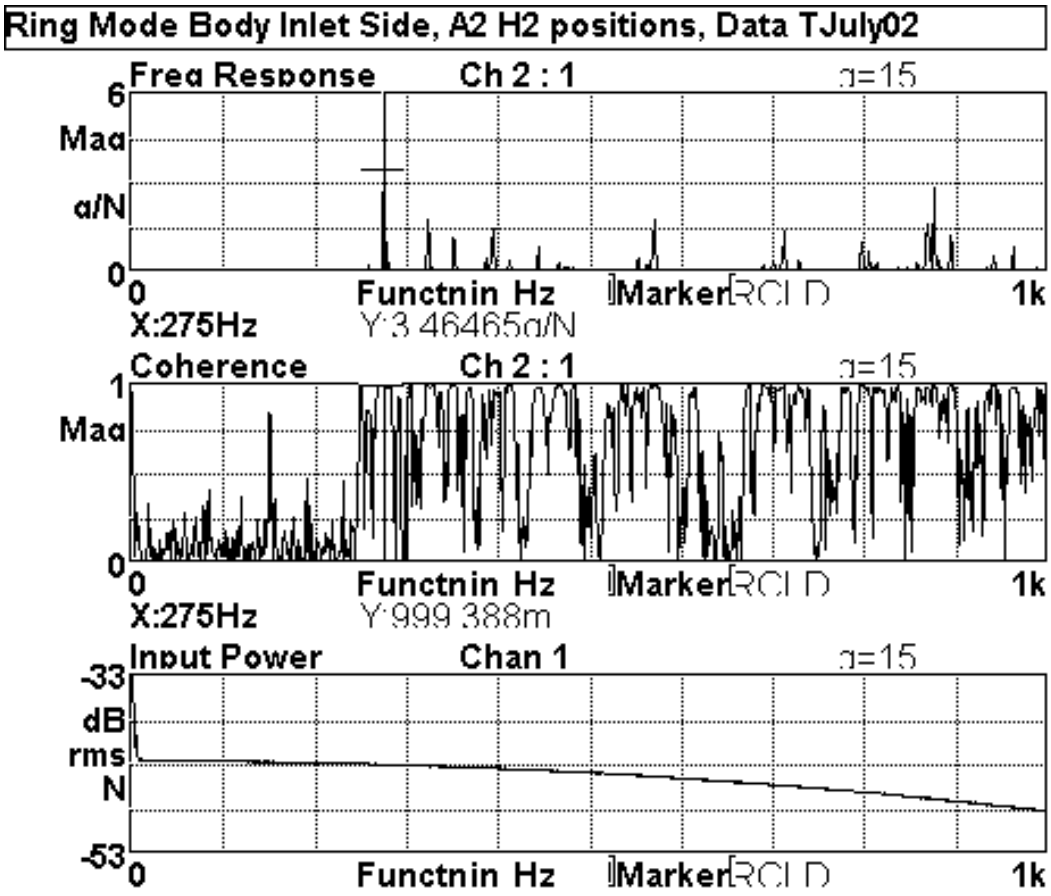

Figure App D.4 FRF, Body Ring Mode, A2 H2, Data Set TJuly02

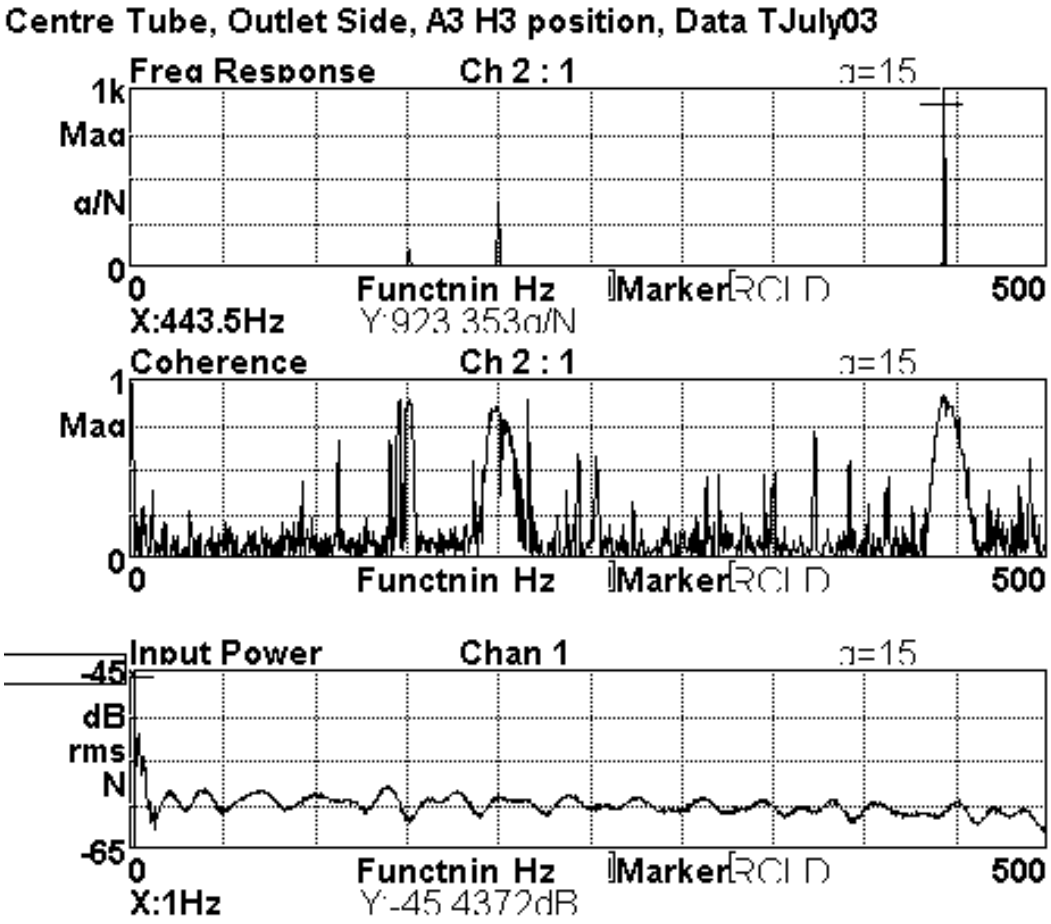

Figure App D.5 FRF, Centre Tube, A3 H3, Data Set TJuly03

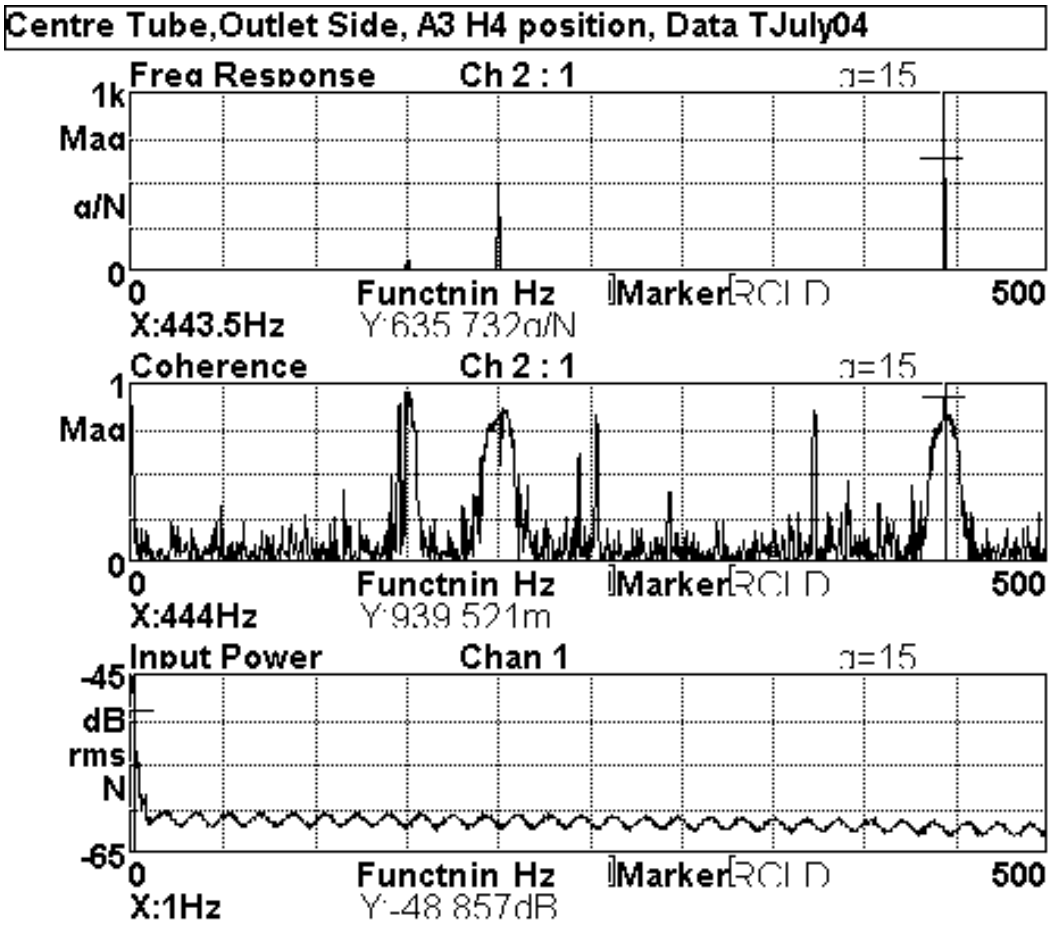

Figure App D.6 FRF, Centre Tube, A3 H4, Data Set TJuly04

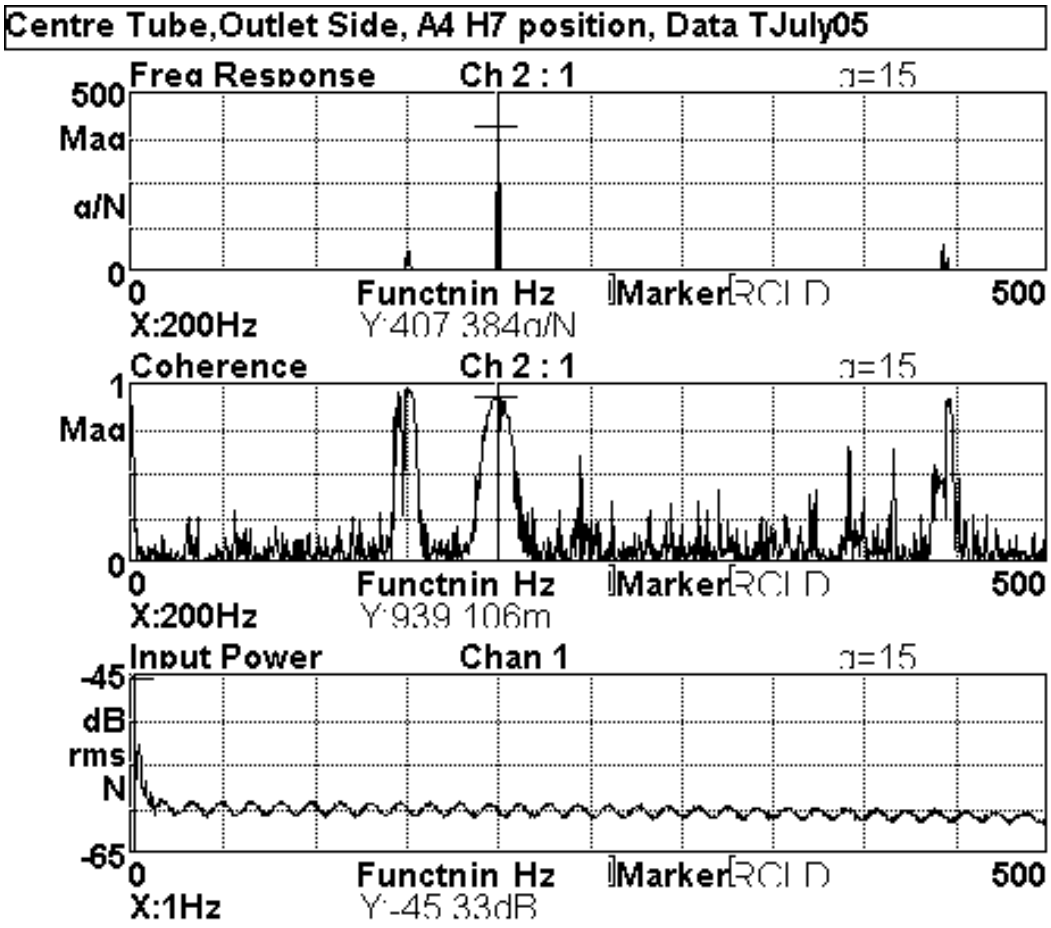

Figure App D.7 FRF, Centre Tube, A4 H7, Data Set TJuly05

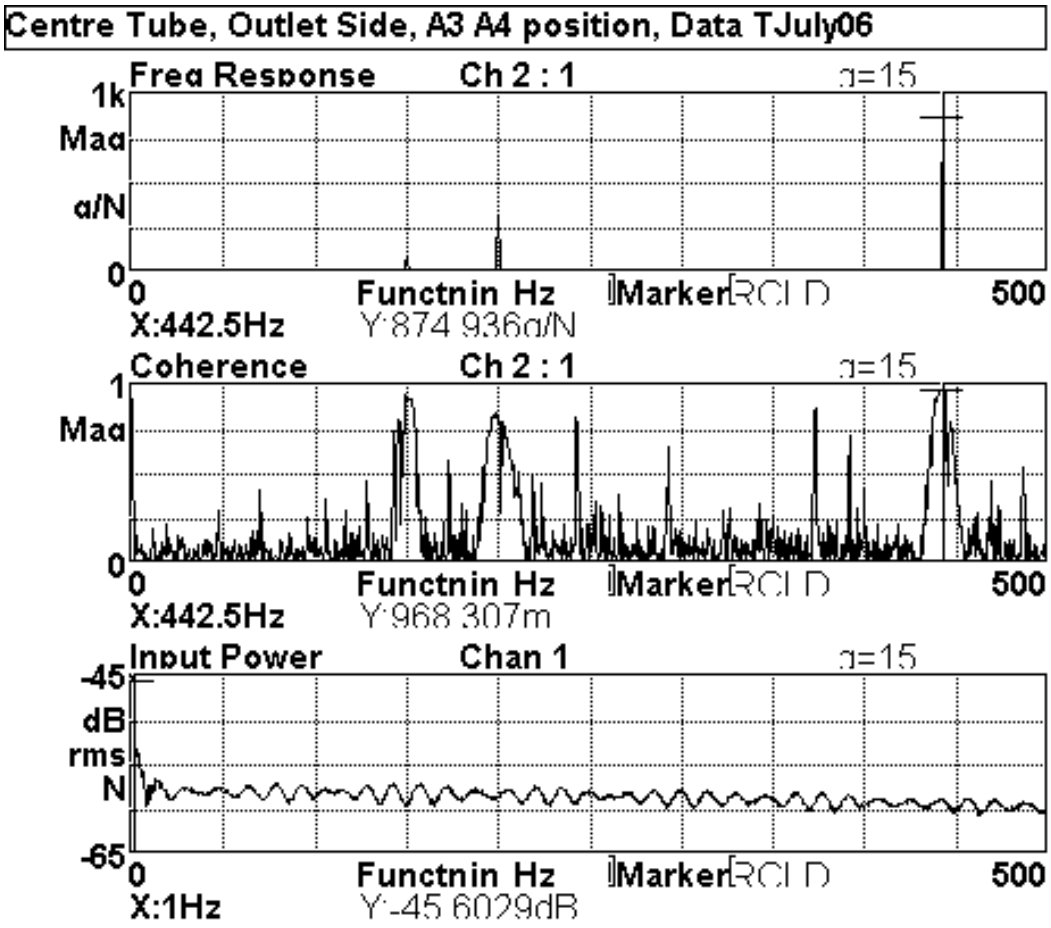

Figure App D.8 FRF, Centre Tube, A4 H5, Data Set TJuly06

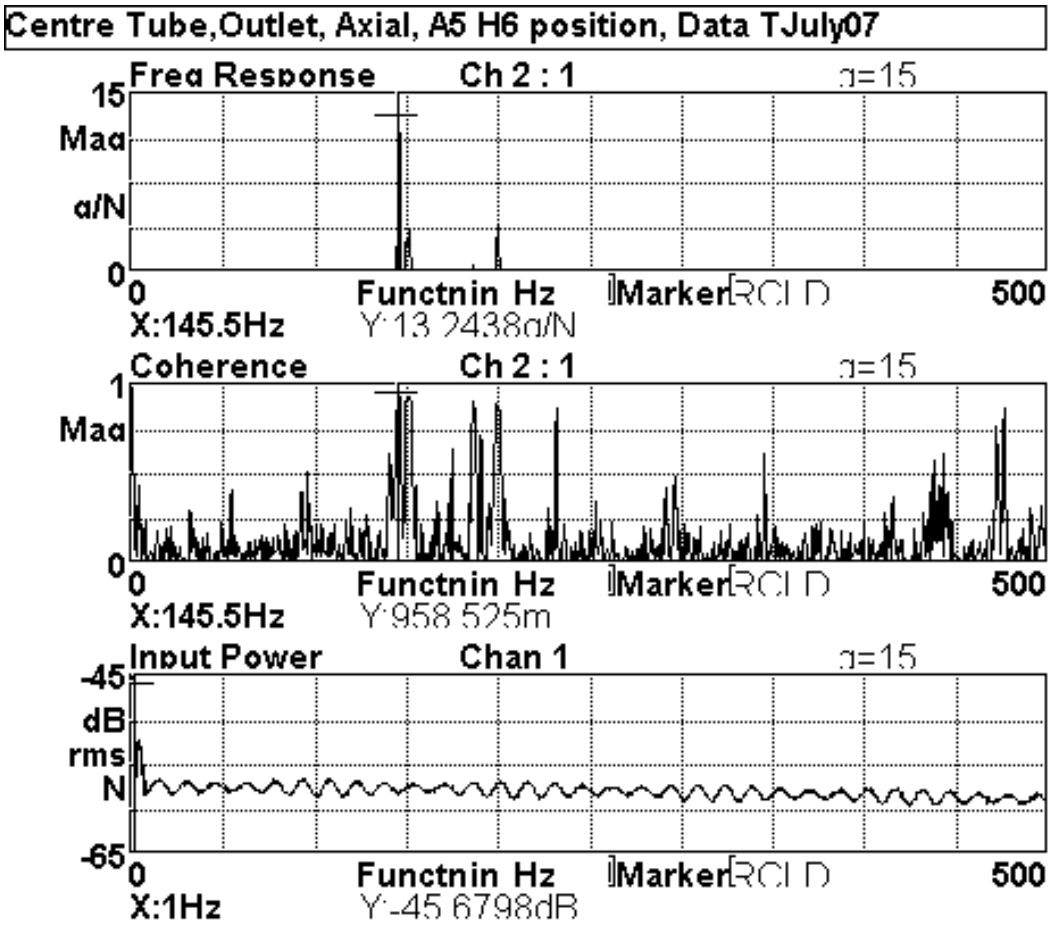

Figure App D.9 FRF, Centre Tube, A5 H6, Data Set TJuly07

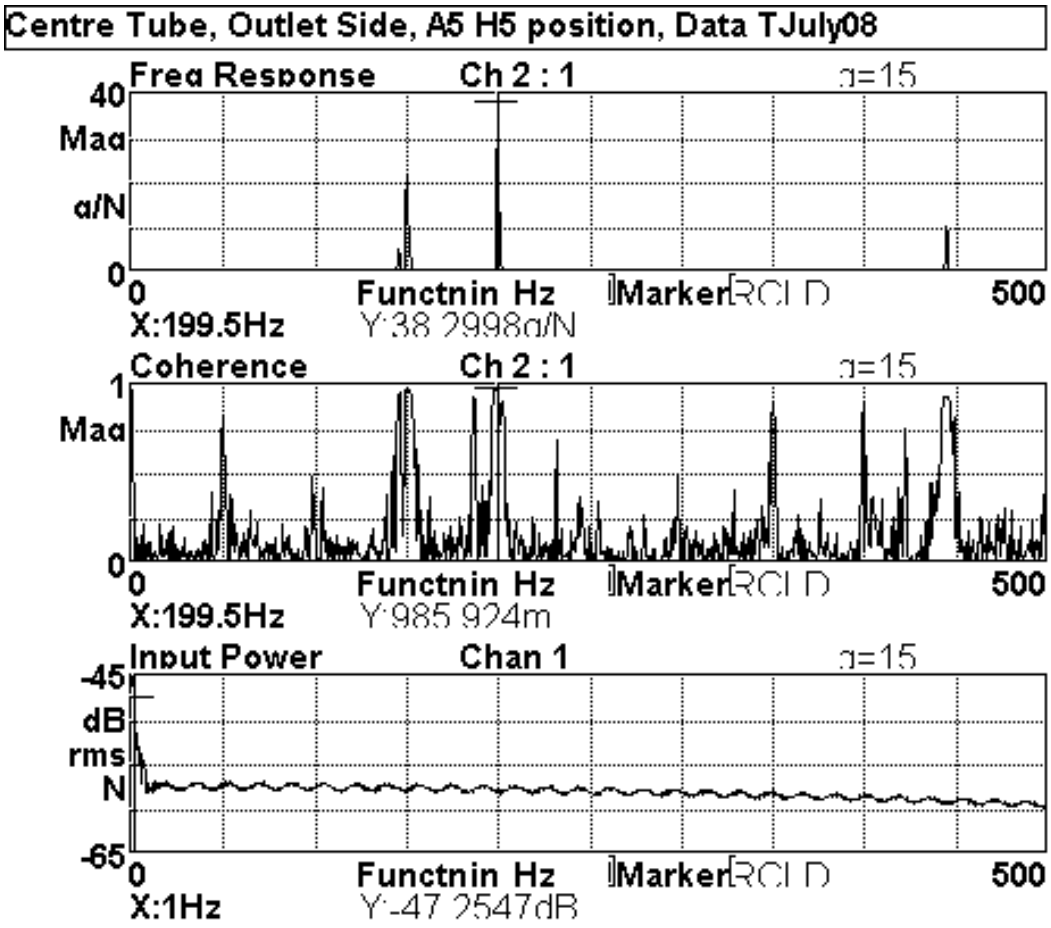

Figure App D.10 FRF, Centre Tube, A5 H5, Data Set TJuly08